Bioresource Processing Institute of Australia (BioPRIA)

Department of Chemical Engineering

Faculty of Engineering

Monash University

ENGINEERED NANOCELLULOSE SUPERABSORBENTS FOR APPLICATION IN AGRICULTURAL SOILS

by

Ruth Melany Barajas-Ledesma
B. Eng. & M. Eng. (Chemical)

A thesis submitted for the degree of Doctor of Philosophy
at Monash University in 2021, Chemical Engineering

MONASH University   BioPRIA

July 2021

THIS PAGE HAS BEEN INTENTIONALLY LEFT BLANK

"It takes a lot of courage to push through hard times.

Never give up.

Good things are coming your way"

THIS PAGE HAS BEEN INTENTIONALLY LEFT BLANK

Copyright notice

Ruth Melany Barajas-Ledesma

THIS PAGE HAS BEEN INTENTIONALLY LEFT BLANK

Table of Contents

Monash University

Thesis including published works declaration

I hereby declare that this thesis contains no material which has been accepted for the award of any other degree or diploma at any university or equivalent institution and that, to the best of my knowledge and belief, this thesis contains no material previously published or written by another person, except where due reference is made in the text of the thesis.

This thesis includes two original papers published in peer reviewed journals (Chapter 2 and Chapter 3) and one publication accepted for publication (Chapter 4). The core theme of the thesis is Engineered nanocellulose superabsorbent for application in agricultural soils. The ideas, development and writing up of all the papers in the thesis were the principal responsibility of myself, the student, working within the Department of Chemical Engineering, Monash University, under the supervision of Professor Gil Garnier, Professor Antonio Patti and Professor Vanessa Wong.

(The inclusion of co-authors reflects the fact that the work came from active collaboration between researchers and acknowledges input into team-based research.)

In the case of *three chapters* my contribution to the work involved the following:

Thesis Chapter	Publication Title	Status (published, in press, accepted or returned for revision, submitted)	Nature and % of student contribution	Co-author name(s) Nature and % of Co-author's contribution*	Co-author(s), Monash student Y/N*
2	*Engineering nanocellulose superabsorbents by controlling the drying rate*	*Published*	*85%. Key ideas, experimental work, analysis of results and writing first draft*	*1) Vikram Singh Raghuwanshi (2%) experimental work.* *2) Vanessa Wong (3%) manuscript feedback and editing* *3) Antonio Patti (5%) feedback and editing* *4) Gil Garnier (5%) feedback and editing.*	*No* *No* *No* *No*
3	*Effect of the counter-ion on nanocellulose hydrogels and their superabsorbent structure and properties*	*Published*	*80%. Key ideas, experimental work, analysis of results and writing first draft*	*Laila Hossain (5%) experimental work.* *Vanessa Wong (5%) manuscript feedback and editing* *Antonio Patti (5%) feedback and editing* *Gil Garnier (5%) feedback and editing.*	*Yes* *No* *No* *No*

				Vanessa Wong (3%) manuscript feedback and editing	No
4	*Carboxylated nanocellulose superabsorbent: biodegradation and soil water retention properties*	*Accepted*	*85%. Key ideas, experimental work, analysis of results and writing first draft*	Karen Little (2%) manuscript feedback and editing	No
				Antonio Patti (5%) feedback and editing	No
				Gil Garnier (5%) feedback and editing.	No

*If no co-authors, leave fields blank

I have renumbered sections of submitted or published papers in order to generate a consistent presentation within the thesis.

Student name: Ruth Melany Barajas-Ledesma

Student signature: **Date:** 2/08/2021

I hereby certify that the above declaration correctly reflects the nature and extent of the student's and co-authors' contributions to this work. In instances where I am not the responsible author I have consulted with the responsible author to agree on the respective contributions of the authors.

Main Supervisor name: Gil Garnier

Main Supervisor signature: **Date:** 2/08/2021

Acknowledgements

First of all, I would like to express my most sincere and humble gratitude to my supervisors, Professor Gil Garnier, Professor Tony Patti and Professor Vanessa Wong, for putting their trust in me. Gil, who I admire for his leadership, for all his support since the beginning of my PhD, for always encouraging me to develop myself professionally. Tony, my sensei, for guiding me at all times. For all his pieces of advice that, without him knowing, helped me to get through the PhD in my most difficult times. For all the gatherings and for always being there for us, his students. Vanessa, for always checking up on me, giving me your best piece of advice. For being my friend more than my supervisor. I could not have asked for better supervisors and for that, I am truly grateful.

I acknowledge the Australian Research Council (ARC), the PALS grant and Monash University, for providing me with the scholarship necessary to make my dream come true.

Many thanks to my colleagues and friends in BioPRIA, without any doubt, they made my PhD journey fun and more enjoyable. I acknowledge Rodrigo Curvello, Diana Alves, David Mendoza and Maoqi Lin, for being the noisiest people in the room, giving me extensive laughs and chats. For all the coffees that we shared together, celebrating every important milestone that we had achieved in our career. Marek, my best friend-enemy, for being so unique and always looking for an interesting topic to talk about like the origin of the micronations, Australian comedians and for supporting my dream to become a sumo wrestler, filling me up with Tim tams. Aysu and Llyza, my empowered women, my inspiration to complete this journey. My gratitude to Craig, Gloria and Hans, the next PALS generation. Craig, for all his help during these last months, I would not have been able to finish on time without him. Gloria, my Spanish speaker friend, for all her support this past year that made me gain more confidence in myself. Christine, I think of her as my young mentor, she was always there to cheer me up, being my shoulder to cry on, making sure that I was always okay, and for that, I am truly and completely grateful. Last, I acknowledge all my colleagues and staff members at BioPRIA for their support and the many parties we had together.

My sincere gratitude to Tony's group: Karen, Alessia, Cuyler, Mark, Gavin, Shivali, Subramoni and Debjani, for always listen and putting up with my infinite practise presentations. Karen, one of the first people I met when I started this journey, for always being there and for providing me her scientific advice in all my projects.

Many thanks to Laila and Maisha, my dearest Bangladeshi friends, for their friendship. We created an excellent team together that formed a published manuscript. A work we did during COVID-19 that I'll never forget. I learnt so much from them, thanks for trusting me.

I acknowledge Thilina, my role model, for motivating me to never give up and to keep fighting. He was one of the first people I met at BioPRIA, and although we shared a little time together, we became really good friends. He is my confidant, thanks for mentoring me, giving me encouragement during these three years, especially when I needed it the most. Thilina, I hope we can do a trail run together any time soon!

My biggest appreciation to my mentor, Dr Nafty, for having so much patience and for believing in me. Since I met him, I have boosted my professional skills. For teaching me to set goals and providing me the tools I needed to get my first job in Australia. For all of these, I am truly and eternally grateful.

With all my affection, I acknowledge my beloved friends, Laura and Carlos, for encouraging me to do a PhD in the first place, when I needed that push. For all the Friday dinners that transformed into the whole weekend. For all the trips and the time we spent together here in Melbourne. Many thanks for being present in the most important moments of my PhD, even in the distance, at more than 16,000 km (I googled it). I love you so much.

I acknowledge my wonderful brothers, Gerardo and Daniel, who are always on my mind. My grandmother, Socorro, who I love with all my heart. Granny, many thanks for always looking after me; for being with me at all times and for always looking for a way to reach me even if that means learning how to use WhatsApp and Facebook. I also acknowledge my auntie, Alisson, who is always in my heart.

I express my infinite gratitude to my beloved husband, Diego, for always believing in me, even when I doubted myself; for encouraging me to follow my dreams and for giving me the freedom to be whoever I wanted. For always being present in every moment of this journey and for pampering me when I needed it.

Finally, I acknowledge my parents, Ruth and Gerardo, for all their encouragement. It is because of them that today I am completing this doctorate degree. For every lesson and piece of advice every day of my life that has made me who I am. My daddy, for making me believe that if I can dream it, I can do it, to do the impossible. Every page, every word, every letter of this thesis is for them and for Diego.

In 2009, when I was doing my bachelor's degree, I expressed in an assignment to one professor my wish of pursuing a PhD and becoming a scientist in chemical engineering. I told him that believing in oneself made everything else come by addition. I knew since that moment that I wanted to become a Doctor; I did not know where, when or how. Today, more than a decade later, I have made my dream come true.

Thank you, God, for never letting me fall.

With all my love, Melany.

Abstract

It is estimated that global need for food will require a doubling in food production by 2050. To meet this demand in a sustainable and environmentally benign way is a major challenge for the agricultural industry, especially because irrigated agriculture is limited and consumes about 70% of the water available for human use worldwide. Superabsorbent polymers (SAP) appear as an attractive strategy to tackle this challenge. These are highly porous, hydrophilic polymers capable of absorbing water at hundreds of times their own weight. However, most of the commercial SAP are based on polyacrylamide (PAM) or polyacrylate (PA) fossil-fuel derived polymers, which degrade extremely slowly into by-products increasingly raising environmental and health concerns. These issues haven driven the development of SAP based on natural polymers such as cellulose, the world's most abundant (bio)polymer. Cellulose is readily available, biodegradable, renewable, has inherent hydrophilicity and other desirable characteristics to produce superabsorbents. Nanocellulose refers to the cellulose fibres with dimensions in the nanometre scale. Apart from the intrinsic properties of cellulose, nanocellulose is easy to functionalise into SAP. There are very few reports in the literature describing the potential of nanocellulose superabsorbents in agriculture and therefore, the topic remains poorly understood. This thesis aims to engineer the physical and chemical properties of nanocellulose SAP to develop a performant and biodegradable material for use in soil water retention in sustainable agriculture.

This doctoral thesis is composed of two sections. The first focuses on the engineering of the physical and chemical structure of nanocellulose for specific use in agriculture. Nanocellulose SAPs are commonly produced in the laboratory through freeze-drying. This technique is not only expensive and difficult to perform on a large-scale, but also produces ultra-low density superabsorbents, which can severely restrict their application in agriculture. By changing the drying method, we demonstrated that superabsorbents of remarkable properties can be produced. Oven-drying at 50 °C achieves

superabsorbents with a higher swelling capacity than those freeze-dried. This is attributed to their high pore area, which increases the interaction between water molecules and cellulose fibres, leading to a stronger physical entrapment of water by capillary forces. Exchanging the Na^+ ions present in the nanocellulose network for NH_4^+ also increases the pore area of the superabsorbents. This is because of the unique ability of the NH_4^+ ions to rotate, creating additional hydrogen bonds with water.

In the second section of the thesis, the potential of nanocellulose SAPs, produced through different drying techniques, to increase water retention in a sandy soil used as a model is analysed. The increase in soil water retention with increasing application rate of SAP confirms the suitability of these materials. Soils amended with freeze-dried SAP reach the highest water retention, while those with SAP oven-dried at 50 °C remain moist the longest. The performance of the SAPs decreases with increasing hydration/dehydration cycles. This is attributed to the SAP biodegradation, which in this soil, occurs after 30 days of exposure.

The development of efficient nanocellulose superabsorbents for agriculture requires to consider their effect on the successive stages of plant growth. This is achieved with two comprehensive pot trials performed in a greenhouse. In the first, tatsoi plants are grown under water stress in a sandy soil amended with 0.5 wt% and 1.0 wt% application of nanocellulose SAP oven-dried at 50 °C. While increasing the application rate of superabsorbent decreases the total water consumption, the plant biomass significantly decreases with the addition of 1.0 wt% of nanocellulose SAP compared to those without superabsorbent. This was attributed to an immobilisation of nitrogen by microbial biomass, where the nanocellulose provides a spike of readily available carbon and energy source. The increase in soil respiration rates with increasing application of nanocellulose further supports this hypothesis.

In the second pot trial, spinach plants are grown in two types of soil, a sandy (SD) and a clay loam (CL) soil, both amended with 0.5 wt% of nanocellulose SAP oven-dried at 50 °C. This study is conducted to evaluate the effect that soil has on the performance of superabsorbent in plant growth.

The results are compared with those of a commercial polyacrylamide-based SAP. Plant biomass varies widely with the type of soil. Plant biomass is the highest in SD soil treated with the commercial SAP, while it significantly decreases in CL soils amended with any type of superabsorbent. This effect is magnified when nanocellulose SAP is used, which is attributed to waterlogging stress and the fast biodegradation of cellulose, where only 50% of the initial mass remains after 5 days of exposure.

This thesis contributes to sustainable agriculture by expanding our knowledge of superabsorbents engineered from natural polymers. Nanocellulose is used as a model to create a performant platform material to replace the current fossil fuel-derived and non-biodegradable synthetic SAP. This research pioneers in the use of nanocellulosic materials in agriculture and will guide the future studies that are needed to modify the nanocellulose SAP structure to provide full benefits for agricultural use.

List of publications

Peer-reviewed journal papers
The following published and submitted papers are included in the body of this thesis as individual chapters. The sections of these published papers have been renumbered in order to generate a consistent presentation within the thesis. Papers in the published format are included as Appendix II.

1. **BARAJAS-LEDESMA, R**.; PATTI, A.; WONG, V.; RAGHUWANSHI, V.; GARNIER, G. Engineering nanocellulose superabsorbents by controlling the drying rate. Colloids and Surfaces A: Physicochemical and Engineering Aspects, vol. 600, p. 124943, doi: https://doi.org/10.1016/j.colsurfa.2020.124943

2. **BARAJAS-LEDESMA, R**.; HOSSAIN, L.; WONG, V.; PATTI, A.; GARNIER, G. Effect of the counter-ion on nanocellulose hydrogels and their superabsorbent structure and properties. Journal of Colloid and Interface Science, vol. 599, pp. 140-148, doi: https://doi.org/10.1016/j.jcis.2021.04.065.

3. **BARAJAS-LEDESMA, R**.; WONG, V.; LITTLE, K.; PATTI, A.; GARNIER, G. Carboxylated nanocellulose superabsorbent: biodegradation and soil water retention properties. (Manuscript accepted by Journal of Applied Polymer Science).

The following published papers are not included in the main body of this thesis and can be found in their published format in Appendix III.

1. HOSSAIN, L.; MALIHA, M.; **BARAJAS-LEDESMA, R**.; KIM, J.; PUTERA, K.; SUBEDI, D.; TANNER, J.; BARR, J.; BANASZAK HOLL, M.; GARNIER, G. Engineering laminated paper for SARS-CoV-2 medical gowns. Polymer, vol 22, p. 123643, doi: https://doi.org/10.1016/j.polymer.2021.123643.

List of figures

Chapter 1

Chapter 4

Chapter 5

Chapter 6

irrespective of soil moisture and (d) WP in soil moisture irrespective of treatment. Values are reported as mean ± standard deviation (n=5). Means followed by the same letter were not significantly different at the $p \leq 0.05$ level (Tukey's HSD), see Table 2 for details of ANOVA results.

Figure 6-5   Shoot dry weight (SDW) of spinach grown in two soil types. For the CL soil (in red), (a) SDW under different levels of soil moisture and treatments, (b) SDW in treatments irrespective of soil moisture, and (c) SDW in soil moisture irrespective of treatment. For the SD soil (in blue), (d) SDW under different levels of soil moisture and treatments, (e) SDW in treatments irrespective of soil moisture and (f) SDW soil moisture irrespective of treatment. Values are reported as mean ± standard deviation (n=5). For each plot, means followed by the same letter were not significantly different at the $p \leq 0.05$ level (Tukey's HSD). Figure a and d highlights the difference at the two-way interaction (Treatment X Soil Moisture). See Table 2 for details of ANOVA results.

Figure 6-6   Cumulative CO_2 emissions of different soil treatments for: (a) CL soil and (b) SD soil. Results are reported as mean ± standard deviation (n=5). The asterisks above each data point show the level of significant difference compared to the control, C0. Here, * is $p \leq 0.01$, and ** shows $p \leq 0.001$.

Figure 6-7   (a) Effect of soil type on the biodegradation of nanocellulose SAP over time. (b) Amount of nanocellulose superabsorbent remained at the end of the plant experiment for both soils. Results are reported as mean ± standard deviation (n=5). Bars followed by the same letter were not significantly different at the $p \leq 0.05$

level (Tukey's HSD). The asterisk above day 7 in (b) shows the level of significant difference at the $p \leq 0.05$.

List of tables

ns = no significant difference, * is p ≤ 0.05, ** represents p ≤ 0.01, and **** is p

≤ 0.0001.

Table 6-III   Total carbon (%), nitrogen (%) and C:N molar ratio of soil treatments measured

by elemental analysis.

List of Abbreviations

$(NH_4)_2SO_4$	Ammonium sulfate
3D	Three-dimensional
ANOVA	Analysis of variance
ARC	Australian research council
BEK	Bleached eucalyptus kraft
BTCA	1,2,3,4-butanetetracarboxylic dianhydride
C	Carbon
C:N	Carbon:nitrogen
C0	Control without fertiliser
C6	Primary alcohol groups
$CaSO_4.\frac{1}{2}H_2O$	Calcium sulfate hemihydrate
CEC	Cation Exchange Capacity
CF	Control with fertiliser
CK	Control
CL	Clay loam soil
CMC	Carboxylmethylcellulose
CNC	Cellulose nanocrystals
CNF	Cellulose nanofibers

CO_2	Carbon dioxide
COO-	Carboxylate groups
$CuSO_4.5H_2O$	Copper (II) sulfate pentahydrate
DS	Degree of substitution
DW	Deionised water
ECH	Epichlorohydrin
f	Ionic sensitivity
FID	Gc-flame ionization detector
FT-IR	Fourier transform infrared
GC	Gas chromatography
GC-TCD	Gas chromatography – thermal conductivity detector
GI	Germination index
HCl	Hydrochloric acid
HCNS	Elemental analysis
HEC	Hydroxyethylcellulose
HID	High intensity discharge
HNO_3	Nitric acid
HPLC	High performance liquid chromatography
HSD	Tukey's honestly significant difference
ICP-OES	Inductively coupled plasma – optical emission spectrometry
ISO	International Organization for Standardization
K_2SO_4	Potassium sulfate
LVR	Linear viscoelastic region
MBA	N, N' methylenebisacrylamide

MC	Methylcellulose
$MgSO_4$	Magnesium sulfate anhydrous
MMt	Montmorillonite
MPS	Multipurpose Sampler
MTG	Mean time to germination
N	Nitrogen
N0.5	Nanocellulose SAP at 0.5 wt%
N1.0	Nanocellulose SAP at 1.0 wt%
Na_2SO_4	Sodium sulfate anhydrous
NaBr	Sodium bromide
NaClO	Sodium hypochlorite
NaOH	Sodium hydroxide
NFC	Nanofibrillar cellulose
NPK	Nitrogen/phosphorus/potassium
P	Phosphorus
PA	Polyacrylate
PAAm	Polyacrylamide
PALS	Processing advance lignocellulosics
PAM	Polyacrylamide
RCF	Relative centrifugal force
S0.5	Commercial SAP at 0.5 wt%
SAP	Superabsorbent polymers
SAXS	Small angle X-ray scattering
SD	Sandy soil

SDW	Shoot dry weight
SEM	Scanning electron microscopy
SFW	Shoot fresh weight
SM	Soil moisture
SW	Saline
TEMPO	2,2,6,6-tetramethylpiperidine-1-oxyl
TW	Tap water
W_{eq}	Swelling properties
WHC	Water holding capacity
WP	Water productivity
WRV	Water retention value
WUE	Water use efficiency
Zn^{2+}	Zinc
$ZnSOz_4.H_2O$	Zinc sulfate monohydrate

List of Nomenclature

%	Percentage
°	Degree
°C	Celsius
Å	Angstrom
atm	Atmosphere
cm	Centimetre
cmol	Centimol
g	Gram

G'	Storage modulus
G"	Loss modulus
h	Hour
ha	Hectare
kg	Kilogram
kg	Kilogram
kHz	Kilohertz
L	Litre
M	Molar
m^2	Square metre
m^3	Cubic metre
MPa	Megapascal
mg	Milligram
min	Minute
mL	Millilitre
mm	Millimetre
mmol	Millimole
mV	Millivolts
mV	Millivolts
MW	Molecular weight
nm	Nanometre
ppm	Parts per million
psia	Pounds per square inch absolute
rpm	Revolutions per minute

s	Seconds
w/v	Weight per volume
wt.	Weight
μg	Microgram
μm	Micrometre

THIS PAGE HAS BEEN INTENTIONALLY LEFT BLANK

CHAPTER 1:
INTRODUCTION AND
LITERATURE REVIEW

THIS PAGE HAS BEEN INTENTIONALLY LEFT BLANK

Chapter 1: Introduction and Literature Review

1.1 Introduction

It is estimated that global demand for food will require a doubling in food production by 2050 [1]. To meet this demand in a sustainable and environmentally benign way is a major challenge for the agricultural industry, especially because irrigated agriculture consumes about 70% of the water available for human use worldwide [2, 3]. Decreasing availability of water, drought and climate change significantly threaten the world's agricultural development in the coming years. According to Müller C. [4], agricultural yields are expected to decline by between 2 – 15% over the next 30 years due to the impact of climate change. Hence, new strategies are needed to optimise the efficient use of the water resources and ensure the long-term sustainability of the agricultural industry.

One possible water conservation strategy is the use of superabsorbent polymers (SAP). These are three-dimensional (3D) networks of hydrophilic polymers capable of absorbing water or fluids at hundreds of times their own weight and remain stable [5-9]. Superabsorbents have been increasingly used in many applications such as biomedical [10], food and beverages [11], personal care and hygiene products [12].

In the agricultural and horticultural industries, SAPs provide an option to prolong water availability in soils, semi-arid and arid lands and during droughts, hence allowing the plants to survive longer under water stress [13]. Superabsorbents can also increase water retention in different types of soil, significantly reducing irrigation water consumption [14]. As soil conditioners and nutrient carriers, SAPs can improve soil properties [15]; thereby, increasing crop yield [16].

Despite all these significant benefits, a major drawback that has limited the use of superabsorbents in agriculture is that most are fossil-fuel derived polymers such as polyacrylate (PA) or polyacrylamide (PAM) [13]. Once exposed to the environment and in soils, these

PA/PAM SAPs degrade very slowly into by-products, raising serious environmental concerns including the formation of microplastic particles which are not only harmful to the soil biota but also to human health [17-19]. Acrylamide-based polymers are known to have carcinogenic effects [20] and the continuous use of polyacrylate can induce occupational asthma [21]. These environmental and health issues have led to the development of SAPs derived from natural polymers such as cellulose [22], chitin [8], starch [23], guar gum [15], and pectin [24] among others[5]. Most of these SAP, however, are still produced as composites with PAM or PA, reducing their biodegradability and sustainability.

Cellulose, the most abundant biopolymer worldwide, emerges as a compelling renewable, biodegradable, non-toxic and sustainable alternative for producing SAPs. Cellulose is made of D-glucose units linked by β-1,4 glycosidic bonds. These bonds determine the structure of this polymer, linear or branched, and dictate its hydrogen bonding ability driven by the presence of an enormous amount of hydroxyl groups [10]. Hydrogen bonds enables the cellulose chains to assemble with each other in a hierarchical structure which dictates their mechanical properties and insolubility in water [25]. The H-bonds also confer cellulose its hydrophilicity and water absorption.

Nanocellulose refers to the cellulose fibres that possess dimensions in the nanometre scale [26]. Nanocellulose-based superabsorbents have been the focus of significant research in the last two decades [27-29]. Its outstanding mechanical properties, low-density, renewability and tunable porous structure make nanocellulose a promising material for a range of applications including reinforced nanocomposites [30], food packaging [31], coatings, printed electronics[26] and biomedical [10].

Nevertheless, few studies have reported the use of nanocellulose based-SAP in agriculture [32, 33]. Indeed, some reviews are available that highlights the use and nanocellulose SAPs in

agriculture [7, 27, 34]. However, these only describe the potential application of nanocellulose, considering other polysaccharides as examples. The effect of nanocellulose SAP in different agricultural soils is less well understood. No studies have engineered the physical and chemical structure of this material to suit specific agricultural needs nor related those to the effect on soil water retention properties and plant growth. This information is crucial for any use in agriculture. The effect of nanocellulose SAP on the soil microbial community and how this affects the nanocellulose longevity needs to be determined.

To address this, the main aim of this doctoral research is to engineer the physical and chemical properties of nanocellulose superabsorbents for agricultural soils and evaluate their performance in several soil types.

The first part of this thesis introduces nanocellulose superabsorbents as promising materials for agriculture. An effective and cheaper method for the production of nanocellulose SAP is presented, while improving the structure and physical properties of this material, making it more feasible and attractive for agriculture. The effect of different cations on the rheological and swelling properties of nanocellulose SAP is determined. This is of particular importance in agriculture as many cations exist in the soil environment which will impact the performance of the superabsorbent.

Following optimisation of the structure and properties, the second part of this thesis measured the effect of varying application rates of nanocellulose SAP on water retention in different soils. The ionic sensitivity of these SAP to the soil solution was measured and related to their swelling performance after several cycles. A pot trial in a greenhouse was carried out to quantify the impact that different application rates of nanocellulose superabsorbent have on the growth of tatsoi under different levels of soil moisture to simulate water stress. Based on the best application rate of nanocellulose, a follow up plant study was conducted to systematically

compare the performance of nanocellulose with that of a commercially available polyacrylamide-based superabsorbent. The effect of these SAP on the growth of spinach in different soils was then determined. Finally, the effect of varying application rates of nanocellulose SAP and fertiliser addition on the superabsorbent biodegradation was quantified and related to the soil microbial activity.

This research demonstrates how nanocellulose superabsorbents can be engineered to improve the agricultural soils properties. It also reports the future studies and functionalisation needed to further maximise the potential of these materials for agriculture.

1.2 Synthesis of nanocellulose superabsorbents

1.2.1 Nanocellulose: types and characteristics

Cellulose exists in plants, fungi, bacteria and certain animals. In plants, cellulose is arranged in an organised hierarchical structure together with other biopolymers such as hemicellulose and lignin. Individual cellulose molecules are brought together to form larger units, also known as elementary fibrils or microfibrils which have a diameter in the range of 3 – 4 nm and length in the range of 1 – 5 µm. These elementary fibrils are packed into larger units, called macrofibrils, which are then assembled into the known cellulose fibres, with diameter ranging from 20 – 50 µm (Figure 1). Two types of nanocellulose can be obtained from lignocellulosic sources: cellulose nanofibers (CNF) and cellulose nanocrystals (CNC). Each with varying dimensions and properties (Figure 2).
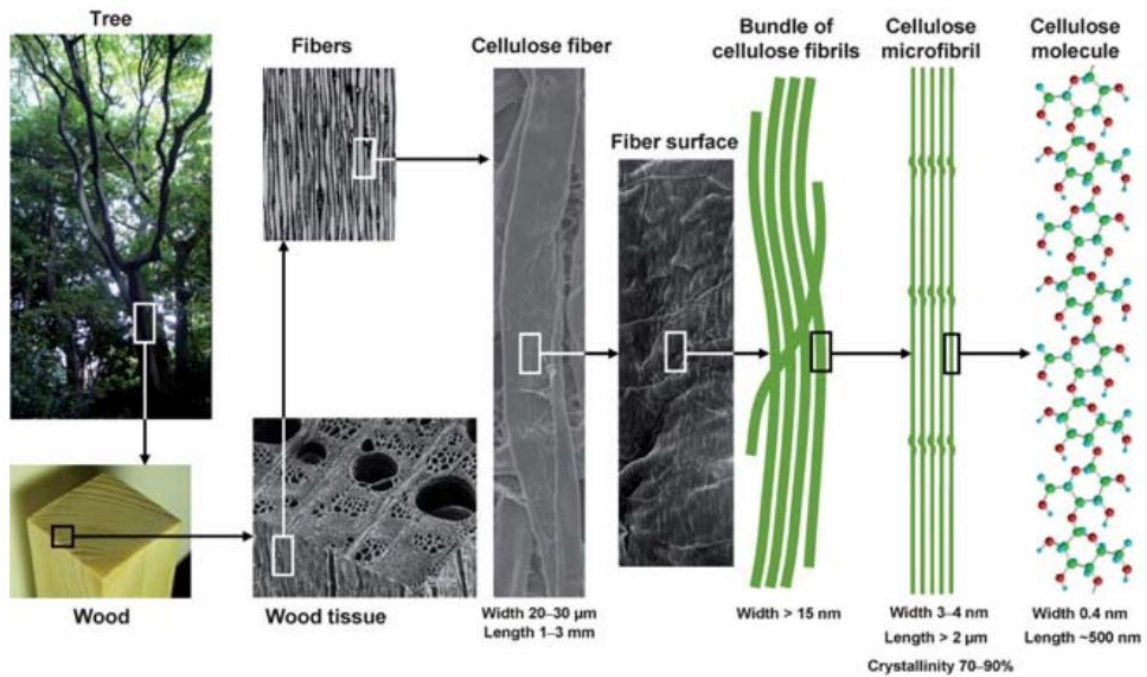
Figure 1. Hierarchical breakdown of wood biomass to cellulose molecules and their characteristic length and structure. Reproduced from [35] with permission from the Royal Society of Chemistry.

Cellulose nanofibers can be extracted from lignocellulosic by mechanical, chemical or enzymatic treatments [27, 36]. CNF sustain a large aspect ratio (length/diameter) which is due to the diameter in the range of 5-100 nm and length in the range of 1-5 micrometres [37]. CNC refers to the crystalline part extracted from the cellulose microfibers by acid, enzymatic, oxidation and ionic liquid treatments [38]. The CNC are rod like nanostructures with diameter in the range of 5-20 nm and lengths between 100-300 nm [39]. The nanoscale dimensions and surface properties of the CNF and CNC allows engineering advanced functional cellulosic materials in the forms of suspension, powder, gels [40], thin films [41, 42] and foam [43].
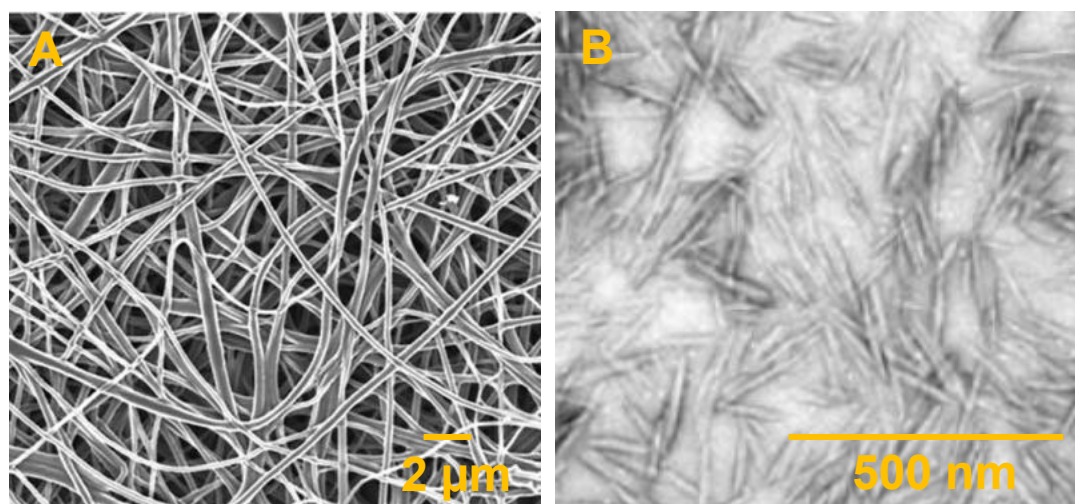
Figure 2. Scanning electron microscopy (SEM) images of (a) CNF and (b) CNC. (a) Published by the Royal Society of Chemistry [44] and (b) Reprinted with permission from [45]. Copyright 2005 American Chemical Society.

Another advantage of the nanoscale cellulose is the possibility to functional their surface with different chemical groups via physical and chemical interactions [46, 47]. The presence of a larger quantity of -OH groups at the nanocellulose fibre surfaces allows functionalising nanocellulose surface with carboxyl (COO^-) [47], azide [48] and phenolic esters [49]. The surface functional groups allow functionality of the nanocellulose for specific applications. For example, the presence of carboxyl groups in CNF is responsible for the high swelling ability in the production of superabsorbents [43]. Though high performant superabsorbents have been prepared using both CNC and CNF, only CNF allows the production of superabsorbents composed entirely from this material. This is because its unique ability to create fibre entanglement, which allows the formation of the highly porous structure needed to accommodate large quantities of water [43]. On the contrary, CNC does not form fibre entanglement nor a porous structure; and for this reason, CNC is mostly used as filler, to reinforce the structure in the production of SAP composites [50].

1.2.2 Production of nanocellulose superabsorbent

The production of superabsorbent from CNF involves two main steps: first, the preparation of a hydrogel from a dispersion; and second, removal of water [26]. The functionalisation and chemical modification of the SAP structure is mainly performed in the first step, whereas the drying technique dictates the physical structure of the SAP [51] Figure 3).
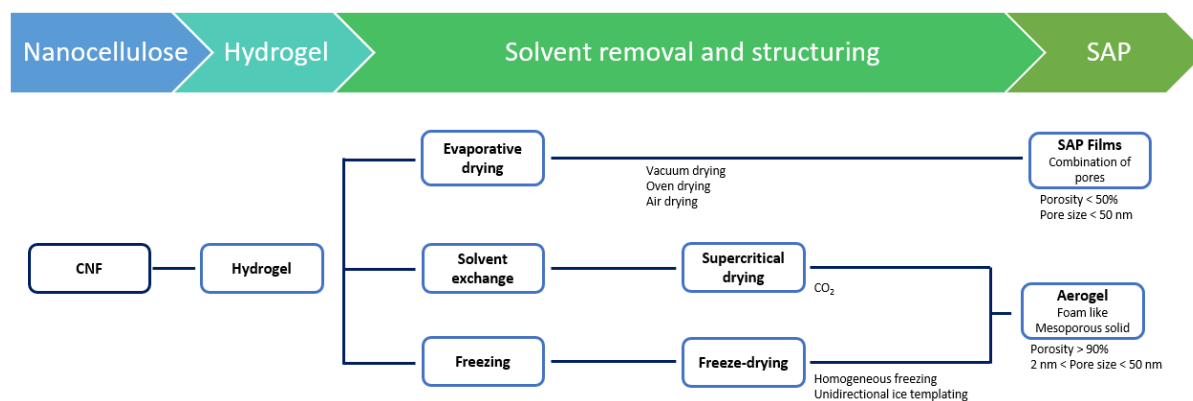
Figure 3. From nanocellulose to nanocellulose superabsorbents. Nanocellulose processing image.

1.2.2.1 Hydrogel preparation

Hydrogels are three-dimensional networks (3D) composed of hydrophilic polymers that are physically or chemically cross-linked (Figure 4). The production of CNF-based hydrogels often requires the modification of the cellulose surface to achieve suspensions with good colloidal stability. Modification of CNF can be accomplished through chemical (carboxylation [35, 43], carboxymethylation [52], quaternization [53], etc.) or enzymatic treatments [54]. Of those, the 2,2,6,6-tetramethylpiperidine-1-oxyl (TEMPO)-mediated oxidation of cellulose, developed by Isogai, et al. [35], is considered one of the most effective methods to produce nanocellulose fibres. This process selectively converts a significant proportion of the CNF surface primary alcohol groups (C6) of the cellulose glucose units into carboxylate groups (COO^-). This surface modification provides the necessary electrostatic repulsion which allows the liberation of fibres upon high shear forces or homogenisation [35], forming nanocellulose hydrogels (Figure 4).
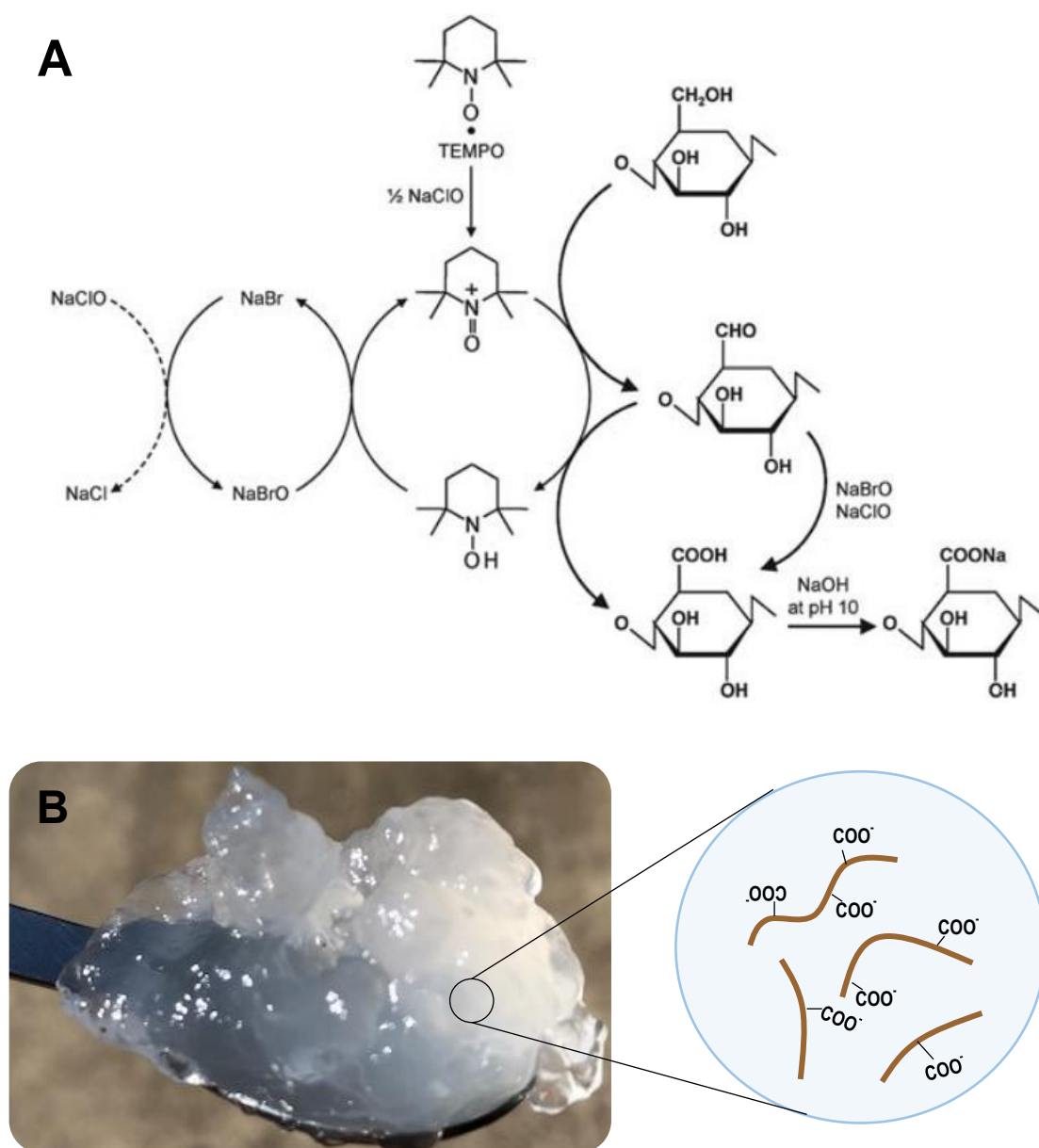
Figure 4. (a) Reaction mechanism of TEMPO-mediated oxidation of cellulose to produce CNF. Reproduced from [35] with permission from the Royal Society of Chemistry. (b) Nanocellulose hydrogel produced through TEMPO-mediated oxidation.

1.2.2.2 Material functionalisation

1.2.2.2.1 Physical cross-linking

Different to most gels that form a solution in water, nanocellulose hydrogels form a colloidal suspension [55]. This is because nanocellulose is insoluble in water, while in the constitutive polymer in other gels is water soluble. Because of this, nanocellulose hydrogels network is due to an entanglement of fibres that are physically cross-linked by electrostatic forces. This structure can be further strengthened by chemical cross-linking [8]. In physical cross-linking, interacting forces such as hydrogen bonding, electrostatic, van der Waals, chain entanglements, ionic and hydrophobic interactions dominate [56]. Physically crosslinked hydrogels and SAPs are not as stable as chemically crosslinked SAPs. The crosslinking strength will depend on pH, temperature and concentration [57].

Physical cross-linking via hydrogen bonding between carboxyl groups can be achieved by freeze-thaw technique. The polymer concentration is increased upon crystallisation of bulk solvent which forces polymer chains to align and form a joined network held by hydrogen bonding and covalent interaction. An increase in the freeze-thaw cycle affects the hydrogel properties, for example, reduction of porosity [58]. High strength PVA hydrogels were made by this technique where the strength came from intra and intermolecular hydrogen bonds [59]. Metal ions can be nucleated and grow on CNF network where there is metal -carboxylate strong interactions between polymer chains and metal ions [60, 61]. Multivalent metal ions (Ca^{2+}, Zn^{2+}, Al^{3+} and Ce^{3+}) were introduced to CNF reinforced polyacrylamide to form ionic interaction with CNF [62]. The ion valency also influences the degree of fibrillation of CNF hydrogels upon mechanical treatment, changing the rheological and swelling properties of the hydrogel and SAP [63]. This is relevant to evaluate the SAP application in soils, considering that the soil water environment contains a mixture of soluble salts.

Fibre entangled cellulose hydrogels and SAP can be formed by introducing electrostatic repulsive COO⁻ groups on cellulose fibre followed by mechanical treatment at a certain fibre concentration [64]. These hydrogels showed dependency on salt and pH as polymer matrix bound water is affected by salt concentration and system pH [65]. In another study, biohybrid hydrogels made from carboxylated cellulose and chitin nanofiber were formed due to the electrostatic repulsion and hydrogen bonding between the negatively charged nanofiber and positively charged chitin nanofiber [66].

Crosslinking by hydrophobic interaction can be formed by introducing hydrophobic groups on cellulose chains. Methyl cellulose can be incorporated as hydrophobic end, showing a thermo responsive behaviour due to hydrophobic interaction of methyl groups and hydroxyl groups upon heating above a specific temperature [67, 68]. The thermal sensitivity is dependent on the relative content of the hydrophilic and hydrophobic groups in the polymer [69].

1.2.2.2.2 Chemical cross-linking

In chemical crosslinking, the polymer chains are linked together by covalent bonding. This type of cross-linking is stronger and permanent. Chemical cross-linking can be achieved by the following ways: (i) using an introduced crosslinker, (ii) reaction between functional groups of polymers, (iii) using photosensitive agents, or, (iv) initiation with enzymes [70, 71].

Different crosslinkers have been studied to produce strong hydrogels with tunable properties. These include: epichlorohydrin (ECH) [72], N, N' methylenebisacrylamide (MBA) [72-74], malic acid, fumaric acid, glutaraldehyde, citric acid, glycidyl ether epoxy compounds [75] and many others [76, 77]. Among them, citric acid is gaining in popularity due to its nontoxicity, inexpensive, hydrophilic and safe nature [58]. Demitri, et al. [78] produced citric acid crosslinked cellulose hydrogel for agricultural use. There are some recent reports on dual crosslinking combining both ionic and covalent bonding. This type of crosslinking is used to

prepare SAP with very high mechanical strength, controlled degradation rate, self-healing and antibacterial properties [79, 80].

Photosensitive groups can be incorporated into a polymer enabling crosslinking under irradiation such as UV light. Chitosan with an incorporated photosensitive azide group formed hydrogel after exposure to UV light. UV radiated crosslinking can also be formed between two polymer chains by introducing photosensitive agents on both polymers. This crosslinked material can release encapsulated growth hormone in a control rate [81].

The preparation method dictates the hydrogel structure and final properties such as mechanical and rheological properties, absorption capacity, porosity and many others. Therefore, understanding the intended application and requirements is vital in choosing the most appropriate method for preparing nanocellulose hydrogels.

1.2.2.3 Removal of water

A major challenge in the production of nanocellulose superabsorbents is to maintain their porous structure during water removal after the hydrogel has been formed. Different drying processes have been evaluated to remove water from hydrogels including supercritical drying, freeze-drying and oven-drying. In supercritical drying preceded by solvent exchange, the pressure and temperature of the hydrogel are raised above the critical point of the solvent employed. Carbon dioxide (CO_2) is the commonly used solvent due to its easily accessible critical temperature and pressure of 31.3 °C and 7.4 MPa, respectively. Because of this, the surface tension and the capillary pressure disappears, conserving the mesoporous structure of the nanocellulose. Though this technique is considered to be the perfect method of drying gels, supercritical drying is not widely used, mostly because of the complexity of the process and the expensive equipment required [26, 82].

Freeze-drying is the preferred method for preparation of highly-porous, ultralow-density solid gels with high water absorption at laboratory scale [26, 82]. Freezing followed by ice sublimation avoids the formation of capillary pressure, conserving the structure of the original dispersion. However, freeze-drying is difficult to perform on a large-scale and is expensive [82]. It also produces ultra-low density superabsorbents [43], which can be difficult to apply in the field.

Oven-drying has also been studied to prepare SAP [83]. This process is generally less desirable as cellulosic fibres tend to aggregate during oven-drying, referred to as hornification [84]. Aggregation of fibres closes the pores of the material, decreasing its absorption capacity, and surface area [85]. However, fibre agglomeration can be minimised if low temperatures are employed. Beaumont, et al. [85] showed that cellulose-based gels oven-dried at 60 °C had better colloidal stability and higher water retention than freeze-dried gels. This was due to the low process temperatures and hydrogel additives, such as carboxylmethylcellulose (CMC) that reduced the hornification effect. Introducing high-density anionic charges such as carboxylate groups or preparing hydrogels at high pH can also prevent fibre agglomeration by electrostatic stabilisation [29, 86].

1.3 Superabsorbent properties for agriculture

1.3.1 Swelling

One of the most important properties of nanocellulose-based superabsorbents for agriculture is their high swelling ability. This will determine the capacity of the SAP to effectively hold and release water and nutrients to the soil environment. The swelling of this material is attributed to the high concentration of carboxylate (COO^-) groups enabling hydrogen bonding with water molecules. The swelling mechanism is governed by the nature of and mobility of ions between the interior of the superabsorbent and the exterior solution, also known as counter-ion entropy,

resulting in a differential in osmotic pressure [87]. The fibre surface charge, also measured as the degree of substitution (DS), also plays an important role in the swelling ability as it dictates the number of participating carboxylate groups able to bind with water [43, 47]. The absorption performance and the swelling rate can be engineered by changing the drying method, process variables and the nature of cations incorporated to balance the surface charge [43, 51, 63]. Mendoza, et al. [43] found that the absorption capacity of freeze-dried nanocellulose SAP can be manipulated by the amount of nanocellulose fibres. Superabsorbents with higher amounts of fibres (1 wt% compared to 0.3 − 0.5wt%) absorbed less water due to a narrower pore distribution which limited the availability of carboxylate groups.

The ionic strength and the pH of the external solution can also influence the swelling behaviour of the superabsorbent [27, 88]. Both elements are of particular importance for agricultural applications because of the numerous amounts of natural exchangeable cations present in the soil and the variability in soil pH. In general, increasing the concentration of salt results in a decrease in swelling [88-90]. This is attributed to the charge screening effect of the carboxylate group that decreases the electrostatic repulsion forces [88]. This leads to a decrease in the osmotic pressure difference, resulting in a decrease in swelling [29]. A decrease in repulsive forces is also observed under acidic conditions, where the low pH enables the protonation of carboxylate groups, resulting in charge neutrality [90]. The ion valency also has an effect on the swelling performance [63]. Spagnol, et al. [91] studied the effect of the ion valency on the swelling of a superabsorbent composite made of CNF and chitosan-graft-poly(acrylic acid). They reported a decrease in the SAP swelling with increasing ion valency in the order of monovalent > divalent > trivalent. This is because the higher the cation charges, the higher the degree of cross-linking. Multivalent ions can not only form additional inter- and intramolecular complexes with the carboxylate groups in the SAP, but are also able to neutralise several charges inside the polymer network, resulting in a decrease in swelling (Figure 5).
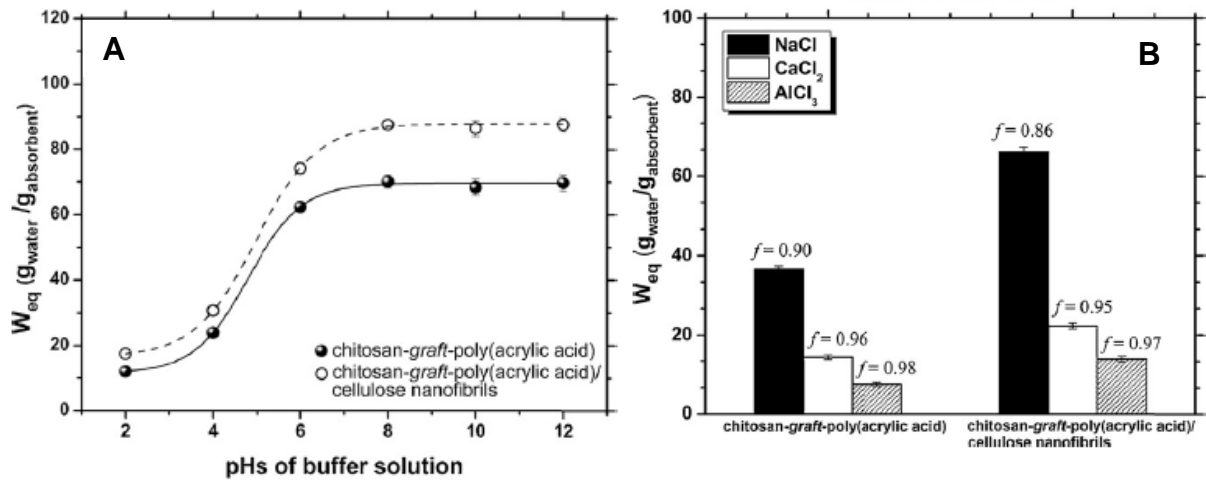
Figure 5. (a) Effect of pH on the swelling properties (W$_{eq}$) of chitosan-graft-poly(acrylic acid) and chitosan-graft-poly(acrylic acid)/cellulose nanofibrils hydrogel composite reinforced with cellulose nanofibrils. (b) Weq of chitosan-graft-poly(acrylic acid) and chitosan-graft-poly(acrylic acid)/cellulose nanofibrils hydrogel composites in aqueous solutions with different salts (conc. equal to 0.15 mg L−1). Both images are from [91]. [1]The salt sensitivity factor, f, determines the ionic sensitivity of the SAP to the salt solution, and is calculated as:

$$f = 1 - \frac{W_{saline}}{W_{water}}.$$ Here, W$_{saline}$ is the swelling of the SAP in saline and W$_{water}$ is that in water.

The chemical composition of the cellulose-based SAP greatly influences the swelling capacity of these polymers. As previously discussed, the swelling is due to the presence of hydrophilic groups such as COO$^-$ in the superabsorbent network. Increasing the amount of available hydrophilic groups results in an increase in swelling. This can be achieved, for example, by grafting the cellulose units onto polyacrylamides or polyacrylates. Suo, et al. [92] reported that the swelling of CMC-based SAP increased from about 100 to 900 g water/g SAP when acrylic acid and acrylamide monomers were introduced. The extent of cross-linking also affects the swelling as it dictates the number of available hydrophilic groups participating in hydrogen bonding with water [22].

1.3.2 Phytotoxicity

The absence of phytotoxicity is the first requirement of superabsorbents to allow their safe application involving plants. Early stage seedling growth and seed germination bioassays are generally used for determining toxicity effects in plants. Studies have evaluated the levels of phytotoxicity of nanocellulosic materials with positive results. Zhang, et al. [33] reported that nanocellulose-based hydrogels could be beneficial for seed germination and plant growth. These hydrogels also exhibited antifungal activity during the breeding and growth of sesame seeds (Figure 6). Barajas-Ledesma, et al. [51] conducted a germination experiment of radish and cress seeds grown nanocellulose SAP. Both, the germination index and mean time to germination of both species treated with SAP was similar to the control. Similar germination studies have been conducted in other cellulose-based SAP such as CMC and hydroxyethylcellulose (HEC), all showing positive effects [93].
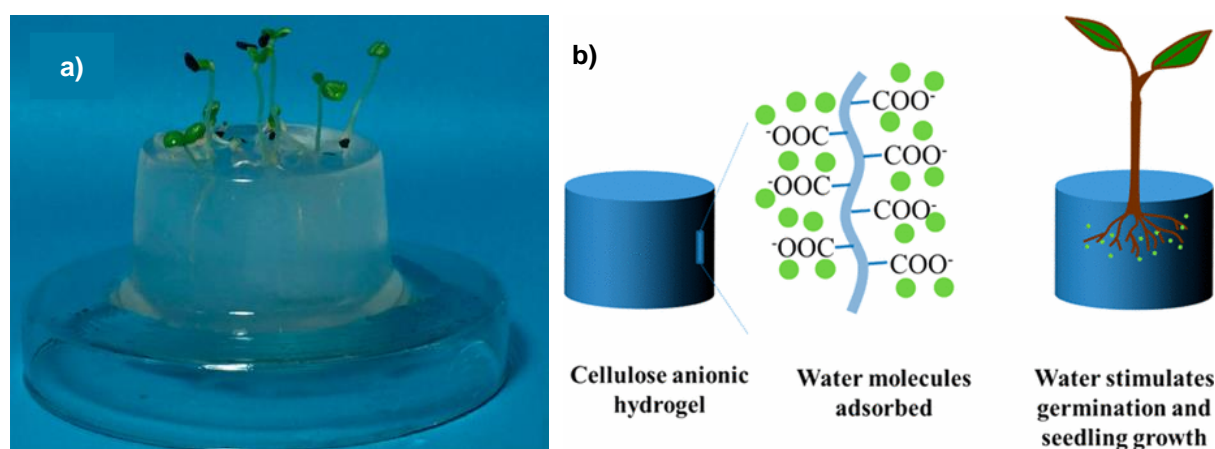
Figure 6. (a) Sesame seeds grown on the surface of a cellulose nanofiber hydrogel after 7 days. (b) Mechanism of seed germination and seedling growth. Both images reprinted with permission [33]. Copyright 2017. American Chemical Society.

1.3.3 Biodegradability

The low biodegradability of fossil-fuel derived superabsorbents has hindered their use in the agricultural field. From this perspective, cellulose is a natural polymer composed of glucose

molecules, and the easily accessible carbon (C) is a source of food for microorganisms. Studies suggest that cellulose, as it is, can be fully degraded over a period of between 16 – 30 days [94, 95]. The biodegradability of cellulose-based materials such as films has also been studied through several techniques. Vikman, et al. [96] investigated the degradation of nanofibrillar cellulose (NFC) films under controlled composting conditions. These films were completely degraded after 3 weeks of composting. In a different protocol, Kono and Fujita [97] tested the degradability of cellulose SAP cross-linked with 1,2,3,4-butanetetracarboxylic dianhydride (BTCA) by enzymatic degradation. The rate of biodegradation was dependent on the concentration of BTCA, where around 95% of the superabsorbent with low molar feed ratios of BTCA (around 0.5) remained after 7 days of exposure compared to 11% when this molar feed ratio was increased to 7.5 BTCA. For TEMPO-oxidised nanocellulose, Homma, et al. [98] reported that the degradation rate is also affected by the type of counter-ion present in the cellulose fibres and films. After treatment with crude cellulase, the authors found that the counter-ion degradation behaviour follows the order of $Na^+ \approx NH_4^+ \approx K^+ \approx Cs^+ \gg Ca^{2+} > H^+ > Cu^{2+}$. A similar trend was observed using soil burial tests (Figure 7). The biodegradation of cellulose is also influenced by the soil type and environmental conditions (temperature and moisture) [94, 95, 99].
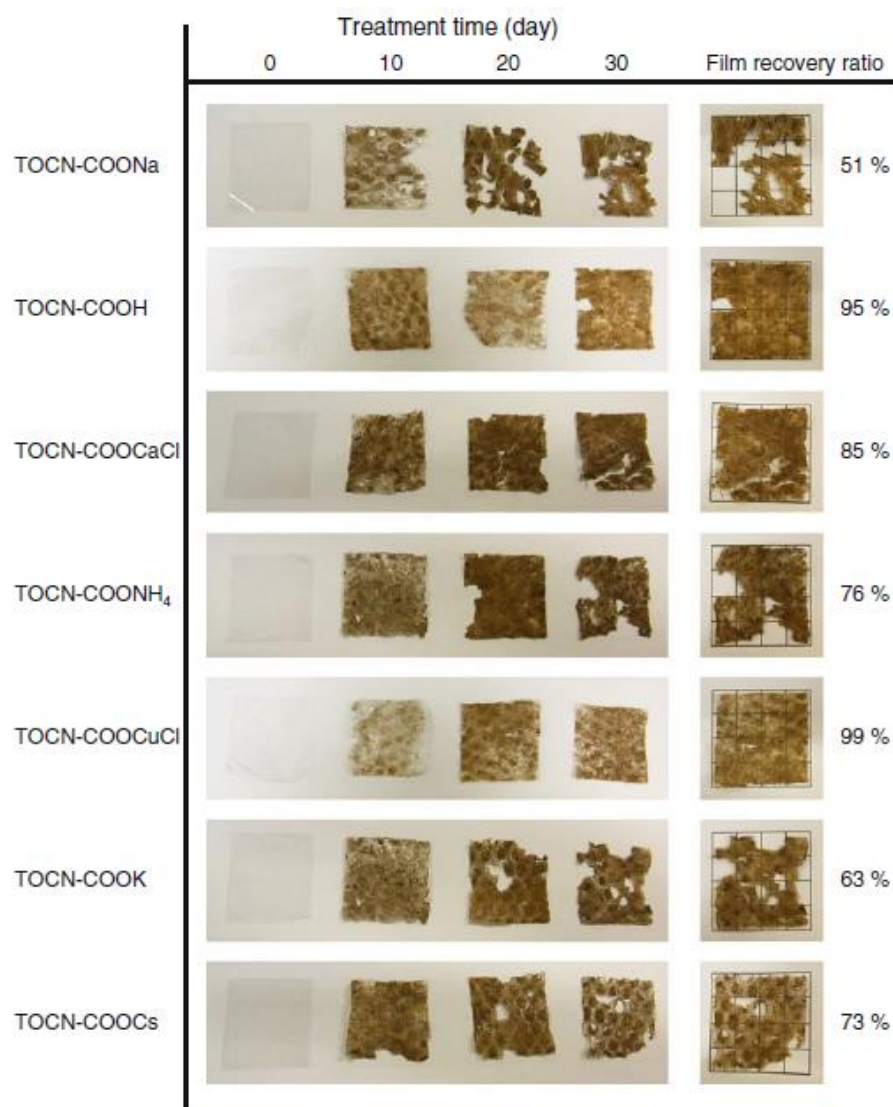
Figure 7. Morphological changes and recovery ratios of TEMPO-oxidised nanocellulose films after soil burial for 0–30 days. Reprinted with permission from Springer. Copyright (2013) [98].

1.4 Agricultural applications of nanocellulose

1.4.1 Water retention agent

One of the most common applications of superabsorbents is as a water retention agent. The addition of cellulose-based superabsorbents to soils has improved soil physical properties such as bulk density, porosity, soil permeability, water retention or water holding capacity, among others [100-102]. Each of these indirectly affect plant growth. An increase in soil porosity leads

to an enhancement in the rate of seedling emergence and seed germination, root growth and density, and soil compaction, reducing soil erosion. Most importantly, it also improves soil aeration, increasing oxygen availability in the root zone of plants and soil microbial activity [15, 23, 93, 102, 103].

SAPs act as 'water reservoirs' in the soil, increasing soil water retention for long periods of time (Figure 8a). This effect was observed by Sawut, et al. [104] who reported that even small additions of 0.8 g of cellulose-based SAP per 200 g of soil could hold soil moisture for up to 30 days compared to 11 days in soil without SAP. Increasing soil water retention not only reduces irrigation water consumption, but also prolongs plant survival for longer periods, delaying the onset of permanent wilting point. Demitri, et al. [22] noticed a controlled and sustained release of water in superabsorbents developed from carboxymethylcellulose (CMC) cross-linked with hydroxyethylcellulose (HEC) which delayed the onset of the permanent wilting point in tomato plants. These plants withered after 22 days of the last irrigation compared to 9 days for plants in soil that did not have SAP. The magnitude of these effects depends, among other factors such as SAP longevity and soil type, on the application rate of the superabsorbent to soils, where, in general, between 0.2 – 2wt% of SAP is applied [105].

Plants are highly sensitive to water stress. Water stress or drought is one of the most important limiting factors that affect plant growth and crop productivity, especially when this occurs at critical growth-stages of a cultivated crop [106]. The addition of cellulose-based SAP to arid or sandy soils (soils with low water retention) has ameliorated the impact of drought in the growth of plants [107]. Montesano, et al. [93] evaluated the effect of water stress in the growth of cucumber plants in sandy soils amended with and without a superabsorbent based on CMC crosslinked with HEC. The authors reported an increase in the fresh weight of plants grown in treatments amended with a superabsorbent which almost doubled compared to that in treatments without SAP. A similar response was observed in other plant parameters such as

leaf fresh biomass, fruit fresh weight and stem fresh weight, among others. In the same way, studies have found that cellulose-based SAP can also promote seed germination in soils with limited water availability. Sánchez - Orozco, et al. [108] noticed that the seedling growth of beans and pumpkins increased with increasing concentrations of a cellulose-based SAP derived from used disposable diapers.

One of the limitations of cellulose-based SAP is that the absorption capacity decreases with increasing number of hydration and dehydration cycles [109] (Figure 8b). This is attributed to a blockage of the active negative sites (e.g. carboxylate groups) of the polymer by the metal ions in the soil that are released in water [110]. This effect was reported by Spagnol, et al. [111], who found an increase formation in crosslinking density by physical interaction of multivalent cations (e.g. Mg^{2+} and Ca^{2+}) with the carboxylate groups of poly(acrylamide-co-acrylate)-based superabsorbents and cellulose nanowhiskers. SAP biodegradation also contributes to the decrease in the swelling performance [93].
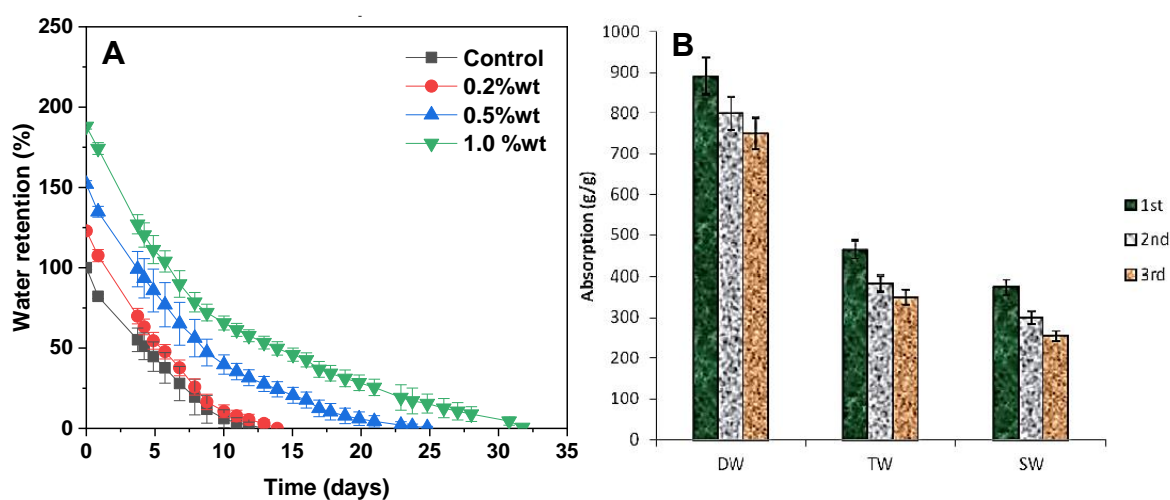
Figure 8. (a) Effect of nanocellulose superabsorbent concentrations on soil water retention with time. (b) SAP absorption in deionised water (DW), tap water (TW) and saline (SW) after the 1st, 2nd and 3rd cycle. Reprinted with permission from MDPI. Copyright (2012) [110].

1.4.2 Carrier for agrochemicals

With a rapidly increasing world population, modern agriculture largely depends on the use of agrochemicals, such as fertilisers, herbicides and fungicides, to supply the growing demand for food. However, studies suggest that only a small proportion of the fertiliser applied to soils is actually used by the plants [112, 113]. Also, agrochemical addition is often inconsistent with the plant needs, as 40 to 70% of the total applied fertiliser is lost to the environment, leading to a loss of valuable resources; more importantly, this loss pollutes the environment [113]. For these reasons, slow release fertilisers have been developed to control the release of nutrients to the soil according to plant demand.

Controlled nutrient release using superabsorbent polymers has been widely studied. The application of cellulose-based SAP to deliver agrochemicals to soils has increased plant growth and crop yield compared to those amended with fertilisers only [114-116]. Essawy, et al. [117] reported that nutrients loaded into SAPs fabricated by grafting polymerisation of acrylic acid and chitosan with cellulose, can take up to 60 days to be released in soils compared to only 5 days without SAP. In general, two approaches are used to load the superabsorbent with agrochemicals. The first one is *in-situ* loading of additives during the preparation of the superabsorbent. This is performed either by chemically cross-linking the SAP with the mineral nutrient, entrapping and bonding the fertiliser molecules onto the structure of the superabsorbent [118, 119], or by forming the superabsorbent in a solution containing the desired nutrient dissolved in [115]. Because the *in-situ* loading involves chemical modification of the SAP, which permanently bonds the mineral nutrients to the SAP structure, only a fraction of the loaded agrochemical is actually released, leaving the rest attached to the polymer network and not accessible to plants [120] (Figure 9a).

The second approach involves loading the superabsorbent with agrochemicals after superabsorbent preparation. This is accomplished by swelling the superabsorbent in a solution

containing the active substance, which diffuses into the SAP structure to absorb or be entrapped. The loading efficiency is related to the osmotic pressure differential and the physical-chemical affinity of the agrochemical for the SAP polymer chains [5] (Figure 9b). In the *post*-loading approach, the agrochemical loading efficiency correlates directly to their concentration in the loading solution, where the efficiency increases with increasing concentration in the loading solution. This is because of an increase in nutrient diffusion from the outside to the inside of the polymer network [121, 122]. The release of agrochemicals to the soil medium increases with increasing loading efficiency. This is because higher loading leads to a faster movement of solvent molecules penetrating the surface of the superabsorbent [121-123]. In general, the *in-situ* approach is preferred over the *post*-loading because of the greater loading efficiency [5].
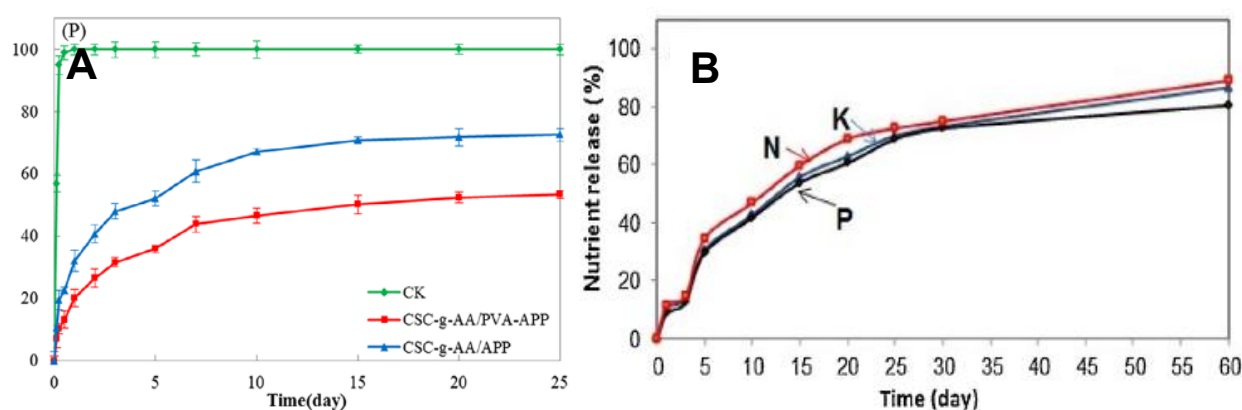
Figure 9. (a) Release behaviour of phosphorus in soil from the control (CK) and cellulose modified superabsorbents. Reprinted with permission from Wiley. Copyright (2020) [120]. (b) Release behaviours of nitrogen, potassium and phosphorus in soil from a cellulose-based superabsorbent polymer formed via graft polymerization of acrylic acid from chitosan-cellulose hybrid. Reprinted with permission from Elsevier. Copyright (2016) [117].

Coating agrochemicals with layers of superabsorbent and other materials such as ethylcellulose, carboxymethylcellulose or hydroxyethylcellulose is another physical method

that was developed for slow-release fertilisers [124-126]. This technique also provides a long release time of approximately 30 days. However, the water retention capability of these materials is lower than that of the other methods and concerns arise regarding the low degradation of the coating materials which remain in the soil after the agrochemicals are released, thus creating an environmental issue[127].

The use of clays in the formulation of superabsorbents has improved the SAP ability to load agrochemicals, as well as delayed their release to the medium [128]. Bortolin, et al. [129] synthetised superabsorbents from methylcellulose (MC), polyacrylamide (PAAm) and montmorillonite (MMt). SAPs were loaded with different formulations of urea and the controlled release was determined. The presence of MMt favoured the slow release kinetics of urea, releasing larger amounts of nutrient at a rate about 200 times slower than pure urea. These results agree with those of Bauli, et al. [32], also reporting that adding different types of clays as "fillers" reduced the release rate of NPK fertiliser encapsulated in CMC-based superabsorbents.

1.5 Perspectives

Nanocellulose superabsorbents are a new class of biodegradable, renewable, engineerable and non-toxic materials. Simple methods such as TEMPO-mediated oxidation followed by mechanical treatment can be used to modify the nanocellulose chemical structure, producing superabsorbents with exceptional swelling properties. Their structure can be further functionalised via physical or chemical cross-linking to enhance their properties for agricultural use. Nanocellulose SAP has the ideal attributes for many applications in agriculture including as water retention agents and carrier for agrochemicals. Though several studies have reported the remarkable properties of nanocellulose, literature has been restricted to other applications of this material such as food packaging or biomedical uses. Few studies have reported the use

of nanocellulose in agriculture. These have targeted its synthesis and functionalisation, demonstrating only with germination studies that these materials could have application in agriculture. Therefore, more research efforts are required to measure and fully understand the effect of nanocellulose in agricultural soils and plant growth. The potential areas to explore have been described in this review and will be summarised as gaps in knowledge in the next section.

1.6 Gaps in knowledge

First and foremost, the literature review identified that few studies have reported the use of nanocellulose, specifically cellulose nanofibres (CNF), in agriculture. Previous research has focussed on the early stage development and synthesis of CNF-based superabsorbents, using germination and seedling growth studies to demonstrate that these materials could have application in agriculture. This creates several significant gaps in knowledge that have limited the application of nanocellulose superabsorbents in agriculture. The most critical to address in specific are:

1. Most studies have focussed on the chemical functionalisation of the superabsorbent by cross-linking in the preparation of the nanocellulose hydrogel, employing freeze-drying as the most common method to produce superabsorbents. This type of drying significantly reduces the application range of these materials for agriculture, as freeze-drying is not only expensive, but also difficult to perform on a large-scale. The effect of different drying techniques on the structure and swelling properties of SAP has not been established.

2. The chemical structure of nanocellulose SAP also needs to be optimised for specific applications in agriculture. Superabsorbents produced through TEMPO-mediated oxidation result in sodium cations remaining in the cellulose fibre network. Adding

sodium to soils can have adverse effects on the soil structure and water availability, imposing a stress on growing crops and decreasing crop yield. The exchange of the cation with others can tailor this material to function not only as a superabsorbent, but also as a nutrient carrier for plants. In addition, understanding the effect that different cations have on the superabsorbent properties is essential for applications in agricultural soils, where there is a natural mixture of exchangeable cations including Ca^{2+}, Mg^{2+}, K^+ and Na^+.

3. The effect of nanocellulose SAPs in agricultural soils has not been evaluated in any detail. Their potential to increase water retention in different soils, its performance after several cycles and how this performance is affected by the longevity and properties of the nanocellulose remains poorly understood. There is a limited understanding of the relationship between soil microbial activity and nanocellulose biodegradation.

4. Most importantly, the impact of nanocellulose-based SAP on plant growth is not well understood, especially under water stress conditions and different levels of plant nutrient availability (i.e. fertilisers). Though some studies have analysed the effect of cellulose-based SAP on the growth of plants, these have been limited to the use of other cellulose derivatives such as carboxymethylcellulose and hydroxyethyl cellulose. A few studies have considered superabsorbents containing nanocellulose; however, these have measured other variables such as phytotoxicity or controlled release of nutrients. None have quantified the effects of varying applications of nanocellulose SAP on soil properties, plant growth and associated nutrient availability through fertilisers.

5. Lastly, there is limited literature about the performance and longevity of nanocellulose SAP depending on the soil type. Soils vary greatly in texture (the

proportions of sand, silt and clay), physical properties (porosity, bulk density), cation exchange capacity (available Ca^{2+}, K^+, Mg^{2+}), organic matter, microbial activity, total soluble salts and pH. Each of these conditions will significantly impact the absorption capacity and biodegradation of nanocellulose SAP. To maximise the SAP benefits for agriculture, it is essential to measure the effect of the superabsorbent in different soils and plants. An understanding of the impact of the microbial community, which changes from soil to soil, is very important as the effectiveness of the superabsorbent will be limited by the rate of biodegradation.

1.7 Research Hypothesis

The research hypothesis that this thesis aims to validate is that nanocellulose superabsorbents produced specifically from the TEMPO-mediated oxidation of cellulose can act as an effective water retention agent in agricultural soils.

1.8 Research Objectives

The research hypothesis is tested by addressing several key aims. The first aim is to optimise the production of nanocellulose superabsorbents for application as soil conditioners in agriculture, and to understand how the nanocellulose structure can be engineered to suit the agricultural needs. The second aim is to evaluate the effect of nanocellulose SAP in two different soils and with selected plants; and how this affects superabsorbent biodegradation.

The specific research objectives are:

1. To engineer and fully characterise novel and cheaper nanocellulose superabsorbents by controlling the drying rate, given by different drying techniques, with appropriate structure and properties for applications in soil

2. To determine the effect of the nanocellulose cation on the gelation mechanism and superabsorbent structure and properties by exchanging the current Na^+ ions present

in the nanocellulose network for different ions such as Mg^{2+}, NH_4^+ and K^+. These will provide a basis in understanding how the superabsorbent behaves in the soil environment where a range of such cations exist.

3. To demonstrate the suitability of nanocellulose SAPs to increase soil water retention; and to measure the biodegradation of these SAPs and determine their relationship to the microbial activity.

4. To quantify the effect of different applications of nanocellulose SAP on plants grown under water stress, and to compare the performance of this superabsorbent with one commercially available based on polyacrylamide.

5. To measure the effect of different soils on water retention of the nanocellulose and how this affects plant growth, and to determine the relationship between soil microbial activity and nanocellulose biodegradation.

1.9 Thesis outline

This thesis consists of five experimental chapters of which three are already published and two are under review. All published manuscripts have been reformatted to keep a consistent presentation whilst the content remains unchanged. The original publications and/or submitted manuscripts are provided in Appendix II.

A chapter-by-chapter outline based on the research objectives, the conducted research studies and the outcomes are presented:

- **Chapter 1: Introduction and literature review.**

This chapter provides a revision of our understanding and the current state-of-art knowledge of nanocellulose superabsorbents for applications in agriculture. The available technologies to produce nanocellulose SAPs, and how the properties of nanocellulose can be engineered for a range of applications are discussed. Special consideration is given for

applications as a soil conditioner and carrier for agrochemicals. This chapter also outlines

the existing opportunities for research and future development.

- **Chapter 2. Engineering nanocellulose superabsorbents by controlling the drying rate**

BARAJAS-LEDESMA, R.; PATTI, A.; WONG, V.; RAGHUWANSHI, V.; GARNIER, G. Engineering nanocellulose superabsorbents by controlling the drying rate. Colloids and Surfaces A: Physicochemical and Engineering Aspects, vol. 600, p. 124943, doi: https://doi.org/10.1016/j.colsurfa.2020.124943

Impact factor: 3.990

The first step in developing the nanocellulose SAP was to determine the relationship

between the absorption performance and the SAP structure, and how this structure can be

engineered by controlling the rate of water removal (drying rate). In chapter 2, TEMPO-

oxidised nanocellulose superabsorbents were prepared using five different drying

techniques, each providing a distinct drying rate: freeze-drying, vacuum-drying, air-drying

and oven-drying at high and low temperatures. The absorption capacity in deionised water

was measured as a function of time and the swelling kinetics was determined, modelled

and related to the superabsorbent structure. The morphology and physical structure of the

superabsorbents were fully characterised using mercury porosimetry, scanning electron

microscopy (SEM) and small angle X-ray scattering (SAXS). By conducting phytotoxicity

tests, this chapter introduced the potential of nanocellulose SAP for agriculture.

- **Chapter 3. Effect of the counter-ion on nanocellulose hydrogels and their superabsorbent structure and properties**

BARAJAS-LEDESMA, R.; HOSSAIN, L.; WONG, V.; PATTI, A.; GARNIER, G. Effect of the counter-ion on nanocellulose hydrogels and their superabsorbent structure and properties. Journal of Colloid and Interface Science, vol. 599, pp. 140-148, doi: https://doi.org/10.1016/j.jcis.2021.04.065.

Impact factor: 7.489

Once the physical structure of the nanocellulose SAP had been optimised, the next step was

to measure the effect of different cations on the swelling performance of nanocellulose.

This is critical for applications in soil and other possible applications in agricultural sectors, considering the numerous amount of natural exchangeable cations that exist in the soil that will affect the SAP absorption capacity. Therefore, Chapter 3 determined the effect of multivalent ions on the gel stability and the superabsorbent properties. Four ions of valency one: H^+, K^+, Na^+ and NH_4^+, and three ions of valency two, Ca^{2+}, Mg^{2+} and Zn^{2+} were tested. The rheology of the hydrogels was characterised and related to the ion valency. The superabsorption performance was measured and linked to the pore properties and the degree of fibrillation, controlled by the type of ion.

- **Chapter 4. Carboxylated nanocellulose superabsorbent: biodegradation and soil water retention properties**

BARAJAS-LEDESMA, R.; WONG, V.; LITTLE, K.; PATTI, A.; GARNIER, G. Carboxylated nanocellulose superabsorbent: biodegradation and soil water retention properties. (Manuscript under review by Journal of Applied Polymer Science).

Impact factor: 2.52

Following the optimisation of the physical properties and chemical structure of nanocellulose SAPs, the next step was to evaluate their performance in soil, as one of the main applications in agriculture is as soil conditioners. Chapter 4 outlines a series of incubation experiments of soil treated with three nanocellulose superabsorbents: freeze-dried and oven-dried at low and high temperatures. The absorption capacity in soil water extracts was measured as a function of time and compared to that in deionised water. The sensitivity of each type of superabsorbent to ionic strength was determined. Soil treatments were amended with different application rates of these superabsorbents and the effects on water retention capacity, microbial community and superabsorbent biodegradation were quantified.

- **Chapter 5. Effect of Nanocellulose-based superabsorbent on the early stage growth of tatsoi (*Brassica rapa narinosa*)**

BARAJAS-LEDESMA, R.; WONG, V.; LITTLE, K.; GARNIER, G; PATTI, A. Effect of Nanocellulose-based superabsorbent on the early stage growth of tatsoi (Manuscript under review by ACS Agricultural Science and Technology).

Impact factor: not available

Throughout the soil incubation studies, it was determined that nanocellulose SAP at 50 °C was the performing material to retain soil water and retained soil water for longer periods of time. Thus, this superabsorbent was considered to move forward into the next stage: the interaction of nanocellulose SAP with plants. Chapter 5 evaluates the effect of different application rates of superabsorbent on the growth of tatsoi under water stress conditions. A pot trial was carried out in a greenhouse where plants were grown in soils treated with two application rates of nanocellulose SAP: 0.5 and 1wt.% and at three levels of soil moisture: 70, 40 and 20%. Total irrigation and water use efficiency were measured. Plant biomass was quantified and correlated to the SAP application rate. All of these parameters were used to determine the best application rate of nanocellulose SAP to soils. Results were compared to soils amended with a commercially available anionic polyacrylamide-based SAP.

- **Chapter 6. Biodegradation of nanocellulose superabsorbent and its effect on the growth of spinach**

BARAJAS-LEDESMA, R.; WONG, V.; LITTLE, K.; GARNIER, G; PATTI, A. Biodegradation of nanocellulose superabsorbent and its effect on the growth of spinach. (Manuscript under review by ACS Agricultural Science and Technology).

Impact factor: not available

Thus far, each investigation has contributed to a process level of understanding of the use of nanocellulose SAP for agricultural soils and how these superabsorbents can be engineered to maximise their feasibility and performance. These findings, however, are

dependent on the soil type. Soils vary greatly in texture (the proportions of sand, silt and clay), physical properties (porosity, bulk density), and chemical properties such as cation exchange capacity (available Ca^{2+}, K^+, Mg^{2+}), and pHEach of these conditions will significantly impact the performance of the superabsorbent. Therefore, Chapter 6 describes the performance of nanocellulose SAP in two different soils: a sandy soil and a clay loam soil. A pot trial whereby spinach plants are grown in these two soils treated with one application rate of nanocellulose was conducted. The effect of the superabsorbent on the soil porosity, soil water retention, water usage and plant yield was measured. The nanocellulose biodegradation was quantified and related to the soil type and soil microbial activity.

- **Chapter 7. Conclusion and perspectives**

Chapter 7 brings together the overall findings and new knowledge that has been developed through this thesis. The perspective for the application of nanocellulose superabsorbents in soils and other agricultural sectors and the future research that needs to be conducted is addressed.

1.10 References

[1]   D. Tilman, C. Balzer, J. Hill, and B. L. Befort, "Global food demand and the sustainable intensification of agriculture," *Proceedings of the National Academy of Sciences,* vol. 108, no. 50, pp. 20260-20264, 2011, doi: 10.1073/pnas.1116437108.

[2]   Organisation for Economic Co-operation and Development. "Managing water sustainably is key to the future of food and agriculture." https://www.oecd.org/agriculture/topics/water-and-agriculture/ (accessed 12/06/2020, 2020).

[3]   W. a. t. E. Department of Agriculture, . "Water for food." Australian Government. https://www.agriculture.gov.au/water/water-for-food (accessed 12/06/2020, 2020).

[4]   B. A. Müller C., Popp A., Waha K., Fader M.,, "Climate change impacts on agricultural yields," in "World Development Report " Potsdam Institute for Climate Impact Research, Germany, 2010.

[5]   M. R. Guilherme *et al.*, "Superabsorbent hydrogels based on polysaccharides for application in agriculture as soil conditioner and nutrient carrier: A review," *European Polymer Journal,* vol. 72, pp. 365-385, 2015, doi: 10.1016/j.eurpolymj.2015.04.017.

[6] E. M. Ahmed, "Hydrogel: Preparation, characterization, and applications: A review," *Journal of Advanced Research,* vol. 6, no. 2, pp. 105-121, 2015/03/01/ 2015, doi: https://doi.org/10.1016/j.jare.2013.07.006.

[7] S. Ghorbani *et al.*, "Hydrogels Based on Cellulose and its Derivatives: Applications, Synthesis, and Characteristics," *Polymer Science, Series A,* vol. 60, no. 6, pp. 707-722, 2019, doi: 10.1134/s0965545x18060044.

[8] X. Shen, J. L. Shamshina, P. Berton, G. Gurau, and R. D. Rogers, "Hydrogels based on cellulose and chitin: fabrication, properties, and applications," *Green Chemistry,* 10.1039/C5GC02396C vol. 18, no. 1, pp. 53-75, 2016, doi: 10.1039/C5GC02396C.

[9] J. R. Gross, "The Evolution of Absorbent Materials," in *Studies in Polymer Science*, vol. 8, L. Brannon-Peppas and R. S. Harland Eds.: Elsevier, 1990, pp. 3-22.

[10] R. Curvello, V. S. Raghuwanshi, and G. Garnier, "Engineering nanocellulose hydrogels for biomedical applications," *Advances in Colloid and Interface Science,* vol. 267, pp. 47-61, 2019/05/01/ 2019, doi: https://doi.org/10.1016/j.cis.2019.03.002.

[11] H. M. Shewan and J. R. Stokes, "Review of techniques to manufacture micro-hydrogel particles for the food industry and their applications," *Journal of Food Engineering,* vol. 119, no. 4, pp. 781-792, 2013/12/01/ 2013, doi: https://doi.org/10.1016/j.jfoodeng.2013.06.046.

[12] A. Bashari, A. Rouhani Shirvan, and M. Shakeri, "Cellulose-based hydrogels for personal care products," *Polymers for Advanced Technologies,* vol. 29, no. 12, pp. 2853-2867, 2018, doi: 10.1002/pat.4290.

[13] M. J. Zohuriaan-Mehr, H. Omidian, S. Doroudiani, and K. Kabiri, "Advances in non-hygienic applications of superabsorbent hydrogel materials," *Journal of Materials Science,* journal article vol. 45, no. 21, pp. 5711-5735, November 01 2010, doi: 10.1007/s10853-010-4780-1.

[14] J. El-Asmar, H. Jaafar, I. Bashour, M. T. Farran, and I. P. Saoud, "Hydrogel Banding Improves Plant Growth, Survival, and Water Use Efficiency in Two Calcareous Soils," *CLEAN – Soil, Air, Water,* vol. 45, no. 7, p. 1700251, 2017, doi: https://doi.org/10.1002/clen.201700251.

[15] N. Thombare, S. Mishra, M. Z. Siddiqui, U. Jha, D. Singh, and G. R. Mahajan, "Design and development of guar gum based novel, superabsorbent and moisture retaining hydrogels for agricultural applications," *Carbohydr Polym,* vol. 185, pp. 169-178, 2018, doi: 10.1016/j.carbpol.2018.01.018.

[16] A. M. AbdAllah, A. M. Mashaheet, and K. O. Burkey, "Super absorbent polymers mitigate drought stress in corn (Zea mays L.) grown under rainfed conditions," *Agricultural Water Management,* vol. 254, p. 106946, 2021/08/01/ 2021, doi: https://doi.org/10.1016/j.agwat.2021.106946.

[17] Z. Steinmetz *et al.*, "Plastic mulching in agriculture. Trading short-term agronomic benefits for long-term soil degradation?," *Science of The Total Environment,* vol. 550, pp. 690-705, 2016/04/15/ 2016, doi: https://doi.org/10.1016/j.scitotenv.2016.01.153.

[18] A. A. Horton, A. Walton, D. J. Spurgeon, E. Lahive, and C. Svendsen, "Microplastics in freshwater and terrestrial environments: Evaluating the current understanding to identify the knowledge gaps and future research priorities," *Science of The Total Environment,* vol. 586, pp. 127-141, 2017/05/15/ 2017, doi: https://doi.org/10.1016/j.scitotenv.2017.01.190.

[19] L. Ramos, G. Berenstein, E. A. Hughes, A. Zalts, and J. M. Montserrat, "Polyethylene film incorporation into the horticultural soil of small periurban production units in Argentina," *Science of The Total Environment,* vol. 523, pp. 74-81, 2015/08/01/ 2015, doi: https://doi.org/10.1016/j.scitotenv.2015.03.142.

[20]   National Cancer Institute. "Acrylamide and cancer risk." https://www.cancer.gov/about-cancer/causes-prevention/risk/diet/acrylamide-fact-sheet (accessed.

[21]   S. M. D. Sánchez-Garcia, M. M. D. Fernández-Nieto, and J. M. D. P. Sastre, "Asthma Induced by a Thermal Printer," (in English), *The New England Journal of Medicine,* vol. 360, no. 22, pp. 2375-6, 2009 May 28

2017-10-31 2009, doi: http://dx.doi.org/10.1056/NEJMc0901008.

[22]   C. Demitri, F. Scalera, M. Madaghiele, A. Sannino, and A. Maffezzoli, "Potential of Cellulose-Based Superabsorbent Hydrogels as Water Reservoir in Agriculture," (in English), *International Journal of Polymer Science,* vol. 2013, 2013 2013, doi: http://dx.doi.org/10.1155/2013/435073.

[23]   D. Sarmah and N. Karak, "Biodegradable superabsorbent hydrogel for water holding in soil and controlledвЂђrelease fertilizer," *Journal of applied polymer science,* vol. 137, no. 13, pp. 48495-n/a, 2020, doi: 10.1002/app.48495.

[24]   M. R. Guilherme, A. V. Reis, A. T. Paulino, T. A. Moia, L. H. C. Mattoso, and E. B. Tambourgi, "Pectin-based polymer hydrogel as a carrier for release of agricultural nutrients and removal of heavy metals from wastewater," *Journal of Applied Polymer Science,* pp. n/a-n/a, 2010, doi: 10.1002/app.32123.

[25]   S. M. F. Kabir, P. P. Sikdar, B. Haque, M. A. R. Bhuiyan, A. Ali, and M. N. Islam, "Cellulose-based hydrogel materials: chemistry, properties and their prospective applications," *Prog Biomater,* vol. 7, no. 3, pp. 153-174, Sep 2018, doi: 10.1007/s40204-018-0095-0.

[26]   N. Lavoine and L. Bergström, "Nanocellulose-based foams and aerogels: processing, properties, and applications," *Journal of Materials Chemistry A,* vol. 5, no. 31, pp. 16105-16117, 2017, doi: 10.1039/c7ta02807e.

[27]   S. Li and G. Chen, "Agricultural waste-derived superabsorbent hydrogels: Preparation, performance, and socioeconomic impacts," *Journal of Cleaner Production,* vol. 251, p. 119669, 2020/04/01/ 2020, doi: https://doi.org/10.1016/j.jclepro.2019.119669.

[28]   C. Liliana Serna and M. A. Guancha-Chalapud, "Natural fibers for hydrogels production and their applications in agriculture," (in English), *Acta Agronómica,* vol. 66, no. 4, pp. 495-505, 2017 2017, doi: http://dx.doi.org/10.15446/acag.v66n4.56875.

[29]   I. H. Mondal, *Cellulose-Based Superabsorbent Hydrogels* (Polymers and Polymeric Composites: A Reference Series). 2019.

[30]   A. a. Dufresne and A. Dufresne, *Nanocellulose : from nature to high performance tailored materials*. Berlin: Berlin

Boston : De Gruyter, 2012.

[31]   A. Ali and S. Ahmed, "Recent Advances in Edible Polymer Based Hydrogels as a Sustainable Alternative to Conventional Polymers," *J Agric Food Chem,* vol. 66, no. 27, pp. 6940-6967, Jul 11 2018, doi: 10.1021/acs.jafc.8b01052.

[32]   C. R. Bauli, G. F. Lima, A. G. de Souza, R. R. Ferreira, and D. S. Rosa, "Eco-friendly carboxymethyl cellulose hydrogels filled with nanocellulose or nanoclays for agriculture applications as soil conditioning and nutrient carrier and their impact on cucumber growing," *Colloids and Surfaces A: Physicochemical and Engineering Aspects,* vol. 623, p. 126771, 2021/08/20/ 2021, doi: https://doi.org/10.1016/j.colsurfa.2021.126771.

[33]   H. Zhang *et al.*, "Cellulose Anionic Hydrogels Based on Cellulose Nanofibers As Natural Stimulants for Seed Germination and Seedling Growth," *J Agric Food Chem,* vol. 65, no. 19, pp. 3785-3791, May 17 2017, doi: 10.1021/acs.jafc.6b05815.

[34]   A. Kalhapure, R. Kumar, V. P. Singh, and D. S. Pandey, "Hydrogels: a boon for increasing agricultural productivity in water-stressed environment," *Current Science,* vol. 111, no. 11, pp. 1773-1779, 2016. [Online]. Available: http://www.jstor.org/stable/24911537.

[35]   A. Isogai, T. Saito, and H. Fukuzumi, "TEMPO-oxidized cellulose nanofibers," *Nanoscale,* 10.1039/C0NR00583E vol. 3, no. 1, pp. 71-85, 2011, doi: 10.1039/C0NR00583E.

[36]   H. Kargarzadeh *et al.*, "Advances in cellulose nanomaterials," *Cellulose,* vol. 25, no. 4, pp. 2151-2189, 2018/04/01 2018, doi: 10.1007/s10570-018-1723-5.

[37]   T. Nissilä, J. Wei, S. Geng, A. Teleman, and K. Oksman, "Ice-Templated Cellulose Nanofiber Filaments as a Reinforcement Material in Epoxy Composites," *Nanomaterials,* vol. 11, no. 2, p. 490, 2021. [Online]. Available: https://www.mdpi.com/2079-4991/11/2/490.

[38]   K. J. De France, T. Hoare, and E. D. Cranston, "Review of Hydrogels and Aerogels Containing Nanocellulose," *Chemistry of Materials,* vol. 29, no. 11, pp. 4609-4631, 2017/06/13 2017, doi: 10.1021/acs.chemmater.7b00531.

[39]   M. Chen, J. Parot, V. A. Hackley, S. Zou, and L. J. Johnston, "AFM characterization of cellulose nanocrystal height and width using internal calibration standards," *Cellulose (London),* vol. 28, no. 4, pp. 1933-1946, 2021, doi: 10.1007/s10570-021-03678-0.

[40]   R. Ajdary, B. L. Tardy, B. D. Mattos, L. Bai, and O. J. Rojas, "Plant Nanomaterials and Inspiration from Nature: Water Interactions and Hierarchically Structured Hydrogels," *Advanced Materials,* vol. n/a, no. n/a, p. 2001085, doi: https://doi.org/10.1002/adma.202001085.

[41]   V. S. Raghuwanshi and G. Garnier, "Cellulose Nano-Films as Bio-Interfaces," (in English), *Frontiers in Chemistry,* Review vol. 7, no. 535, 2019-July-30 2019, doi: 10.3389/fchem.2019.00535.

[42]   Z. Huang, V. S. Raghuwanshi, and G. Garnier, "Functionality of Immunoglobulin G and Immunoglobulin M Antibody Physisorbed on Cellulosic Films," (in eng), *Front Bioeng Biotechnol,* vol. 5, p. 41, 2017, doi: 10.3389/fbioe.2017.00041.

[43]   L. Mendoza, L. Hossain, E. Downey, C. Scales, W. Batchelor, and G. Garnier, "Carboxylated nanocellulose foams as superabsorbents," *J Colloid Interface Sci,* vol. 538, pp. 433-439, Mar 7 2019, doi: 10.1016/j.jcis.2018.11.112.

[44]   V. Kuzmenko *et al.*, "Cellulose-derived carbon nanofibers/graphene composite electrodes for powerful compact supercapacitors," *RSC Advances,* 10.1039/C7RA07533B vol. 7, no. 73, pp. 45968-45977, 2017, doi: 10.1039/C7RA07533B.

[45]   M. A. S. Azizi Samir, F. Alloin, and A. Dufresne, "Review of Recent Research into Cellulosic Whiskers, Their Properties and Their Application in Nanocomposite Field," *Biomacromolecules,* vol. 6, no. 2, pp. 612-626, 2005/03/01 2005, doi: 10.1021/bm0493685.

[46]   D. Trache *et al.*, "Nanocellulose: From Fundamentals to Advanced Applications," (in English), *Frontiers in Chemistry,* Review vol. 8, no. 392, 2020-May-06 2020, doi: 10.3389/fchem.2020.00392.

[47]   D. J. Mendoza, L. Hossain, C. Browne, V. S. Raghuwanshi, G. P. Simon, and G. Garnier, "Controlling the transparency and rheology of nanocellulose gels with the extent of carboxylation," (in eng), *Carbohydrate polymers,* vol. 245, p. 116566, 2020/10// 2020, doi: 10.1016/j.carbpol.2020.116566.

[48]   A. Herreros-López *et al.*, "Synthesis and Catalytic Activity of Gold Nanoparticles Supported on Dendrimeric Nanocellulose Hybrids," *European Journal of Organic*

Chemistry, vol. 2016, no. 19, pp. 3186-3192, 2016, doi: https://doi.org/10.1002/ejoc.201600148.

[49]   D. J. Mendoza *et al.*, "Phenolic Ester-Decorated Cellulose Nanocrystals as UV-Absorbing Nanoreinforcements in Polyvinyl Alcohol Films," *ACS Sustainable Chemistry & Engineering,* vol. 9, no. 18, pp. 6427-6437, 2021/05/10 2021, doi: 10.1021/acssuschemeng.1c01148.

[50]   A. Olad, F. Doustdar, and H. Gharekhani, "Fabrication and characterization of a starch-based superabsorbent hydrogel composite reinforced with cellulose nanocrystals from potato peel waste," *Colloids and Surfaces A: Physicochemical and Engineering Aspects,* vol. 601, p. 124962, 2020/09/20/ 2020, doi: https://doi.org/10.1016/j.colsurfa.2020.124962.

[51]   R. M. Barajas-Ledesma, A. F. Patti, V. N. L. Wong, V. S. Raghuwanshi, and G. Garnier, "Engineering nanocellulose superabsorbent structure by controlling the drying rate," *Colloids and Surfaces A: Physicochemical and Engineering Aspects,* vol. 600, p. 124943, 2020/09/05/ 2020, doi: https://doi.org/10.1016/j.colsurfa.2020.124943.

[52]   I. Siró, D. Plackett, M. Hedenqvist, M. Ankerfors, and T. Lindström, "Highly transparent films from carboxymethylated microfibrillated cellulose: The effect of multiple homogenization steps on key properties," *Journal of Applied Polymer Science,* vol. 119, no. 5, pp. 2652-2660, 2011, doi: https://doi.org/10.1002/app.32831.

[53]   A. Pei, N. Butchosa, L. A. Berglund, and Q. Zhou, "Surface quaternized cellulose nanofibrils with high water absorbency and adsorption capacity for anionic dyes," *Soft Matter,* 10.1039/C2SM27344F vol. 9, no. 6, pp. 2047-2055, 2013, doi: 10.1039/C2SM27344F.

[54]   M. Henriksson, G. Henriksson, L. A. Berglund, and T. Lindström, "An environmentally friendly method for enzyme-assisted preparation of microfibrillated cellulose (MFC) nanofibers," *European Polymer Journal,* vol. 43, no. 8, pp. 3434-3441, 2007/08/01/ 2007, doi: https://doi.org/10.1016/j.eurpolymj.2007.05.038.

[55]   L. Mendoza, W. Batchelor, R. F. Tabor, and G. Garnier, "Gelation mechanism of cellulose nanofibre gels: A colloids and interfacial perspective," *J Colloid Interface Sci,* vol. 509, pp. 39-46, Jan 1 2018, doi: 10.1016/j.jcis.2017.08.101.

[56]   N. Kayra and A. Ö. Aytekin, "Synthesis of cellulose-based hydrogels: Preparation, formation, mixture, and modification," *Cellulose-Based Superabsorbent Hydrogels,* pp. 407-434, 2019.

[57]   L. Liang, S. Bhagia, M. Li, C. Huang, and A. J. Ragauskas, "Cross-linked nanocellulosic materials and their applications," *ChemSusChem,* vol. 13, no. 1, 2019.

[58]   S. H. Zainal, N. H. h Mohd, N. Suhaili, F. H. Anuar, A. M. Lazim, and R. Othaman, "Preparation of Cellulose-based Hydrogel: A Review," *Journal of Materials Research and Technology,* 2020.

[59]   X. Zhang *et al.*, "Innovative application of PVA hydrogel for the forming of porous Si3N4 ceramics via freeze-thaw technique," *Ceramics International,* vol. 44, no. 11, pp. 13409-13413, 2018.

[60]   L. Zhu *et al.*, "Shapeable fibrous aerogels of metal–organic-frameworks templated with nanocellulose for rapid and large-capacity adsorption," *ACS nano,* vol. 12, no. 5, pp. 4462-4468, 2018.

[61]   C. A. Maestri, P. Bettotti, and M. Scarpa, "Fabrication of complex-shaped hydrogels by diffusion controlled gelation of nanocellulose crystallites," *Journal of Materials Chemistry B,* vol. 5, no. 40, pp. 8096-8104, 2017.

[62] J. Yang, F. Xu, and C.-R. Han, "Metal ion mediated cellulose nanofibrils transient network in covalently cross-linked hydrogels: mechanistic insight into morphology and dynamics," *Biomacromolecules,* vol. 18, no. 3, pp. 1019-1028, 2017.

[63] R. M. Barajas-Ledesma, L. Hossain, V. N. L. Wong, A. F. Patti, and G. Garnier, "Effect of the counter-ion on nanocellulose hydrogels and their superabsorbent structure and properties," *Journal of Colloid and Interface Science,* vol. 599, pp. 140-148, 2021/10/01/ 2021, doi: https://doi.org/10.1016/j.jcis.2021.04.065.

[64] R. Curvello, V. S. Raghuwanshi, and G. Garnier, "Engineering nanocellulose hydrogels for biomedical applications," *Advances in colloid and interface science,* 2019.

[65] L. Mendoza, W. Batchelor, R. F. Tabor, and G. Garnier, "Gelation mechanism of cellulose nanofibre gels: A colloids and interfacial perspective," *Journal of Colloid And Interface Science,* vol. 509, pp. 39-46, 2018, doi: 10.1016/j.jcis.2017.08.101.

[66] X. Zhang, I. Elsayed, C. Navarathna, G. T. Schueneman, and E. B. Hassan, "Biohybrid hydrogel and aerogel from self-assembled nanocellulose and nanochitin as a high-efficiency adsorbent for water purification," *ACS applied materials & interfaces,* vol. 11, no. 50, pp. 46714-46725, 2019.

[67] L. Li, P. Thangamathesvaran, C. Yue, K. Tam, X. Hu, and Y. Lam, "Gel network structure of methylcellulose in water," *Langmuir,* vol. 17, no. 26, pp. 8062-8068, 2001.

[68] Y. Sekiguchi, C. Sawatari, and T. Kondo, "A gelation mechanism depending on hydrogen bond formation in regioselectively substituted O-methylcelluloses," *Carbohydrate Polymers,* vol. 53, no. 2, pp. 145-153, 2003.

[69] J. Garner and K. Park, "Chemically modified natural polysaccharides to form gels," *Polysaccharides, Springer International Publishing, Cham,* pp. 1555-1582, 2015.

[70] S. Khan, A. Ullah, K. Ullah, and N.-u. Rehman, "Insight into hydrogels," *Designed monomers and polymers,* vol. 19, no. 5, pp. 456-478, 2016.

[71] F. Ullah, M. B. H. Othman, F. Javed, Z. Ahmad, and H. M. Akil, "Classification, processing and application of hydrogels: A review," *Materials Science and Engineering: C,* vol. 57, pp. 414-433, 2015.

[72] C. Chang, B. Duan, J. Cai, and L. Zhang, "Superabsorbent hydrogels based on cellulose for smart swelling and controllable delivery," *European Polymer Journal,* vol. 46, no. 1, pp. 92-100, 2010, doi: 10.1016/j.eurpolymj.2009.04.033.

[73] T. Fekete, J. Borsa, E. Takács, and L. Wojnárovits, "Synthesis of cellulose-based superabsorbent hydrogels by high-energy irradiation in the presence of crosslinking agent," *Radiation Physics and Chemistry,* vol. 118, pp. 114-119, 2016.

[74] T. Fekete, J. Borsa, E. Takács, and L. Wojnárovits, "Synthesis of carboxymethylcellulose/starch superabsorbent hydrogels by gamma-irradiation," *Chemistry Central Journal,* vol. 11, no. 1, p. 46, 2017.

[75] O. S. Lawal, M. Yoshimura, R. Fukae, and K. Nishinari, "Microporous hydrogels of cellulose ether cross-linked with di- or polyfunctional glycidyl ether made for the delivery of bioactive substances," *Colloid and Polymer Science,* vol. 289, no. 11, pp. 1261-1272, 2011/07/01 2011, doi: 10.1007/s00396-011-2458-0.

[76] K. M. Salleh *et al.*, "Chemically crosslinked hydrogel and its driving force towards superabsorbent behaviour," *International journal of biological macromolecules,* vol. 118, pp. 1422-1430, 2018.

[77] V. S. Ghorpade, A. V. Yadav, and R. J. Dias, "Citric acid crosslinked cyclodextrin/hydroxypropylmethylcellulose hydrogel films for hydrophobic drug delivery," *International journal of biological macromolecules,* vol. 93, pp. 75-86, 2016.

[78] C. Demitri *et al.*, "Novel superabsorbent cellulose-based hydrogels crosslinked with citric acid," *Journal of Applied Polymer Science,* vol. 110, no. 4, pp. 2453-2460, 2008.

[79] Q. Cheng *et al.*, "Dual Cross-Linked Hydrogels with Injectable, Self-Healing, and Antibacterial Properties Based on the Chemical and Physical Cross-Linking," *Biomacromolecules,* vol. 22, no. 4, pp. 1685-1694, 2021.

[80] S. J. Buwalda, "Bio-based composite hydrogels for biomedical applications," *Multifunctional Materials,* vol. 3, no. 2, p. 022001, 2020.

[81] H. S. Yoo, "Photo-cross-linkable and thermo-responsive hydrogels containing chitosan and Pluronic for sustained release of human growth hormone (hGH)," *Journal of Biomaterials Science, Polymer Edition,* vol. 18, no. 11, pp. 1429-1441, 2007.

[82] Z. Pakowski, "Modern Methods of Drying Nanomaterials," *Transport in Porous Media,* vol. 66, no. 1-2, pp. 19-27, 2006, doi: 10.1007/s11242-006-9019-x.

[83] N. Buchtová and T. Budtova, "Cellulose aero-, cryo- and xerogels: towards understanding of morphology control," *Cellulose,* journal article vol. 23, no. 4, pp. 2585-2595, August 01 2016, doi: 10.1007/s10570-016-0960-8.

[84] N. Butchosa and Q. Zhou, "Water redispersible cellulose nanofibrils adsorbed with carboxymethyl cellulose," *Cellulose,* journal article vol. 21, no. 6, pp. 4349-4358, December 01 2014, doi: 10.1007/s10570-014-0452-7.

[85] M. Beaumont, J. König, M. Opietnik, A. Potthast, and T. Rosenau, "Drying of a cellulose II gel: effect of physical modification and redispersibility in water," *Cellulose,* vol. 24, no. 3, pp. 1199-1209, 2017, doi: 10.1007/s10570-016-1166-9.

[86] T. Lindstrom, Carlsson, G., , "The effect of carboxyl groups and their ionic form during drying on the hornification of cellulose fibers," *svensk papperstidning,* p. R146, 1982.

[87] J. Grignon and A. M. Scallan, "Effect of pH [hydrogen-ion concentration] and neutral salts upon the swelling of cellulose gels," *J. Appl. Polym. Sci,* vol. 25, no. 12, pp. 2829-2843, 1980, doi: 10.1002/app.1980.070251215.

[88] B. Bahrami, T. Behzad, A. Zamani, P. Heidarian, and B. Nasri-Nasrabadi, "Synthesis and characterization of carboxymethyl chitosan superabsorbent hydrogels reinforced with sugarcane bagasse cellulose nanofibers," *Materials Research Express,* vol. 6, no. 6, p. 065320, 2019/03/29 2019, doi: 10.1088/2053-1591/ab0eb8.

[89] L. Hossain, E. Eastman, M. De Rango, V. S. Raghuwanshi, J. Tanner, and G. Garnier, "Absorption kinetics of nanocellulose foams: Effect of ionic strength and surface charge," *Journal of colloid and interface science,* vol. 601, pp. 124-132, 2021, doi: 10.1016/j.jcis.2021.05.092.

[90] T. S. Anirudhan and S. R. Rejeena, "Poly(acrylic acid-co-acrylamide-co-2-acrylamido-2-methyl-1-propanesulfonic acid)-grafted nanocellulose/poly(vinyl alcohol) composite for the in vitro gastrointestinal release of amoxicillin," *Journal of Applied Polymer Science,* vol. 131, no. 17, 2014, doi: https://doi.org/10.1002/app.40699.

[91] C. Spagnol, F. H. A. Rodrigues, A. G. B. Pereira, A. R. Fajardo, A. F. Rubira, and E. C. Muniz, "Superabsorbent hydrogel composite made of cellulose nanofibrils and chitosan-graft-poly(acrylic acid)," *Carbohydrate polymers,* vol. 87, no. 3, pp. 2038-2045, 2012, doi: 10.1016/j.carbpol.2011.10.017.

[92] A. Suo, J. Qian, Y. Yao, and W. Zhang, "Synthesis and properties of carboxymethyl cellulose-graft-poly(acrylic acid-co-acrylamide) as a novel cellulose-based superabsorbent," *Journal of Applied Polymer Science,* vol. 103, no. 3, pp. 1382-1388, 2007, doi: https://doi.org/10.1002/app.23948.

[93]   F. F. Montesano, A. Parente, P. Santamaria, A. Sannino, and F. Serio, "Biodegradable Superabsorbent Hydrogel IncreasesWater Retention Properties of Growing Media and Plant Growth," *Agriculture and Agricultural Science Procedia,* vol. 4, pp. 451-458, 2015, doi: 10.1016/j.aaspro.2015.03.052.

[94]   A. Hadas, L. Kautsky, M. Goek, and E. Erman Kara, "Rates of decomposition of plant residues and available nitrogen in soil, related to residue composition through simulation of carbon and nitrogen turnover," *Soil Biology and Biochemistry,* vol. 36, no. 2, pp. 255-266, 2004/02/01/ 2004, doi: https://doi.org/10.1016/j.soilbio.2003.09.012.

[95]   A. Hadas, S. Feigenbaum, M. Sofer, J. A. E. Molina, and C. E. Clapp, "Decomposition of Nitrogen-15-Labeled Wheat and Cellulose in Soil: Modeling Tracer Dynamics," *Soil Science Society of America Journal,* https://doi.org/10.2136/sssaj1993.03615995005700040019x vol. 57, no. 4, pp. 996-1001, 1993/07/01 1993, doi: https://doi.org/10.2136/sssaj1993.03615995005700040019x.

[96]   M. Vikman, J. Vartiainen, I. Tsitko, and P. Korhonen, "Biodegradability and Compostability of Nanofibrillar Cellulose-Based Products," (in English), *Journal of Polymers and the Environment,* vol. 23, no. 2, pp. 206-215, Jun 2015

2015-07-06 2015, doi: http://dx.doi.org/10.1007/s10924-014-0694-3.

[97]   H. Kono and S. Fujita, "Biodegradable superabsorbent hydrogels derived from cellulose by esterification crosslinking with 1,2,3,4-butanetetracarboxylic dianhydride," *Carbohydrate Polymers,* vol. 87, no. 4, pp. 2582-2588, 2012, doi: 10.1016/j.carbpol.2011.11.045.

[98]   I. Homma, H. Fukuzumi, T. Saito, and A. Isogai, "Effects of carboxyl-group counter-ions on biodegradation behaviors of TEMPO-oxidized cellulose fibers and nanofibril films," *Cellulose,* vol. 20, no. 5, pp. 2505-2515, 2013, doi: 10.1007/s10570-013-0020-6.

[99]   H. P. Hartmann and T. Appel, "Calibration of near infrared spectra for measuring decomposing cellulose and green manure in soils," *Soil Biology and Biochemistry,* vol. 38, no. 5, pp. 887-897, 2006/05/01/ 2006, doi: https://doi.org/10.1016/j.soilbio.2005.08.005.

[100]   Y. G. Han, P. L. Yang, Y. P. Luo, S. M. Ren, L. X. Zhang, and L. Xu, "Porosity change model for watered super absorbent polymer-treated soil," *Environmental Earth Sciences,* vol. 61, no. 6, pp. 1197-1205, 2010/09/01 2010, doi: 10.1007/s12665-009-0443-4.

[101]   X. Hou, R. Li, W. He, X. Dai, K. Ma, and Y. Liang, "Superabsorbent polymers influence soil physical properties and increase potato tuber yield in a dry-farming region," *Journal of Soils and Sediments,* vol. 18, no. 3, pp. 816-826, 2018/03/01 2018, doi: 10.1007/s11368-017-1818-x.

[102]   N. Thombare, S. Mishra, M. Z. Siddiqui, U. Jha, D. Singh, and G. R. Mahajan, "Design and development of guar gum based novel, superabsorbent and moisture retaining hydrogels for agricultural applications," *Carbohydrate Polymers,* vol. 185, pp. 169-178, 2018/04/01/ 2018, doi: https://doi.org/10.1016/j.carbpol.2018.01.018.

[103]   H. A. A. El-Rehim, E.-S. A. Hegazy, and H. L. A. El-Mohdy, "Radiation synthesis of hydrogels to enhance sandy soils water retention and increase plant performance," *Journal of Applied Polymer Science,* vol. 93, no. 3, pp. 1360-1371, 2004, doi: https://doi.org/10.1002/app.20571.

[104]   A. Sawut, M. Yimit, W. Sun, and I. Nurulla, "Photopolymerisation and characterization of maleylatedcellulose-g-poly(acrylic acid) superabsorbent polymer,"

(in eng), *Carbohydr Polym,* vol. 101, pp. 231-9, Jan 30 2014, doi: 10.1016/j.carbpol.2013.09.054.

[105] A. Saha, S. Sekharan, and U. Manna, "Superabsorbent hydrogel (SAH) as a soil amendment for drought management: A review," *Soil and Tillage Research,* vol. 204, p. 104736, 2020/10/01/ 2020, doi: https://doi.org/10.1016/j.still.2020.104736.

[106] G. Bodner, A. Nakhforoosh, and H.-P. Kaul, "Management of crop water under drought: a review," *Agronomy for Sustainable Development,* vol. 35, no. 2, pp. 401-442, 2015/04/01 2015, doi: 10.1007/s13593-015-0283-4.

[107] F. Nnadi and C. Brave, "Environmentally friendly superabsorbent polymers for water conservation in agricultural lands," *Journal of Soil Science and Environmental Management,* vol. 2, pp. 206-211, 07/01 2011.

[108] R. Sánchez - Orozco, B. Timoteo Cruz, T. Torres-Blancas, and F. Ureña-Nuñez, "Valorization of superabsorbent polymers from used disposable diapers as soil moisture retainer," *International Journal of Research - GRANTHAALAYAH,* vol. 5, pp. 115-117, 05/01 2017, doi: 10.5281/zenodo.569984.

[109] G. Cannazza, A. Cataldo, E. De Benedetto, C. Demitri, M. Madaghiele, and A. Sannino, "Experimental Assessment of the Use of a Novel Superabsorbent polymer (SAP) for the Optimization ofWater Consumption in Agricultural Irrigation Process," *Water,* vol. 6, no. 7, pp. 2056-2069, 2014, doi: 10.3390/w6072056.

[110] S. A. Shahid, A. A. Qidwai, F. Anwar, I. Ullah, and U. Rashid, "Improvement in the Water Retention Characteristics of Sandy Loam Soil Using a Newly Synthesized Poly(acrylamide-co-acrylic Acid)/AlZnFe2O4 Superabsorbent Hydrogel Nanocomposite Material," (in English), *Molecules,* vol. 17, no. 8, pp. 9397-9412, 2012 2012, doi: http://dx.doi.org/10.3390/molecules17089397.

[111] C. Spagnol *et al.*, "Nanocomposites based on poly(acrylamide-co-acrylate) and cellulose nanowhiskers," *European Polymer Journal,* vol. 48, no. 3, pp. 454-463, 2012, doi: 10.1016/j.eurpolymj.2011.12.005.

[112] A. Shaviv, "Advances in controlled-release fertilizers," in *Advances in Agronomy*, vol. 71: Academic Press, 2001, pp. 1-49.

[113] Y. P. Timilsena, R. Adhikari, P. Casey, T. Muster, H. Gill, and B. Adhikari, "Enhanced efficiency fertilisers: a review of formulation and nutrient release patterns," *J Sci Food Agric,* vol. 95, no. 6, pp. 1131-42, Apr 2015, doi: 10.1002/jsfa.6812.

[114] S. Hashim and W. A. Laftah, "Preparation and Possible Agricultural Applications of Polymer Hydrogel Composite as Soil Conditioner," *Advanced materials research,* vol. 626, pp. 6-10, 2012, doi: 10.4028/

[115] D. W. Davidson, M. S. Verma, and F. X. Gu, "Controlled root targeted delivery of fertilizer using an ionically crosslinked carboxymethyl cellulose hydrogel matrix," *Springerplus,* vol. 2, no. 1, pp. 1-9, 2013, doi: 10.1186/2193-1801-2-318.

[116] W. Wang, Z. Yang, A. Zhang, and S. Yang, "Water retention and fertilizer slow release integrated superabsorbent synthesized from millet straw and applied in agriculture," *Industrial crops and products,* vol. 160, 2021, doi: 10.1016/j.indcrop.2020.113126.

[117] H. A. Essawy, M. B. M. Ghazy, F. A. El-Hai, and M. F. Mohamed, "Superabsorbent hydrogels via graft polymerization of acrylic acid from chitosan-cellulose hybrid and their potential in controlled release of soil nutrients," *Int J Biol Macromol,* vol. 89, pp. 144-151, 2016, doi: 10.1016/j.ijbiomac.2016.04.071.

[118] X. Li, Q. Li, X. Xu, Y. Su, Q. Yue, and B. Gao, "Characterization, swelling and slow-release properties of a new controlled release fertilizer based on wheat straw cellulose

hydrogel," *Journal of the Taiwan Institute of Chemical Engineers,* vol. 60, pp. 564-572, 2016, doi: 10.1016/j.jtice.2015.10.027.

[119] K. Zhong, X.-L. Zheng, X.-Y. Mao, Z.-T. Lin, and G.-B. Jiang, "Sugarcane bagasse derivative-based superabsorbent containing phosphate rock with waterвЂ"fertilizer integration," *Carbohydr Polym,* vol. 90, no. 2, pp. 820-826, 2012, doi: 10.1016/j.carbpol.2012.06.006.

[120] W. Wang, S. Yang, A. Zhang, and Z. Yang, "Preparation and properties of novel corn straw celluloseвЂ"based superabsorbent with waterвЂђretaining and slowвЂђrelease functions," *Journal of applied polymer science,* vol. 137, no. 32, pp. 48951-n/a, 2020, doi: 10.1002/app.48951.

[121] K. Hemvichian, A. Chanthawong, and P. Suwanmala, "Synthesis and characterization of superabsorbent polymer prepared by radiation-induced graft copolymerization of acrylamide onto carboxymethyl cellulose for controlled release of agrochemicals," *Radiation physics and chemistry (Oxford, England : 1993),* vol. 103, pp. 167-171, 2014, doi: 10.1016/j.radphyschem.2014.05.064.

[122] A. I. Raafat, M. Eid, and M. B. El-Arnaouty, "Radiation synthesis of superabsorbent CMC based hydrogels for agriculture applications," *Nuclear Instruments and Methods in Physics Research Section B: Beam Interactions with Materials and Atoms,* vol. 283, pp. 71-76, 2012, doi: 10.1016/j.nimb.2012.04.011.

[123] P. Calcagnile, T. Sibillano, C. Giannini, A. Sannino, and C. Demitri, "Biodegradable poly(lactic acid)/celluloseвЂђbased superabsorbent hydrogel composite material as water and fertilizer reservoir in agricultural applications," *Journal of applied polymer science,* vol. 136, no. 21, pp. 47546-n/a, 2019, doi: 10.1002/app.47546.

[124] B. Ni, M. Liu, and S. LГј, "Multifunctional slow-release urea fertilizer from ethylcellulose and superabsorbent coated formulations," *Chemical engineering journal (Lausanne, Switzerland : 1996),* vol. 155, no. 3, pp. 892-898, 2009, doi: 10.1016/j.cej.2009.08.025.

[125] L. Wu and M. Liu, "Preparation and characterization of cellulose acetate-coated compound fertilizer with controlled-release and water-retention," *Polym. Adv. Technol,* vol. 19, no. 7, pp. 785-792, 2008, doi: 10.1002/pat.1034.

[126] B. Ni, M. Liu, S. LuM€, L. Xie, and Y. Wang, "Environmentally Friendly Slow-Release Nitrogen Fertilizer," *J. Agric. Food Chem,* vol. 59, no. 18, pp. 10169-10175, 2011, doi: 10.1021/jf202131z.

[127] X. Li, Q. Li, Y. Su, Q. Yue, B. Gao, and Y. Su, "A novel wheat straw cellulose-based semi-IPNs superabsorbent with integration of water-retaining and controlled-release fertilizers," *Journal of the Taiwan Institute of Chemical Engineers,* vol. 55, pp. 170-179, 2015, doi: 10.1016/j.jtice.2015.04.022.

[128] A. Bortolin, A. R. Serafim, F. A. Aouada, L. H. C. Mattoso, and C. Ribeiro, "Macro- and Micronutrient Simultaneous Slow Release from Highly Swellable Nanocomposite Hydrogels," *J. Agric. Food Chem,* vol. 64, no. 16, pp. 3133-3140, 2016, doi: 10.1021/acs.jafc.6b00190.

[129] A. Bortolin, F. A. Aouada, L. H. Mattoso, and C. Ribeiro, "Nanocomposite PAAm/methyl cellulose/montmorillonite hydrogel: evidence of synergistic effects for the slow release of fertilizers," *J Agric Food Chem,* vol. 61, no. 31, pp. 7431-9, Aug 7 2013, doi: 10.1021/jf401273n.

THIS PAGE HAS BEEN INTENTIONALLY LEFT BLANK

THIS PAGE HAS BEEN INTENTIONALLY LEFT BLANK

CHAPTER 2:

ENGINEERING NANOCELLULOSE SUPERABSORBENTS BY CONTROLLING THE DRYING RATE

THIS PAGE HAS BEEN INTENTIONALLY LEFT BLANK

PREFACE

The use of superabsorbent polymers (SAPs) in soils provides an option to improve the efficient use of water and land resources. They can increase water retention in different types of soil, significantly reducing irrigation water consumption. Most of the commercially available superabsorbents are fossil-fuel derived polymers which are non-biodegradable and non-renewable. The production of SAPs from the TEMPO-mediated oxidation of cellulose appears as an ideal alternative to replace these synthetic polymers. However, the preparation of these cellulosic SAP is commonly performed through freeze-drying. This technique is difficult to perform on a large-scale, energy intensive and expensive, which can limit their application in agriculture. Therefore, this chapter explores the preparation of nanocellulose SAP by controlling the drying rate. We raise the hypothesis that the drying rate controls the structure of the resulting SAP. Five drying methods, each providing a different rate of water removal, were evaluated. The swelling capacity at equilibrium and the swelling kinetics were measured and related to the SAP structure. The morphology and pore properties of the SAPs were characterised by scanning electron microscopy, mercury porosimetry and small angle X-ray scattering (SAXS). Phytotoxicity tests on plants were conducted to confirm the safe application of nanocellulose SAPs to soils.

This published chapter in *Colloids and Surfaces A: Physicochemical and Engineering Aspects* addresses the first objective of this research, which is to engineer and characterise novel and cost-effective nanocellulose superabsorbents by controlling the drying rate, producing SAPs with appropriate structure and properties for applications in agricultural soils.

THIS PAGE HAS BEEN INTENTIONALLY LEFT BLANK

Chapter 2: Engineering nanocellulose superabsorbents by controlling the drying rate

THIS PAGE HAS BEEN INTENTIONALLY LEFT BLANK

Engineering nanocellulose superabsorbent structure by controlling the drying rate

Ruth M. Barajas-Ledesma[a], Antonio F. Patti[b], Vanessa N.L. Wong[c], Vikram Singh Raghuwanshi[a] and Gil Garnier[a*]

[a]Bioresource Processing Institute of Australia (BioPRIA) and Department of Chemical Engineering, Monash University, Clayton, VIC 3800, Australia
[b]School of Chemistry, Monash University, Clayton, VIC 3800, Australia
[c]School of Earth, Atmosphere & Environment, Monash University, Clayton, VIC 3800, Australia

*For correspondence: Gil.Garnier@Monash.edu

2.1 Abstract

Hypothesis: The absorption performance and structure of superabsorbents prepared from carboxylated nanocellulose are strongly influenced by the rate of water removal. Their structure can be engineered by changing the drying profile.

Experiments: TEMPO-oxidised nanocellulose superabsorbents were prepared using five different drying techniques, each providing a distinct drying rate. The absorption capacity of deionised water was measured as a function of time and the swelling kinetics was determined, modelled and related to the superabsorbent structure. Superabsorbent phytotoxicity was assessed through seed emergence tests.

Findings: The absorption performance of nanocellulose superabsorbents is controlled by the drying rate. In most cases, drying the nanocellulose superabsorbents via evaporation increases the absorption capacity compared to freeze-dried superabsorbents. The best nanocellulose superabsorbent was the air-dried, absorbing around 230 g water/g dry fibre. The high absorption capacity of the evaporative dried superabsorbents is due to their high pore area which increases the interaction between water molecules and fibres. This leads to a stronger physical entrapment of water by capillary forces. Seed germination studies demonstrated that

oven-dried 50 °C superabsorbent increased germination by 40%. Carboxylated nanocellulose superabsorbents emerge as high-performance renewable materials which can be used extensively in many applications, including agriculture.

2.2 Keywords

Superabsorbent, TEMPO-mediated oxidation, Nanocellulose, Structure, Drying, Hornification.

2.3 Graphical Abstract
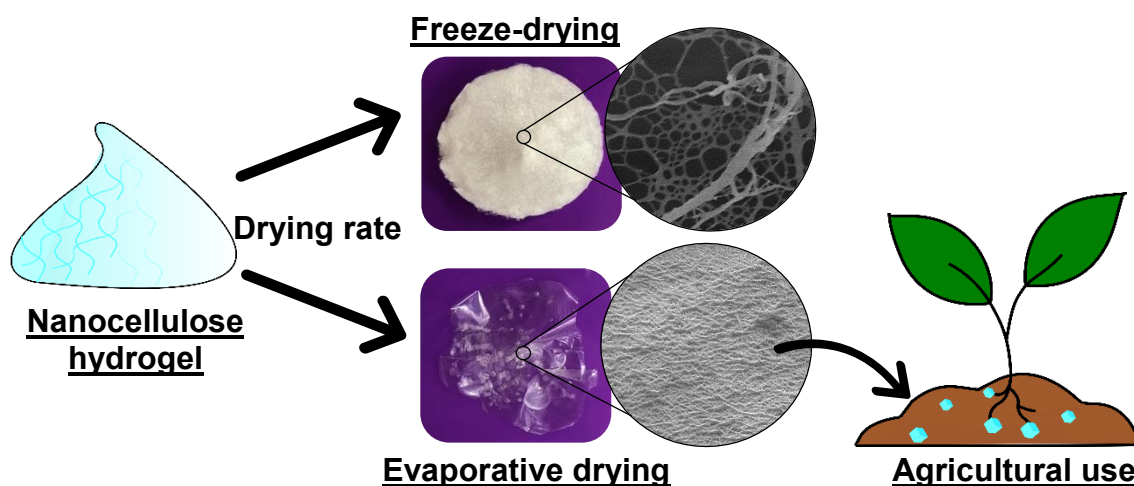
2.4 Introduction

Superabsorbent polymers (SAP) are physically or chemically cross-linked three-dimensional (3D) networks made of linear or branched hydrophilic polymers [1]. Superabsorbents can absorb water or fluids at hundreds of times their own weight and remain stable in the swollen state [1-4]. The degree of swelling is governed by the mobility of ions from the external solution toward the centre of the superabsorbent, also known as counter-ion entropy, that induces an osmotic pressure difference across the material network [5, 6]. Superabsorbents have been used in many applications including biomedicine [5], food and beverages [7],

personal care and hygiene products [8], soil remediation and wastewater treatment [9] and agriculture [10]. In agriculture, SAPs can ameliorate water availability for plants [11]. These serve as soil conditioners, improving soil properties, reducing the irrigation water consumption, and increasing crop yield [12, 13], and as nutrient carriers [13].

Most of the commercial superabsorbents are synthetic polymers, such as polyacrylamides or polyacrylates, which are non-biodegradable. Growing environmental and health concerns have driven the search for natural polymer-based superabsorbents, especially those made of polysaccharides, such as pectin or starch [14, 15]. Cellulose, the most abundant polymer on earth, has also been investigated as a superabsorbent for its availability, low-cost, biodegradability, renewability and hydrophilicity [13, 16]. Different synthesis methods have been examined to produce cellulose-based SAPs [17]. Among those, the TEMPO-mediation oxidation of cellulose is currently considered one of the most effective method for producing nanocellulose-based SAPs [6, 18]. This process oxidises the easily accessible primary alcohol groups (C6) to the carboxylic acid, resulting in a cellulose structure containing some C6 carbons in carboxylic acid form. This surface modification provides the necessary electrostatic repulsion which assists the liberation of nanocellulose fibres upon mechanical fibrillation [19]. The resulting material, also referred to as hydrogel, consists of an entanglement of cellulose nanofibres (CNF) creating a porous material of high specific surface area [20]. Several reviews on nanocellulose-based material properties, production, structure and applications have been published [17, 20-22].

A major challenge in the production of nanocellulose-based superabsorbents is to retain their porous structure during water removal. Different drying rates determined by the drying process have been examined to remove the water from hydrogels. Among these, freeze-drying has become the preferred method for laboratory preparation of highly-porous, ultralow-density solid SAPs of high water retention and swelling properties [20, 23]. These are commonly

known as foams or aerogels [20]. Freezing followed by sublimation of ice prevents the formation of capillary pressure, preserving the structure of the original dispersion. However, freeze-drying is not only expensive and difficult to perform on a large-scale [23], but it also produces low-density and fast swelling superabsorbents of limited application range. In agriculture, for example, a fast swelling rate can selectively sequester water, thus restricting the water availability to plants creating an undesirable water stress environment [12]. Thus, controlling the superabsorbent properties and structure which affect plant growth is crucial.

Evaporative-drying presents an alternative. Buchtová and Budtova [24] reported the evaporative vacuum drying at room temperature of microcrystalline cellulose dissolved in ionic liquids to produce superabsorbents with a volume shrinkage of 90%, very low porosity and no measurable surface area because of the collapse of the porous polymer network. Beaumont et al. [25] compared the effects of oven-drying at 60 °C and freeze-drying on the redispersibility of TENCEL gel, composed of spherical cellulose II microparticles. Surprisingly, they showed that oven-dried superabsorbents had better colloidal stability and higher water retention than freeze-dried superabsorbents. This was attributed to the low process temperatures and superabsorbent additives, such as carboxylmethylcellulose, that minimises the agglomeration and collapse of fibres during drying, referred to as hornification [26]. Hornification can also be minimised by preparing superabsorbents at high pH or by carboxylation of cellulose; a high-density of dissociated carboxylic groups prevents agglomeration by electrostatic stabilization [22, 27].

While several studies have investigated the synthesis and formulation of cellulose-based superabsorbents, none have systematically compared the effect of drying rate and profile on the structure of nanocellulose superabsorbents nor related those to the absorption capacity and swelling kinetics. The effect of the drying rate on the morphology, porosity and pore properties

of nanocellulose superabsorbent and how these properties influence plant growth remains poorly understood.

In this study, carboxylated nanocellulose hydrogels were prepared via TEMPO oxidation followed by high-pressure homogenization. This standard carboxylated nanocellulose hydrogel was dried to create a superabsorbent using five different drying techniques, each providing a different drying rate: freeze-drying, air-drying, vacuum drying, and oven-drying at high and low temperature. The superabsorbent absorption properties and the swelling kinetics were quantified. It is our objective to analyse the effect that drying rate has on the resulting superabsorbent structure and to establish the relationship with its absorption characteristics. Of special interest is the production of cellulose-based superabsorbents as hydro-retentor materials for applications in sustainable agriculture.

2.5 Materials and Methods

2.5.1 Materials

Bleached Eucalyptus Kraft (BEK) pulp, containing around 90% w/w of moisture was provided by Australian Paper, Maryvale, Australia. The chemical composition of the BEK pulp is displayed in Table I [28]. 2,2,6,6-tetramethylpiperidine-1-oxyl (TEMPO) and sodium bromide (NaBr) were purchased from Sigma-Aldrich. Sodium hydroxide (NaOH) and hydrochloric acid (HCl) were diluted for solutions as required and purchased from Merck and ACL Laboratories, respectively. 12% w/v sodium hypochlorite (NaClO) was purchased from Thermo Fisher Scientific and used as received. Radish (*Raphanus Sativus*) and cress (*Lepidium sativum L.*) seeds were purchased from Mr. Fothergill's (South Windsor, Australia).

Table I. Chemical composition of BEK pulp in dry basis.

Chemical composition	Average content (% ± standard deviation)
Cellulose	78.7 ± 0.8

Hemicellulose	17.7 ± 0.4
Lignin	3.2 ± 0.1
Extractives	0.3 ± 0.1
Ash	0.2 ± 0.1

2.5.2 Superabsorbent preparation

Nanocellulose superabsorbent was prepared following the TEMPO-mediated oxidation process developed by Isogai et al. [19]. Briefly, 25 g (dry weight) of BEK pulp was suspended in 2500 mL of water containing 0.4 g and 2.5 g of dissolved TEMPO and NaBr, respectively. The 12% w/v NaClO was initially adjusted to pH 10 through addition of 36% w/v HCl. The oxidation process started by adding 100 mL NaClO (6.6 mmol NaClO/g cellulose) drop-wise to the suspension under constant stirring. The pH of the reaction was kept at 10 via addition of 0.5M NaOH. The reaction was maintained for 3 h or until no decrease in pH was observed. The oxidised fibres were washed with deionised water, recovered by filtration. The TEMPO-oxidised cellulose had a carboxylate content of 1.4 mmol/g as determined by conductivity titration [29].

The TEMPO-oxidised cellulose was then dispersed in deionised water to achieve a concentration of 0.5% w/v. Fibrillation was accomplished by using a high-pressure homogeniser (GEA Niro Soavi Homogeniser Panda) at 1000 bar and two passes.

After fibrillation, five drying techniques were employed to produce the superabsorbent: freeze-drying, air-drying, vacuum-drying at 50 °C and oven-drying at 50 °C and 105 °C. Freeze-dried nanocellulose superabsorbent was prepared by freezing the nanocellulose samples for at least 12 h at -80 °C. Once frozen, samples were freeze-dried (Christ Alpha 2-4 LD Plus) for 2 days. Air-dried samples were allowed to dry at ambient temperature (approx. 23 °C) until no

difference in mass was observed. Vacuum oven-dried nanocellulose samples were prepared by drying in a vacuum oven (Thermoline Scientific Vacuum drying oven) at 50 °C until no difference in mass was observed. Oven-dried nanocellulose samples were prepared by drying in an oven at either 50 °C or 105 °C until no difference in mass was observed.

2.5.3 Characterisation

The structural morphology of all superabsorbents was analysed by SEM using a FEI Nova NanoSEM and a FEI Magellan 400. Samples were mounted on a metal stub coated with an Iridium layer less than 2 nm thick. Micrographs were obtained in high vacuum-mode.

The pore size distribution, porosity (total and at P=1 atm) and pore surface of all samples were determined by mercury porosimetry (Micromeritics Autopore IV). Samples were degassed at 50 °C for at least 24 h prior to testing. Two replicates per sample were conducted. In all measurements, the contact angle at the Hg-sample interface was assumed to be 130 ° and a testing pressure range from 0.1 to 60,000 psia was applied. The desired values were obtained through the Washburn Equation:

$$D = \frac{-4\gamma cos\theta}{P} \tag{1}$$

where D is the pore diameter, γ is the surface tension of mercury, θ refers to the contact angle between the mercury and the pore wall, and P is the applied pressure.

SAXS measurements were performed at the X-ray facility laboratory, Monash University with a Bruker N8 Horizon instrument using a CuKα (λ = 1.54 Å) micro-source. The sample to detector distance was 0.6 m which covers the q range between~0.015 to 0.3 Å^{-1}. The scattered photons from the sample were collected on a 2D Vantec-500 detector (pixel size ~70 μm × 70 μm). Final scattering curves were obtained by radial averaging of scattering images with the Bruker EVA software.

2.5.4 Swelling and water retention studies

The swelling capacity of the superabsorbents prepared was evaluated in deionised water. Both swelling capacity and swelling rate were measured. The swelling capacity was determined by weighing the samples before and after immersion in deionised water for at least 24 h. The swelling capacity was calculated as follows:

$$Swelling\ capacity, Q = \frac{m_t - m_d}{m_d} \tag{2}$$

where m_t is the weight of the swollen superabsorbent at time t and m_d refers to the weight of the dried sample.

The swelling rate was evaluated by monitoring the weight gain of the samples after immersion in water over different periods of time and expressed as Q variations. Results are reported as the average and standard deviation of triplicates.

The water retention value (WRV) of all rehydrated superabsorbents was performed in triplicates following ISO 17190-6 [30]. The set up was adapted from Qingzheng Cheng [31]. Briefly, superabsorbent samples were immersed in deionised water for at least 48 h prior to testing. Each wet sample was placed in a polypropylene mesh placed inside empty centrifugation tubes (Figure S1, see APPENDIX I). Centrifugation was carried out 3 minutes at a relative centrifugal force (RCF) of 250 G at room temperature. After centrifugation, the "wet weight" of the samples was measured. The samples were oven dried at 105 °C until they reached constant mass. The WRV was calculated as follows:

$$WRV = \frac{m_c - m_d}{m_d} \tag{3}$$

where m_c is the weight of the wet sample after centrifugation and m_d refers to the weight of the dry sample.

2.5.5 Seed germination tests

The impact of the superabsorbents, freeze-dried and oven-dried at 50 °C, on the germination and growth of two plant species was assessed. The species selected were radish and cress.

Superabsorbent effects on seed germination were evaluated at concentrations of 2, 5, 10 g of superabsorbent/L. The application rate was within the recommended range for commercial superabsorbents [32]. For each treatment, different amounts of the nanocellulose before drying were spread on a filter paper according to the desired concentration. The filter paper was later freeze-dried or oven-dried at 50°C, assuring even distribution of the superabsorbent on the filter paper. Once dried, the filter paper with the superabsorbent was placed in a 90 mm Petri dish and 5 mL of deionised water was poured. After the addition of water, 10 seeds of each species were placed on the wetted filter paper. Dishes were placed at room temperature in the dark. Four replicates of each treatment and the control (0 g/L – 5 ml of deionised water – dH$_2$O) were performed. Seed germination, defined as the seed having a radicle length > 5mm [33], was evaluated 12-hourly over a period of 7 days. The mean time to germination (MTG) of each plant species was calculated as follows:

$$MTG = \sum \frac{n \times d}{N} \tag{4}$$

where n is the number of seeds that germinated between each time period, d is the incubation period in minutes at that point and N is the total number of seeds that germinated in the treatment.

The germination index (GI) was determined for each species over a period of 48 h using the germination percentage and the radicle length:

$$\text{Germination index (GI\%)} = \frac{G_s}{G_c} \times \frac{L_s}{L_c} \times 100 \tag{5}$$

where Gs and Gc are the number of seeds that germinated in the sample and the control and Ls and Lc are the root lengths of the sample and the control, respectively. Germination index was measured as a percentage of control.

The germination studies data was analysed statistically using a One-way ANOVA (analysis of variance) to evaluate differences between the means of the different treatments. The Dunn's test was used to determine any significant differences ($p < 0.05$). ANOVA and Dunn's analyses were performed using SigmaPlot 13 (Sysstat, Chicago, IL).

2.6 Results

2.6.1 Swelling behaviour

The swelling capacity of the five nanocellulose superabsorbents was measured in deionised water as a function of time (Figure 1). In general, all superabsorbents show a similar behaviour. After an initial absorption rate, swelling levels up to reach a plateau. The time required to reach maximum capacity ranged from a couple of hours, for freeze-dried superabsorbent, to 48 h for air-dried. Lyophilised superabsorbent is characterised by an initial rapid swelling with most of it occurring during the first minutes. These results are consistent with literature on freeze-dried nanocellulose superabsorbents [6]. For the samples dried via evaporation, the swelling rate is slower. Both freeze-dried and vacuum-dried samples reached their equilibrium capacity within 5 h whereas oven-dried samples at low and high temperature achieved equilibrium after 24 h.

The absorption capacity at equilibrium of all samples was measured over time until constant mass was observed (Figure 1). The swelling at equilibrium is a function of the drying rate employed, dictated by the drying technique. Surprisingly, in all cases- except for oven drying at 105 °C-, drying the nanocellulose by evaporation increased its equilibrium capacity over freeze-dried superabsorbents. Air-dried superabsorbent has the highest water absorption capacity at 230 g water/g dry fibre.
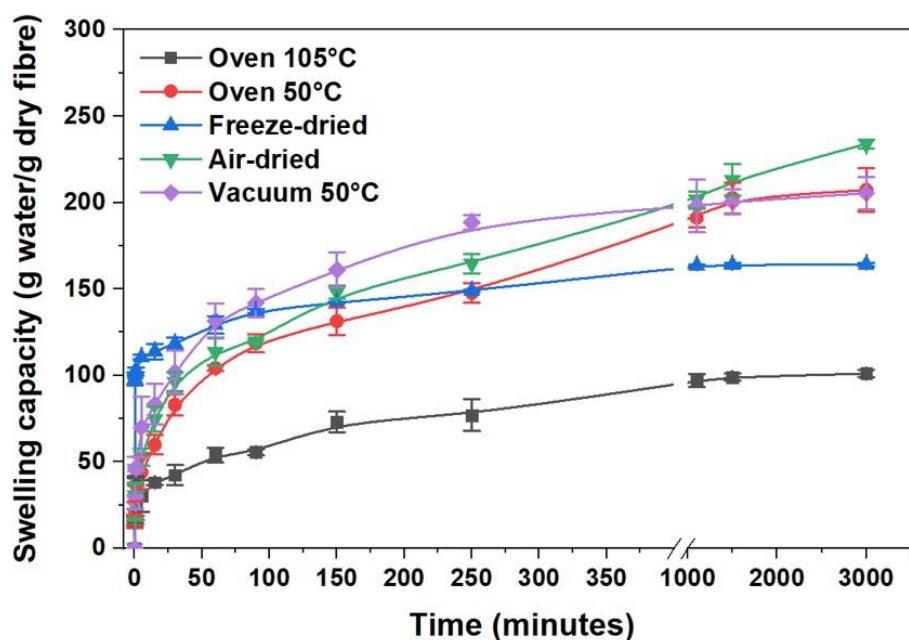
Figure 1. Swelling capacity of nanocellulose superabsorbents produced using five different drying techniques as a function of time. Results are reported as mean ± standard deviation (n=3).

The rate of water removal as a function of time was measured for all the superabsorbents (Figure 2). A direct relationship between the absorption capacity and the drying rate is observed. Among evaporative-dried superabsorbents, air-dried superabsorbents show the slowest drying followed by oven-dried 50 °C and vacuum-dried 50 °C. Oven-dried 105 °C superabsorbents display the fastest drying rate and also the lowest swelling capacity.
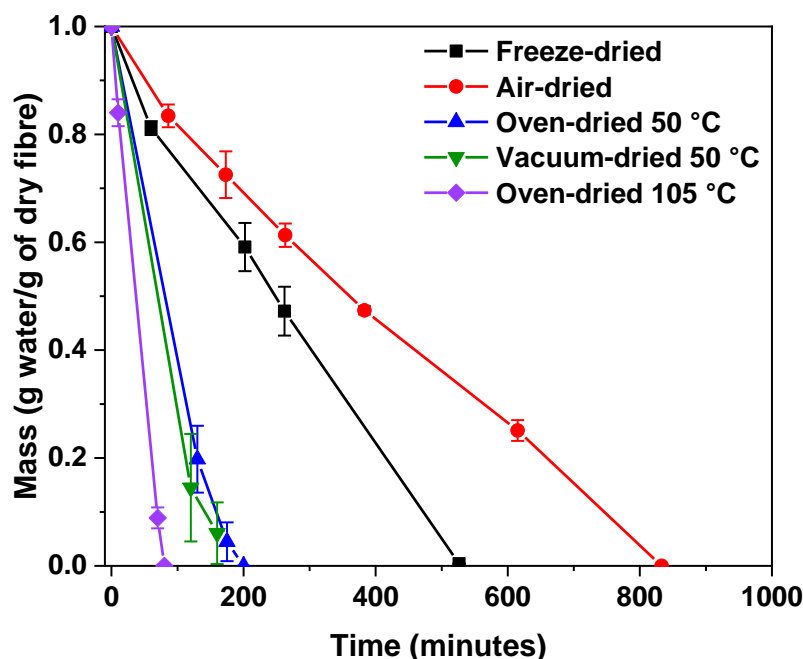
Figure 2. Rate of water removal as a function of time of nanocellulose superabsorbents produced using five different drying techniques. Results are reported as mean ± standard deviation (n=3).

2.6.2 Pore size distribution

Mercury porosimetry was used to measure the pore size distribution of the nanocellulose superabsorbents prepared with the different drying techniques (Figure 3). Pore size distribution notably changed depending on the drying mode categorized as freeze-drying or evaporative drying. Both freeze-dried superabsorbent and oven-dried 105°C superabsorbent are characterised by a macroporous structure as defined by IUPAC [34] with no pores observed at a scale lower than 50 nm. Air-dried, oven 50 °C and vacuum-dried superabsorbents all present a combination of macro, meso and micropores [34].
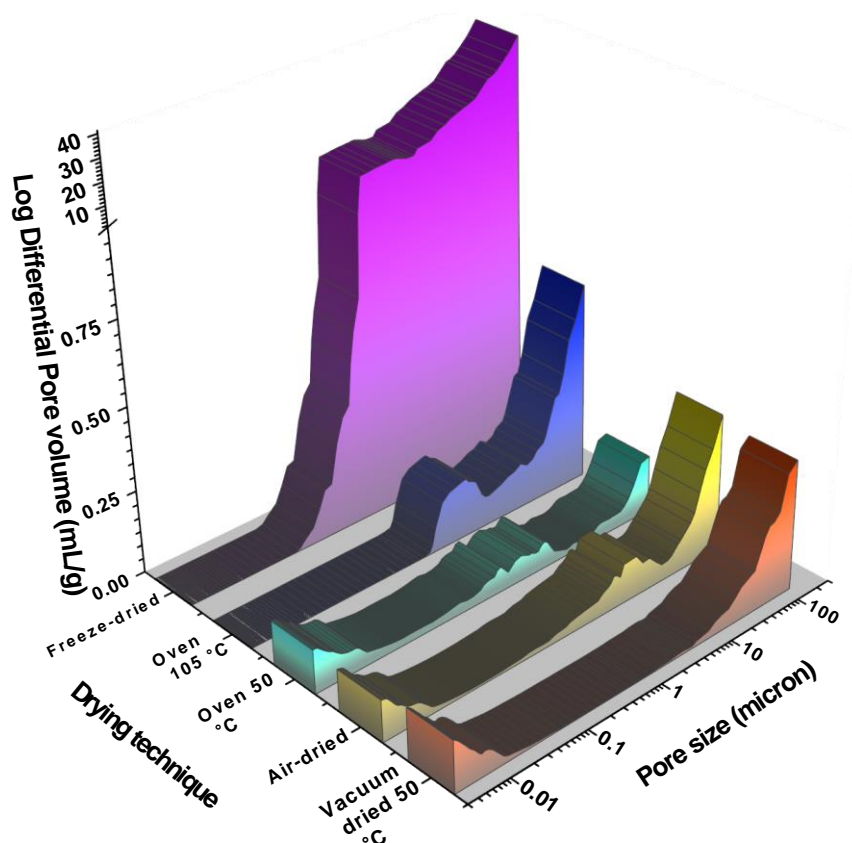
Figure 3. Pore size distribution of nanocellulose superabsorbents using different drying techniques.

The relationship between bulk density, porosity, pore area (surface area) and volume of the superabsorbent is shown as a function of the drying technique in Figure 4. Freeze-drying the nanocellulose superabsorbent produced an ultralight and highly porous material having a density lower than 170 kg/m^3 and a porosity higher than 90%. These characteristics are typical of freeze-dried superabsorbents also referred to as nanocellulose foams [20]. In all cases, evaporative drying produced porous nanocellulose superabsorbents of porosities ranging from 50 to 60% and with densities in between 1000 and 1400 kg/m^3. Vacuum-drying produced the superabsorbent of highest density (1400 kg/m^3). Freeze-drying and oven-drying at 105 °C produced superabsorbents with the lowest pore area. These values were around 7 times lower than with the other drying techniques. Freeze-dried nanocellulose superabsorbents have the

highest pore volume: around 20 mL/g. This value is 60 times higher than for superabsorbents prepared through evaporative-drying.

Figure 4. (a) Porosity and bulk density of the different nanocellulose superabsorbents. (b) Pore area and pore volume obtained through mercury porosimetry. Total porosity was calculated as: Total porosity $= \left(\frac{pore\ volume}{skeletal\ volume\ +\ pore\ volume} \right) x\ 100\%$.

2.6.3 Structure

To analyse the structural morphology of the superabsorbents, scanning electron microscopy (SEM) imaging was performed (Figure 5). The visual appearance of each superabsorbent is shown in Figure S2, APPENDIX I. The morphology of the superabsorbents strongly depends on the drying rate. At low magnification, freeze-dried superabsorbent is characterised by a sheet-like network of fibres with interconnected pores of several microns in diameter. This morphology is typical of freeze-dried materials [20, 24]. In contrast, evaporative-dried superabsorbents present a transparent film-like structure with no visible pores in the micrometre scale. For these, increasing the drying rate or temperature leads to an increase in surface roughness. Air-dried superabsorbent structure is homogeneous, soft and glassy whereas more micro-irregularities become evident as the temperature increases from 50 °C to 105 °C. These are due to fibre hornification which increases with temperature. At high magnification, freeze-dried superabsorbent forms a three-dimensional nanoporous network of fibres (Figure 5a). The fibres are clearly visible and pore diameters range from 50 to 200 nm. The superabsorbents prepared by evaporation are characterised by two-dimensional structures of compact frames made of elemental entangled fibrils stacked on top of each other. Though the presence of small pores is observed in these cases, their diameter is difficult to measure by SEM due to the high density of fibres (Figure 5b-d). The number of pores in oven-dried superabsorbent at 105 °C (Figure 5e) is much lower than for the other evaporative-dried superabsorbents.
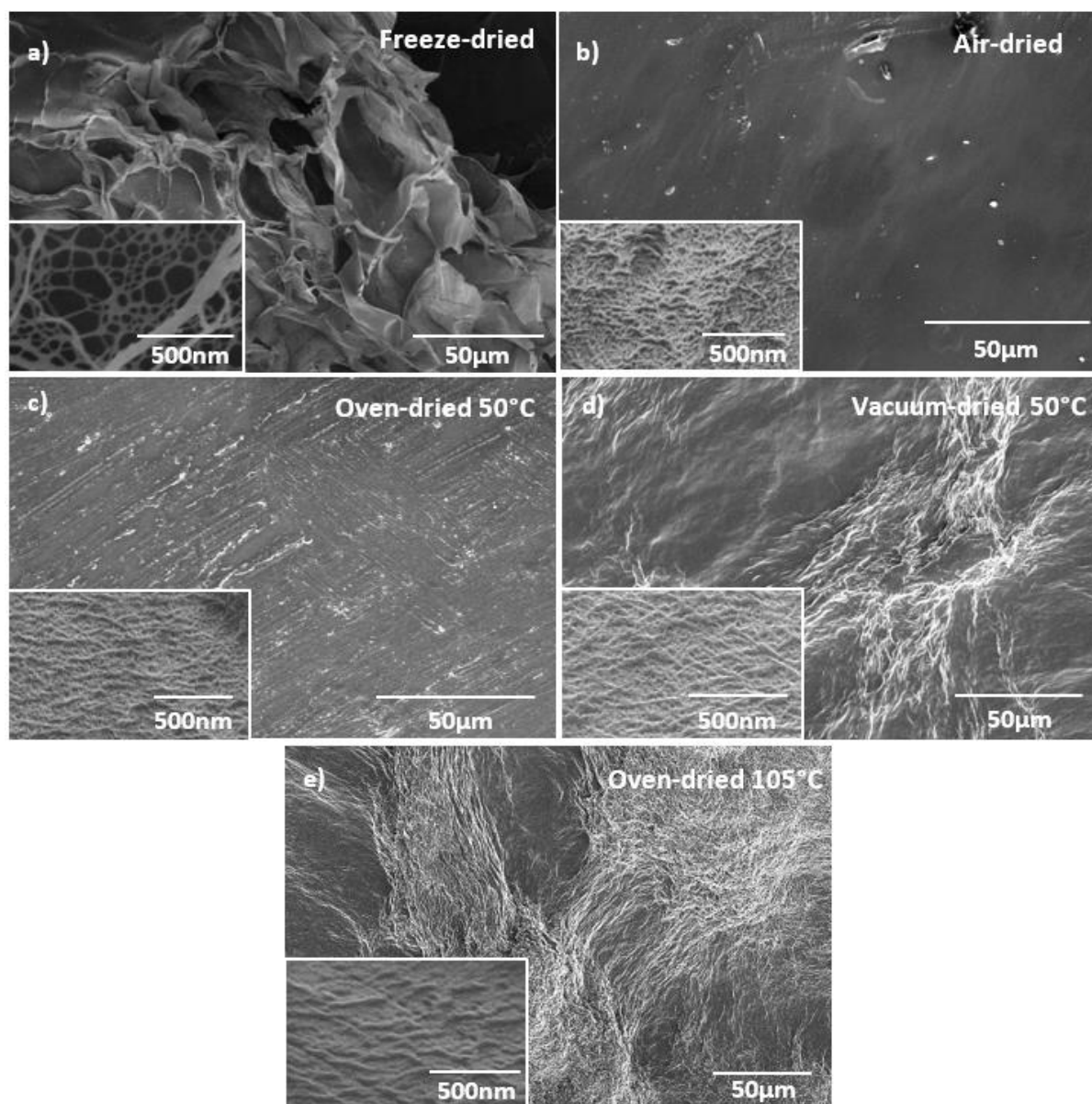
Figure 5. SEM micrographs of the nanocellulose superabsorbent produced by changing the drying rate with the drying methods: (a) freeze-drying, (b) air-dried, (c) oven-dried at 50 °C, (d) vacuum oven-dried at 50 °C and (e) oven-dried 105 °C.

Small angle X-ray scattering (SAXS) was used to evaluate the pore structure and their distribution in the superabsorbents (Figure 6). SAXS is a non -destructive method providing the morphology and distribution of nanoscale structures over a complete volume [35-37]. The pore structure and distribution of the superabsorbents are dependent on the drying technique. In SAXS, superabsorbents air-dried, oven-dried 50 °C and vacuum-dried at 50 °C display a uniform isotropic scattering. The pore size distribution from the SAXS curves were obtained

by modelling the scattering using the sphere shape model [38] combined with the lognormal pore distribution. The pore size distribution evaluated from SAXS curve fitting is similar to the pore distributions from mercury porosimetry (Figure 6d). However, the SAXS images of freeze-dried and oven-dried 105 °C superabsorbents show anisotropic scattering (Figure S3, see APPENDIX I) revealing the pores are not distributed in a particular direction. In both cases, the pore sizes are large and beyond the size range measurement of lab SAXS setup.
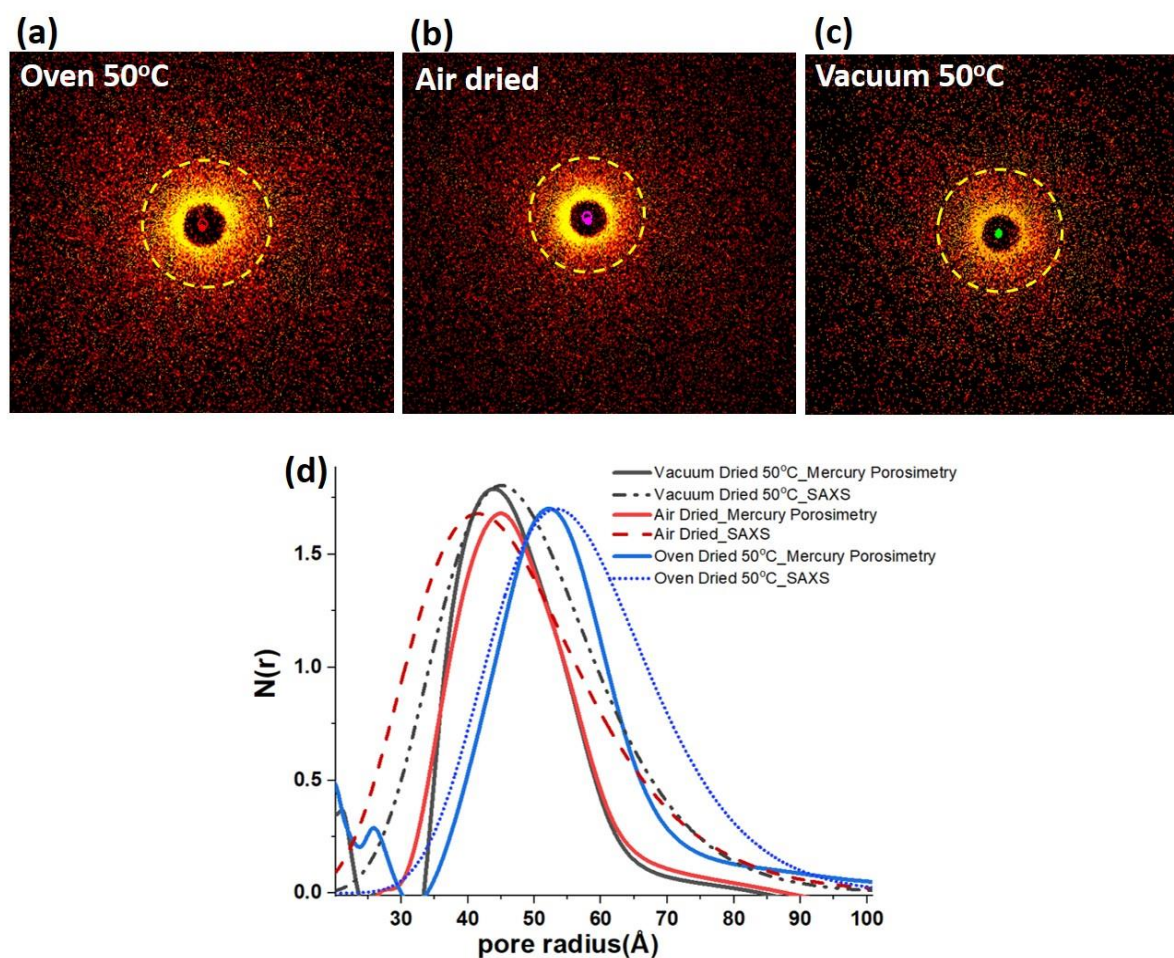
Figure 6. Small angle X-ray scattering (SAXs) images of the nanocellulose superabsorbent produced at different drying rates: (a) air-dried, (b) oven-dried at 50 °C, (c) vacuum oven-dried at 50 °C. (d) Pore distribution of SAXs and mercury porosimetry tests. SAXS images of freeze-dried and oven-dried at 105 °C displayed in Figure S3, APPENDIX I.

2.6.4 Phytotoxicity assays

To determine the effect of the superabsorbents in plants, a germination experiment was conducted. Radish and cress seeds were treated with three different concentrations of 2 types of superabsorbents: freeze-dried and oven-dried 50°C (to represent superabsorbents produced via evaporation). The mean time to germination (MTG) of both species is shown in Figure 7. There was no significant difference in the MTG between the dH_2O control (0 g/L) and the freeze-dried or oven-dried 50 °C treatments. The MTG remains constant in all cases.
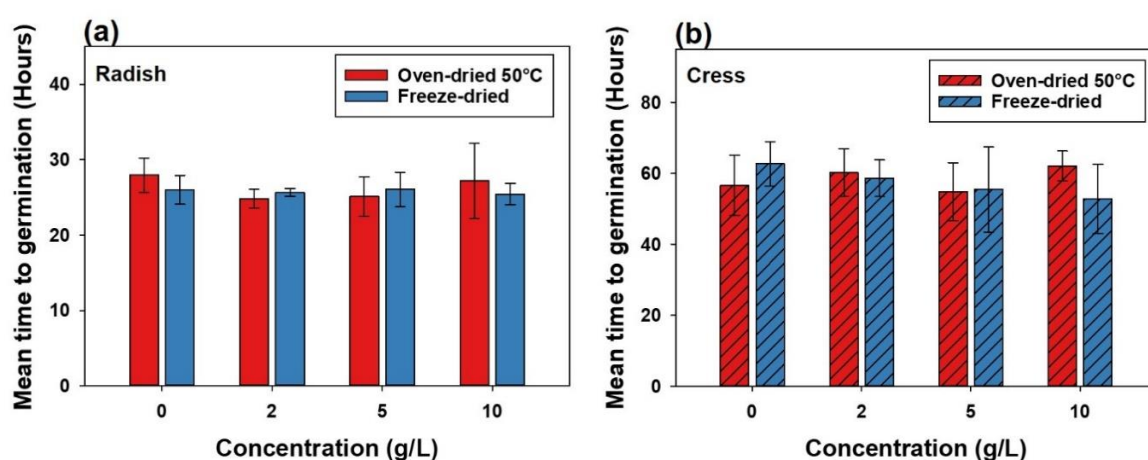
Figure 7. Mean time to germination of (a) radish and (b) cress in the presence of increasing concentrations of two different types of superabsorbents: oven-dried 50 °C and freeze-dried. Results are reported as mean ± standard deviation (n=4). Pictures of the phytotoxicity tests are shown in Figure S4, see APPENDIX I.

The germination index (GI) was calculated by measuring the radicle length of seeds grown on the superabsorbents for 48 h (Figure 8). Radish and cress seeds grown over freeze-dried superabsorbent show no significant difference between the dH_2O control and any of the freeze-dried concentrations. Radish seeds treated with oven-dried 50 °C superabsorbent exhibit an increase in GI between the concentrations of 2 to 5 g/L (compared with the control). In contrast, a slight decrease in GI is observed in cress seeds treated with oven-dried 50 °C superabsorbent at the highest concentration of 10 g/L.
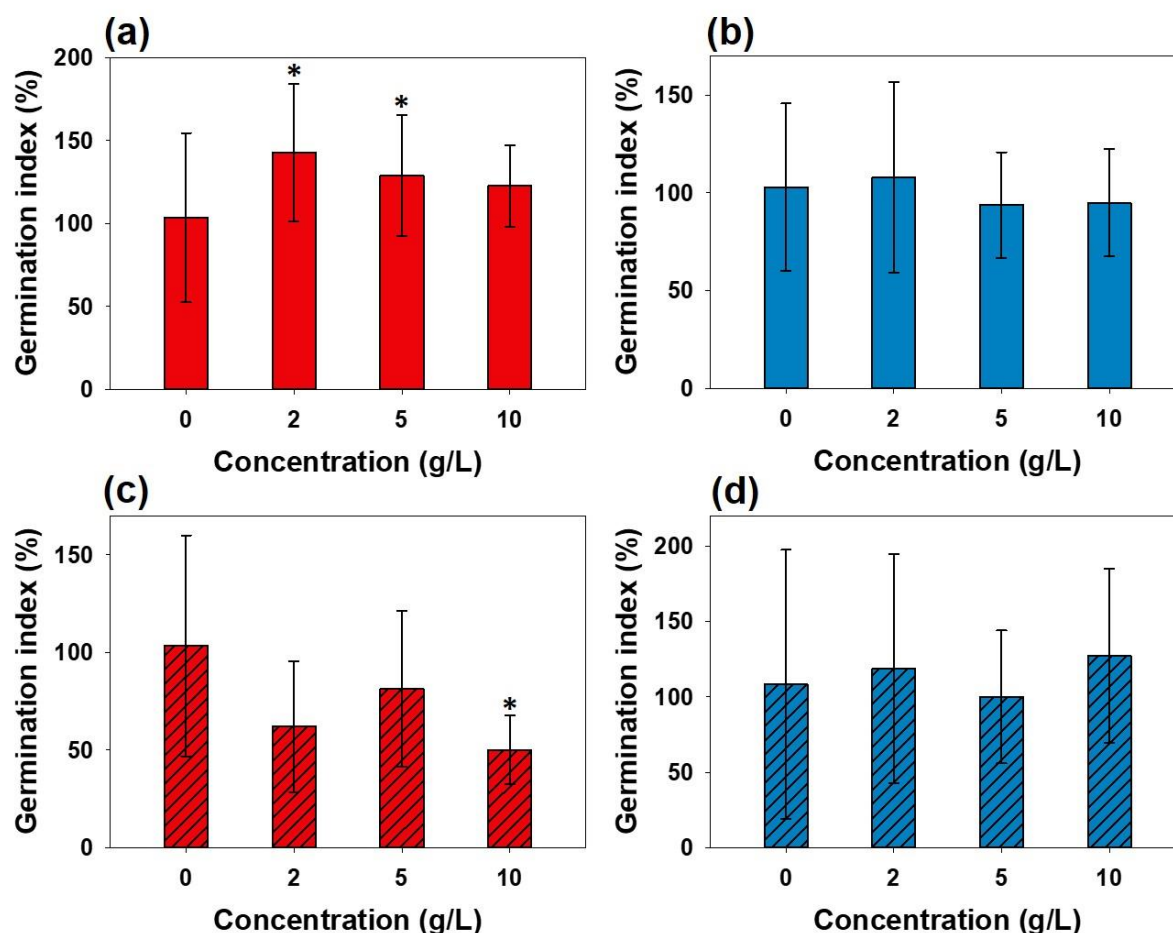
Figure 8. Germination index of radish species treated with (a) oven-dried 50 °C and (b) freeze-dried superabsorbents, and cress species treated with (c) oven-dried 50 °C and (d) freeze-dried superabsorbents. Statistical difference according to ANOVA analysis followed by Dunn's test against 0 g/L concentration as control indicated as *P < 0.05, N=4.

2.7 Discussion

2.7.1 Effect of drying rate on the superabsorbent structure and swelling rate

Nanocellulose-based superabsorbents of varying structures were prepared by adjusting the drying rate controlled with the drying mode. We raised the hypothesis that the rate of water removal from the hydrogel network controls its micro and nano structure. The effect of the structure on the swelling rate and superabsorption of nanocellulose was measured.

The structure of the superabsorbents was analysed by scanning electron microscopy (SEM), mercury porosimetry and small angle X-ray scattering (SAXS). While SEM provides three-dimensional and high-resolution images in a wide range of magnification, this technique is limited in quantifying material size and distribution [39]. Mercury porosimetry measures the pore size distribution which is used to calculate specific surface area and density. However, Hg porosiometry cannot quantify closed pores and measures the largest entrance of pores - not the actual inner size [40]. SAXS measurement generates the particle size, distribution and shape variations [37]. The combination of these three techniques can define the superabsorbent structure both at the micro and nanoscale with certainty.

Freeze-dried superabsorbent achieved the fastest absorption rate (Figure 1). This is due to their high porosity with the network of fibres forming pores ranging from 50 nm to 100 μm. Kuśtrowski et al. [41] also reported similar pore properties for fast-swelling polysaccharides superabsorbents. High porosity polymeric networks allow fast water diffusion across the superabsorbent [13]. In general, superabsorbents dried by evaporation have a much slower swelling rate, with around 10% of their capacity reached during the first minutes.

Two distinct regimes are observed in the swelling kinetics of nanocellulose superabsorbents: (i) a steep initial uptake of water and (ii) an asymptotical process towards the equilibrium swelling ratio. The effect of the drying technique on the swelling ratio was analysed using Schott's second-order kinetics model [42]

$$\frac{t}{Q_t} = \frac{1}{K_s Q_\infty^2} + \frac{1}{Q_\infty} t \tag{6}$$

where Q_∞ denotes the swelling capacity at equilibrium, K_s is the swelling rate constant, Q_t is the swelling capacity at time t. Because $K_{is} = K_s Q_\infty^2$, equation (6) can be expressed as:

$$\frac{t}{Q_t} = \frac{1}{K_{is}} + \frac{1}{Q_\infty} t \tag{7}$$

where K_{is} refers to the initial swelling rate constant [43]. Plots of the average swelling rate (t/Q_t) versus time (t) are displayed in Figure 9; the expected straight lines are achieved ($R^2 >$ 0.99) in all cases. This confirms that the swelling process follows a second-order kinetic model. This model successfully described semicrystalline polymers such as cellulose or gelatin [6, 42, 43].
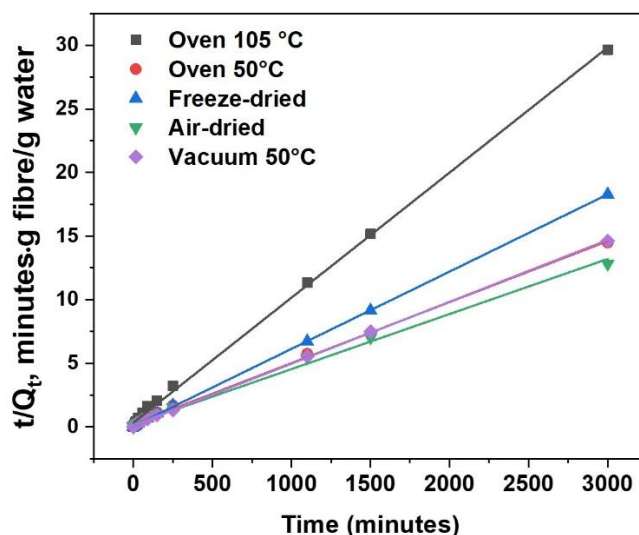
Figure 9. Plots of t/Qt vs t according to Eq. 7 based on the experimental data displayed in Figure 1.

The swelling kinetic parameters K_s, K_{is} and Q_∞ obtained from the slopes and intercepts of the plots (Figure 9) are listed in Table II. The theoretical absorption capacity at equilibrium (Q_{theo}) is similar to the experimental absorption capacity (Q_{actual}) in all cases. Both the initial (K_{is}) and actual (K_s) swelling rate constants varied accordingly to the drying technique. K_{is} indicates the point where the buffer solution has permeated the entire film but before the polymer network stress relaxation retards swelling [42]. For freeze-dried superabsorbents, high porosity and pore size speed up the diffusion rate of water molecules into the superabsorbent, resulting in the highest K_{is}. In contrast, air-dried superabsorbents present a K_{is} around four times lower which indicates a slower diffusion rate of water molecules induced by the material porosity.

The swelling rate constant, K_s, is related to the solvent diffusion and relaxation process of the polymer chains [44]. Low values K_s suggest a rate controlled by stress relaxation in the swelling polymer network- not by diffusion-controlled swelling [42]. Air-dried superabsorbent presented the lowest K_s. The water molecules in this material diffused throughout the material during the first hour of immersion as shown by their soft and transparent appearance; however, equilibrium swelling was reached after 24 h. This indicates that the rate determining process is stress relaxation of the fibre network driven by the osmotic swelling pressure [42]. The same absorption mechanism applies to oven-dried at 50 °C and vacuum-dried at 50 °C. Freeze-dried superabsorbent reached saturation during the first minutes of experiment, suggesting a diffusion driven process. For the oven-dried superabsorbents at 105 °C, the swelling rate constant is higher than those from the other drying evaporation techniques. This indicates superabsorbent reaching saturation at a faster rate due to hornification, result in superabsorbents of smaller pores and inaccessible carboxylate groups, lowering swelling capacity.

Table II. Swelling kinetic parameters of the different superabsorbents.

Type	Q_{actual} (g/g)	Q_{theo} (g/g)	K_{is} (g/g min)	K_s (10^{-5}, g/g min)
Oven-dried 105 °C	101.16	102.04	3.11	29.94
Oven-dried 50 °C	207.25	208.33	4.98	11.48
Freeze-dried	164.13	163.93	17.93	66.73
Air-dried	233.93	232.55	4.75	8.78
Vacuum 50 °C	205.43	204.08	9.95	23.91

2.7.2 Swelling capacity and water retention of nanocellulose superabsorbents

Two main variables are responsible for the superabsorption behaviour of nanocellulose. The first is porosity that enables diffusion of water molecules into the fibre network. This leads to

the physical entrapment of water loosely held between nanofibres by capillary forces [6]. The second is the superabsorbent surface area. This facilitates the interaction between water and carboxylate groups (COO^-) and promotes hydrogen bonding. The fibre network expands and accommodates the influx of water through the relaxation of fibres driven by osmotic pressure [22, 42]. The type of cations in the superabsorbent matrix also impacts water uptake [45]. However, only Na^+ was investigated in this study. Hence, the effects in the swelling capacity are directly related to the drying rate defining the structure of the superabsorbents.

Surprisingly, in all cases – except those dried at 105 °C – evaporative drying resulted in superabsorbents of higher swelling capacity than those produced by sublimation/freeze-drying. This contrasts from literature which reports that freeze-dried superabsorbent have higher absorption capacity than evaporative-dried superabsorbent [20, 22, 24, 46]. This is because hornification in evaporative drying produces capillary pressure-induced stresses, shrinking pores and decreasing swelling capacity [24, 25]. However, low-temperature drying and introducing anionic charges into the cellulose structure, such as carboxylate groups, minimise hornification of cellulose fibres [22, 25, 27]. These techniques were selected in our study.

Nevertheless, the high absorption capacity of our nanocellulose superabsorbents prepared by evaporative drying cannot be solely explained by the minimisation of hornification. Such performance is due to a combination of factors, all controlled by the drying rate. First, porosity and pore size enable physical entrapment of water into the superabsorbent network. This property is accentuated in freeze-dried superabsorbent having a porosity of >90%, which partly explains its absorption capacity [6]. The high absorption capacity of evaporative-dried superabsorbents is attributed largely to their high pore area higher than 45 m^2/g (Figure 10). This increases the number of accessible COO^- groups participating in hydrogen bonding with water compared to freeze-dried superabsorbents, increasing the interaction of water adsorbed

onto the polymer chains and swelling of the fibre network [47]. This, coupled with the pore size, lead to a stronger physical entrapment of water in between nanofibres by capillary forces.

These characteristics of evaporative-dried superabsorbents are given by rate of water removal. A relationship between this rate and the absorption capacity is observed. For these superabsorbents, Figures 1 and 2 show that the slower the drying rate, the higher the absorption capacity achieved. This is because slow rates lead to a more uniform arrangement of fibres, producing superabsorbents with macro, meso and micropores which results in high absorption capacity.

These hypotheses are also supported by the water retention values (WRV) shown in Figure 10. A relationship between the pore area and the WRV is observed. Evaporative dried superabsorbents – except for those oven-dried at 105 °C – exhibit high pore area and high-water retention properties, while freeze-dried superabsorbent shows low pore area and low WRV. This is attributed to the large pore size which promotes the release of water molecules from the superabsorbent matrix.
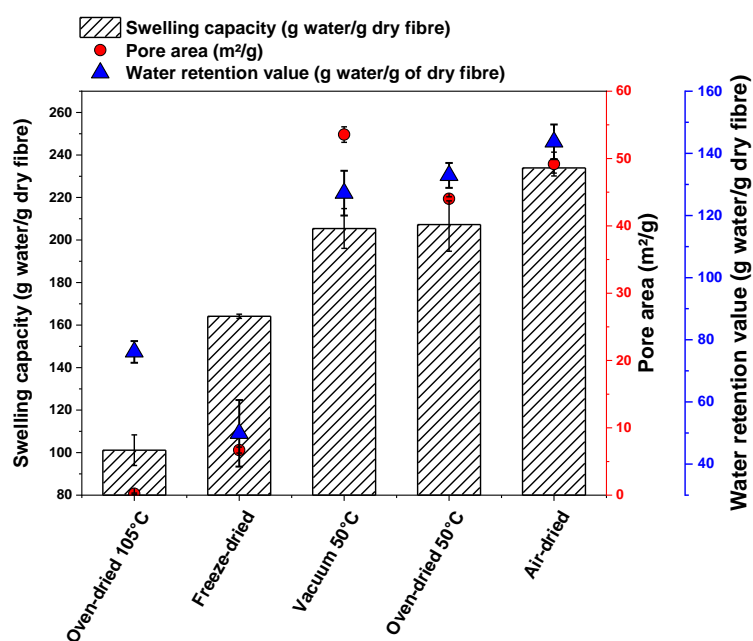
Figure 10. Relationship between the drying technique, the swelling capacity, pore area and water retention value of nanocellulose superabsorbent.

2.7.3 Importance of nanocellulose superabsorbent structure in agriculture

Seed germination is one of the most important phases in the life cycle of a plant and is highly dependent on the existing environment [48]. Seed germination bioassays and early stage seedling growth studies are commonly used for determining toxicity effects in plants. In the development of novel materials as growing media, the absence of phytotoxicity is the first requirement [11]. In this study, seed germination and early stage seedling growth tests of radish and cress were conducted on two materials: freeze-dried and oven-dried 50 °C. The freeze-dried superabsorbent was chosen because of its difference in morphology compared to evaporative-dried superabsorbents, while oven-dried 50°C was selected to represent superabsorbents dried via evaporation – the best condition for industrial scale production. Results show that any of the superabsorbents used in this study influenced the mean time to germination of either radish or cress seeds compared to the control (deionized water – dH_2O). This indicates that if seeds were to be grown in soil with nanocellulose superabsorbent, the time to emergence is unlikely to be affected, and hence its application in agriculture is safe for plants.

Moreover, radish seeds treated with oven-dried 50 °C exhibit an increase in the germination index by 30 – 40%. Such results are not observed in seeds treated with freeze-dried superabsorbent. This increase is attributed to the swelling kinetics of evaporative-dried superabsorbent being slower than freeze-dried superabsorbent, which increases the water availability at the early stage of seed germination. These positive effects confirm the results reported on superabsorbents improving seedling growth, regulating plants available water and reducing the detrimental effects produced by water stress [11, 49].

2.8 Conclusion

A series of nanocellulose superabsorbents varying in pore properties was characterized in structure and swelling behaviour for application as hydro retentor in agriculture. Nanocellulose superabsorbents were prepared from TEMPO oxidized cellulose superabsorbents [6]. The structure of the nanocellulose superabsorbent was controlled with the drying rate of the superabsorbent. This was engineered with the drying process. Five methods, each providing a different rate of water removal, were studied. These include: freeze-dried, air-dried, vacuum-dried at 50 °C, and oven-dried at 50 °C and 105 °C. The effect of drying on the superabsorbent structure, swelling capacity, absorption rate, water retention and seed germination was analysed.

The structure of the nanocellulose superabsorbent, measured in terms of porosity, pore volume and area, is governed by the drying technique used. This structure directly impacts swelling capacity and kinetics. Freeze-dried superabsorbents are characterised by a three-dimensional macroporous network of fibres and pores ranging from 50 nm to 100 µm, whereas evaporative-dried superabsorbents form two-dimensional network of entangled fibrils stacked on top of each other. The high porosity and large pore size of freeze-dried superabsorbents are responsible for their fastest absorption rate. These superabsorbents exhibit a diffusion-controlled swelling mechanism. The absorption mechanism of evaporative-dried superabsorbents is dictated by stress relaxation of the fibre network. Both mechanisms are described by a second-order kinetics model [42]. Air-dried superabsorbents have the highest swelling capacity. This is attributed to pore area and strong water bond interaction. Superabsorbents oven-dried at 105 °C have the lowest swelling capacity due to fibre hornification [25].

Seed germination of radish and cress seeds demonstrates that the nanocellulose-based superabsorbents tested in this study are suitable for agricultural use; the SAP performance was independent of the drying process. This study identified evaporative drying as the best drying technique to produce high capacity superabsorbents. This technique is far easier and cheaper than freeze-drying, decreasing production costs of nanocellulose superabsorbents.

2.9 Acknowledgement

2.10 References

[1]   J. R. Gross, "The Evolution of Absorbent Materials," in *Studies in Polymer Science*, vol. 8, L. Brannon-Peppas and R. S. Harland Eds.: Elsevier, 1990, pp. 3-22.

[2]   E. M. Ahmed, "Hydrogel: Preparation, characterization, and applications: A review," *Journal of Advanced Research,* vol. 6, no. 2, pp. 105-121, 2015/03/01/ 2015, doi: https://doi.org/10.1016/j.jare.2013.07.006.

[3]   S. Ghorbani *et al.*, "Hydrogels Based on Cellulose and its Derivatives: Applications, Synthesis, and Characteristics," *Polymer Science, Series A,* vol. 60, no. 6, pp. 707-722, 2019, doi: 10.1134/s0965545x18060044.

[4]   X. Shen, J. L. Shamshina, P. Berton, G. Gurau, and R. D. Rogers, "Hydrogels based on cellulose and chitin: fabrication, properties, and applications," *Green Chemistry,* 10.1039/C5GC02396C vol. 18, no. 1, pp. 53-75, 2016, doi: 10.1039/C5GC02396C.

[5]   R. Curvello, V. S. Raghuwanshi, and G. Garnier, "Engineering nanocellulose hydrogels for biomedical applications," *Advances in Colloid and Interface Science,* vol. 267, pp. 47-61, 2019/05/01/ 2019, doi: https://doi.org/10.1016/j.cis.2019.03.002.

[6]   L. Mendoza, L. Hossain, E. Downey, C. Scales, W. Batchelor, and G. Garnier, "Carboxylated nanocellulose foams as superabsorbents," *J Colloid Interface Sci,* vol. 538, pp. 433-439, Mar 7 2019, doi: 10.1016/j.jcis.2018.11.112.

[7]   H. M. Shewan and J. R. Stokes, "Review of techniques to manufacture micro-hydrogel particles for the food industry and their applications," *Journal of Food Engineering,* vol. 119, no. 4, pp. 781-792, 2013/12/01/ 2013, doi: https://doi.org/10.1016/j.jfoodeng.2013.06.046.

[8]   A. Bashari, A. Rouhani Shirvan, and M. Shakeri, "Cellulose-based hydrogels for personal care products," *Polymers for Advanced Technologies,* vol. 29, no. 12, pp. 2853-2867, 2018, doi: 10.1002/pat.4290.

[9]   S. Basak, N. Nandi, S. Paul, I. W. Hamley, and A. Banerjee, "A tripeptide-based self-shrinking hydrogel for waste-water treatment: removal of toxic organic dyes and lead (Pb2+) ions," *Chemical Communications,* 10.1039/C7CC01774J vol. 53, no. 43, pp. 5910-5913, 2017, doi: 10.1039/C7CC01774J.

[10]   T. M. Neethu, P. K. Dubey, and A. R. Kaswala, "Prospects and Applications of Hydrogel Technology in Agriculture," *International Journal of Current Microbiology and Applied Sciences,* vol. 7, no. 05, pp. 3155-3162, 2018, doi: 10.20546/ijcmas.2018.705.369.

[11]   F. F. Montesano, A. Parente, P. Santamaria, A. Sannino, and F. Serio, "Biodegradable Superabsorbent Hydrogel IncreasesWater Retention Properties of Growing Media and Plant Growth," *Agriculture and Agricultural Science Procedia,* vol. 4, pp. 451-458, 2015, doi: 10.1016/j.aaspro.2015.03.052.

[12]   M. J. Zohuriaan-Mehr, Kabiri, Kourosh.,, "Superabsorbent Polymer Materials: A review," *Iranian Polymer Journal,* vol. 17, no. 6, pp. 451-477, 2008.

[13]   M. R. Guilherme *et al.*, "Superabsorbent hydrogels based on polysaccharides for application in agriculture as soil conditioner and nutrient carrier: A review," *European Polymer Journal,* vol. 72, pp. 365-385, 2015, doi: 10.1016/j.eurpolymj.2015.04.017.

[14]   M. R. Guilherme, A. V. Reis, A. T. Paulino, T. A. Moia, L. H. C. Mattoso, and E. B. Tambourgi, "Pectin-based polymer hydrogel as a carrier for release of agricultural nutrients and removal of heavy metals from wastewater," *Journal of Applied Polymer Science,* pp. n/a-n/a, 2010, doi: 10.1002/app.32123.

[15]   J. Zhang, L. Wang, and A. Wang, "Preparation and Swelling Behavior of Fast-Swelling Superabsorbent Hydrogels Based On Starch-g-Poly(acrylic acid-co-sodium acrylate)," *Macromolecular Materials and Engineering,* vol. 291, no. 6, pp. 612-620, 2006, doi: 10.1002/mame.200500387.

[16]   S. Varanasi, R. He, and W. Batchelor, "Estimation of cellulose nanofibre aspect ratio from measurements of fibre suspension gel point," *Cellulose,* vol. 20, no. 4, pp. 1885-1896, 2013, doi: 10.1007/s10570-013-9972-9.

[17]   S. M. F. Kabir, P. P. Sikdar, B. Haque, M. A. R. Bhuiyan, A. Ali, and M. N. Islam, "Cellulose-based hydrogel materials: chemistry, properties and their prospective applications," *Prog Biomater,* vol. 7, no. 3, pp. 153-174, Sep 2018, doi: 10.1007/s40204-018-0095-0.

[18]   Q. Li, S. McGinnis, C. Sydnor, A. Wong, and S. Renneckar, "Nanocellulose Life Cycle Assessment," *ACS Sustainable Chemistry & Engineering,* vol. 1, no. 8, pp. 919-928, 2013/08/05 2013, doi: 10.1021/sc4000225.

[19]   A. Isogai, T. Saito, and H. Fukuzumi, "TEMPO-oxidized cellulose nanofibers," *Nanoscale,* 10.1039/C0NR00583E vol. 3, no. 1, pp. 71-85, 2011, doi: 10.1039/C0NR00583E.

[20]   N. Lavoine and L. Bergström, "Nanocellulose-based foams and aerogels: processing, properties, and applications," *Journal of Materials Chemistry A,* vol. 5, no. 31, pp. 16105-16117, 2017, doi: 10.1039/c7ta02807e.

[21]   K. J. De France, T. Hoare, and E. D. Cranston, "Review of Hydrogels and Aerogels Containing Nanocellulose," *Chemistry of Materials,* vol. 29, no. 11, pp. 4609-4631, 2017/06/13 2017, doi: 10.1021/acs.chemmater.7b00531.

[22]   I. H. Mondal, *Cellulose-Based Superabsorbent Hydrogels* (Polymers and Polymeric Composites: A Reference Series). 2019.

[23]   Z. Pakowski, "Modern Methods of Drying Nanomaterials," *Transport in Porous Media,* vol. 66, no. 1-2, pp. 19-27, 2006, doi: 10.1007/s11242-006-9019-x.

[24] N. Buchtová and T. Budtova, "Cellulose aero-, cryo- and xerogels: towards understanding of morphology control," *Cellulose,* journal article vol. 23, no. 4, pp. 2585-2595, August 01 2016, doi: 10.1007/s10570-016-0960-8.

[25] M. Beaumont, J. König, M. Opietnik, A. Potthast, and T. Rosenau, "Drying of a cellulose II gel: effect of physical modification and redispersibility in water," *Cellulose,* vol. 24, no. 3, pp. 1199-1209, 2017, doi: 10.1007/s10570-016-1166-9.

[26] N. Butchosa and Q. Zhou, "Water redispersible cellulose nanofibrils adsorbed with carboxymethyl cellulose," *Cellulose,* journal article vol. 21, no. 6, pp. 4349-4358, December 01 2014, doi: 10.1007/s10570-014-0452-7.

[27] T. Lindstrom, Carlsson, G., , "The effect of carboxyl groups and their ionic form during drying on the hornification of cellulose fibers," *svensk papperstidning,* p. R146, 1982.

[28] S. Ang, V. Haritos, and W. Batchelor, "Cellulose nanofibers from recycled and virgin wood pulp: A comparative study of fiber development," *Carbohydrate Polymers,* vol. 234, p. 115900, 2020/04/15/ 2020, doi: https://doi.org/10.1016/j.carbpol.2020.115900.

[29] T. Saito and A. Isogai, "TEMPO-Mediated Oxidation of Native Cellulose. The Effect of Oxidation Conditions on Chemical and Crystal Structures of the Water-Insoluble Fractions," *Biomacromolecules,* vol. 5, no. 5, pp. 1983-1989, 2004/09/01 2004, doi: 10.1021/bm0497769.

[30] *Urine-absorbing aids for incontinence - Test methods for characterizing polymer-based absorbent materials* ISO 17190-6, Geneva, 2001.

[31] J. W. Qingzheng Cheng, Joseph F. McNeel, Peter M. Jacobson,, "Water retention value measurements of cellulosic materials using a centrifuge technique," *BioResources,* vol. 5, no. 3, pp. 1945-1954, 2010.

[32] S. Karnani and Viji. "Hydrogel Agriculture Technology." http://vikaspedia.in/agriculture/best-practices/sustainable-agriculture/crop-management/hydrogel-agriculture-technology (accessed 06/02/2020, 2020).

[33] K. P. Mosse, A. F. Patti, E. W. Christen, and T. R. Cavagnaro, "Winery wastewater inhibits seed germination and vegetative growth of common crop species," *J Hazard Mater,* vol. 180, no. 1-3, pp. 63-70, Aug 15 2010, doi: 10.1016/j.jhazmat.2010.02.069.

[34] IUPAC, *Compendium of Chemical Terminology, 2nd ed. (the "Gold Book")*. Oxford: Blackwell Scientific Publications, 1997.

[35] V. S. Raghuwanshi *et al.*, "Cationic polyacrylamide induced nanoparticles assembly in a cellulose nanofiber network," *Journal of Colloid and Interface Science,* vol. 529, pp. 180-186, 2018/11/01/ 2018, doi: https://doi.org/10.1016/j.jcis.2018.06.009.

[36] V. S. Raghuwanshi, U. M. Garusinghe, J. Ilavsky, W. J. Batchelor, and G. Garnier, "Effect of nanoparticles size and polyelectrolyte on nanoparticles aggregation in a cellulose fibrous matrix," *Journal of Colloid and Interface Science,* vol. 510, pp. 190-198, 2018/01/15/ 2018, doi: https://doi.org/10.1016/j.jcis.2017.09.064.

[37] O. Glatter and O. Kratky, *Small angle x-ray scattering*. London, New York: Academic Press, 1982.

[38] V. S. Raghuwanshi, M. Ochmann, F. Polzer, A. Hoell, and K. Rademann, "Self-assembly of gold nanoparticles on deep eutectic solvent (DES) surfaces," *Chemical Communications,* 10.1039/C4CC02588A vol. 50, no. 63, pp. 8693-8696, 2014, doi: 10.1039/C4CC02588A.

[39] L. C. Gomes, J. M. R. Moreira, M. Simões, L. F. Melo, and F. J. Mergulhão, "Biofilm localization in the vertical wall of shaking 96-well plates," (in eng), *Scientifica (Cairo),* vol. 2014, pp. 231083-231083, 2014, doi: 10.1155/2014/231083.

[40] H. Giesche, "Mercury Porosimetry: A General (Practical) Overview," *Particle & Particle Systems Characterization,* vol. 23, no. 1, pp. 9-19, 2006/06/01 2006, doi: 10.1002/ppsc.200601009.

[41]   P. Kuśtrowski, P. Natkański, A. Rokicińska, and E. Witek, "Polymer Hydrogel-Clay (Nano)Composites," in *Polymer Gels*, (Gels Horizons: From Science to Smart Materials, 2018, ch. Chapter 1, pp. 1-62.

[42]   H. Schott, "Swelling kinetics of polymers," *Journal of Macromolecular Science, Part B,* vol. 31, no. 1, pp. 1-9, 2006, doi: 10.1080/00222349208215453.

[43]   X. Shi, W. Wang, and A. Wang, "pH-responsive sodium alginate-based superporous hydrogel generated by an anionic surfactant micelle templating," *Carbohydrate Polymers,* vol. 94, no. 1, pp. 449-455, 2013/04/15/ 2013, doi: https://doi.org/10.1016/j.carbpol.2013.01.019.

[44]   F. Rosa, J. Bordado, and M. Casquilho, "Kinetics of water absorbency in AA/AMPS copolymers: applications of a diffusion–relaxation model," *Polymer,* vol. 43, no. 1, pp. 63-70, 2002/01/01/ 2002, doi: https://doi.org/10.1016/S0032-3861(01)00596-1.

[45]   I. Homma, H. Fukuzumi, T. Saito, and A. Isogai, "Effects of carboxyl-group counter-ions on biodegradation behaviors of TEMPO-oxidized cellulose fibers and nanofibril films," *Cellulose,* vol. 20, no. 5, pp. 2505-2515, 2013, doi: 10.1007/s10570-013-0020-6.

[46]   J. Nemoto, T. Soyama, T. Saito, and A. Isogai, "Nanoporous networks prepared by simple air drying of aqueous TEMPO-oxidized cellulose nanofibril dispersions," *Biomacromolecules,* vol. 13, no. 3, pp. 943-6, Mar 12 2012, doi: 10.1021/bm300041k.

[47]   Z. Xia, M. Patchan, J. Maranchi, J. Elisseeff, and M. Trexler, "Determination of crosslinking density of hydrogels prepared from microcrystalline cellulose," *Journal of Applied Polymer Science,* vol. 127, no. 6, pp. 4537-4541, 2013, doi: 10.1002/app.38052.

[48]   A. G. Rombola *et al.*, "Relationships between Chemical Characteristics and Phytotoxicity of Biochar from Poultry Litter Pyrolysis," *J Agric Food Chem,* vol. 63, no. 30, pp. 6660-7, Aug 5 2015, doi: 10.1021/acs.jafc.5b01540.

[49]   M. K. Akhter J., Malik K.A., Mardan A., Ahmad M., M.M. Iqbal, "Effects of hydrogel amendment on water storage of sandy loam and loam soils and seedling growth of barley, wheat and chickpea," *Plant, Soil and Environment,* vol. 50, no. 10, pp. 463-469, 2004.

THIS PAGE HAS BEEN INTENTIONALLY LEFT BLANK

THIS PAGE HAS BEEN INTENTIONALLY LEFT BLANK

CHAPTER 3:

EFFECT OF THE COUNTER-ION ON NANOCELLULOSE HYDROGELS AND THEIR SUPERABSORBENT STRUCTURE AND PROPERTIES

THIS PAGE HAS BEEN INTENTIONALLY LEFT BLANK

PREFACE

The TEMPO-mediated oxidation of cellulose produces a material where a significant number of primary hydroxyl groups on the fibre surfaces are oxidised to carboxyl groups. These are isolated in the sodium carboxylate form (i.e. COO^-Na^+). The sodium ion is readily exchangeable with other cations. Previous studies have revealed that the swelling performance of the SAPs varies depending on the ionic strength of the external solution. However, only limited ions such as Mg^{2+} or Ca^{2+}, and under specific preparation protocols, have been tested. Understanding how the superabsorption performance is affected by the type of cation is important especially for applications in agricultural soils, where there is a natural mixture of exchangeable cations including Zn^{2+}, Mg^{2+}, K^+ and Na^+. This chapter evaluated the effect of different cations on the nanocellulose hydrogel and SAP properties. Four ions of valency one: H^+, K^+, Na^+ and NH_4^+, and three ions of valency two, Ca^{2+}, Mg^{2+} and Zn^{2+} were tested. The addition of the desired cations, as well as the amount, was confirmed through Fourier Transform Infrared spectroscopy (FT-IR) and Inductively Coupled Plasma Optical Emission Spectroscopy (ICP-OES). The rheology of the hydrogels was analysed and the pore properties of the SAP produced were characterised using mercury porosimetry and scanning electron microscopy. The absorption capacity and kinetics were measured and linked to the SAP pore properties, which were related to the type of cation.

This published chapter in the *Journal of Colloid and Interface Science* addresses the second objective, which is to determine the effect of the nanocellulose cation on the gelation mechanism and superabsorbent structure and properties by exchanging the current Na^+ ions present in the oxidised nanocellulose for different ions such as Mg^{2+}, NH_4^+ and K^+. The studies performed in this chapter provided the basis to understand how the superabsorbent behaves in the soil environment where a range of such cations exist.

THIS PAGE HAS BEEN INTENTIONALLY LEFT BLANK

Chapter 3: Effect of the counter-ion on nanocellulose hydrogels and their superabsorbent structure and properties

THIS PAGE HAS BEEN INTENTIONALLY LEFT BLANK

Effect of the counter-ion on nanocellulose hydrogels and their superabsorbent structure and properties

Ruth Barajas-Ledesma[a], Laila Hossain[a], Vanessa N.L. Wong[b], Antonio Patti[c] and Gil Garnier[a*]

[a]Bioresource Processing Research Institute of Australia (BioPRIA) and Department of Chemical Engineering, Monash University, Clayton, VIC 3800, Australia
[b]School of Earth, Atmosphere & Environment, Monash University, Clayton, VIC 3800, Australia
[c]School of Chemistry, Monash University, Clayton, VIC 3800, Australia

*For correspondence: Gil.Garnier@Monash.edu

3.1 Abstract

Hypothesis: Carboxylated nanocellulose gels and superabsorbents (SAPs) can be engineered by ion exchange of TEMPO treated cellulose fibers with different cations prior to shearing, thus creating a nanofibrous network ionically cross-linked. The structure and properties of these materials are highly influenced by the type of counter-ion used as it controls both the degree of fibrillation and crosslinking.

Experiments: Functionalised nanocellulose SAPs were made using TEMPO-mediated oxidation followed by ion-exchange before fibrillation into a hydrogel and freeze-drying. Seven different cations were tested: 4 of valency 1 (H, Na, K, NH_4), and 3 of valency 2 (Ca, Mg, and Zn). The effect of the counter-ion on the gelation mechanism and the superabsorbent performance was evaluated. The SAP absorption capacity in deionised water was related to the superabsorbent structure and morphology.

Findings: The gel stability of nanocellulose superabsorbents is governed by the counter-ion type and valency. The viscoelastic properties of all nanocellulose hydrogels are controlled by its elastic regime, that is storage modulus (G') > loss modulus (G''). The type of cation dictates

the rheology of these gels by altering the fibrillation efficiency due to the extent of ionic cross-links occurring before and after fibrillation. The driving force for gelation in monovalent gels is due to the coupling of nanofibrils by physical interactions, creating an electrostatic stabilisation of the ionised COO^- groups at high shear forces. Cation – carboxylate interactions dominate the gelation in divalent gels by supressing the repulsive charges generated by the COO^- and also creating interfibril connections via ionic-crosslinks, as confirmed by the zeta potentials. The superabsorption performance is dominated by the counter-ion and is in the order of: $NH_4^+ > K^+ > Na^+ > Mg^{2+} > Zn^{2+} > Ca^{2+}$. NH_4^+-SAPs present the slowest kinetics and the highest absorption capacity. Their high pore area, which extends the number of accessible carboxyl groups that participate in hydrogen bonding with water, is responsible for this behaviour. Nanocellulose SAPs are attractive renewable materials, suited for many applications, including as nutrient cation carriers in agriculture.

3.2 Keywords

Carboxylated nanocellulose, TEMPO, cation, valency, superabsorbent, gelation, hydrogel, foam, aerogel.

3.3 Graphical Abstract
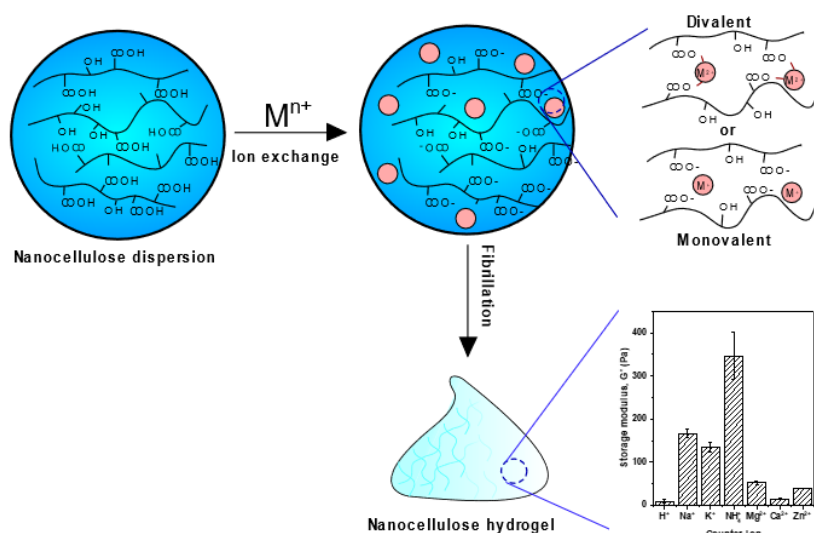
3.4 Introduction

Hydrogels are characterised by cross-linked networks of hydrophilic polymers that hold large amounts of water and remain stable [1-4]. The gelation mechanism is controlled by the density and type of cross-linking, physical or chemical. For physically cross-linked hydrogels, gelation is due to physical interacting forces such as van der Waals, hydrogen bonding, electrostatic and chain entanglements, among others [5]. Chemically cross-linked hydrogels undergo chemical reactions that covalently cross-link the polymer network. These hydrogels are typically strong and permanent [5]. The formation of ionically-crosslinked hydrogels has been reported when metal salts are added to the polymer network, inducing gelation by screening repulsive charges [6, 7].

Hydrogels can be used as superabsorbent polymers (SAPs) by removing the water of the network which, for nanocellulose, is often achieved by freeze-drying [8, 9]. The resulting material from freeze-drying appears as a foamy-like structure, also referred to as nanocellulose foam or aerogel [8, 10]. Their swelling is dictated by the movement of the counter-ions from outside to inside the superabsorbent, causing an osmotic pressure difference across the network [11]. These materials are found in numerous applications such as hygiene and personal care products [12], agriculture [13] and biomedicine [14]. In agriculture, SAPs can act as soil conditioners, increasing plant water availability and soil water retention [15, 16], and as slow release fertilisers or nutrient carriers [16].

The majority of the available superabsorbents are fossil fuel derived polymers which degrade slowly and raise health and environmental concerns due to the formation of microplastic particles that can be harmful to soil biota [17-19]. These environmental issues have driven the development of superabsorbents from natural polymers, especially those made of starch [20], pectin [21], alginate [22], or cellulose [23, 24]. Among these, cellulose, the most abundant

carbohydrate and biopolymer on earth, is often preferred as source material due to its biodegradability, availability and hydrophilicity [16, 25]. Cellulose-based SAPs can be produced through the 2,2,6,6-tetramethylpiperidine-1-oxyl (TEMPO)-mediated oxidation of cellulose followed by (freeze)drying. This process converts the primary alcohol groups of cellulose into sodium carboxylate groups [26], and adds the required electrostatic repulsion which forms nanocellulose hydrogels upon mechanical fibrillation. Nanocellulose-based SAPs are regarded as highly-porous materials with high swelling and water retention properties [8, 27].

The sodium ions present in the polymer matrix are not desirable for agricultural related applications of nanocellulose superabsorbents. Adding sodium to soils will have an adverse effect on soil structure, oxygen and water availability and can impose a stress on growing crops, resulting in a decrease of yields or crop failure [28]. The exchange of the counter-ion with others can tailor this material not only as a superabsorbent, but also as a nutrient carrier for plants. Literature suggests that the cation can significantly influence the properties of cellulose-based materials. Homma, Fukuzumi, Saito and Isogai [29] found that the biodegradation rate of TEMPO-oxidised nanofibril films is greatly influenced by the counter-ion; Na^+ is reported to have the fastest rate and Cu^{2+} the lowest. Dong, Snyder, Williams and Andzelm [6] revealed that the storage modulus (G') of cellulose nanofibril hydrogels increases with increasing valency of the metal cation and is strongly associated to the binding energy of the COO^- groups with the nanofibers. Yang, Xu and Han [7] showed that cellulose nanofibers (CNF) covalently cross-linked with polyacrylamide (PAM) can be reinforced with multivalent cations to create hydrogels of high stiffness and toughness. The addition of these ionic-links between the metal cation and CNF improves hardness and elasticity by 600% compared to pristine gels.

Ionically cross-linked nanocellulose hydrogels can be prepared by subjecting the TEMPO-oxidised nanocellulose to an aqueous salt solution before or after fibrillation, with most of the

studies using the latter. This technique consists on adding the salt solution dropwise to a dispersion of TEMPO-oxidised cellulose nanofibers, without stirring, which are left standing overnight [6, 7, 30, 31]. This process selectively substitutes the sodium ions present in the dispersion with another ion of stronger affinity. However, this technique is not only slow – which can sometimes take up to 5 days [30]- but also challenging to scale up, thus limiting the application range.

While several studies investigated the effect that different metal cations have on the gelation of nanocellulose-based hydrogels, none have studied the effect of the different cations on the viscoelastic properties of nanocellulose hydrogels nor associated those to the superabsorption performance. Similarly, while some studies suggested that the addition of salt solution after fibrillation results in the formation of heterogenous clumps and the loss of the gel structure [32], the effect of the cation on the fibrillation efficiency upon homogenisation is unknown.

Here, TEMPO-mediated oxidation was used to prepare carboxylated nanocellulose hydrogels. The oxidised fibres were subjected to an acid wash with HCl to remove all Na^+ cations present, followed by fibre re-suspension in different salt solutions, homogenisation and freeze-drying. The fibrillation efficiency, hydrogel rheology and SAP structure and swelling properties were measured. This study innovates by the technique used to prepare ionically cross-linked SAPs. The addition of these cations can not only assist in the transition of the superabsorbent as a hydro-retentor material to a nutrient carrier material for applications in sustainable agriculture, but can also help in understanding the behaviour of superabsorbent in soils where there is a natural mixture of exchangeable cations, including Ca^{2+}, Mg^{2+} and K^+.

3.5 Materials and Methods

3.5.1 Materials

Bleached Eucalyptus Kraft (BEK) pulp was provided by Australian Paper, Maryvale, Australia with a chemical composition of cellulose (78.8% $\pm$ 0.8), hemicellulose (17.7% $\pm$ 0.4), lignin (3.2% $\pm$ 0.1), extractives (0.3% $\pm$ 0.1) and ash (0.2% $\pm$ 0.1)[33]. Sodium hypochlorite (NaClO) at 12% w/v was purchased from Thermo Fisher Scientific and used as received. 2,2,6,6-Tetramethylpiperidine-1-oxyl (TEMPO) and Sodium bromide (NaBr) were purchased from Sigma-Aldrich. Sodium hydroxide (NaOH) and hydrochloric acid (HCl) were purchased from ACL Laboratories and Merck, respectively, and diluted for solutions as needed. Zinc sulfate monohydrate (ZnSOz_4.H$_2$O), sodium sulfate anhydrous (Na$_2$SO$_4$), ammonium sulfate ((NH$_4$)$_2$SO$_4$) and potassium sulfate (K$_2$SO$_4$) were purchased from Sigma-Aldrich. Calcium sulfate hemihydrate (CaSO$_4$.½H$_2$O) and Copper (II) sulfate pentahydrate (CuSO$_4$.5H$_2$O) were purchased from Westlab. Magnesium sulfate anhydrous (MgSO$_4$) was purchased from Merck. 70% Nitric acid (HNO$_3$) was purchased from Ajax Finechem.

3.5.2 Synthesis of carboxylated cellulose

The oxidation process was based on a previously developed method [26]. In brief, 25 g of BEK pulp (dry basis) was dispersed in 2500 mL of water with 2.5 g and 0.4 g of dissolved sodium bromide and TEMPO, respectively. Prior to the oxidation process, the sodium hypochlorite at 12% w/v was adjusted to pH 10 through the addition of hydrochloric acid at 36% w/v. To achieve a carboxylate content of 1.4 mmol/g of dry fibre, 100 mL of sodium hypochlorite was added drop-wise to the suspension whilst stirring. The pH of the reaction was maintained at 10 by adding 0.5 M NaOH. The reaction was complete when the change in pH was negligible. The oxidised cellulose was washed with deionised water, filtrated and stored refrigerated at 4 °C until required. The sodium carboxylate content of the TEMPO oxidised cellulose was 1.4 mmol/g dry fibre and was measured by conductivity titration [34].

3.5.3 Ion exchange treatment of carboxylated cellulose

The ion exchange treatment employed was based on a previously reported method [29]. Briefly, 1 g of the TEMPO-oxidised fibres, containing sodium carboxylate groups, was suspended in 1 L of 0.01 M HCl and stirred for 1 h. The oxidised cellulose pulp was later washed with Milli-Q water and filtrated. The oxidised pulp with protonated carboxyl groups was then re-suspended in 1 L of salt solution and stirred for 3 h at room temperature. The number of moles of salt dissolved in the suspension was fixed to be 10 times as much as the calculated carboxylate groups present in the oxidised cellulose. After 3 h, the salt treated cellulose fibres were washed with Milli-Q water, filtrated and stored refrigerated at 4 °C until required. The following solutions were used for the ion-exchange treatment: hydrochloric acid (HCl), sodium sulfate (Na_2SO_4), zinc sulfate ($ZnSO_4$), potassium sulfate (K_2SO_4), ammonium sulfate (($NH_4)_2SO_4$), copper (II) sulfate ($CuSO_4$), calcium sulfate ($CaSO_4$), magnesium sulfate ($MgSO_4$). Sulfate anion salts were selected to negate the effect of the anion and for its suitability for agriculture.

3.5.4 Preparation of nanocellulose hydrogel and superabsorbent

To prepare the nanocellulose hydrogel, the TEMPO-oxidised fibres treated with the various counter-ions were suspended in Milli-Q water to achieve a concentration of solids of 0.5% w/v and fibrillated through high pressure homogenisation (GEA Niro Soavi Homogeniser Panda) at 800 bar and two passes. To produce the nanocellulose superabsorbent, the resulting hydrogel from homogenisation was stored for at least 12 h at -80°C and freeze-dried for 48 h using a Christ Alpha 2-4 LD Plus.

3.5.5 Characterisation

Freeze-dried nanocellulose SAP was characterised using a Fourier Transform Infrared (FTIR) spectrometer (Agilent Technologies Cary 630 FTIR).

The counter-ion content in nanocellulose hydrogels was analysed by either elemental analysis (HCNS) using a Perkin Elmer 2400 Series II analyser, for NH_4^+ and H^+ gels, or by inductively coupled plasma – optical emission spectrometry (ICP-OES), for all other ions. For ICP-OES analysis, 3 g of nanocellulose hydrogel was placed in crucibles and ashed using a muffle furnace, based on a previously reported method [35]. Temperature was ramped to 600 °C over 3 h and was kept for a further 3 h. The metal residues left in the crucible were dissolved using 1 mL of 70% HNO_3 and diluted with Milli-Q water to achieve a total volume of 15 mL. The dissolved metals were then analysed by ICP-OES using a Perkin-Elmer Avio 200. Each sample was analysed in triplicate.

The zeta potential of the nanocellulose hydrogels was measured following the method described by Mendoza, Hossain, Browne, Raghuwanshi, Simon and Garnier [36]. Briefly, 1 mL of each salt treated gel was diluted to a concentration 0.01% and sonicated using an ultrasonic homogeniser at 70% amplitude (ON/OFF, 5s) and 19.5 kHz for 2 min. Large cellulose fibres were removed by centrifugation for 5 min at 4,400 rpm. The zeta potential was measured using a Brookhaven Nanobrook Omni. Each sample was analysed 5 times.

The viscoelastic properties of nanocellulose hydrogels were evaluated using a rheometer (Anton Paar MCR302) at 25 °C. A cone (0.997°) and plate (49.975 mm) geometry was selected for Na^+, K^+ and NH_4^+ and a cup and bob for H^+, Mg^{2+}, Ca^{2+} and Zn^{2+} ions. During the measurements, a solvent trap was employed to maintain a constant temperature. The amplitude sweep was varied from 0.01 to 100% at a constant frequency of 1 Hz.

The morphology of the SAPs was observed using scanning electron microscopy (SEM) (FEI Magellan 400). Nanocellulose foams were placed on a metal stub and coated with an Iridium layer of less than 2 nm thick.

The porosity, pore size distribution and pore properties of all SAPs were measured by mercury porosimetry (Micromeritics Autopore IV). Samples were degassed at 50 °C for at least 24 h prior to testing and analysed in triplicates. A testing pressure ranged from 0.1 to 60,000 psi was applied.

The swelling or absorption capacity of nanocellulose SAPs was quantified in Milli-Q water. The swelling rate and absorption were measured by weighing the samples before and after immersion in water over different periods of time (1, 5, 15, 30, 60, 90, and 150 minutes) at room temperature. The following equation was used to determine the swelling capacity:

$$Swelling\ capacity, Q = \frac{m_t - m_d}{m_d} \qquad (5)$$

where m_t refers to the weight of the swollen gel at time t and m_d is the weight of the dried sample.

3.6 Results

TEMPO-oxidised BEK pulp, which had a carboxylate content of 1.4 mmol/g dry fibre and was washed with acid, was first dispersed into different salt solutions of varying valency and cation type and then homogenised under high shear forces, thus forming hydrogels. These hydrogels were characterised in chemical structure and ion content. Rheology was used to evaluate the cross-linking density and fibrillation efficiency. Hydrogels were then lyophilised and the aerogels produced were analysed for morphology, pore size distribution and swelling in water.

3.6.1 Ion exchange of carboxyl-group counter-ions

The FT-IR spectra and the zeta potential of the hydrogels prepared with the various counter-ions is displayed in Figure 1a and b, respectively. The presence of a band at 1720 cm^{-1} for the H$^+$-hydrogel indicates the conversion of the Na$^+$ carboxylate groups from the TEMPO-mediated oxidation to carboxylic acid groups using the acid treatment (Figure 1a). All samples

with monovalent ions (Na^+, K^+ and NH_4^+) and divalent ions (Mg^{2+}, Ca^{2+} and Zn^{2+}) show a sharp peak at $1600 \, cm^{-1}$, distinctive of the C=O stretching groups, which confirms the presence of the respective carboxylate counter-ions. Interestingly, the zeta potential of the nanocellulose hydrogels decreased with increasing ion valency. Monovalent hydrogels have a zeta potential ranging from -80 mV to -74mV; for divalent, it ranges from -50 to -35mV. Ca^{2+}-hydrogels have the lowest surface charge of all samples (Figure 1b). The difference among the valencies is significant, as previously reported [37].
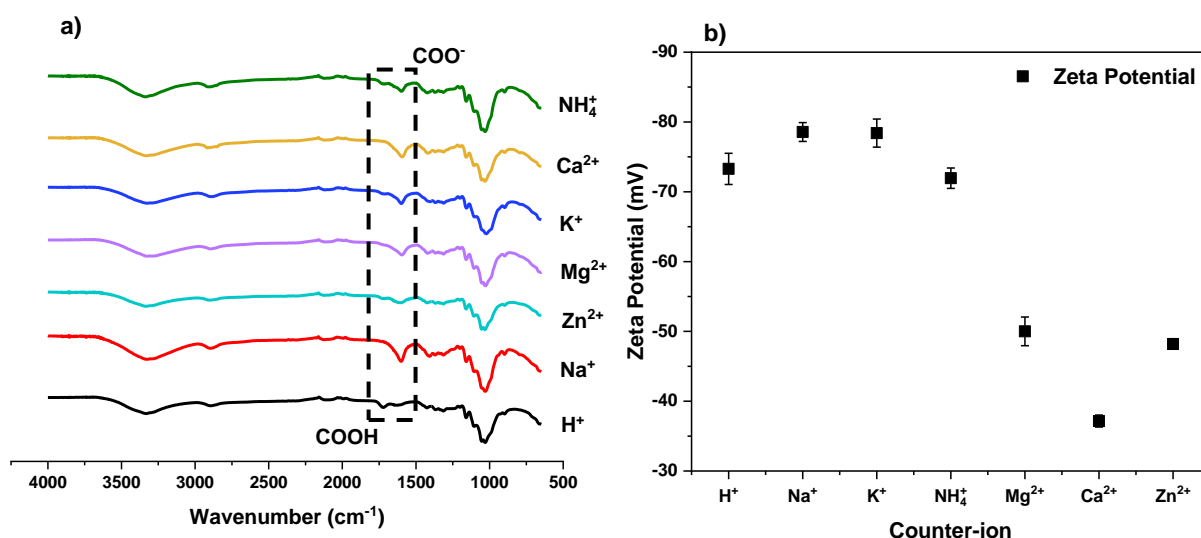
Figure 1. (a) FT-IR spectra and (b) zeta potential of TEMPO-oxidised nanocellulose pretreated with different counter-ions. The dashed line highlights the absorption bands for COO- and COOH groups. Results are reported as mean ± standard deviation (n=3).

The degree of counter-ion exchange from the protonated carboxyl group to other cations was evaluated through ICP-OES analysis (Figure 2). NH_4^+ ions were determined by HCNS analysis, also shown in Figure 2. Except for Zn^{2+}-gels, the measured counter-ion content of all ions is similar to that calculated by stoichiometry – 1.4 and 0.7 mmol/g dry fibre for mono and divalent cation gels, respectively. This confirms the complete conversion of the protonated carboxyl groups to their respective carboxylate salts. Samples with divalent ions formed

cationic carboxylate groups with 1:2 (cation-COO-) molar ratio, corresponding to (COO)$_2$-cation structures ionically cross-linked. The increase in the measured counter-ion content of Zn^{2+}-gels, which is higher than the calculated value, can be attributed to an excess of salt solution that was not completely removed upon washing.
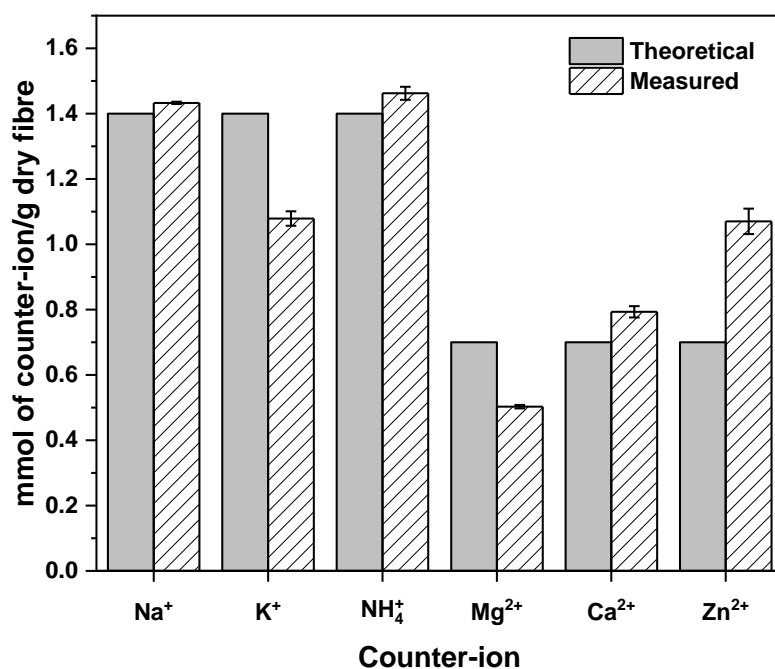
Figure 2. Counter-ion content of the TEMPO-oxidised nanocellulose sheared after the ion exchange treatment. Measurements are determined from ICP-OES and HCNS analysis. Results are reported as mean ± standard deviation (n=3).

3.6.2 Viscoelastic properties

The effect of the counter-ions on the gelation properties of the nanocellulose hydrogels was measured by rheology. The viscosity curves of all gels are presented in Figure 3a. In general, increasing shear rate decreases viscosity. This is known as a shear-thinning behaviour and is common in nanocellulose gels [38, 39]. Gels with divalent ions have lower shear viscosity than those with monovalent ions.

The storage modulus or solid-like behaviour (G') and the loss modulus or liquid-like behaviour (G'') were evaluated as a function of shear strain in oscillatory flow mode (Figure 3d-e). The

viscoelastic properties of the nanocellulose gels is governed by the elastic regime in all cases, noted by a higher G' than G'' over the strain range. The storage modulus of the gels decreases with increasing ion valency. Monovalent gels, except those with H^+ ion, exhibit an elastic modulus an order of magnitude higher than all divalent ions providing an indication of fibre crosslinking in between the gel matrix [7]. Gel stiffness, described by the G' values (Figure 3b), is in the order of $NH_4^+ \gg Na^+ > K^+ > Mg^{2+} > Zn^{2+} > Ca^{2+} > H^+$. Similarly, gel relaxation, described by G'' values (Figure 3c), is in the decreasing order of $NH_4^+ \gg Na^+ > K^+ > Mg^{2+} > Ca^{2+} \sim Zn^{2+} > H^+$. The linear viscoelastic region (LVR) changes for both curves, G' and G'', depending on the valency and type of counter-ion. Both hydrogels display a similar LVR regime that drops at a shear strain of 10%. Finally, the difference between the G' and the G'' values for monovalent gels is an order of magnitude higher than for divalent gels. This suggests that monovalent gels are mostly dominated by the elastic character, whereas divalent and H^+ gels are dictated by both the elastic and the viscous behaviour in the same proportion.
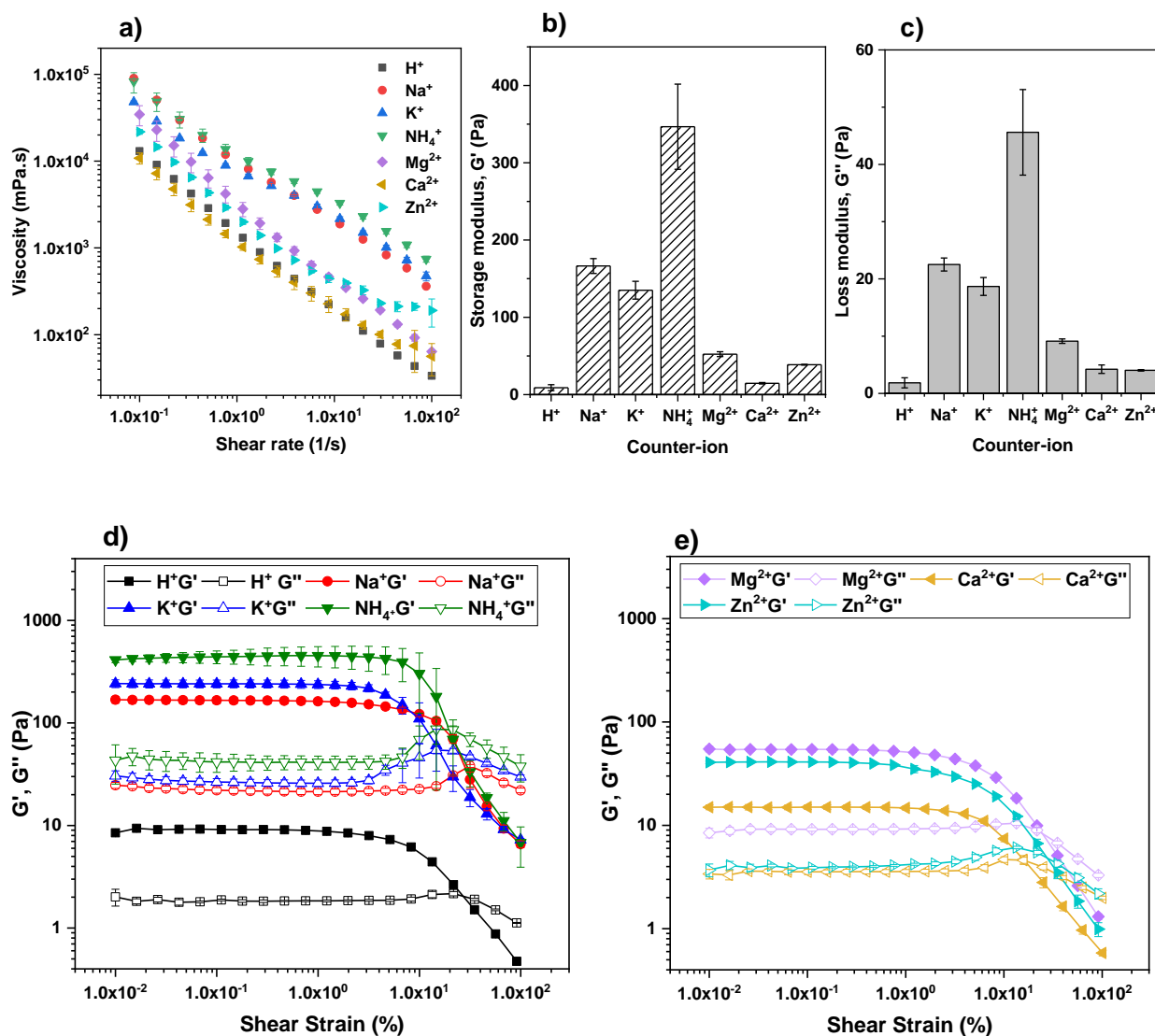
Figure 3. Rheological properties of TEMPO-oxidised nanocellulose sheared with different

counter-ions: (a) viscosity curves, (b) nanocellulose gel stiffness and (c) relaxation

represented by the storage modulus (G') and the loss modulus (G''), storage (G')

and loss (G'') modulus of (d) monovalent and (e) divalent ions. Results are

reported as mean ± standard deviation (n=3).

3.6.3 Morphology

Nanocellulose-based aerogels were prepared by freeze-drying. SEM imaging was employed to

analyse the morphology (Figure 4). The internal structure strongly depends on the counter-ion

present in the superabsorbent. Though all treatments produced SAPs with very porous

structures, the pore shape, size and fibre arrangement differ. Monovalent ions form SAPs characterised by an entanglement of fibres which results in open and porous three-dimensional assemblies (Figure 4a-d). Fibres are clearly visible, forming foam structures with pore diameters ranging from 10 – 300 nm. In contrast, superabsorbents with divalent ions are characterised by a more homogeneous and organised structure. Pores are detected, but the cellulose fibres are still connected to each other, not entangled (Figure 4e-g). Pore diameters range between 30 – 200 nm.
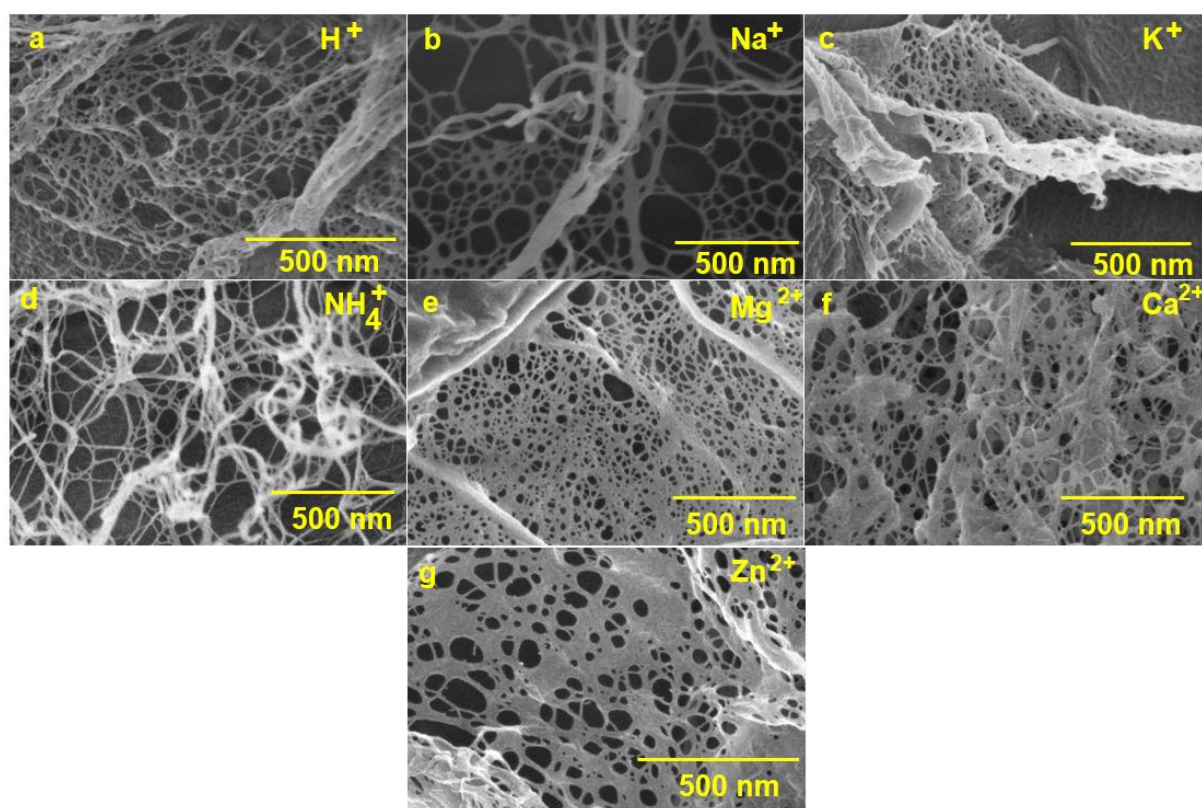
Figure 4. SEM images of the nanocellulose superabsorbent made from freeze-drying nanocellulose hydrogels of TEMPO-treated cellulose sheared with different counter-ions: (a) H^+, (b) Na^+, (c) K^+, (d) NH_4^+, (e) Mg^{2+}, (f) Ca^{2+} and (g) Zn^{2+}.

3.6.4 Pore size

The pore size distribution of the nanocellulose superabsorbents was evaluated using mercury porosimetry (Figure 5a). Pore size distribution is controlled by the counter-ion present in the

SAP. Apart from NH_4^+, all monovalent and divalent ions form SAP with a microporous structure. No visible pores are noted at a scale lower than 2 µm. Superabsorbents made with NH_4^+ counter-ion display a combination of micro, meso and macropores of size ranging from 5 nm to up to 100 µm, as classified by IUPAC [40].

The pore properties of the superabsorbents are expressed as a function of the counter-ion (Figure 5a-c). NH_4^+-based superabsorbents exhibit the highest pore area, more than 15 times higher than any of the other SAPs. They also have the smallest pore diameter, in the range of 2 – 5 nm, which is about 6 times smaller than for the other materials. Apart from this, there are no other major differences observed in the SAPs prepared with the other monovalent and divalent ions. The pore volume is slightly smaller for superabsorbents with monovalent ions than for divalent ions, ranging from 25 – 30 mL/g and 32 – 37 mL/g, respectively. The porosity of all the SAPs is between 90 – 94%, which is typical of freeze-dried superabsorbents [8].
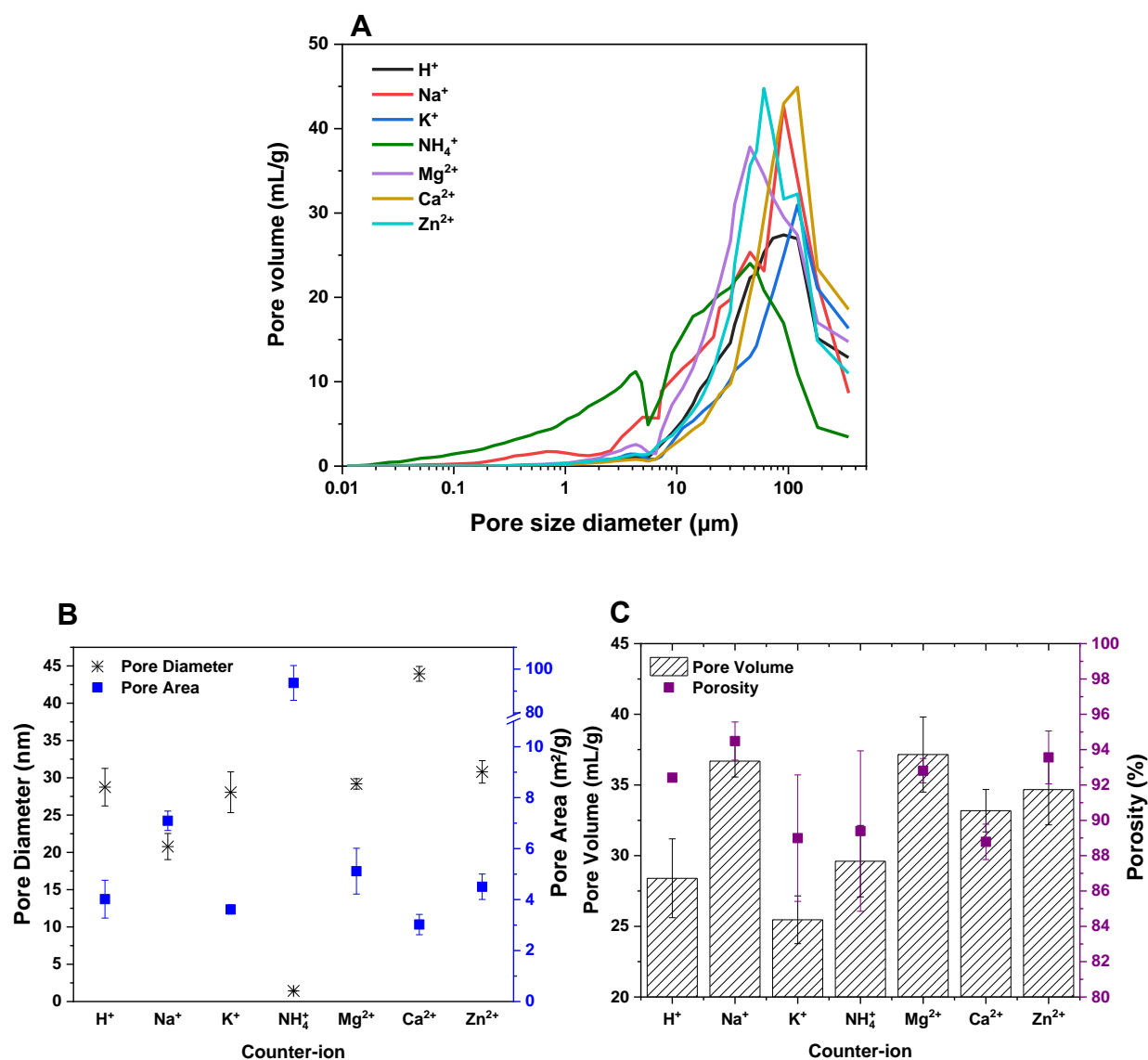
Figure 5. Pore properties of the nanocellulose superabsorbents with different counter-ions: (a) pore size distribution (b) pore diameter and pore area, and (c) porosity and pore volume. Results are reported as mean ± standard deviation (n=3).

3.6.5 Swelling

The degree of swelling of the nanocellulose SAPs was quantified in Milli-Q water and evaluated as over time (Figure 6). All superabsorbents perform similarly, with swelling uptake reaching a plateau after an initial absorption rate. Apart from NH_4^+, superabsorbents show an

initial rapid swelling, achieving equilibrium as soon as they are immersed in water. SAP with

NH_4^+ counter-ion is characterised a slow swelling rate.

The type of counter-ion dictates the SAP swelling at equilibrium (Figure 7). Ammonium-based

SAP achieves the highest swelling capacity of approximately 130 g water/g dry fibre. This is

followed by the other monovalent ions, K^+ and Na^+, in order, respectively. SAPs with valency

two ions report a lower swelling capacity, with Ca^{2+} being the lowest of all.
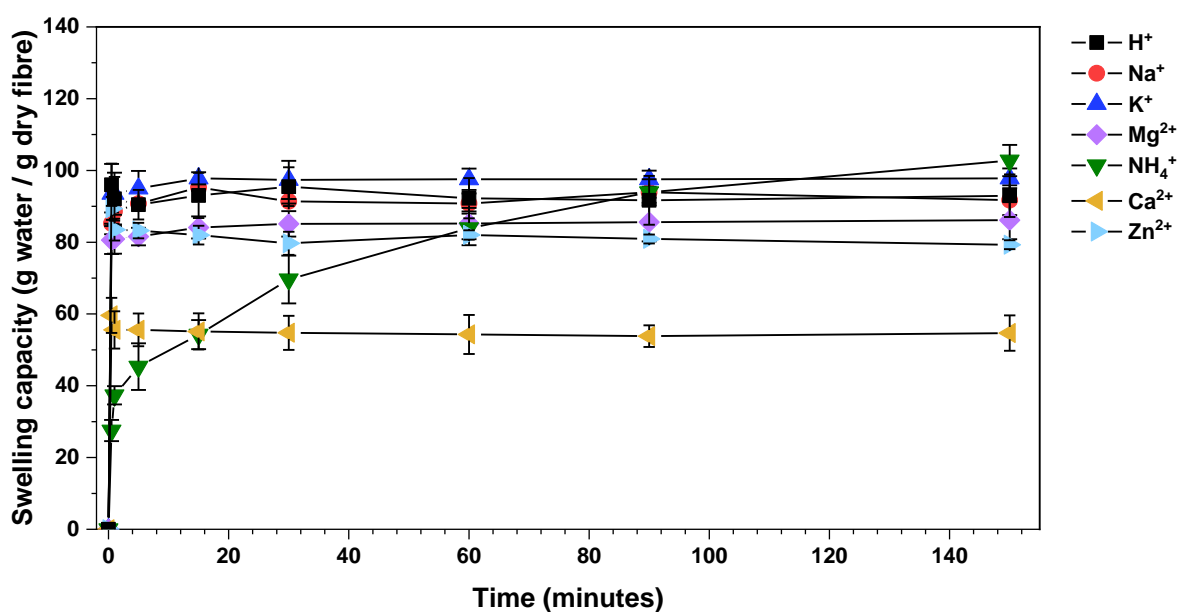
Figure 6. Effect of the counter-ion on the degree of swelling of nanocellulose superabsorbents

over time. Results are reported as mean ± standard deviation (n=3).
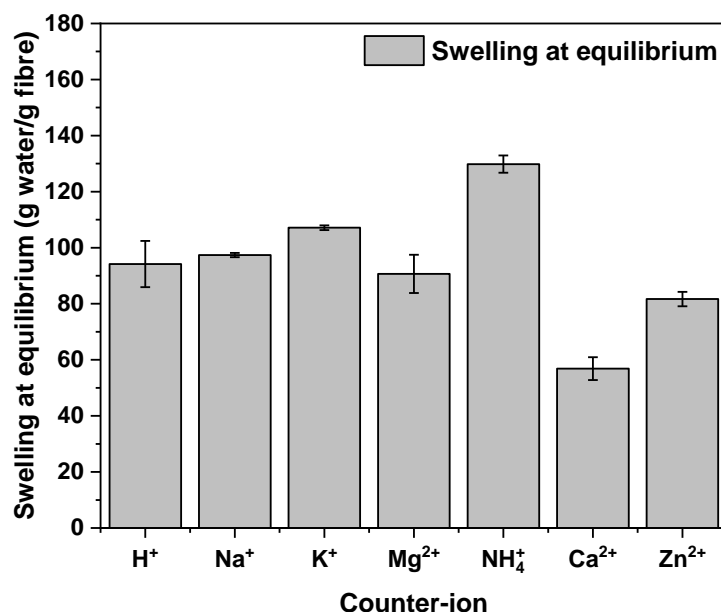
Figure 7. Effect of the counter-ion on the swelling capacity of nanocellulose superabsorbents at equilibrium. Results are reported as mean ± standard deviation (n=3).

3.7 Discussion

TEMPO-mediated oxidation is the most commonly used method to produce nanocellulose hydrogels. This introduces sodium carboxylates at the C6 glycosidic position which contributes to the liberation of cellulose fibres upon homogenisation. However, the presence of sodium counter-ions may limit the application range of this material. This study evaluated the effects that different counter-ions have on the properties of both nanocellulose hydrogels and superabsorbents via ion exchange treatment prior fibrillation.

The FT-IR spectra analysis confirms the evidence of the carboxylate groups balanced by different cations or protonated carboxyl groups. This is noted by the presence of their characteristic peak of metal carboxylate group at ~1600 cm^{-1}. However, the intensity of this peak is lower for hydrogels with Zn^{2+} and NH_4^+ ions. In these cases, the FT-IR spectra also show a small peak at ~1720 cm^{-1} which corresponds to protonated carboxyl groups. This suggests that not all the carboxyl groups were converted to the corresponding metal carboxylate

group [29, 41]. This is because of the pH of $ZnSO_4$ and NH_4SO_4 solutions being 4.8 and 5.5 respectively, which promotes the partial formation of free carboxylic acid.

Except for Zn^{2+}-gels, the addition of multivalent ions forms cation carboxylate groups with molar ratios of 1:1 and 1:2 for monovalent cations (NH_4^+, H^+, Na^+, K^+) and divalent cations (Zn^{2+}, Ca^{2+}, Mg^{2+}), respectively. Divalent cations have a higher solvation volume and binding energy than monovalent cations which allows interfibril interactions, leading to ionic cross-linking between multiple fibres [6]. These ionic links generate strong interactions with numerous carboxylate groups, bridging cellulose nanofibers by attractive forces that screen the electrostatic repulsion between neighbouring nanofibres [7]. This screening effect governs the gel stability and increases with increasing concentration and counter-ion valency [42]. This is confirmed with the surface charge of the hydrogels, being almost half that of monovalent gels, indicating the formation of significant cohesive interactions between nanofibrils due to the strength of these interfibril connections [6]. The surface charge, measured by zeta potential, is related to the physical stability of these gels by electrostatic repulsion of individual fibres. Values higher than ±30 mV can develop enough repulsive force to reach good colloidal stability. On the other hand, smaller values can lead to flocculation and particle aggregation [43]. In this case, the low zeta potential values of divalent gels, with Ca^{2+}-gels being close to the threshold of agglomeration, led to a decrease in the degree of nanofibrillation, exhibited by the substantial fibril aggregation observed in the nanocellulose dispersion after fibrillation and in the morphology of the aerogels upon drying (Figure 4) [36]. Fibril aggregation was also observed in gels with H^+ ions. In this case, gel stability is governed by the protonated carboxyl groups which decrease the electrostatic repulsion and surface charge, allowing the fibres to come closer as the van der Waals forces become dominant, resulting in a decrease in the degree of fibrillation [32, 44]. In contrast, monovalent ionic gels lack the interfibril cross-linking interactions as observed with the viscoelastic properties. Thus, the driving force for gelation is

due to the coupling of nanofibrils by physical interactions that creates an electrostatic stabilisation of the ionised COO^- groups when high shear forces are applied to the oxidised fibres [6, 32], forming stronger and more stable materials.

The type of counter-ion governs the superabsorption performance. The interaction of the counter-ion with the cellulose nanofibers can be explained by two main variables. For monovalent ions, the swelling at equilibrium follows the Hofmeister effect. This effect relates the behaviour of hydrophilic colloids in the presence of salts and is attributed to the size and hydration of ions [45]. According to the Hofmeister effect, stability of hydrophilic particles follows the indirect series as: $NH_4^+ > K^+ > Na^+$ where ions on the left will adsorb more strongly to a hydrophilic substrate [45]. This cation specificity coincides with the measured values of swelling capacity and is attributed to negative volume exclusion entropy generated by the cation hydration. This results in an increase of the strength of the electrostatic repulsive forces which increases the entanglement of nanocellulose fibres [46, 47]. Thus, increasing the absorption capacity due to the increase in hydrogen bonding between the COO^- available to interact with water [48] and also contributing to the swelling of the fibre network [10].

These repulsive forces are screened in the presence of divalent cations, as van der Waals forces become dominant and strong cation-carboxylate bonds are created [6]. Cellulose nanofibers come closer, decreasing the fibre ability to entangle upon fibrillation and thus, decreasing the swelling capacity. In this case, swelling is mainly attributed to the available pore volume, where swelling increases with increasing pore volume and decreases in the order of $Mg^{2+} > Zn^{2+} > Ca^{2+}$. This difference in pore volume depending on the counter-ion can be associated to the cation radii, where the increment in ionic radii of valency two cations results in a decrease in swelling (Mg^{2+} (72 pm) $< Ca^{2+}$ (100 pm)) [49].

Lastly, of all the cations studied, NH_4^+ produced gels and superabsorbents with remarkable properties: high gel stiffness and stability, high SAP pore area and swelling, and slow swelling kinetics. Such performance is attributed to the unique ability of the ammonium cation to rotate [50]. This ability creates additional hydrogen bonds between the water molecules and the nanofiber network, resulting in a higher fibrillation efficiency upon homogenisation. This increase in fibre entanglement is observed in the small pore size and wide pore distribution of this SAP (Figures 4d, 5a and 5b), increasing the pore area by an order of magnitude. This expands the number of available carboxyl groups able to participate with hydrogen bonding, resulting in a high gel stiffness. This also increases the swelling of the nanofiber network and the amount of water adsorbed to the polymer chains, responsible for the high swelling of this superabsorbent [51].

3.8 Conclusion

A number of nanocellulose hydrogels varying in the extent of cellulose fiberization and ion cross-linking was prepared and freeze-dried into superabsorbents (SAPs). Gel and SAP were characterized in terms of rheology, aerogel structure, gelation mechanism and swelling behaviour. Carboxylated nanocellulose was prepared from TEMPO-oxidized cellulose followed by ion exchange in a series of salt solutions prior to high shear homogenization into a gel [10]. Seven cations were ion exchanged to the COO^- groups. These are: H^+, Na^+, K^+, NH_4^+, Ca^{2+}, Mg^{2+} and Zn^{2+}; the anion was sulfate. The effect of the cation on the gelation properties and mechanism, superabsorbent structure, swelling capacity and absorption rate was analysed.

FT-IR and ICP-OES analyses confirm the formation of metal carboxylate groups with 1:1 (metal-COO-) molar ratio for monovalent cations and 1:2 molar ratio for divalent cations, which corresponds to $(COO)_2$-metal structures ionically cross-linked. The gel stability of the

nanocellulose is governed by the valency and the type of cation. Gelation in monovalent gels is due to the coupling of nanofibrils by physical interactions which creates an electrostatic stabilisation of the ionised carboxyl groups during the high shear forces of homogenizing [6, 32]. In contrast, for divalent gels, the driving force for gelation is due to strong interfibril connections via ionic-crosslinks which screen the repulsive forces between carboxylate groups, enabling fibres to associate together. The type of ion and their interaction with the COO^- groups determine the efficiency of fibrillation during homogenization, which affects the structure of the hydrogels and aerogels made of those. This aerogel structure directly impacts swelling capacity and kinetics. Swelling at equilibrium is in order of: $NH_4^+ > K^+ > Na^+ > Mg^{2+} > Zn^{2+} > Ca^{2+}$. The swelling capacity of monovalent SAPs follows the Hofmeister effect and is related to the size and hydration of ions. For divalent SAPs, absorption is caused by their difference in pore volume given by the ionic radii. The remarkable properties of NH_4^+ gel and SAP, compared to the other cations, are attributed to the ability of the ammonium cation to rotate, which increases the number of available carboxyl groups that engage in hydrogen bonding, resulting in an increase in pore area, gel stiffness and SAP swelling [51].

This study not only demonstrates the potential of nanocellulose-based SAPs with different cations to suit a range of applications but also innovates on the preparation method, that is by performing ion exchange before fibrillation -and not after- resulting in a cheaper and faster process than the conventional treatment. The addition of these cations can assist in the transition of the superabsorbent as a hydro-retentor to a nutrient carrier material, increasing the benefits of this material for agricultural and food use.

3.9 Acknowledgement

Financial support was from the Australian Research Council (ARC), Norske Skog, Visy, the

Government of Tasmania and Opal through the Industry Transformation Research Hub

Processing Advance Lignocellulosics (PALS) grant IH130100016.

3.10 References

[1] E.M. Ahmed, Hydrogel: Preparation, characterization, and applications: A review, Journal of Advanced Research 6(2) (2015) 105-121.

[2] S. Ghorbani, H. Eyni, S.R. Bazaz, H. Nazari, L.S. Asl, H. Zaferani, V. Kiani, A.A. Mehrizi, M. Soleimani, Hydrogels Based on Cellulose and its Derivatives: Applications, Synthesis, and Characteristics, Polymer Science, Series A 60(6) (2019) 707-722.

[3] X. Shen, J.L. Shamshina, P. Berton, G. Gurau, R.D. Rogers, Hydrogels based on cellulose and chitin: fabrication, properties, and applications, Green Chemistry 18(1) (2016) 53-75.

[4] J.R. Gross, The Evolution of Absorbent Materials, in: L. Brannon-Peppas, R.S. Harland (Eds.), Studies in Polymer Science, Elsevier1990, pp. 3-22.

[5] R. Curvello, V.S. Raghuwanshi, G. Garnier, Engineering nanocellulose hydrogels for biomedical applications, Advances in Colloid and Interface Science 267 (2019) 47-61.

[6] H. Dong, J.F. Snyder, K.S. Williams, J.W. Andzelm, Cation-Induced Hydrogels of Cellulose Nanofibrils with Tunable Moduli, Biomacromolecules 14(9) (2013) 3338-3345.

[7] J. Yang, F. Xu, C.-R. Han, Metal Ion Mediated Cellulose Nanofibrils Transient Network in Covalently Cross-linked Hydrogels: Mechanistic Insight into Morphology and Dynamics, Biomacromolecules 18(3) (2017) 1019-1028.

[8] N. Lavoine, L. Bergström, Nanocellulose-based foams and aerogels: processing, properties, and applications, Journal of Materials Chemistry A 5(31) (2017) 16105-16117.

[9] K.J. De France, T. Hoare, E.D. Cranston, Review of Hydrogels and Aerogels Containing Nanocellulose, Chemistry of Materials 29(11) (2017) 4609-4631.

[10] L. Mendoza, L. Hossain, E. Downey, C. Scales, W. Batchelor, G. Garnier, Carboxylated nanocellulose foams as superabsorbents, J Colloid Interface Sci 538 (2019) 433-439.

[11] J. Grignon, A.M. Scallan, Effect of pH and neutral salts upon the swelling of cellulose gels, Journal of Applied Polymer Science 25(12) (1980) 2829-2843.

[12] A. Bashari, A. Rouhani Shirvan, M. Shakeri, Cellulose-based hydrogels for personal care products, Polymers for Advanced Technologies 29(12) (2018) 2853-2867.

[13] T.M. Neethu, P.K. Dubey, A.R. Kaswala, Prospects and Applications of Hydrogel Technology in Agriculture, International Journal of Current Microbiology and Applied Sciences 7(05) (2018) 3155-3162.

[14] R. Curvello, G. Garnier, Cationic Cross-Linked Nanocellulose-Based Matrices for the Growth and Recovery of Intestinal Organoids, Biomacromolecules 22(2) (2021) 701-709.

[15] M.J. Zohuriaan-Mehr, Kabiri, Kourosh.,, Superabsorbent Polymer Materials: A review, Iranian Polymer Journal 17(6) (2008) 451-477.

[16] M.R. Guilherme, F.A. Aouada, A.R. Fajardo, A.F. Martins, A.T. Paulino, M.F.T. Davi, A.F. Rubira, E.C. Muniz, Superabsorbent hydrogels based on polysaccharides for application in agriculture as soil conditioner and nutrient carrier: A review, European Polymer Journal 72 (2015) 365-385.

[17] Z. Steinmetz, C. Wollmann, M. Schaefer, C. Buchmann, J. David, J. Tröger, K. Muñoz, O. Frör, G.E. Schaumann, Plastic mulching in agriculture. Trading short-term agronomic

benefits for long-term soil degradation?, Science of The Total Environment 550 (2016) 690-705.

[18] A.A. Horton, A. Walton, D.J. Spurgeon, E. Lahive, C. Svendsen, Microplastics in freshwater and terrestrial environments: Evaluating the current understanding to identify the knowledge gaps and future research priorities, Science of The Total Environment 586 (2017) 127-141.

[19] L. Ramos, G. Berenstein, E.A. Hughes, A. Zalts, J.M. Montserrat, Polyethylene film incorporation into the horticultural soil of small periurban production units in Argentina, Science of The Total Environment 523 (2015) 74-81.

[20] P. Chen, W.A. Zhang, W. Luo, Y.e. Fang, Synthesis of superabsorbent polymers by irradiation and their applications in agriculture, Journal of Applied Polymer Science 93(4) (2004) 1748-1755.

[21] M.R. Guilherme, A.V. Reis, A.T. Paulino, T.A. Moia, L.H.C. Mattoso, E.B. Tambourgi, Pectin-based polymer hydrogel as a carrier for release of agricultural nutrients and removal of heavy metals from wastewater, Journal of Applied Polymer Science (2010) n/a-n/a.

[22] X. Shi, W. Wang, A. Wang, pH-responsive sodium alginate-based superporous hydrogel generated by an anionic surfactant micelle templating, Carbohydrate Polymers 94(1) (2013) 449-455.

[23] A. Sannino, C. Demitri, M. Madaghiele, Biodegradable Cellulose-based Hydrogels: Design and Applications, Materials 2(2) (2009) 353-373.

[24] J. De Guzman, K. Dela Peña, J. Ytac Dorothy, T. Tumolva, Synthesis and Characterization of Ionically-Crosslinked κ- Carrageenan/Sodium Alginate/Carboxymethyl Cellulose Hydrogel Blends for Soil Water Retention and Fertilizer Release, Solid State Phenomena 304 (2020) 59-65.

[25] S. Varanasi, R. He, W. Batchelor, Estimation of cellulose nanofibre aspect ratio from measurements of fibre suspension gel point, Cellulose 20(4) (2013) 1885-1896.

[26] A. Isogai, T. Saito, H. Fukuzumi, TEMPO-oxidized cellulose nanofibers, Nanoscale 3(1) (2011) 71-85.

[27] Z. Pakowski, Modern Methods of Drying Nanomaterials, Transport in Porous Media 66(1-2) (2006) 19-27.

[28] E. Bresler, Saline and Sodic Soils Principles-Dynamics-Modeling, 1st ed. 1982. ed., Berlin, Heidelberg : Springer Berlin Heidelberg : Imprint: Springer1982.

[29] I. Homma, H. Fukuzumi, T. Saito, A. Isogai, Effects of carboxyl-group counter-ions on biodegradation behaviors of TEMPO-oxidized cellulose fibers and nanofibril films, Cellulose 20(5) (2013) 2505-2515.

[30] H. Dong, J.F. Snyder, D.T. Tran, J.L. Leadore, Hydrogel, aerogel and film of cellulose nanofibrils functionalized with silver nanoparticles, Carbohydrate Polymers 95(2) (2013) 760-767.

[31] M. Chau, S.E. Sriskandha, D. Pichugin, H. Thérien-Aubin, D. Nykypanchuk, G. Chauve, M. Méthot, J. Bouchard, O. Gang, E. Kumacheva, Ion-Mediated Gelation of Aqueous Suspensions of Cellulose Nanocrystals, Biomacromolecules 16(8) (2015) 2455-2462.

[32] L. Mendoza, W. Batchelor, R.F. Tabor, G. Garnier, Gelation mechanism of cellulose nanofibre gels: A colloids and interfacial perspective, J Colloid Interface Sci 509 (2018) 39-46.

[33] S. Ang, V. Haritos, W. Batchelor, Cellulose nanofibers from recycled and virgin wood pulp: A comparative study of fiber development, Carbohydrate Polymers 234 (2020) 115900.

[34] T. Saito, A. Isogai, TEMPO-Mediated Oxidation of Native Cellulose. The Effect of Oxidation Conditions on Chemical and Crystal Structures of the Water-Insoluble Fractions, Biomacromolecules 5(5) (2004) 1983-1989.

[35] M. Maliha, M. Herdman, R. Brammananth, M. McDonald, R. Coppel, M. Werrett, P. Andrews, W. Batchelor, Bismuth phosphinate incorporated nanocellulose sheets with antimicrobial and barrier properties for packaging applications, Journal of Cleaner Production 246 (2020) 119016.

[36] D.J. Mendoza, L. Hossain, C. Browne, V.S. Raghuwanshi, G.P. Simon, G. Garnier, Controlling the transparency and rheology of nanocellulose gels with the extent of carboxylation, Carbohydrate Polymers 245 (2020) 116566.

[37] R. Prathapan, R. Thapa, G. Garnier, R.F. Tabor, Modulating the zeta potential of cellulose nanocrystals using salts and surfactants, Colloids and Surfaces A: Physicochemical and Engineering Aspects 509 (2016) 11-18.

[38] I. Besbes, S. Alila, S. Boufi, Nanofibrillated cellulose from TEMPO-oxidized eucalyptus fibres: Effect of the carboxyl content, Carbohydrate Polymers 84(3) (2011) 975-983.

[39] O. Nechyporchuk, M.N. Belgacem, F. Pignon, Current Progress in Rheology of Cellulose Nanofibril Suspensions, Biomacromolecules 17(7) (2016) 2311-2320.

[40] IUPAC, Compendium of Chemical Terminology, 2nd ed. (the "Gold Book"), Blackwell Scientific Publications, Oxford, 1997.

[41] T. Saito, T. Uematsu, S. Kimura, T. Enomae, A. Isogai, Self-aligned integration of native cellulose nanofibrils towards producing diverse bulk materials, Soft Matter 7(19) (2011) 8804-8809.

[42] J.N. Israelachvili, Intermolecular and surface forces, 3rd ed. ed., Burlington, Massachusetts : Academic Press2011.

[43] E. Joseph, G. Singhvi, Chapter 4 - Multifunctional nanocrystals for cancer therapy: a potential nanocarrier, in: A.M. Grumezescu (Ed.), Nanomaterials for Drug Delivery and Therapy, William Andrew Publishing2019, pp. 91-116.

[44] A.B. Fall, S.B. Lindström, O. Sundman, L. Ödberg, L. Wågberg, Colloidal Stability of Aqueous Nanofibrillated Cellulose Dispersions, Langmuir 27(18) (2011) 11332-11338.

[45] T. Oncsik, G. Trefalt, M. Borkovec, I. Szilagyi, Specific Ion Effects on Particle Aggregation Induced by Monovalent Salts within the Hofmeister Series, Langmuir 31(13) (2015) 3799-3807.

[46] H. Huang, E. Ruckenstein, Effect of Hydration of Ions on Double-Layer Repulsion and the Hofmeister Series, The Journal of Physical Chemistry Letters 4(21) (2013) 3725-3727.

[47] E. Ruckenstein, H. Huang, Specific ion effects on double layer forces through ion hydration, Colloids and Surfaces A: Physicochemical and Engineering Aspects 459 (2014) 151-156.

[48] R.M. Barajas-Ledesma, A.F. Patti, V.N.L. Wong, V.S. Raghuwanshi, G. Garnier, Engineering nanocellulose superabsorbent structure by controlling the drying rate, Colloids and Surfaces A: Physicochemical and Engineering Aspects 600 (2020) 124943.

[49] R.D. Shannon, Revised effective ionic radii and systematic studies of interatomic distances in halides and chalcogenides, Acta Crystallographica Section A 32(5) (1976) 751-767.

[50] J. Guo, L. Zhou, A. Zen, A. Michaelides, X. Wu, E. Wang, L. Xu, J. Chen, Hydration of NH4+ in Water: Bifurcated Hydrogen Bonding Structures and Fast Rotational Dynamics, Physical Review Letters 125(10) (2020) 106001.

[51] Z. Xia, M. Patchan, J. Maranchi, J. Elisseeff, M. Trexler, Determination of crosslinking density of hydrogels prepared from microcrystalline cellulose, Journal of Applied Polymer Science 127(6) (2013) 4537-4541.

THIS PAGE HAS BEEN INTENTIONALLY LEFT BLANK

CHAPTER 4:

CARBOXYLATED NANOCELLULOSE SUPERABSORBENT: BIODEGRADATION AND SOIL WATER RETENTION PROPERTIES

THIS PAGE HAS BEEN INTENTIONALLY LEFT BLANK

PREFACE

One of the main applications of superabsorbents is as water retention agents in agricultural soils. Once the physical structure and chemical composition of the nanocellulose SAP have been engineered, the next step is to evaluate its performance in soil. In this chapter, a series of incubation experiments of soil treated with three different nanocellulose superabsorbents: freeze-dried and oven-dried at low and high temperatures - was conducted. The absorption capacity of the SAPs immersed in soil-water extracts was measured and compared to those in deionised water. The ionic sensitivity of each type of superabsorbent was determined. Soil was amended with different application rates of these superabsorbents and the effects on soil water retention were quantified. The performance of the SAPs after several hydration/dehydration cycles was analysed and related to the SAP biodegradation, measured through soil respiration studies and acid digestion methods.

By addressing the third research objective, this chapter demonstrates the suitability of nanocellulose SAPs to increase soil water retention. This chapter was submitted for publication to the *Journal of Applied Polymer Science* and acceptation is pending – following the successful second review.

THIS PAGE HAS BEEN INTENTIONALLY LEFT BLANK

Chapter 4: Carboxylated nanocellulose superabsorbent: biodegradation and soil water retention properties

THIS PAGE HAS BEEN INTENTIONALLY LEFT BLANK

Carboxylated nanocellulose superabsorbent: biodegradation and soil water retention properties

Ruth M. Barajas-Ledesma[a], Vanessa N.L. Wong[b], Karen Little[c], Antonio F. Patti[c]and Gil Garnier[a*]*

[a]Bioresource Processing Research Institute of Australia (BioPRIA) and Department of Chemical Engineering, Monash University, Clayton, VIC 3800, Australia
[b]School of Earth, Atmosphere & Environment, Monash University, Clayton, VIC 3800, Australia
[c]School of Chemistry, Monash University, Clayton, VIC 3800, Australia

*Email of corresponding authors: Gil.Garnier@Monash.edu and Antonio.Patti@Monash.edu

4.1 Abstract

In this study, TEMPO (2,2,6,6-tetramethylpiperidine-1-oxyl)-oxidized nanocellulose superabsorbents are prepared using three different drying techniques: freeze-dried, and oven-dried at low and high temperatures. The benefits are investigated by evaluating the superabsorbent structure, composition and application rate. The absorption performance of nanocellulose superabsorbents is affected by the concentration and type of salts in the soil water extracts. Oven-dried at 50 °C SAP presents the highest ionic sensitivity attributed to its large number of accessible carboxylate groups. The water retention of the soil treatments increases with increasing application rate. Soil treated with the freeze-dried superabsorbent shows the highest water retention, whereas those amended with the 50 °C oven-dried SAP remain moist the longest. The biodegradation rate of these materials depends on the application rate and nutrient availability. Carboxylated nanocellulose superabsorbents emerge as high-performance biodegradable materials for agricultural use, able to replace the current non-biodegradable petrochemical-based superabsorbents.

4.2 Keywords

Carboxylated nanocellulose, water retention, swelling, biodegradation, agriculture, microbial activity.

4.3 Graphical Abstract
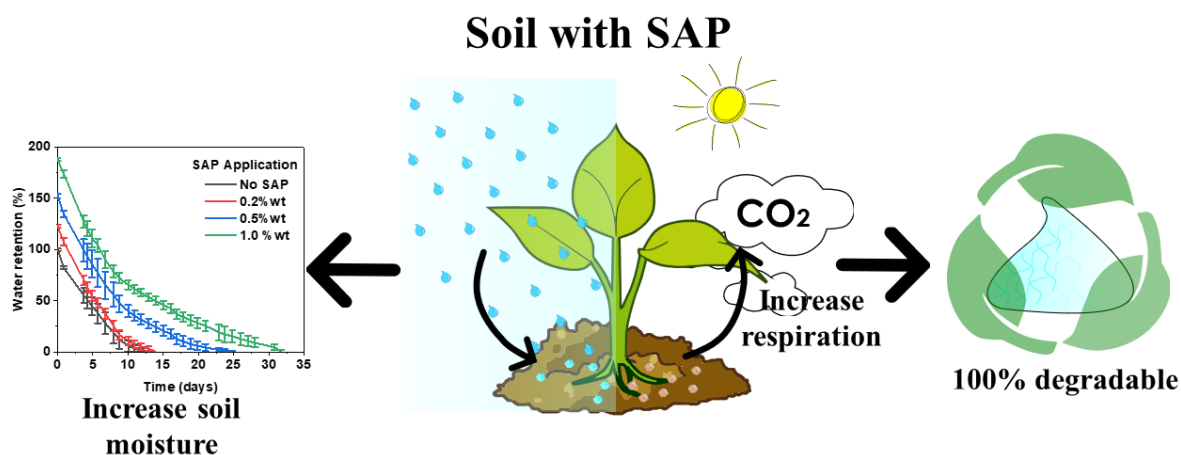
4.4 Introduction

Fresh water is critical for agricultural production and food security. Irrigated agriculture uses about 70% of the water available for human consumption worldwide and accounts for 59% of the total fresh water in Australia [1, 2]. Water availability has been impacted by climate change, drought and water shortage; its decrease has affected world agricultural development in recent years. According to Müller C. [3], agricultural yields will decline between 2 – 15% over the next 30 years due to climate change. Hence, the efficient use of water resources is crucial for the long-term sustainability of the agricultural industry.

One strategy to optimize water retention in soils and hence making it more available to crops, is the use of superabsorbent polymers (SAPs) [4]. SAPs are three-dimensional (3D) networks of linear or branched hydrophilic polymers physically or chemically cross-linked [5]. SAPs can absorb and hold water at hundreds of times their own weight and remain stable in their swollen state [6-9]. They have been extensively used in many applications including biomedicine [10],

food and beverages [11], personal care and hygiene products [12]. In the agricultural and horticultural industries, SAPs have a range of applications which includes seed coatings, seed additives and root dips [13]. The use of SAPs in soil has improved water availability for plants [14]. SAPs have also contributed to water retention in different types of soil, significantly reducing the irrigation water consumption [15, 16]. SAPs also serve as soil conditioners and nutrient carriers [5], thereby improving soil properties and increasing crop yield [4, 5, 17].

Most of the commercially available SAPs in agriculture are petrochemical-based and made of polyacrylate (PA) or polyacrylamide (PAM). Such PA/PAM SAPs degrade very slowly into by-products increasingly raising health concerns including the formation of microplastic particles which can be harmful to soil biota [18-20]. These environmental issues have led to the development of superabsorbents from natural polymers such as starch [21], pectin [22], chitin, chitosan, alginate, and lignin, among others [23]. Most of these are still produced as composites in combination with synthetic polymers, decreasing their biodegradability.

Some of the major limitations of naturally derived SAPs are their low mechanical resistance, high-cost, restricted longevity in soils and also low-absorption capacity [5, 13]. Cellulose, and especially nanocellulose, has the potential to overcome these limitations because of its availability, low-cost, biodegradability, hydrophilicity and high surface area [5, 24]. Nanocellulose refers to the individual cellulose chains, also called elementary fibrils, which have a diameter of $3 - 4$ nm and a length $> 1 - 2$ µm [25]. Its low-density, high-strength, flexibility and tunable surface chemistry make nanocellulose attractive as a material for superabsorbents.

Nanocellulose-based SAPs can be produced from TEMPO-mediated oxidation of cellulose, currently considered as one of the most effective methods [26-28]. This process selectively converts the primary alcohols (C6) into carboxylate groups (Figure 1). This surface

modification provides the necessary electrostatic repulsion which produces nanoscale fibers upon mechanical fibrillation [29]. Recent studies have shown that the resulting material can be dried either by freeze-drying or evaporative-drying to create a highly porous superabsorbent consisting of an entanglement of cellulose nanofibers (CNF) of high surface area [30]. Despite these advantages, few nanocellulose-based superabsorbents have been developed for application in agriculture. Though several studies have investigated cellulose-based superabsorbents, most of them are crosslinked with acrylamide or acrylic acid [31], reducing their biodegradability and sustainability. Few studies have analyzed nanocellulose-based superabsorbents for agriculture. Zhang et al. found that chemically cross-linked nanocellulose superabsorbent can be beneficial for seed germination. These superabsorbents can be applied as soilless culture mediums for plant growth [32]. Mendoza et al. reported that the absorption capacity of carboxylated nanocellulose superabsorbents is dictated by the charge density and fiber content [26]. Zhou et al. stated that carboxymethylcellulose–acrylamide based superabsorbents containing carboxylated CNF have a distilled water absorption capacity higher than CNF-free superabsorbent [33]. Yet, none of these studies has evaluated the ability of nanocellulose-based superabsorbents as a water retention agent in a controlled soil environment nor their biodegradability under realistic conditions.
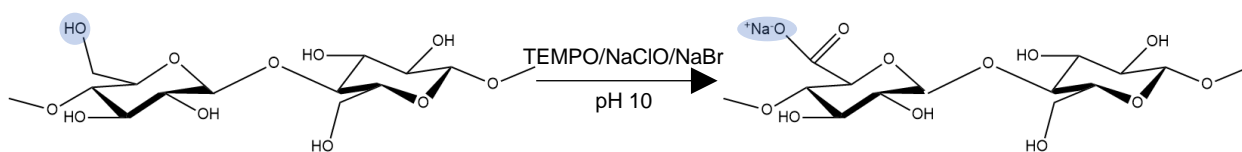
Figure 1. Schematic representation of the selective TEMPO-mediated oxidation reaction of cellulose.

While some studies have evaluated the synthesis and formulation of nanocellulose-based superabsorbents [31, 34, 35], none has systematically compared the effect of application rate

on soil water retention properties nor related those to soil microbial activity. These steps are crucial for any agriculture use, potentially compromising food security, environment and human health. The effect of a novel generation of nanocellulose superabsorbent produced from different drying methods on the superabsorbent longevity needs to be quantified.

In this study, carboxylated nanocellulose superabsorbents were prepared via TEMPO oxidation followed by high-pressure homogenization. This standard carboxylated nanocellulose was dried using three different drying techniques: freeze-drying or oven-drying at high and low temperatures. The water retention of the soil treated with these superabsorbents was quantified for agriculture use at three different application rates. Our objective is to analyze the effect of nanocellulose-based superabsorbents on microbial activity and establish a relationship with its biodegradation. This is to enable nanocellulose superabsorbent as a new class of performance, cheap and sustainable hydro-retentor for agriculture use.

4.5 Experimental Section/Methods

4.5.1 Materials

Bleached Eucalyptus Kraft (BEK) pulp was provided by Australian Paper (Maryvale, Australia). Sodium bromide (NaBr) and 2,2,6,6-tetramethylpiperidine-1-oxyl (TEMPO) were purchased from Sigma-Aldrich (Melbourne, Australia). Hydrochloric acid (HCl) and sodium hydroxide (NaOH) were diluted for solutions as required and purchased from ACL Laboratories, (Melbourne, Australia) and Merck (Bayswater, Australia), respectively. 12% w/v sodium hypochlorite (NaClO) was purchased from Thermo Fisher Scientific (Scoresby, Australia) and used as received. Urea, super phosphate and potassium sulphate of potash were purchased from Richgro (Jandakot, Australia).

Soil was collected from a wheat growing property located in Ouyen, north-west Victoria (34°58'0.16"S; 142°20'45.85"E) (alkaline Calcarosol [36]), soil was collected at a depth of 20-

40 cm, air-dried and sieved to <2 mm. The soil was then characterized for a range of key physicochemical properties including pH, electrical conductivity and available and exchangeable cations (Table S1). Analysis was conducted by Environmental Analysis Laboratories, at Southern Cross University [37], using Rayment and Lyons [38] standard methods.

4.5.2 Superabsorbent Preparation

Nanocellulose superabsorbent was prepared following the TEMPO-mediated oxidation process developed by Isogai et al. [29] to achieve a carboxylate content of 1.4 mmol/g. In brief, 25 g (dry weight) of BEK pulp was suspended in 2500 mL of deionized water containing 0.4 g and 2.5 g of dissolved TEMPO and NaBr, respectively. Before the reaction started, 100 mL of 12% w/v NaClO were adjusted to pH 10 through the addition of 36% w/v HCl. The oxidation process started by adding the 100 mL of NaClO (6.6 mmol NaClO/g cellulose) drop-wise to the suspension under constant stirring. The pH of the reaction was kept at 10 via addition of 0.5M NaOH [39, 40]. The reaction was maintained for 3 h or until no decrease in pH was observed. The oxidized fibers were washed with deionized water, filtrated and stored refrigerated at 4 °C.

The TEMPO-oxidized pulp was dispersed in deionized water to prepare a solution of 0.5% w/v which was further fibrillated using a high-pressure homogenizer (GEA Niro Soavi Homogenizer Panda) at 1000 bar and two passes. To produce the superabsorbent materials, the resulting product from homogenization was either freeze-dried or oven-dried. Freeze-dried superabsorbent was accomplished by freezing the nanocellulose for at least 12 h at -80 °C followed by freeze-drying (Christ Alpha 2-4 LD Plus) for 2 days. Oven-dried superabsorbent was prepared by drying the nanocellulose in an oven (Thermoline BTC-9090) at either 50 °C or 105 °C until no mass loss was observed.

4.5.3 Soil Water Retention Studies

(i) Soil water holding capacity. The soil water holding capacity (WHC) or field capacity was determined gravimetrically by adding an excess of deionized water to 100 g of soil into a Buchner funnel with a filter paper placed at the bottom. Water was then allowed to drain and the saturated soil was left covered at room temperature for 48 h. After this period, the saturated soil was weighed and oven dried. The WHC was calculated as follows:

$$WHC = \ m_w - m_d \tag{1}$$

Where m_w refers to the weight of the saturated soil and m_d is the mass of the dried soil. The units of WHC are in g water/100 g of soil.

(ii) Water retention tests. Soils were subjected to two experiments to test the effect of freeze-dried or oven-dried superabsorbent prepared at 50 °C or 105 °C. For both studies, polypropylene containers (120 mL) were drilled with four holes of 4 mm diameter and a filter paper was placed at the bottom of each. Each experiment was then prepared as follows: superabsorbent was added to the soil at rates of 0.2, 0.5 and 1 wt.% to prepare a total of 50 g of soil treatment. Each treatment was thoroughly mixed and placed in the 120 mL containers which were then fully immersed in deionized water for 24 h to allow the superabsorbent to reach equilibrium. A control treatment without the superabsorbent was also prepared and underwent the same immersion treatment. Five replicates of each treatment were conducted. After 24 h, the containers were raised to drain the excess water until no further water was observed coming out of the bottom of the container and the weight was recorded. The containers were then placed without any covering into a temperature/humidity control cabinet (Thermoline L+M – 150-GD) kept at 23 °C and 80% relative humidity. Samples were weighed every day. Water retention was calculated as follows:

$$\text{Water retention (\%)} = \frac{m_i}{m_o} \times 100 \qquad (2)$$

Where m_i refers to the mass of the sample at day i, and m_o is the mass of the control after being fully saturated with water (day 0).

During the first experiment, samples were allowed to dry without any further addition of deionized water. This experiment concluded when no further mass loss was detected.

During the second experiment, samples were prepared and incubated under the same conditions as described previously, over a period of 28 days. In this case, further addition of deionized water was performed whenever the percentage of the water in the control treatment had decreased to 10% or less. This typically required between 10 – 12 mL of water at 8 – 10-day intervals. This same volume of water was added to all the other treatments at that point.

4.5.4 Microbial Activity Studies

Soil incubation studies were performed with two types of superabsorbent: freeze-dried and oven-dried at 50 °C. For each type, treatments were prepared by adding the superabsorbent at the same application rates as mentioned in section 4.5.3 to prepare 50 g of soil mixture. Deionized water was added to reach 60% WHC. Two different control treatments were prepared: one without any superabsorbent and another with a basal application of fertilizer and 1% wt. of superabsorbent. The fertilizer was applied at an equivalent rate of 60 kg ha^{-1} of N, 70 kg ha^{-1} of P and 60 kg ha^{-1} of K based on the soil analysis. The fertilizer was thoroughly mixed with the soil. Five replicates were conducted for each treatment. Samples were incubated at 23 °C and 80% relative humidity in a temperature/humidity control cabinet (Thermoline L+M – 150-GD).

Gas samples were collected at days 1, 3, 5, 7, 14, 21 and 28 using the static chamber method adapted from van Zwieten et al. [41]. Briefly, the containers containing the incubated, treated

soils were sealed and soil gas emissions were allowed to accumulate for exactly 10 minutes

(based on a CO_2 emission curve previously conducted). A gas tight syringe (SGE Analytical

Scientific) was used to extract an aliquot of soil gas emissions through a chlorobutyl septum

and was then introduced into a pre-evacuated Labco® exetainer vial. Collected gases were

analyzed for CO_2 using an Agilent Technologies 7890A Gas Chromatography – Thermal

Conductivity Detector (GC-TCD) and GC-Flame Ionization Detector (FID).

The flux rate, F_{CO2}, was calculated using equation 3 and noted as mg CO_2/m^2h:

$$F_{CO_2} = \frac{b \text{ x } V_{CH} \text{ x } MW_{CO_2} \text{ x } 60 \text{ x } 10^6}{A_{CH} \text{ x } MV_{corr} \text{ x } 10^9} \tag{3}$$

Where b is the CO_2 concentration measured in ppm/minute, V_{CH} is the volume of the measuring

chamber, MW_{CO_2} is the molecular weight of CO_2 (44 g/mol), A_{CH} refers to the basal area of the

measuring chamber and MV_{corr} is the temperature corrected molecular weight volume

calculated using equation 4:

$$MV_{corr} = 0.02241 \text{ x } \left(\frac{273.15+T}{273.15}\right) \tag{4}$$

Where T is the air temperature during the measurement and 0.02241 is the molar volume of

an ideal gas at 273.15 K, 1 atm.

4.5.5 Biodegradation Studies

Superabsorbent biodegradation was evaluated for two types of superabsorbent: freeze-dried

and oven-dried at 50 °C. For each type, superabsorbent was added to soil at the application

rates specified in section 4.5.3 to an overall weight of 10 g. Deionized water was added to reach

60% WHC. Similar to the microbial activity studies, two different control treatments were

prepared: one without any superabsorbent and another with a basal rate of fertilizer and 1 wt.%

of superabsorbent, as previously described. The latter was to review the effect of the fertilizer

on superabsorbent biodegradation. Five replicates were conducted for each treatment. Samples

were incubated at 23 °C and 80% relative humidity in a temperature/humidity control cabinet

(Thermoline L+M – 150-GD). Samples were destructively sampled at days 1, 3, 5, 7, 14, 21 and 28, dried in an oven at 60 °C and stored frozen at -20 °C until required.

Biodegradation was measured using the acid digestion method adapted from Sluiter et al. [42] to hydrolyze cellulose in the soil to glucose and glucuronic acid which were then measured. In brief, 3 mL of 72% sulfuric acid was added to 5 g of treated soil at room temperature. The mixture was placed in a water bath at 30 °C and incubated for 60 minutes. During this time, the mixture was occasionally stirred every 5 to 10 minutes to ensure even acid – soil contact. Dilution to 4% sulfuric acid was made by adding 83 mL of deionized water followed by autoclaving for 60 minutes at 121 °C. After cooling to room temperature, the soil was removed by filtration and the supernatant retained and neutralized to pH 5 – 6 using calcium carbonate. When neutralization was completed, the solids were separated by centrifugation at 4400 rpm for 10 minutes. The supernatant was collected and analyzed through high performance liquid chromatography (HPLC) using a BioRad Amminex HPX-87H column, 0.005M sulfuric acid as the mobile phase, with a refractive index detector at a temperature of 40 °C and a flow rate of 0.4 mL/minute. A scheme of the experimental set up is shown in Figure S1.

4.5.6 Swelling Studies

(i) Soil water extract. Water was extracted from the soil according to the saturation extract method adapted from Sparks et al. [43]. A mass of 1 kg of air-dried soil was weighed into a beaker. Deionized water was added to the soil until it was nearly saturated and the mixture was left at room temperature for 3 h to allow the dissolution of the soluble salts. More deionized water was added while stirring, until the soil paste shined and a soil-water paste was formed. The soil paste was left at room temperature for another 2 h. The soil paste was then filtered under vacuum using a Buchner funnel and filter paper. The filtrate (i.e. soil water extract) was centrifuged at 4400 rpm for 10 minutes to further separate any remaining solids from the soil water extract.

The soil water extract was characterized by Environmental Analysis Laboratories, at Southern Cross University [37], using Rayment and Lyons [38] standard methods (Table S2).

(ii) Swelling capacity: The swelling capacity of the superabsorbents was measured in the soil water extracts obtained in previous section to simulate real environment conditions, with comparison to deionized water. The swelling capacity and swelling rate were determined by weighing the samples before and after immersion in the soil water extract over different periods of time (1, 5, 15, 30, 60, 90, 150, 250 and 1440 minutes) at room temperature following the method described by Mendoza et al. [26]. The swelling capacity was calculated as follows [26, 44]:

$$\text{Swelling capacity}, Q = \frac{m_t - m_d}{m_d} \tag{5}$$

where m_t is the weight of the swollen gel at time t and m_d refers to the weight of the dried sample. Results are reported as the average and standard deviation of triplicates. Photographs of the experimental set up are shown in Figure S2.

4.5.7 Scanning electron microscopy (SEM)

The morphology of freeze-dried and oven-dried at 50 °C superabsorbents was evaluated by SEM on a FEI Magellan 400 and a Nova NanoSEM. SAPs were mounted on a metal stub coated with a 2 nm layer of Iridium. Micrographs were obtained in high vacuum-mode. Additional pore properties of these SAP are displayed in Table S3.

Data Analysis: The microbial activity data was analyzed statistically using a One-way ANOVA (analysis of variance) to evaluate differences between the means of the control and treatments. Dunnett's test was used to determine any significant differences between the control and the treatments. Biodegradation studies were analyzed statistically using a t-test analysis to evaluate

differences between the means the treatments. Both analyses were performed using GraphPad Prism 9.0.2.

4.6 Results

4.6.1 Swelling

The swelling capacity of the three nanocellulose superabsorbents in soil water extracts is expressed as a function of time (Figure 2). All superabsorbents show a similar behavior. Swelling uptake reaches a plateau after an initial absorption rate. In all cases, superabsorbents required up to 150 minutes to reach maximum capacity. Freeze-dried superabsorbent is characterized by an initial rapid swelling with most of it occurring during the first minutes. In contrast, superabsorbents dried via evaporation show a slower swelling rate.

Swelling at equilibrium is dictated by the drying technique used to prepare the superabsorbent and the swelling media employed (Figure 3). While SAP oven-dried at 50 °C achieves the highest absorption capacity in deionized water, freeze-dried SAP has the highest swelling capacity in soil water extracts of 90 g water/g superabsorbent. This is followed by SAP oven-dried at 50 °C and at 105 °C being 55 and 40 g water/g superabsorbent, respectively.
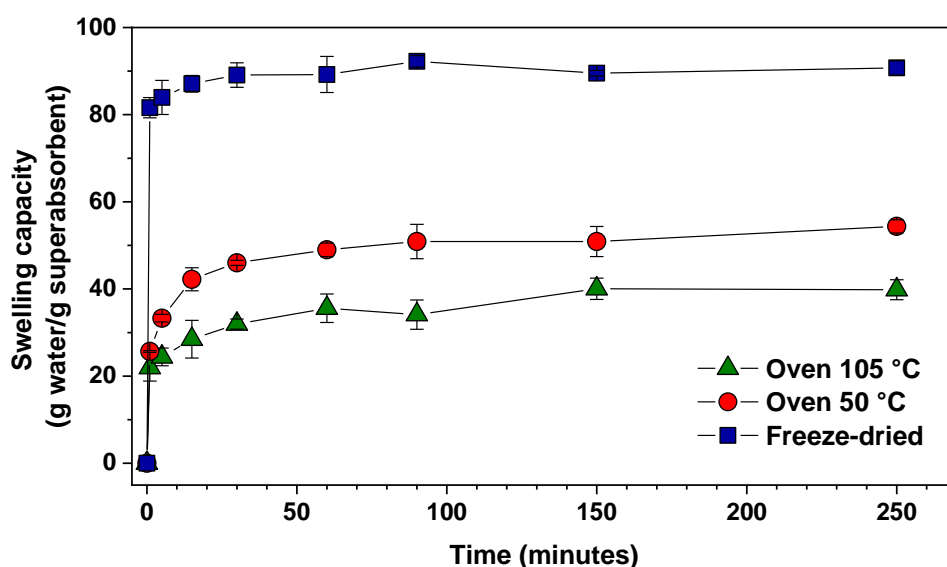
Figure 2. Effect of the drying process on the swelling capacity of nanocellulose superabsorbents immersed in soil water as a function of time. Results are reported as mean ± standard deviation (n=3).
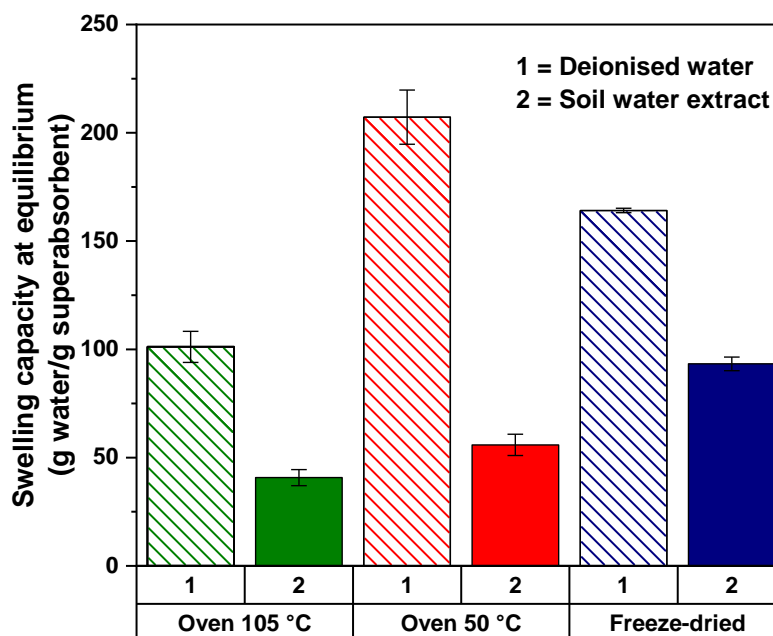
Figure 3. Effect of the drying process on the swelling capacity of nanocellulose superabsorbents at equilibrium. Comparison of deionized water with soil water extract. Results are reported as mean +/- standard deviation (n=3).

4.6.2 Soil Water Retention

The water retention of the soil amended with the nanocellulose superabsorbents was evaluated under two conditions: with and without further addition of deionized water after the initial irrigation – day 0 (Figure 4a-f). In all treatments, soil water retention increases as the nanocellulose SAP application rate increases. This is independent of the superabsorbent type. Soil amended with freeze-dried SAP shows the maximum water retention of 2.3 times higher than soils without superabsorbent (control) (Figure 4a). While controls required approximately 10 days to reach constant weight, soils amended with 1 wt.% application rate of any superabsorbent took between 25 to 33 days, 2.3 to 3 times longer time compared to the control.

For all treatments, the water retention effectiveness decreases with increasing number of irrigation cycles. This is noted via two different indicators. Firstly, the water retention of the soil treated with any superabsorbent decreases with increasing irrigation cycles. For example, the water retention of the soil treated with 1.0 wt.% oven-dried at 50 °C SAP changes from 170% in the first cycle to 110% and 85% in the second and third irrigation cycles, respectively. Secondly, the difference between the water retention of the soil treatments and the control decreases as the irrigation number increases. Both indicators suggest a decrease in the superabsorbent efficiency.
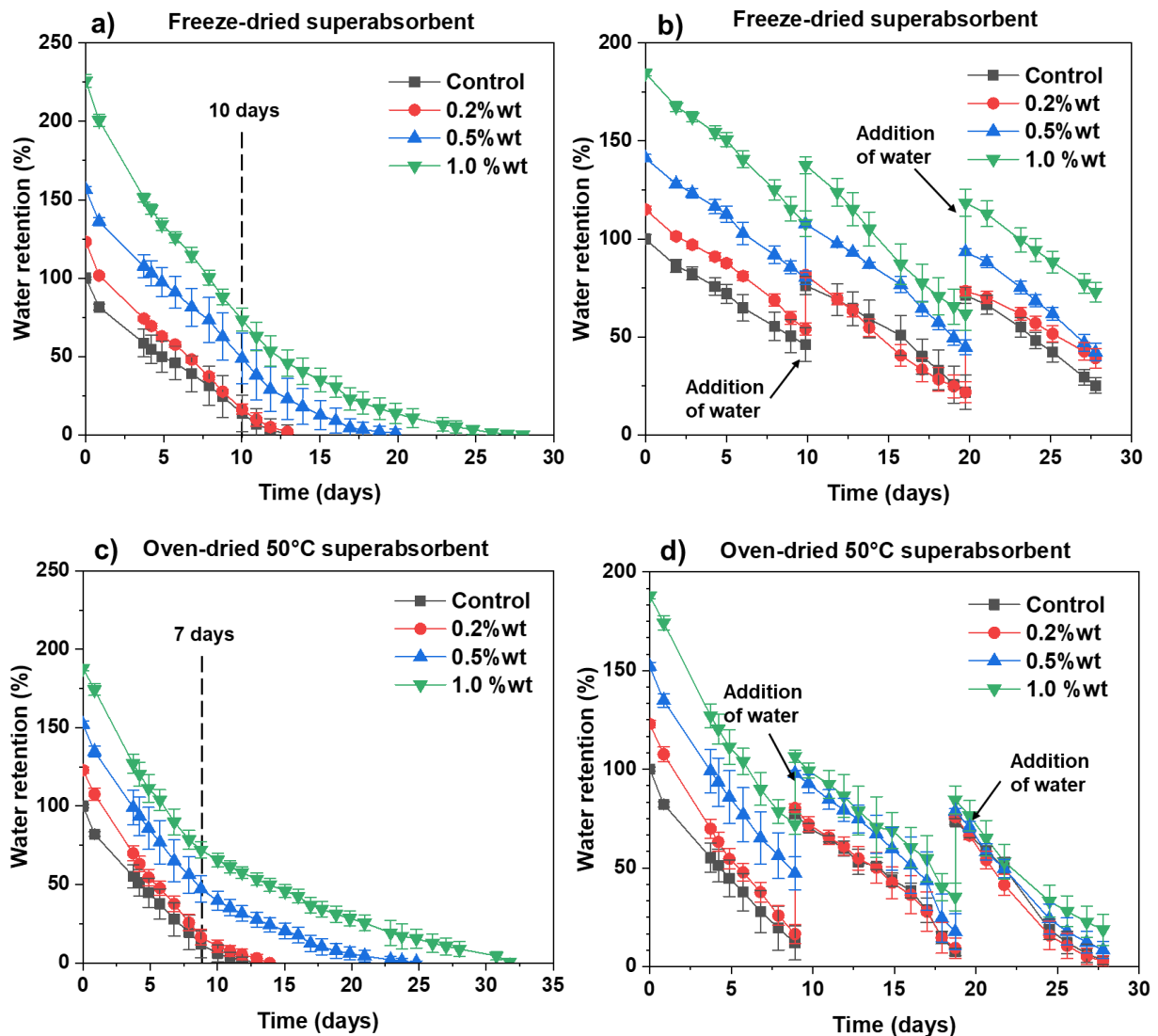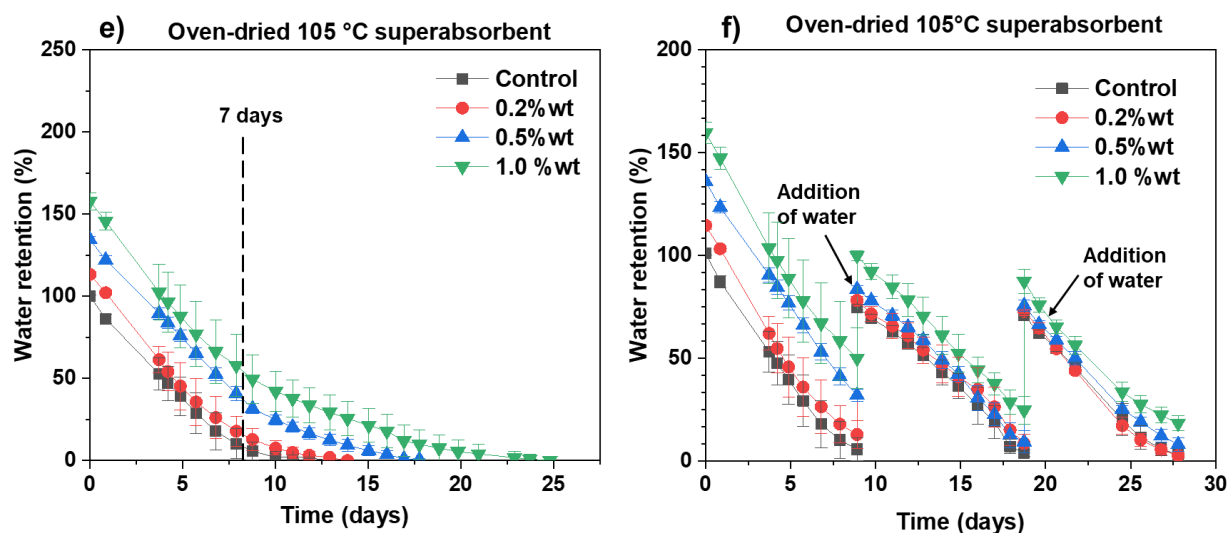
Figure 4. Water retention of soil treated with different nanocellulose superabsorbents over a period of 28 days with and without further addition of deionized water after initial irrigation: (a and b) freeze-dried SAP, (c and d) oven-dried 50 °C SAP and (e and f) oven-dried 105 °C SAP. Results are reported as mean ± standard deviation (n=5).

4.6.3 Microbial Activity

In general, for both types of superabsorbent, CO_2 emissions (i.e. respiration rates) increase with time and with application rate of SAP (Figure 5). This increase is more statistically significant when freeze-dried superabsorbent is used. The difference between the control and soil treated with 1 wt.% SAP ranges between 900 mg CO_2/m^2h to 1800 mg CO_2/m^2h for 50 °C oven-dried and freeze-dried SAP, respectively. These respiration rates signify the response of the soil microbial community to the presence of this nanocellulose superabsorbent. Similarly, fertilized soil amended with 1 wt.% of any SAP exhibits an increase of CO_2 emissions compared to the soil treatments without fertilizer.
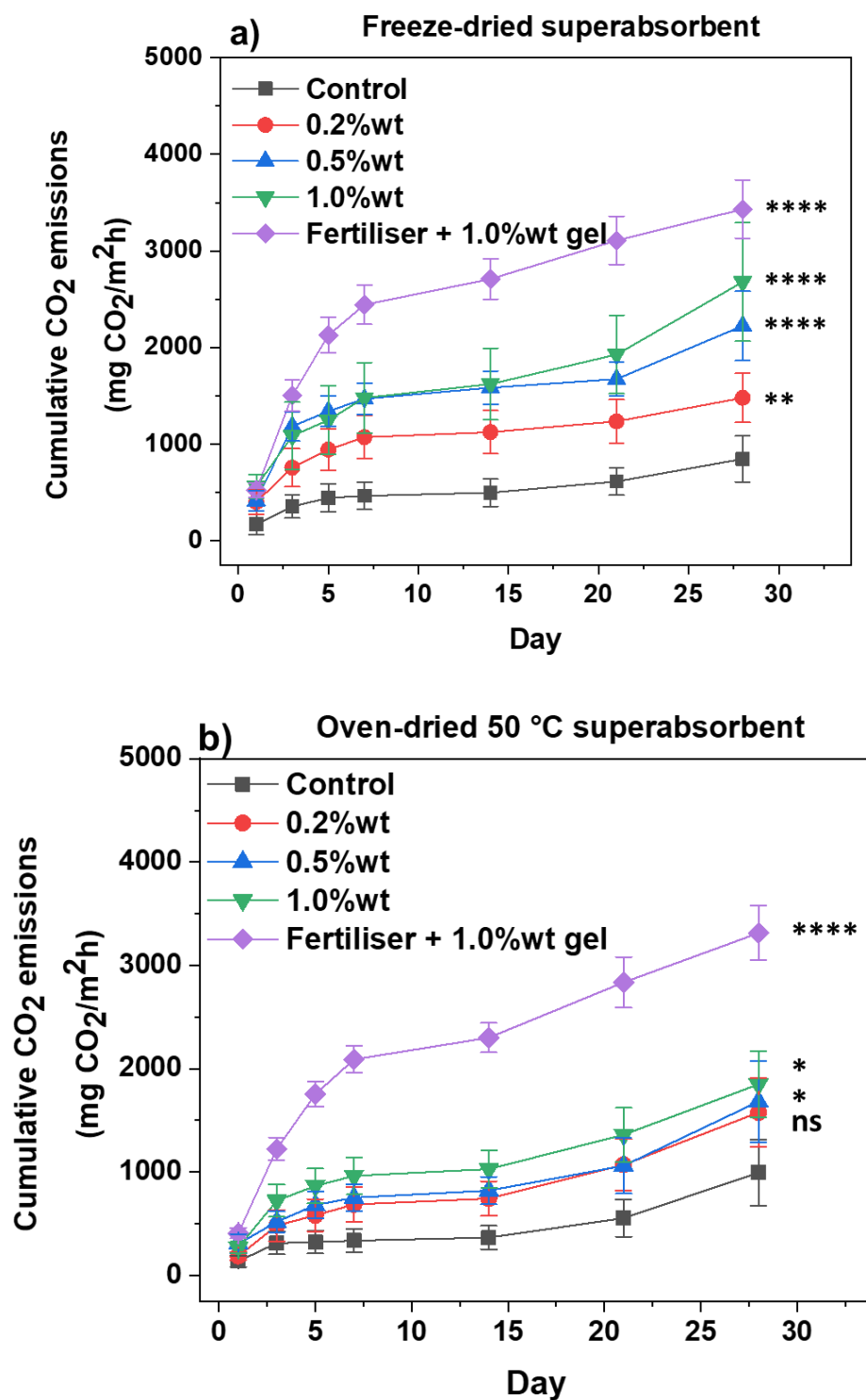
Figure 5. Cumulative CO_2 emissions of soil treated with different application rates of (a) freeze-dried superabsorbent and (b) oven-dried 50 °C superabsorbent. Results are reported as mean ± standard deviation (n=5). Statistical difference according to One-way ANOVA analysis followed by Dunnett's test against control is indicated. Here,

ns = no significant difference, * represents p ≤ 0.05, ** denotes p ≤ 0.01 and ****
is p ≤ 0.0001.

4.6.4 Biodegradation

For the soil used in this study, the rate of biodegradation is dependent upon the type and application rate of superabsorbent (Figure 6). For soil treated with 0.2 wt.% superabsorbent, both freeze-dried and oven-dried SAP follow the same degradation trend and approximately 40% of the initial SAP remains after 28 days exposure. No statistical difference is observed between soil treatments with either 0.2 wt.% or 0.5 wt.% application rate of superabsorbent. However, a difference in the biodegradation rate and SAP type is observed when the application rate increases. For the 1 wt.% treatment, freeze-dried SAP degradation starts after 7 days exposure, whereas degradation of oven-dried SAP throughout the 28 days of exposure is slow and almost negligible. Fertilizer addition to 1 wt.% treatment significantly increases the degradation rate; both nanocellulose superabsorbents exhibit similar rates compared to 0.2 wt.% treatment.
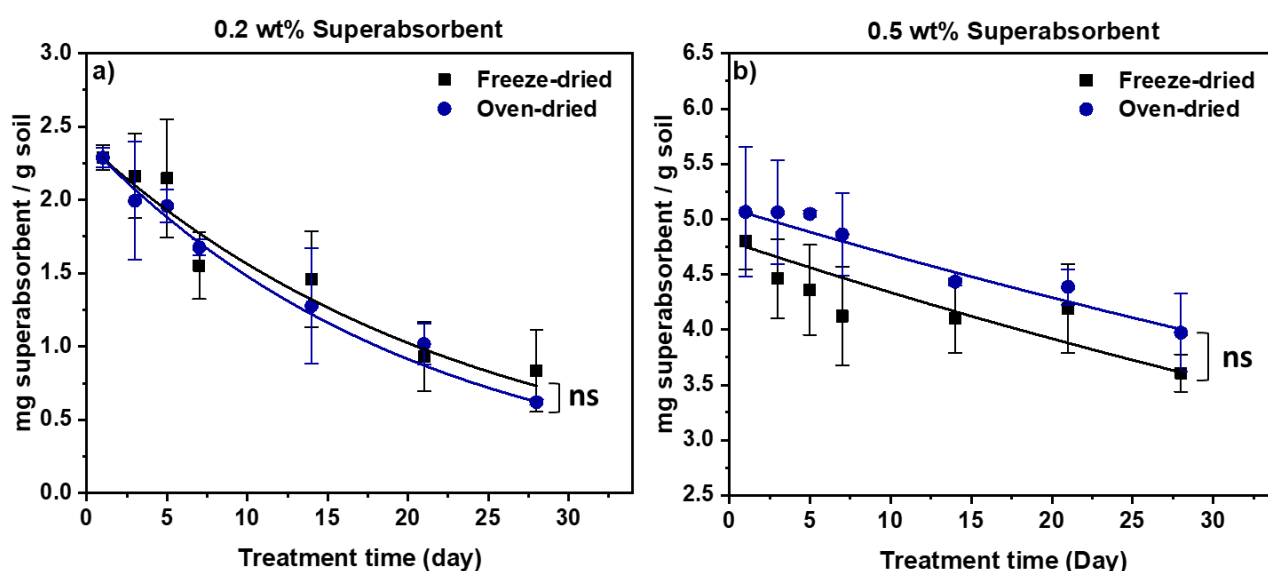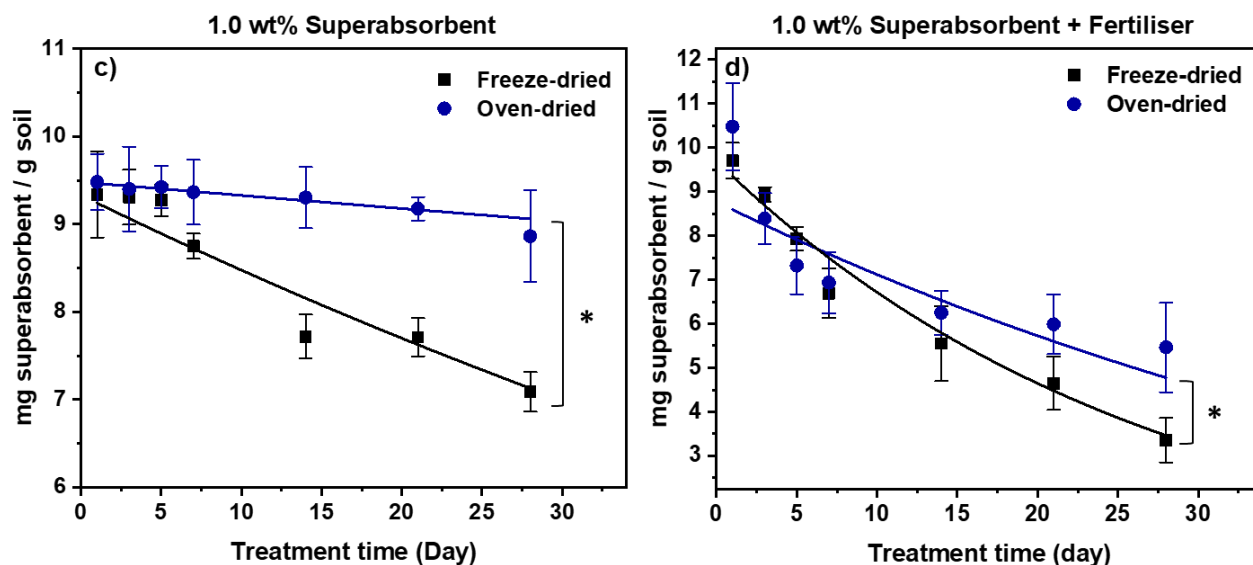
Figure 6. Effect of drying process on the superabsorbent biodegradation overtime in soil. (a) 0.2 wt.%, (b) 0.5 wt.%, (c) 1 wt.% and (d) 1 wt.% superabsorbent application rate + fertilizer addition. Results are reported as mean ± standard deviation (n=5). Statistical difference according to unpaired t-test. Here, ns= no significant difference between treatments, * is p ≤ 0.05.

4.7 Discussion

4.7.1 Effect of Ionic Strength on Superabsorbent Performance

The swelling capacity of nanocellulose-based superabsorbent was measured in the soil-water to evaluate their performance. A decrease in the absorption capacity of the superabsorbent results when salt concentration increases, independent of its type. This is because the swelling ability is driven by the difference in osmotic pressure inside and outside the polymer network caused by the movement of the counterions in the system [26]. These osmotic effects are diminished with increasing concentrations of salt, resulting in a decrease in swelling [35]. To measure the sensitivity of the superabsorbent materials towards the soil water extracts, the ionic sensitivity was measured as follows [45]:

$$\text{Ionic sensitivity, } f = 1 - \frac{Q_s}{Q_d} \qquad (6)$$

Where Q_s refers to the swelling in salt solution and Q_d is the swelling in deionized water, both in g of water/ g of SAP. Superabsorbents with lower f values are preferred for their performance, as higher f values mean a higher absorbency loss of the superabsorbent in salt solutions [35].

The ionic sensitivity (f) value of the superabsorbents studied is displayed in Figure 7. Oven-dried 50 °C SAP shows a higher ionic sensitivity compared to the others. This is attributed to its morphology, characterized by a high pore area and large number of small pores in the nanometer scale (Table S3 and Figure S3) [30]. This increases the number of accessible COO⁻ groups in the superabsorbent network, whereas the swelling mechanism of freeze-dried SAP is mainly driven by physical entrapment of water [26]. A higher number of accessible COO⁻ groups indicates a higher anion charge [46], which in the presence of salt solutions, results in a higher salt sensitivity and absorbency loss for oven-dried 50 °C superabsorbents.
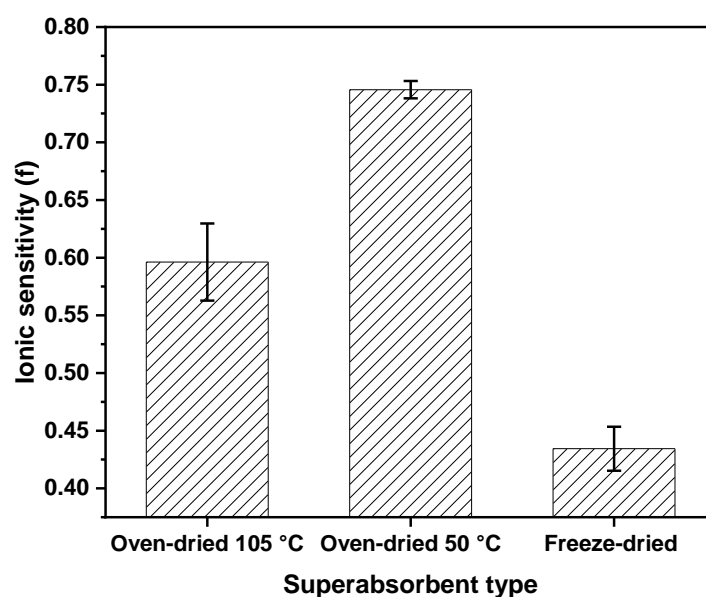
Figure 7. Ionic sensitivity value of the superabsorbents treated with soil water extracts. A low
f value indicates a lower drop of swelling capacity when salt solution replace water.
Results are reported as mean ± standard deviation (n=3).

4.7.2 Effect of Application Rate on Soil Water Retention

Addition of nanocellulose superabsorbent increases the water retention of the soil tested. Soil amended with freeze-dried superabsorbent achieved the highest water retention, at all application rates, followed by 50 °C oven-dried and 105 °C oven-dried SAP. These results are directly related to the SAP porous structure [30]. Such an increase in water content is hypothesized to increase the period of water available for the plant, as measured from the soils water evaporation rates. The evaporation rates of the soils amended with the highest superabsorbent application (1.0 wt.%) were slower than those of the controls. This results in a delay of the permanent wilting point by up to 20 days, reducing the water requirement of plants [47, 48]. This also confirms that nanocellulose derived SAP can retain water in soils for significantly longer periods [49]. The absorption capacity of these SAPs is in the range of what other authors have reported for cellulose-based SAP. Cannazza et al. [49] prepared superabsorbents based on carboxymethylcellulose and hydroxyethyl cellulose cross-linked with citric acid with a swelling capacity of up to 75 and 40 g water/g superabsorbent in deionized and tap water, respectively.

There are three different drying regimes for each type of superabsorbent and application rate. The first corresponds to the water evaporating from the soil. This regime starts from day 0 up to day 8-10 for freeze-dried and oven-dried SAPs. This is followed by a transitionary phase, as the soil is completely dried and the superabsorbent starts to release water. Finally, the last drying regime corresponds to the evaporation of water from the superabsorbent itself. This regime is indicated by the different slopes of each SAP depending on the application rate and lasts from the transitionary phase onwards. These regimes can be used to correlate the soil moisture and superabsorbent efficiency over time.

Interestingly, soil treated with 1.0 wt.% of freeze-dried SAP loses water at a faster rate than oven-dried 50 °C SAP. This difference in drying rate is attributed to their difference in SAP

structure and the influence of soil structure and how it interacts with the SAP. Freeze-dried superabsorbent is a foamy-like material characterized by an open structure, whereas oven-dried SAP is a thin-film with pores ranging in the nanometer scale [30]. When the freeze-dried nanocellulose SAP dries, its structure collapses, leaving large pores in the soil which increase soil matrix porosity and facilitate water evaporation [50].

Comparing water retention of the soil treatments after several irrigation cycles, all treatments presented a similar behavior: high-water absorption in the first cycle which decreased in the subsequent cycles. This was independent of the application rate. This decrease is mainly attributed to two factors. Firstly, the metal ions in the soil that are released in the presence of water. When the superabsorbent absorbs this water, these ions strongly bind to the carboxylate groups of the nanocellulose, blocking their active negative sites and decreasing absorbency. SAP blockage increases with each further cycle of irrigation and drying [51]. This effect was reported previously by Spagnol et al., who found an increase formation of crosslinking points due to the physical interaction of multivalent cations (e.g. Mg^{2+} and Ca^{2+}) and the carboxylate groups present in superabsorbents based on poly(acrylamide-co-acrylate) and cellulose nanowhiskers [52]. The second main factor affecting the SAP efficiency is its degradation [49].

4.7.3 Superabsorbent Effect on Microbial Community and Its Biodegradation

Respiration rates of the soil amended with nanocellulose SAP increased with increasing application rate. This is because the addition of a carbon source to the soil increases the population of carbon decomposing microbes which results in an increase in respiration rate [53-56]. Adding fertilizer further accelerates soil respiration rates for both types of superabsorbent. This is because of the increase in microbial biomass by nutrient addition which boosts the decomposition rate of soil carbon [55].

Respiration rates of each treatment are related to the superabsorbent degradation rate in soil which follows the negative exponential function [57]:

$$C(t) = C_0 e^{-kt} \tag{7}$$

Where $C(t)$ stands for the superabsorbent concentration (mg/g) in the soil at time t of incubation, C_0 is the superabsorbent concentration at day 0, and k is the rate constant of the superabsorbent decay with time (day^{-1}). The decay rate constants, k, for all the treatments are listed in Table I. Decay rate constants varied widely from 0.001 d^{-1} to 0.048 d^{-1} depending on the SAP type and application rate. This model successfully described decomposition rates of carbon sources such as cellulose or manure [58-60]. The decay rate constant of the soil amended with 0.2 wt.% SAP was similar for nanocellulose freeze-dried and oven-dried 50 °C, ranging between 0.042 and 0.048 d^{-1}, respectively. The rate of superabsorbent decomposition in soil is independent of the type of superabsorbent (either freeze-dried or oven-dried). Considering that the SAP is composed of more than 90% cellobiose units with the remainder being oxidized glucose units, its decomposition rate can be compared to that of cellulose, reported to range from 0.03 and 0.06 d^{-1} [57, 60]. The calculated values of soil amended with 0.2 wt.% SAP correspond to this range. The rate of superabsorbent breakdown is affected by soils and incubation conditions: moisture content and temperature.

This rate is also governed by the initial population of microbes and nutrients available in the soil. For example, decomposition of 0.5 wt.% oven-dried SAP in soil is delayed until day 5. This is due to the time required to build up the microbial biomass in soil necessary to kick off the decomposition process. Such effect is not observed in soil amended with freeze-dried SAP because of its porous structure which increases soil porosity. This increases oxygen diffusion and air permeability [61], which facilitates the increase in microbial biomass. However, a delay in degradation is observed as the application rate increases. This is most likely due to nutrient depletion impacting the microbial population. This is supported by the fertilizer addition to 1 wt.% soil treatments which accelerates SAP breakdown, exhibiting similar rates to 0.2 wt.% SAP in soil without fertilizer.

Table I. Decay rate constants of freeze-dried and oven-dried superabsorbents. Results are reported as mean ± standard deviation (n=5).

Cellulose application rate (wt.%)	Cellulose initial concentration (mg/g)	Decay rate constant (day^{-1})	R^2
Freeze-dried			
0.2 wt.%	2.28 ± 0.08	0.042 ± 0.0038	0.97
0.5 wt.%	4.80 ± 0.25	0.010 ± 0.0006	0.90
1.0 wt.%	9.33 ± 0.48	0.009 ± 0.0007	0.91
1.0 wt.% + Fertilizer	9.70 ± 0.41	0.037 ± 0.0022	0.97
Oven-dried 50 °C			
0.2 wt.%	2.28 ± 0.06	0.048 ± 0.0007	0.99
0.5 wt.%	5.06 ± 0.58	0.008 ± 0.0009	0.81
1.0 wt.%	9.48 ± 0.32	0.001 ± 0.0001	0.91
1.0 wt.% + Fertilizer	10.47 ± 0.99	0.017 ± 0.0052	0.74

4.8 Conclusion

Carboxylated nanocellulose superabsorbent polymers (SAPs) were evaluated as water retention agents for agricultural use. SAPs were made from TEMPO mediated oxidation of cellulose followed by high pressure homogenization and drying. Three drying methods were studied: freeze-dried and oven-dried at low (50 °C) and high (105 °C) temperatures. The effect of the nanocellulose superabsorbents on the soil water retention and microbial community in a calcarosol soil was analyzed and the swelling capacity on soil water and biodegradation rate were determined.

The water retention of soil increases with application rate of superabsorbent. The extent of this increase in water holding capacity and the profile of water retention over time are dependent on the type of SAP. These water retention properties decrease as the superabsorbent degrades.

Soil amended with freeze-dried superabsorbent has the highest water retention, followed by 50 °C oven-dried and 105 °C oven-dried SAP. The high ionic sensitivity of 50 °C oven-dried SAP is due to its high pore area and numerous accessible COO^- groups. Soil amended with this superabsorbent remains moist the longest. This increase in water content prolongs the period of water available for the plant, delaying the permanent wilting point by up to 20 days.

Soil respiration rate increases as a function of superabsorbent application rate. This is related to the SAP decomposition rate which, in the calcarosol soil used in this study, mainly occurs within 30 days exposure, independently of the type of nanocellulose superabsorbent. This decomposition rate is governed by the nutrient availability and the initial microbial biomass in the soil. Carboxylated nanocellulose-based superabsorbents are attractive alternatives to replace our current non-biodegradable and unsustainable petroleum SAP for agricultural use. The full characterization of plant growth, including crop productivity and soil sustainability as well as refinements of the SAP structural alteration required to prolong its biodegradability are now needed.

4.9 Acknowledgement

4.10 References

[1]   Organisation for Economic Co-operation and Development. "Managing water sustainably is key to the future of food and agriculture." https://www.oecd.org/agriculture/topics/water-and-agriculture/ (accessed 12/06/2020, 2020).

[2]   W. a. t. E. Department of Agriculture, . "Water for food." Australian Government. https://www.agriculture.gov.au/water/water-for-food (accessed 12/06/2020, 2020).

[3]   B. A. Müller C., Popp A., Waha K., Fader M.,, "Climate change impacts on agricultural yields," in "World Development Report " Potsdam Institute for Climate Impact Research, Germany, 2010.

[4]   M. J. Zohuriaan-Mehr, Kabiri, Kourosh.,, "Superabsorbent Polymer Materials: A review," *Iranian Polymer Journal,* vol. 17, no. 6, pp. 451-477, 2008.

[5]   M. R. Guilherme *et al.*, "Superabsorbent hydrogels based on polysaccharides for application in agriculture as soil conditioner and nutrient carrier: A review," *European Polymer Journal,* vol. 72, pp. 365-385, 2015, doi: 10.1016/j.eurpolymj.2015.04.017.

[6]   E. M. Ahmed, "Hydrogel: Preparation, characterization, and applications: A review," *Journal of Advanced Research,* vol. 6, no. 2, pp. 105-121, 2015/03/01/ 2015, doi: https://doi.org/10.1016/j.jare.2013.07.006.

[7]   S. Ghorbani *et al.*, "Hydrogels Based on Cellulose and its Derivatives: Applications, Synthesis, and Characteristics," *Polymer Science, Series A,* vol. 60, no. 6, pp. 707-722, 2019, doi: 10.1134/s0965545x18060044.

[8]   X. Shen, J. L. Shamshina, P. Berton, G. Gurau, and R. D. Rogers, "Hydrogels based on cellulose and chitin: fabrication, properties, and applications," *Green Chemistry,* 10.1039/C5GC02396C vol. 18, no. 1, pp. 53-75, 2016, doi: 10.1039/C5GC02396C.

[9]   J. R. Gross, "The Evolution of Absorbent Materials," in *Studies in Polymer Science*, vol. 8, L. Brannon-Peppas and R. S. Harland Eds.: Elsevier, 1990, pp. 3-22.

[10]   R. Curvello, V. S. Raghuwanshi, and G. Garnier, "Engineering nanocellulose hydrogels for biomedical applications," *Advances in Colloid and Interface Science,* vol. 267, pp. 47-61, 2019/05/01/ 2019, doi: https://doi.org/10.1016/j.cis.2019.03.002.

[11]   H. M. Shewan and J. R. Stokes, "Review of techniques to manufacture micro-hydrogel particles for the food industry and their applications," *Journal of Food Engineering,* vol. 119, no. 4, pp. 781-792, 2013/12/01/ 2013, doi: https://doi.org/10.1016/j.jfoodeng.2013.06.046.

[12]   A. Bashari, A. Rouhani Shirvan, and M. Shakeri, "Cellulose-based hydrogels for personal care products," *Polymers for Advanced Technologies,* vol. 29, no. 12, pp. 2853-2867, 2018, doi: 10.1002/pat.4290.

[13]   M. J. Zohuriaan-Mehr, H. Omidian, S. Doroudiani, and K. Kabiri, "Advances in non-hygienic applications of superabsorbent hydrogel materials," *Journal of Materials Science,* journal article vol. 45, no. 21, pp. 5711-5735, November 01 2010, doi: 10.1007/s10853-010-4780-1.

[14]   F. F. Montesano, A. Parente, P. Santamaria, A. Sannino, and F. Serio, "Biodegradable Superabsorbent Hydrogel IncreasesWater Retention Properties of Growing Media and Plant Growth," *Agriculture and Agricultural Science Procedia,* vol. 4, pp. 451-458, 2015, doi: 10.1016/j.aaspro.2015.03.052.

[15]   E. S. Abrisham *et al.*, "Effects of a super absorbent polymer on soil properties and plant growth for use in land reclamation," *Arid Land Research and Management,* vol. 32, no. 4, pp. 407-420, 2018/10/02 2018, doi: 10.1080/15324982.2018.1506526.

[16]   S. Behera and P. A. Mahanwar, "Superabsorbent polymers in agriculture and other applications: a review," *Polymer-Plastics Technology and Materials,* vol. 59, no. 4, pp. 341-356, 2020/03/03 2020, doi: 10.1080/25740881.2019.1647239.

[17]   Reddy Kathi S., "Effect of different doses of superabsorbent polymer (SAP) on water and nitrogen retention in soil, and on the growth and development of tomato and determination of optimal rate of SAP," Master of Science, Plant and soil science College of Graduate Studies Texas A&M University-Kingsville, Texas, 2019.

[18] Z. Steinmetz *et al.*, "Plastic mulching in agriculture. Trading short-term agronomic benefits for long-term soil degradation?," *Science of The Total Environment,* vol. 550, pp. 690-705, 2016/04/15/ 2016, doi: https://doi.org/10.1016/j.scitotenv.2016.01.153.

[19] A. A. Horton, A. Walton, D. J. Spurgeon, E. Lahive, and C. Svendsen, "Microplastics in freshwater and terrestrial environments: Evaluating the current understanding to identify the knowledge gaps and future research priorities," *Science of The Total Environment,* vol. 586, pp. 127-141, 2017/05/15/ 2017, doi: https://doi.org/10.1016/j.scitotenv.2017.01.190.

[20] L. Ramos, G. Berenstein, E. A. Hughes, A. Zalts, and J. M. Montserrat, "Polyethylene film incorporation into the horticultural soil of small periurban production units in Argentina," *Science of The Total Environment,* vol. 523, pp. 74-81, 2015/08/01/ 2015, doi: https://doi.org/10.1016/j.scitotenv.2015.03.142.

[21] P. Chen, W. A. Zhang, W. Luo, and Y. e. Fang, "Synthesis of superabsorbent polymers by irradiation and their applications in agriculture," *Journal of Applied Polymer Science,* vol. 93, no. 4, pp. 1748-1755, 2004, doi: 10.1002/app.20612.

[22] M. R. Guilherme, A. V. Reis, A. T. Paulino, T. A. Moia, L. H. C. Mattoso, and E. B. Tambourgi, "Pectin-based polymer hydrogel as a carrier for release of agricultural nutrients and removal of heavy metals from wastewater," *Journal of Applied Polymer Science,* pp. n/a-n/a, 2010, doi: 10.1002/app.32123.

[23] G. Ö. Kayan and A. Kayan, "Composite of Natural Polymers and Their Adsorbent Properties on the Dyes and Heavy Metal Ions," *Journal of Polymers and the Environment,* 2021/04/24 2021, doi: 10.1007/s10924-021-02154-x.

[24] S. Varanasi, R. He, and W. Batchelor, "Estimation of cellulose nanofibre aspect ratio from measurements of fibre suspension gel point," *Cellulose,* vol. 20, no. 4, pp. 1885-1896, 2013, doi: 10.1007/s10570-013-9972-9.

[25] N. Lavoine and L. Bergström, "Nanocellulose-based foams and aerogels: processing, properties, and applications," *Journal of Materials Chemistry A,* vol. 5, no. 31, pp. 16105-16117, 2017, doi: 10.1039/c7ta02807e.

[26] L. Mendoza, L. Hossain, E. Downey, C. Scales, W. Batchelor, and G. Garnier, "Carboxylated nanocellulose foams as superabsorbents," *J Colloid Interface Sci,* vol. 538, pp. 433-439, Mar 7 2019, doi: 10.1016/j.jcis.2018.11.112.

[27] Q. Li, S. McGinnis, C. Sydnor, A. Wong, and S. Renneckar, "Nanocellulose Life Cycle Assessment," *ACS Sustainable Chemistry & Engineering,* vol. 1, no. 8, pp. 919-928, 2013/08/05 2013, doi: 10.1021/sc4000225.

[28] S. M. F. Kabir, P. P. Sikdar, B. Haque, M. A. R. Bhuiyan, A. Ali, and M. N. Islam, "Cellulose-based hydrogel materials: chemistry, properties and their prospective applications," *Prog Biomater,* vol. 7, no. 3, pp. 153-174, Sep 2018, doi: 10.1007/s40204-018-0095-0.

[29] A. Isogai, T. Saito, and H. Fukuzumi, "TEMPO-oxidized cellulose nanofibers," *Nanoscale,* 10.1039/C0NR00583E vol. 3, no. 1, pp. 71-85, 2011, doi: 10.1039/C0NR00583E.

[30] R. M. Barajas-Ledesma, A. F. Patti, V. N. L. Wong, V. S. Raghuwanshi, and G. Garnier, "Engineering nanocellulose superabsorbent structure by controlling the drying rate," *Colloids and Surfaces A: Physicochemical and Engineering Aspects,* vol. 600, 2020, doi: 10.1016/j.colsurfa.2020.124943.

[31] S. Li and G. Chen, "Agricultural waste-derived superabsorbent hydrogels: Preparation, performance, and socioeconomic impacts," *Journal of Cleaner Production,* vol. 251, p. 119669, 2020/04/01/ 2020, doi: https://doi.org/10.1016/j.jclepro.2019.119669.

[32]   H. Zhang *et al.*, "Cellulose Anionic Hydrogels Based on Cellulose Nanofibers As Natural Stimulants for Seed Germination and Seedling Growth," *J Agric Food Chem,* vol. 65, no. 19, pp. 3785-3791, May 17 2017, doi: 10.1021/acs.jafc.6b05815.

[33]   Y. Zhou, S. Fu, L. Zhang, and H. Zhan, "Superabsorbent nanocomposite hydrogels made of carboxylated cellulose nanofibrils and CMC-g-p(AA-co-AM)," *Carbohydrate Polymers,* vol. 97, no. 2, pp. 429-435, 2013/09/12/ 2013, doi: https://doi.org/10.1016/j.carbpol.2013.04.088.

[34]   C. Liliana Serna and M. A. Guancha-Chalapud, "Natural fibers for hydrogels production and their applications in agriculture," (in English), *Acta Agronómica,* vol. 66, no. 4, pp. 495-505, 2017 2017, doi: http://dx.doi.org/10.15446/acag.v66n4.56875.

[35]   I. H. Mondal, *Cellulose-Based Superabsorbent Hydrogels* (Polymers and Polymeric Composites: A Reference Series). 2019.

[36]   R. F. Isbell, *The Australian soil classification*, Second edition. ed. Clayton South, VIC, Australia : CSIRO Publishing, 2016.

[37]   S. C. U. Environmental Analysis Laboratory, . "Agricultural soil testing." https://www.scu.edu.au/environmental-analysis-laboratory---eal/analytical-services/agricultural-soil-testing/ (accessed 31/07/2020, 2020).

[38]   G. E. Rayment, *Soil chemical methods Australasia*. Collingwood, Vic.: Collingwood, Vic. : CSIRO Pub., 2011.

[39]   P. Sar, S. Ghosh, Y. D. Gordievskaya, K. G. Goswami, E. Y. Kramarenko, and P. De, "pH-Induced Amphiphilicity-Reversing Schizophrenic Aggregation by Alternating Copolymers," *Macromolecules,* vol. 52, no. 21, pp. 8346-8358, 2019/11/12 2019, doi: 10.1021/acs.macromol.9b01804.

[40]   K. G. Goswami *et al.*, "Self-Assembly of Amphiphilic Copolymers with Sequence-Controlled Alternating Hydrophilic–Hydrophobic Pendant Side Chains," *ACS Applied Polymer Materials,* vol. 2, no. 5, pp. 2035-2045, 2020/05/08 2020, doi: 10.1021/acsapm.0c00204.

[41]   L. van Zwieten *et al.*, "Influence of biochars on flux of N2O and CO2 from Ferrosol," (in English), *Australian Journal of Soil Research,* Article vol. 48, p. 555+, 2010 2010. [Online]. Available: https://link.gale.com/apps/doc/A241179274/AONE?u=monash&sid=AONE&xid=088435d9.

[42]   A. Sluiter *et al.*, "Determination of structural carbohydrates and lignin in biomass, in: Laboratory Analytical Procedure (LAP)," *National Renewable Energy Laboratory,* 01/01 2008.

[43]   D. L. e. Sparks, *Methods of soil analysis. Part 3, Chemical methods*. Madison, Wisconsin : Soil Science Society of America : American Society of Agronomy, 1996.

[44]   R. M. Barajas-Ledesma, A. F. Patti, V. N. L. Wong, V. S. Raghuwanshi, and G. Garnier, "Engineering nanocellulose superabsorbent structure by controlling the drying rate," *Colloids and Surfaces A: Physicochemical and Engineering Aspects,* vol. 600, p. 124943, 2020/09/05/ 2020, doi: https://doi.org/10.1016/j.colsurfa.2020.124943.

[45]   K. Kabiri, S. Faraji-Dana, and M. J. Zohuriaan-Mehr, "Novel sulfobetaine-sulfonic acid-contained superswelling hydrogels," *Polymers for Advanced Technologies,* vol. 16, no. 9, pp. 659-666, 2005, doi: 10.1002/pat.637.

[46]   L. Hossain, E. Eastman, M. De Rango, V. S. Raghuwanshi, J. Tanner, and G. Garnier, "Absorption kinetics of nanocellulose foams: Effect of ionic strength and surface charge," *Journal of colloid and interface science,* vol. 601, pp. 124-132, 2021, doi: 10.1016/j.jcis.2021.05.092.

[47]   M. K. Akhter J., Malik K.A., Mardan A., Ahmad M., M.M. Iqbal, "Effects of hydrogel amendment on water storage of sandy loam and loam soils and seedling growth of barley, wheat and chickpea," *Plant, Soil and Environment,* vol. 50, no. 10, pp. 463-469, 2004.

[48]   C. Demitri, F. Scalera, M. Madaghiele, A. Sannino, and A. Maffezzoli, "Potential of Cellulose-Based Superabsorbent Hydrogels as Water Reservoir in Agriculture," (in English), *International Journal of Polymer Science,* vol. 2013, 2013 2013, doi: http://dx.doi.org/10.1155/2013/435073.

[49]   G. Cannazza, A. Cataldo, E. De Benedetto, C. Demitri, M. Madaghiele, and A. Sannino, "Experimental Assessment of the Use of a Novel Superabsorbent polymer (SAP) for the Optimization ofWater Consumption in Agricultural Irrigation Process," *Water,* vol. 6, no. 7, pp. 2056-2069, 2014, doi: 10.3390/w6072056.

[50]   K. Beven and P. Germann, "Macropores and water flow in soils," *Water Resources Research,* vol. 18, no. 5, pp. 1311-1325, 1982, doi: 10.1029/WR018i005p01311.

[51]   S. A. Shahid, A. A. Qidwai, F. Anwar, I. Ullah, and U. Rashid, "Improvement in the Water Retention Characteristics of Sandy Loam Soil Using a Newly Synthesized Poly(acrylamide-co-acrylic Acid)/AlZnFe2O4 Superabsorbent Hydrogel Nanocomposite Material," (in English), *Molecules,* vol. 17, no. 8, pp. 9397-9412, 2012 2012, doi: http://dx.doi.org/10.3390/molecules17089397.

[52]   C. Spagnol *et al.*, "Nanocomposites based on poly(acrylamide-co-acrylate) and cellulose nanowhiskers," *European Polymer Journal,* vol. 48, no. 3, pp. 454-463, 2012, doi: 10.1016/j.eurpolymj.2011.12.005.

[53]   W. H. Schlesinger and J. A. Andrews, "Soil respiration and the global carbon cycle," (in English), *Biogeochemistry,* vol. 48, no. 1, pp. 7-20, Jan 2000 2000, doi: http://dx.doi.org/10.1023/A:1006247623877.

[54]   P. Högberg and A. Ekblad, "Substrate-induced respiration measured in situ in a C3-plant ecosystem using additions of C4-sucrose," *Soil Biology and Biochemistry,* vol. 28, no. 9, pp. 1131-1138, 1996/09/01/ 1996, doi: https://doi.org/10.1016/0038-0717(96)00124-1.

[55]   A. Gallardo and W. H. Schlesinger, "Factors limiting microbial biomass in the mineral soil and forest floor of a warm-temperate forest," *Soil Biology and Biochemistry,* vol. 26, no. 10, pp. 1409-1415, 1994/10/01/ 1994, doi: https://doi.org/10.1016/0038-0717(94)90225-9.

[56]   S. Fontaine, G. Bardoux, D. Benest, B. Verdier, and et al., "Mechanisms of the Priming Effect in a Savannah Soil Amended with Cellulose," (in English), *Soil Science Society of America Journal,* vol. 68, no. 1, pp. 125-131, Jan/Feb 2004 2004.

[57]   H. P. Hartmann and T. Appel, "Calibration of near infrared spectra for measuring decomposing cellulose and green manure in soils," *Soil Biology and Biochemistry,* vol. 38, no. 5, pp. 887-897, 2006/05/01/ 2006, doi: https://doi.org/10.1016/j.soilbio.2005.08.005.

[58]   G. Cabassi, P. M. Gallina, S. Barzaghi, T. M. P. Cattaneo, and L. Bechini, "Near Infrared Monitoring of Mineralisation of Liquid Dairy Manure in Agricultural Soils," *Journal of Near Infrared Spectroscopy,* vol. 16, no. 1, pp. 59-69, 2008, doi: 10.1255/jnirs.762.

[59]   D. Chmolowska, N. Hamda, and R. Laskowski, "Cellulose decomposed faster in fallow soil than in meadow soil due to a shorter lag time," *Journal of Soils and Sediments,* vol. 17, no. 2, pp. 299-305, 2017/02/01 2017, doi: 10.1007/s11368-016-1536-9.

[60]   A. Hadas, L. Kautsky, M. Goek, and E. Erman Kara, "Rates of decomposition of plant residues and available nitrogen in soil, related to residue composition through

simulation of carbon and nitrogen turnover," *Soil Biology and Biochemistry,* vol. 36, no. 2, pp. 255-266, 2004/02/01/ 2004, doi: https://doi.org/10.1016/j.soilbio.2003.09.012.

[61]   H. Domżał, J. Gliński, and J. Lipiec, "Soil compaction research in Poland," *Soil and Tillage Research,* vol. 19, no. 2, pp. 99-109, 1991/02/01/ 1991, doi: https://doi.org/10.1016/0167-1987(91)90079-D.

THIS PAGE HAS BEEN INTENTIONALLY LEFT BLANK

CHAPTER 5:

EFFECT OF NANOCELLULOSE-BASED SUPERABSORBENT ON THE EARLY STAGE GROWTH OF TATSOI (BRASSICA RAPA NARINOSA)

THIS PAGE HAS BEEN INTENTIONALLY LEFT BLANK

PREFACE

Chapter 4 established that the SAPs used in this study have a limited lifetime in terms of biodegradability and associated effectiveness in wetting-drying cycles. In the development of nanocellulose SAPs for agricultural soils, understanding the effect of these SAP on plant growth is vital. Soil incubation studies revealed that the nanocellulose SAP oven-dried at 50 °C was the best material to retain soil water for the longest period of time. This chapter evaluates the effect of different application rates of this SAP on Tatsoi plants grown under water stress; thus, addressing the fourth objective in this study; which is to quantify the effect of different applications of nanocellulose SAP on plants grown under water stress, and to compare the performance of this superabsorbent with a commercial SAP based on polyacrylamide

To do this, a pot trial was carried out in a greenhouse where plants were grown in soils amended with two application rates of nanocellulose, SAP: 0.5 and 1 wt.% and at three levels of soil moisture: 70, 40 and 20%. The total water added and water use efficiency were determined. Plant biomass was measured and related to the SAP application rate. These parameters were used to determine the most suitable application rate of nanocellulose SAP to soils. Likewise, the performance of this SAP was compared to an anionic polyacrylamide-based SAP which is commercially available.

THIS PAGE HAS BEEN INTENTIONALLY LEFT BLANK

Chapter 5: Effect of Nanocellulose-based superabsorbent on the early stage growth of tatsoi (*Brassica rapa narinosa*)

THIS PAGE HAS BEEN INTENTIONALLY LEFT BLANK

Effect of Nanocellulose-based superabsorbent on the early stage growth of tatsoi (*Brassica rapa narinosa*)

5.1 Abstract

In this study, tatsoi plants were grown in soils amended with varying application rates of nanocellulose-based superabsorbent (SAP) and under water stress. Total water added, water use efficiency (WUE) and plant yield were measured. Results were compared to soils treated with a commercially available polyacrylamide-based SAP. WUE significantly increased, by a factor of 4, in soils amended with commercial SAP compared to those without superabsorbent. While there is no difference in the plant biomass between treatments of 0.5 wt% of nanocellulose and the fertilised control, it significantly decreased when the SAP application rate was increased to 1.0 wt%. This was attributed to an immobilisation of nitrogen by microbial biomass. These results were supported by the microbial activity, where soil respiration rates increased with increasing application of nanocellulose SAP. Future studies are needed to modify the nanocellulose structure, prolonging its biodegradation and overcoming the nitrogen drawdown effect.

5.2 Keywords

Nanocellulose superabsorbent, plant growth, tatsoi, brassica rapa narinosa, bok choy, water use efficiency, nitrogen drawdown.

5.3 Graphical Abstract
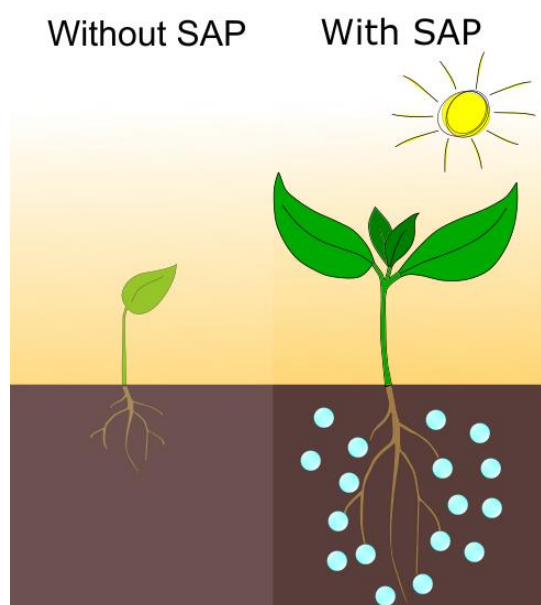
5.4 Introduction

Access to clean water and food security are ranked in the top ten global challenges facing mankind today [1]. Both elements are essential for a healthy, dynamic society and to reduce extreme poverty. With the increase in world's population, there is an increasing demand for food and fresh water. Irrigated agriculture consumes around 70% of the water available for human use worldwide [2, 3]. Water availability has been impacted by drought and water shortage; with agricultural yields expected to decline between 2 – 15% over the next 30 years due to climate change [4]. Hence, the efficient use of water resources is critical for the long-term sustainability of the agricultural industry. Any improvements in water efficiency will have significant benefits in fresh water availability.

One water conservation strategy is the use of superabsorbent polymers (SAPs) [5]. These are hydrophilic polymers capable of absorbing water at hundreds of times their own weight and yet remain stable [6-9]. SAPs have been extensively used in many applications including personal care and hygiene products [10], food and beverages [11] and biomedicine [12]. In the horticultural and agricultural industries, their use in soil has improved water availability for

plants [13]. As water reservoirs, SAPs have increased water retention in different types of soil, significantly reducing the irrigation water consumption [14, 15]. Their effect on plant growth has also been investigated, showing an increase in crop yield [16]. Reddy Kathi S. [17] reported an increase in the growth of tomato plants when soil was amended with different rates of SAP. Sivapalan Siva [18] also confirmed an increase in soybean yield using an anionic polyacrylamide-based SAP.

Most of the commercially available SAPs in agriculture are fossil fuel derived polyacrylates (PA) or polyacrylamides (PAM) which exhibit poor environmental degradability. This lack of sustainability has led to the development of environmentally-friendly superabsorbents from natural polymers, including polysaccharides such as starch [19] or pectin [20]. Most of these, however, are produced as composites in combination with synthetic polymers, decreasing their biodegradability.

Cellulose, the world's most abundant biopolymer, has also been studied because of its desirable properties such as renewability, biodegradability and hydrophilicity [21, 22]. Several studies have developed superabsorbents based on cellulose derivatives such as carboxymethyl cellulose (CMC) [23, 24] or hydroxyethyl cellulose (HEC) [25], exhibiting remarkable swelling properties. Most of these are crosslinked with acrylamide or acrylic acid [26]. Cellulose-based SAP can also be prepared through TEMPO-mediated oxidation [27]. This process selectively converts the primary alcohols (C6) groups in the cellulose fibres into carboxylate groups. This surface modification provides the required electrostatic repulsion to produce nanoscale fibres upon mechanical fibrillation [28]. The resulting material can be oven-dried, creating a highly porous superabsorbent consisting of an entanglement of nanocellulose fibres (NCF) with high swelling properties [29]. Despite these remarkable characteristics, limited research on the application of nanocellulose-based superabsorbents has been conducted in soils. Few studies have analysed these SAPs for agriculture [30]. Zhang, et al. [31] prepared

chemically cross-linked superabsorbents made from NCF that exhibited antifungal activity during the breeding and growth of sesame seeds. Zhou, et al. [32] reported that adding NCF to CMC–acrylamide based superabsorbents increased water absorption capacity and improved salt resistance compared to NCF-free superabsorbent.

While several studies have prepared and investigated the properties of nanocellulose-based superabsorbents [22, 33], none have systematically compared the effect of application rate on soil water efficiency nor related those to plant growth and soil microbial activity. A clear understanding of these responses is critical for their application in agriculture.

In this study, we present the results of a greenhouse study in which we sought to determine the effect of varying application rates of nanocellulose SAP on the growth of tatsoi (a bok choy variety) plants grown under different levels of soil moisture to simulate water-stress conditions. Results were compared to plants grown in soil amended with a PAM-based SAP (commercially available). It is our objective to measure the effect of these SAPs on water use efficiency (the amount of water consumed related to the biomass produced) and to establish a relationship with the crop yield and microbial activity.

5.5 Materials and methods

5.5.1 Materials

Bleached Eucalyptus Kraft (BEK) pulp was provided by Australian Paper, Maryvale, Australia. Its chemical composition was: cellulose (78.8% $\pm$ 0.8), hemicellulose (17.7% $\pm$ 0.4), lignin (3.2% $\pm$ 0.1), extractives (0.3% $\pm$ 0.1) and ash (0.2% $\pm$ 0.1) [34]. Water\$ave BA was purchased from Polymer Innovations. This is a commercially available anionic polyacrylamide-based superabsorbent polymer (SAP). Hydrochloric acid (HCl) and sodium hydroxide (NaOH) were purchased from ACL Laboratories and Merck, respectively, and were diluted for solutions as required. Sodium bromide (NaBr) and 2,2,6,6-Tetramethylpiperidine-1-oxyl (TEMPO) were

purchased from Sigma-Aldrich. 12% w/v sodium hypochlorite (NaClO) was purchased from Thermo Fisher Scientific. Urea, super phosphate and sulphate of potash were purchased from Richgro (Jandakot, Australia). Tatsoi (*Brassica rapa narinosa*) seeds were purchased from Mr. Fothergill's (South Windsor, Australia). Seed raising mix was purchased from Yates.

Soil was collected from a vegetable farm converted from pasture located in Cranbourne, Victoria (38°11'6"S; 145°18'50"E). The soil was classified as a Podosol, according to the Australian Soil Classification criteria [35]. Soil was collected at a depth of 0 – 20 cm, air-dried and sieved to <2 mm. A subsample of 200 g was then analysed for a range of key physicochemical properties (Table I) [36]. More physicochemical properties are found in the supplementary material (Table SI).

Table I. Characteristics of the podosol soil selected for the experiments.

Parameter	Podosol
pH	6.16
Total Carbon (%)	1.4
Total Nitrogen (%)	0.06
C:N	26
Organic Matter (%)	2.5
Effective Cation Exchange Capacity (cmol$^+$/Kg)	2.6
Basic texture	Sandy soil
Water holding capacity (g water/100 g soil)	23

5.5.2 Superabsorbent preparation

Nanocellulose SAP was prepared following the TEMPO-mediated oxidation of BEK pulp previously published [37], a method adapted from Isogai, et al. [28]. In brief, to achieve a carboxylate content of 1.4 mmol/g, 25 g (dry basis) of BEK pulp were suspended in 2500 mL of water containing 0.4 g and 2.5 g of dissolved TEMPO and NaBr, respectively. Prior to the oxidation process, sodium hypochlorite at 12% w/v was adjusted to pH 10 through the addition of hydrochloric acid at 36% w/v. The oxidation process started by adding the 100 mL of NaClO (6.6 mmol NaClO/g cellulose) drop-wise to the suspension under constant stirring. The pH of the reaction was kept at 10 via addition of 0.5M NaOH. The reaction was maintained for 3 h or until no decrease in pH was observed. The oxidised fibres were washed with deionised water. Fibres were then re-dispersed in deionised water to prepare a solution of 0.5% w/v which was further fibrillated using a high-pressure homogeniser (GEA Niro Soavi Homogeniser Panda) at 1000 bar and two passes. To produce the superabsorbent, the resulting product from homogenisation was oven-dried at 50 °C (Thermoline BTC-9090) for at least 48 h or until no mass loss was observed.

5.5.3 Soil water holding capacity

The soil water holding capacity (WHC) or field capacity was measured gravimetrically following the method by Dane and Topp [38]. The value is displayed in Table I as g water / 100 g of soil.

5.5.4 Greenhouse tatsoi (*Brassica rapa narinosa*) pot experiments

The experimental design was set up in a greenhouse located at Monash University Clayton campus to investigate effects of water stress, superabsorbent type and application rate on the growth of tatsoi.

Three treatments of soil amended with superabsorbent were evaluated: nanocellulose at 0.5 wt% (N0.5), nanocellulose at 1.0 wt% (N1.0) and commercial SAP at 0.5 wt% (S0.5). Each

treatment was thoroughly mixed and placed in free-draining plastic pots of 14 cm diameter to reach a total weight of 1.5 kg of soil and superabsorbent. The pots were then immersed in deionised water for 24 h to allow the superabsorbent to reach equilibrium in water uptake. After 24 h, the pots were raised and excess water was drained until no further water was observed coming out of the bottom of the pot. The experiment also included two control treatments in which the soils were not amended with superabsorbent, one without fertiliser (C0) and another with fertiliser (CF). Both controls were irrigated to saturation to be in line with the other treatments. A basal application of fertiliser was then added to the pots with superabsorbent and the fertilised control at an equivalent rate of 100 kg ha^{-1} of N (from urea), 100 kg ha^{-1} of P (as super phosphate) and 100 kg ha^{-1} of K (sulphate of potash) based on grower management practice [39]. Treatments were then allowed to equilibrate for a further 24 h. Seedlings of tatsoi, previously grown in trays with seed raising mix, were then transplanted at the two-leaf stage into the pots with soil treatments. Three levels of soil moisture were studied for each treatment: 70, 40 or 20%. Each treatment had five replicates, giving 75 pots in total.

Once the seedlings were transplanted, the soil moisture was measured and recorded daily. This was done gravimetrically by weighing of the pots and determining the water loss. Treatments were then allowed to reach the desired level of soil moisture (70, 40 or 20%) and irrigated accordingly to maintain the required level at a range ± 5%. A further fertiliser addition was conducted weekly at a rate of 20 kg ha^{-1} of N, 20 kg ha^{-1} of P and 20 kg ha^{-1} of K. Pots were all arranged in a completely randomized block design. A schematisation and picture of the experimental setup is displayed in Figure 1. In the greenhouse, supplemental lighting was used to maintain light levels (12 h day length). The temperature conditions were: 26 °C ± 3 °C day and 16 °C ± 2 °C night.
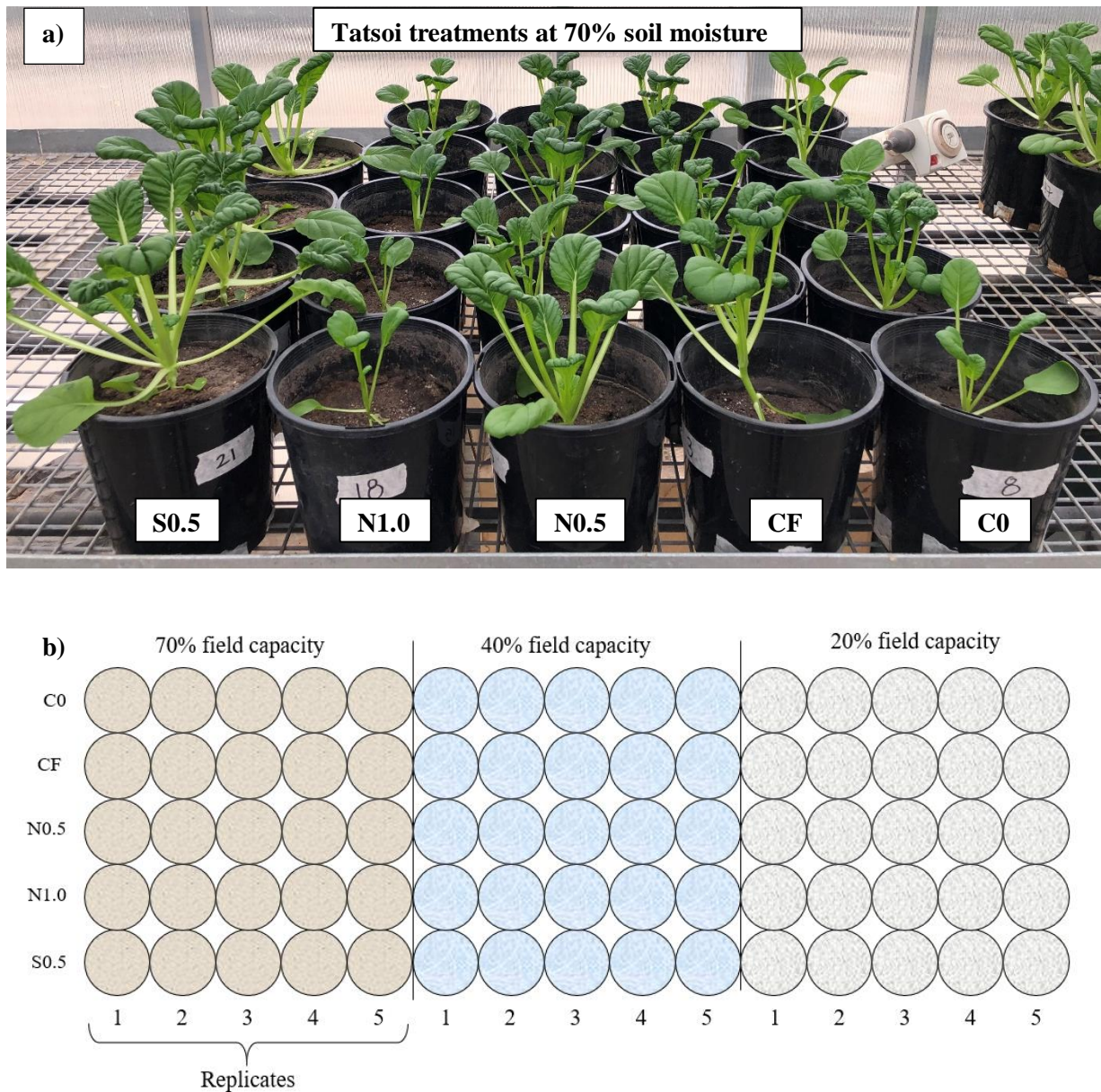
Figure 1. (a) Picture of the experimental setup, tatsoi treatments at 70% of soil moisture after 4 weeks post-transplanting. (b) Schematisation of the plant growth experiment. [1:] The schematisation of the experiment aims to highlight the number of treatments only. All plants were arranged in a completely randomised design.

5.5.5 Plant harvesting and analysis

Plants were harvested 4 weeks post-transplanting. This was done by cutting the plant in each pot just below the cotyledons. Above-ground biomass or shoots were immediately weighed

and the mass was recorded as shoot fresh weight (SFW). The fresh shoots were then oven-dried for 3 days at 55 °C and the shoot dry weight (SDW) was determined.

Soil respiration rates were determined by measuring the CO_2 emissions from each treatment using the static chamber method adapted from van Zwieten, et al. [40]. In brief, soil samples of 50 g were collected from each pot immediately after harvesting and placed into 120 mL polypropylene containers. The containers were then sealed and soil gas emissions were allowed to accumulate for exactly 10 minutes (based on a timed CO_2 emission curve previously established). A gas tight syringe (SGE Analytical Scientific) was used to extract an aliquot of soil gas emissions through a chlorobutyl septum and was then introduced into a pre-evacuated Labco® 12 mL exetainer vial. Collected gases were analysed for CO_2 using an Agilent Technologies 7890A Gas Chromatography – Thermal Conductivity Detector (GC-TCD) and GC-Flame Ionization Detector (FID). The detector temperature was 250 °C. Helium was used as the carrier gas at 21 mL/min. The temperature of the column and oven was 60 °C.

5.5.6 Water parameters

The soil water retention was measured per pot after the 24 h immersion in deionised water following equation 1:

$$Water \ retention \ (\%) = \frac{m_i}{m_o} \ x \ 100 \qquad (1)$$

Where m_i is the mass of the treatment i, and m_o refers to the mass of the control.

The total water added was determined at the end of the experiment and values were used to calculate the water use efficiency (WUE) per pot [41] as follows:

$$Water \ use \ effieciency \ (WUE) = \frac{Shoots \ dry \ weight}{Total \ water \ added} \qquad (2)$$

5.5.7 Data analysis

All plant growth, soil respiration and water usage data were analysed by two-way ANOVA (analysis of variance) with the factors in the analysis being treatment and soil moisture. Where significant differences were identified, pairwise comparisons were made with Tukey's honestly significant difference (HSD) test. Analyses were performed using GraphPad Prism 9.0.2.

5.6 Results

5.6.1 Soil water retention

Water retention was calculated for each treatment after 24 h of immersion in deionised water (Figure 2). In general, water retention increases with the addition of SAP, independent of the superabsorbent type. Soils treated with commercial SAP show the maximum water retention of about 2.2 times more than soil without superabsorbent (control). This is followed by treatments with nanocellulose at 1.0 wt% and 0.5 wt%, being approximately 1.5 and 1.2 times higher than the control, respectively.
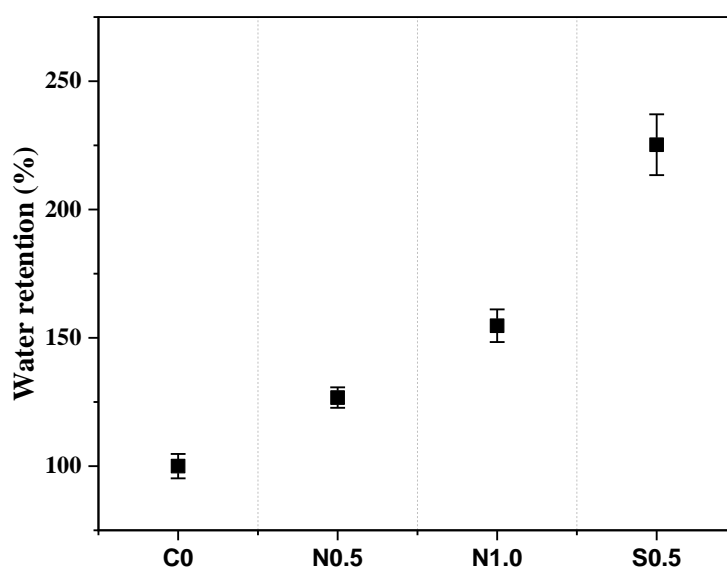
Figure 2. Water retention of soil treated with varying application and types of superabsorbent. Results are reported as mean ± standard deviation (n=15).

5.6.2 Pot trial summary analysis

In this study, the effect of different applications of superabsorbent on plants grown under limited water availability was quantified. For this purpose, the influence of two factors, treatment (T) and soil moisture (SM), was measured. Significant two-way interactions were found among the different response variables with results shown in Table II.

Table II. ANOVA summary table for all response variables. Factors in the analysis were treatment (T) and soil moisture (SM). Both main effects and interactions are indicated. Here, ns = no significant difference, * is $p \leq 0.05$, ** represents $p \leq 0.01$, and **** is $p \leq 0.0001$.

	T	SM	T $\times$ SM
Total water added	****	****	****
Water use efficiency (WUE)	****	ns	*
Shoot dry weight (SDW)	****	**	**
Shoot fresh weight (SFW)	****	ns	ns
CO_2 emissions	****	ns	ns

5.6.3 Effect of SAP on water management

Total water added is calculated for each treatment and soil moisture (Figure 3a and 3b). Analysis of the water added to tatsoi plants shows a significant two-way interaction between the treatment and the soil moisture (Table II). At all levels of soil moisture, total water added in pots with 1.0 wt% of nanocellulose SAP is significantly lower than any other treatment and approximately 20% less than the controls.

The water use efficiency (WUE) is displayed separately for different treatments and levels of soil moisture (Figure 3c and 3d). Data analysis reveals significant two-way interactions between soil moisture and treatment (Table II). Soils treated with commercial SAP achieve the highest WUE, being 3 to 4 times higher than the control, independently of the soil moisture.

This is followed by the control with fertiliser and treatment with 0.5 wt% application of nanocellulose superabsorbent. No correlation between the total water added and WUE was observed.
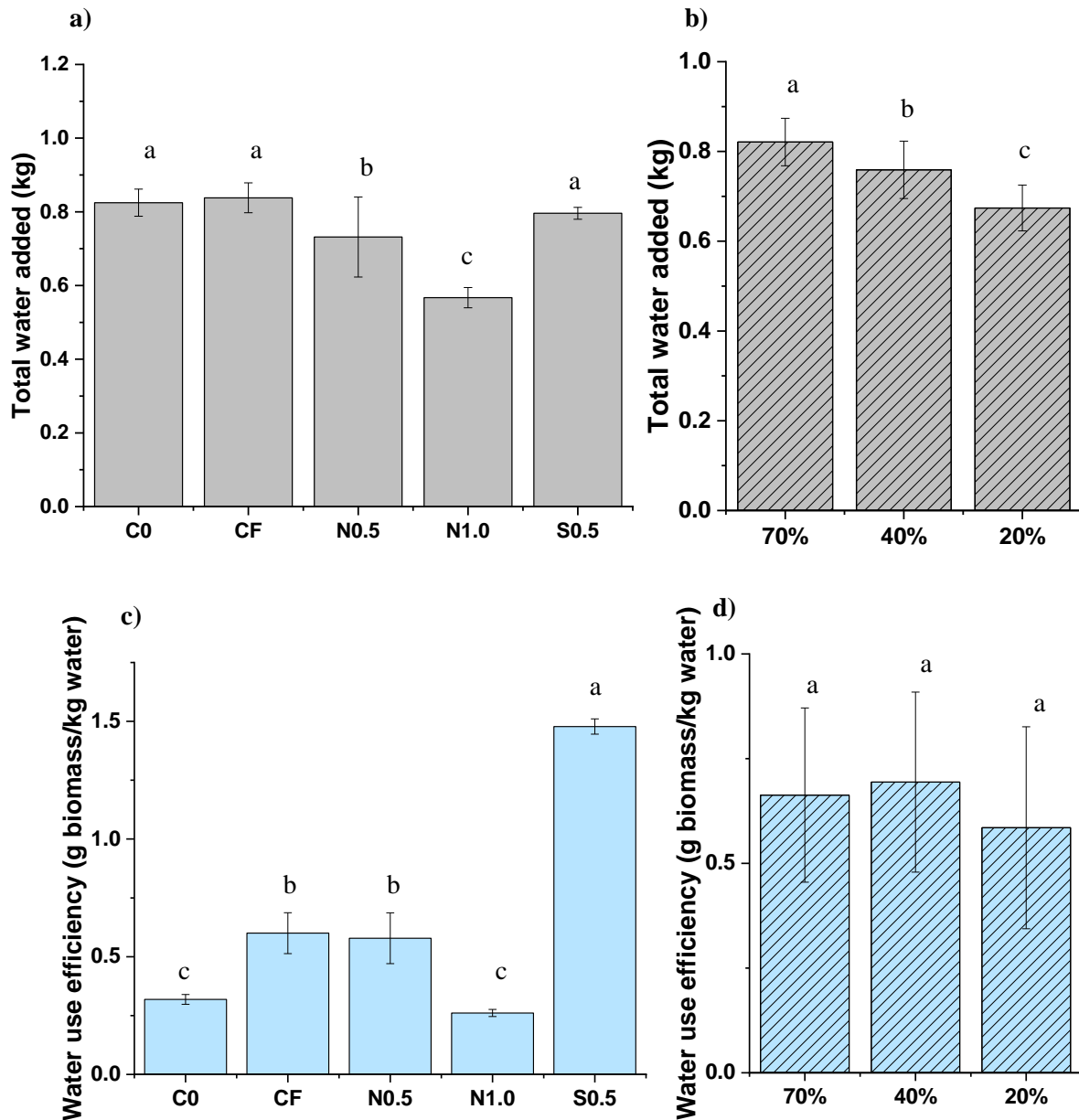
Figure 3. Total water added of tatsoi grown in (a) different treatments irrespective of soil moisture and (b) soil moisture irrespective of treatment. Water use efficiency (WUE) of (c) treatments irrespective of soil moisture and (d) soil moisture irrespective of treatments. Values are reported as mean ± standard deviation (n=5). Means followed

by the same letter were not significantly different at the $p \leq 0.05$ level (Tukey's HSD), see Table II for details of ANOVA results and Figure S1 for the effects of the interaction on the total water added.

5.6.4 Plant biomass

Shoot dry weights. For SDW, there is a significant two-way interaction between soil treatment and the level of soil moisture (Table II). Considering the soil treatment only, treatments with commercial superabsorbent had the highest response in SDW of tatsoi plants, irrespective of soil moisture (Figure 4a). Adding 0.5 wt% of nanocellulose SAP to soil shows no significant difference with respect to the fertilised control. However, there is a significant decrease in SDW when 1.0 wt% nanocellulose is applied. A slight decrease in SDW is observed when soil moisture is decreased to 20%, irrespective of the treatment (Figure 4b), which highlights the impact in plant growth under water stress.

Shoot fresh weights. Similar to SDW, the SFW of tatsoi increases when commercial SAP is used, irrespective of soil moisture (Figure 4c). The SFW of these treatments is approximately two times greater than that of the fertilised controls. The SFW is significantly lower in soils treated with 1.0 wt% of nanocellulose superabsorbent. These treatments have an average SFW of 2 g, compared to 8 g in fertilised controls. Lastly, soil amended with 0.5 wt% of nanocellulose shows no significant difference compared to the control with fertiliser.
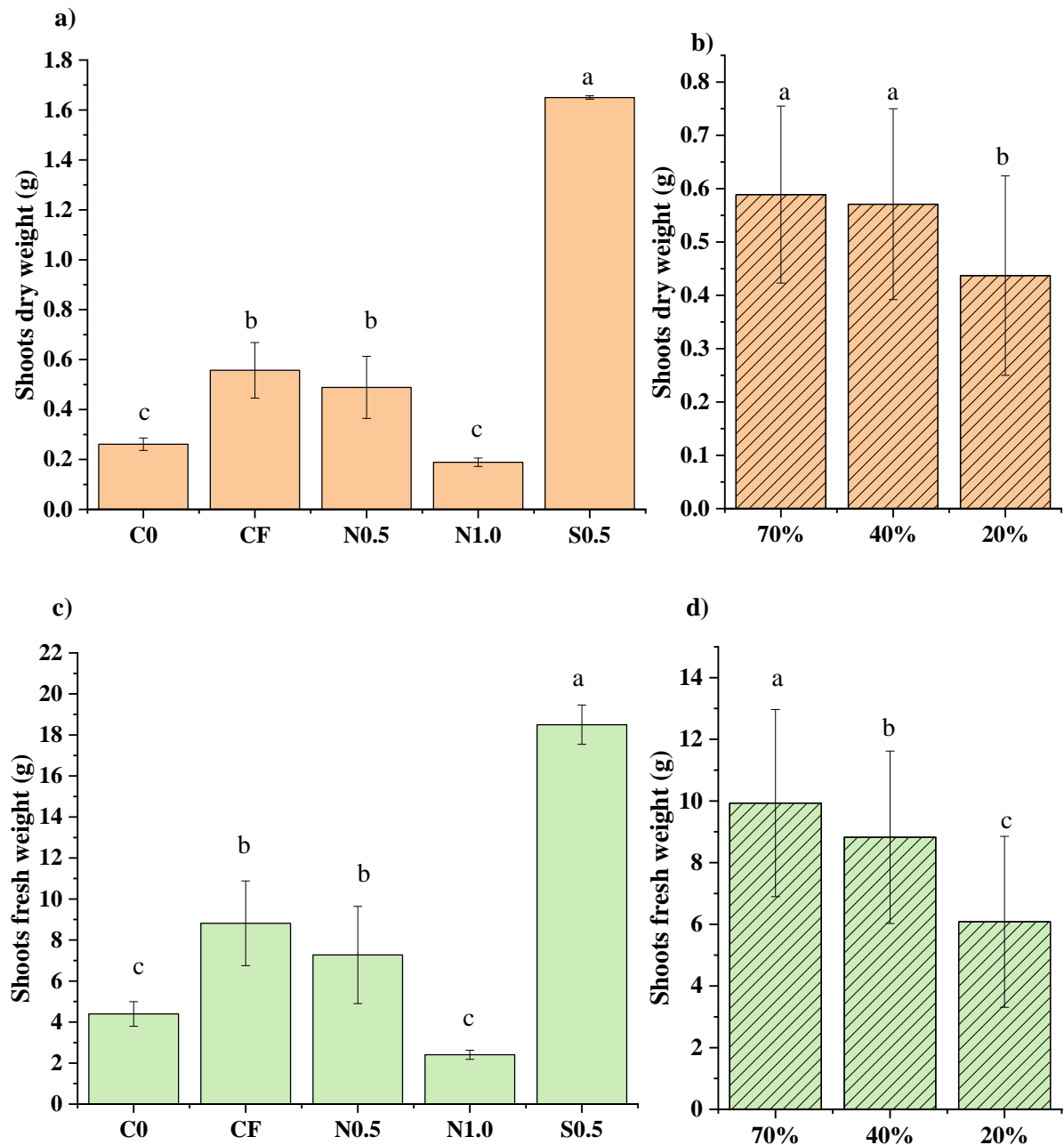
Figure 4. Shoot dry weights (SDW) of Tatsoi plants grown in (a) treatments irrespective of soil moisture and (b) soil moisture irrespective of treatment. Shoot fresh weights (SFW) of Tatsoi plants grown in (c) treatments irrespective of soil moisture and (d) soil moisture irrespective of treatment. Values are reported as mean ± standard deviation (n=5). Means followed by the same letter were not significantly different at the p ≤ 0.05 level (Tukey's HSD), see Table II for details of ANOVA results, Figure S2 for the effects of the interaction on both SDW and SFW.

5.6.5 Microbial activity

CO_2 emissions (i.e. respiration rates) are expressed as a function of soil moisture and treatment (Figure 5a and 5b). No significant interactions between the soil moisture and treatment are observed (Table II). However, there is a significant increase in respiration rates with increasing application rate of nanocellulose superabsorbent, irrespective of soil moisture (Figure 5a). In this case, the difference between the controls and soil amended with 0.5 wt% and 1.0 wt% application rate of nanocellulose SAP is between 300 mg CO_2/m^2h and 600 mg CO_2/m^2h, respectively. These results signify the response of the soil microbial community to the presence of this superabsorbent. Soil amended with commercial superabsorbent, however, does not exhibit a significant difference with respect to any of the controls which is likely to be related to its biodegradation. The change in soil moisture has no impact in the respiration rates irrespective of soil treatment.
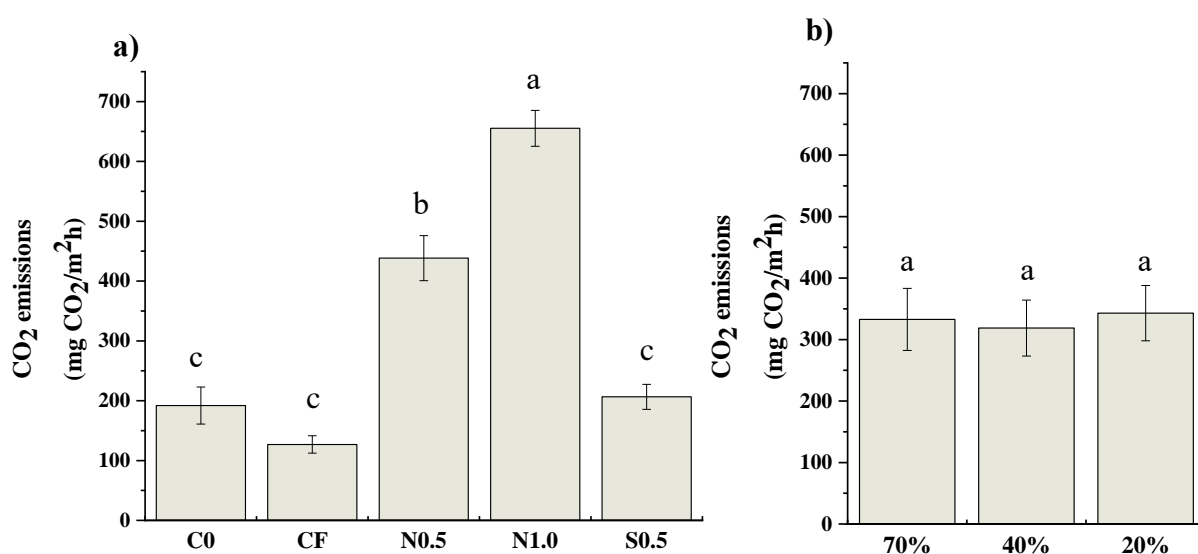
Figure 5. CO_2 emissions of (a) soil treated with different treatments of superabsorbent irrespective of soil moisture and (b) CO_2 emissions of soil moisture irrespective of treatment. Results are reported as mean ± standard deviation (n=5). Means followed by the same letter were not significantly different at the $p \leq 0.05$ level (Tukey's HSD), see Table II for details of ANOVA results.

5.7 Discussion

Soil water retention significantly increased with increasing application rate of superabsorbent, independent of its type. This response is the highest in treatments with commercial superabsorbent. This increase in soil water retention with SAP addition has been observed before [42, 43] and is attributed to the SAP granules occupying all the empty pore spaces in the soil and filling them with additional water [44, 45], increasing the soil water holding capacity. The total water added to each treatment significantly decreased with increasing application rate of nanocellulose SAP, while treatments with commercial superabsorbent showed no difference in this response with respect to both of the controls. Indeed, total water added or total irrigation is a useful variable to measure water deficit; however, this variable only accounts for the volume of water added to soils and does not consider other factors such as the effects on plant growth. Hence, it cannot be solely used to evaluate the efficient use of water resources.

The water use efficiency (WUE) can serve as an indicator to quantify the efficiency. WUE relates the total biomass produced per unit of water consumed. Higher WUE values are preferred to achieve a maximum throughput. In this study, WUE increased in treatments with commercial SAP, while it significantly decreased in treatments with 1.0 wt% nanocellulose superabsorbent. Both effects were irrespective of soil moisture and are related to the plant biomass. Plant biomass was the highest in treatments with commercial SAP, these results are consistent with previous studies and signify the benefits of using superabsorbents in agriculture [16, 46]. For treatments with nanocellulose, plant growth significantly decreased compared to the fertilised control, which was unexpected and indicated that there were other factors operating.

Both the SDW and the SFW of tatsoi plants were significantly reduced with increasing application rate of nanocellulose SAP, irrespective of soil moisture. Though this result differs

from literature that suggests the use of SAP to promote plant growth [16, 47, 48], it has been observed before when cellulose-based SAP materials are used. For example, studies made by Satriani, et al. [46] reveal that the growth of bean significantly decreases in soils amended with a superabsorbent made of carboxylmethylcellulose cross-linked with hydroxyethylcellulose compared to soils without SAP. The authors attributed this outcome to an irrigation deficit.

Nevertheless, in this study, the decrease in plant biomass when nanocellulose SAP is applied is likely to be associated to an immobilisation of nitrogen, also called a nitrogen drawdown effect [49]. This effect occurs when large amounts of materials high in organic carbon and low in nitrogen are added to soils. As a natural carbon source, nanocellulose addition to soil leads to an increase in the population of carbon decomposing microbes. This increase in microbial biomass leads to an increase in nitrogen requirements. Microbes require nitrogen for both growth and reproduction. Consequently, soil microbes draw down the nitrogen reserves in the soil, leaving limited nitrogen for plant growth. Other plant nutrients may also become limiting in these conditions. This results in slower plant growth and nitrogen deficiency. Immobilisation of nitrogen has been observed in potting media containing lignocellulosic sources such as sawdust or pine bark. Sharman and Whitehouse [49] reported a significant decrease in the shoot dry weight of *Nephrolepis* grown in sawdust media, which required nitrogen addition for an optimum plant growth. Similarly, studies made by Handreck [50] exhibited a higher rate of nitrogen immobilisation and poor development of cabbage seedlings grown in potting media composed of aged pine barks compared to those grown in peat media. Literature suggests that nitrogen drawdown appears when the carbon:nitrogen (C:N) molar ratio is higher than 25:1 [51, 52]. In this study, after the fertiliser addition, the C:N molar ratios changed from 28 to 29 and 34 with the application of 0.5 and 1.0 wt% of nanocellulose SAP, respectively. This further supports our hypothesis, suggesting the plants were nutrient limited and exhibited nutrient

deficiency which required additional fertiliser additions beyond what was added in this study (Table III).

Lastly, soil respiration rates significantly increased with increasing application of nanocellulose. This not only signifies the fast biodegradation of this SAP, but also further suggests that the increase in microbial biomass may have led to nitrogen drawdown. Soil respiration has been found to be positively correlated to nitrogen immobilisation. Jackson, et al. [53] evaluated nitrogen immobilisation in different substrates with a range of fertiliser addition, finding an increase in both carbon dioxide rates and nitrogen immobilisation when pine tree chips were used as compared to peat-lite. They also found these to be minimised when higher levels of fertiliser were added.

Table III. Total carbon (%), nitrogen (%) and C:N molar ratio of soil treatments measured by elemental analysis.

Treatment	Total carbon (%)	Total nitrogen (%)	C:N molar ratio
C0	1.2	0.05	28
CF	1.2	0.06	24
N0.5	1.4	0.06	29
N1.0	1.7	0.06	34

5.8 Conclusion

This study evaluated the effect of nanocellulose superabsorbent polymer (SAP) on the growth of tatsoi and its potential for agricultural use. Plants were grown in soils amended with varying rates of SAP and at different levels of soil moisture to simulate water stress conditions. Results were compared with those grown in soils amended with an anionic polyacrylamide-based SAP (commercially available). Total irrigation significantly decreased with increasing application

rate of SAP at all soil moisture levels. Plants grown in soils with commercial SAP had the lowest amount of water added. Water use efficiency (WUE) significantly increased, by a factor of 4, in treatments with commercial SAP compared to the controls. WUE in treatments with 0.5 wt% nanocellulose SAP was similar to controls with fertiliser, but significantly decreased when the application rate was increased to 1.0 wt%. This is associated to the plant biomass that significantly decreases with increasing application rate of nanocellulose.

Both shoots dry weight (SDW) and shoots fresh weight (SFW) were the highest in soils amended with commercial SAP, independently of soil moisture. While these remained similar in soils with 0.5 wt% nanocellulose SAP compared to the fertilised controls, they significantly decreased when the application rate of this superabsorbent increased to 1.0 wt%. This finding is attributed to an immobilisation of nitrogen. This hypothesis is supported by the significant increase in soil respiration rates when nanocellulose SAP is used which also increased with increasing application rate, independently of soil moisture. The high respiration rates also signify the fast biodegradation of this superabsorbent.

There was no significant difference in the CO_2 emissions between soils with commercial SAP and both controls, which further evidences its slow biodegradation. This study identifies the commercial superabsorbent to have a superior performance compared to nanocellulose-based SAP. Further studies are now needed to modify the nanocellulose SAP structure, decreasing the rate of biodegradation and overcoming the nitrogen drawdown effect.

5.9 References

[1] FAO, "The State of Food and Agriculture 2020. Overcoming water challenges in agriculture.," Rome, Italy, 2020.

[2] Organisation for Economic Co-operation and Development. "Managing water sustainably is key to the future of food and agriculture." https://www.oecd.org/agriculture/topics/water-and-agriculture/ (accessed 12/06/2020, 2020).

[3] W. a. t. E. Department of Agriculture, . "Water for food." Australian Government. https://www.agriculture.gov.au/water/water-for-food (accessed 12/06/2020, 2020).

[4] B. A. Müller C., Popp A., Waha K., Fader M.,, "Climate change impacts on agricultural yields," in "World Development Report " Potsdam Institute for Climate Impact Research, Germany, 2010.

[5] M. J. Zohuriaan-Mehr, Kabiri, Kourosh.,, "Superabsorbent Polymer Materials: A review," *Iranian Polymer Journal,* vol. 17, no. 6, pp. 451-477, 2008.

[6] E. M. Ahmed, "Hydrogel: Preparation, characterization, and applications: A review," *Journal of Advanced Research,* vol. 6, no. 2, pp. 105-121, 2015/03/01/ 2015, doi: https://doi.org/10.1016/j.jare.2013.07.006.

[7] S. Ghorbani *et al.*, "Hydrogels Based on Cellulose and its Derivatives: Applications, Synthesis, and Characteristics," *Polymer Science, Series A,* vol. 60, no. 6, pp. 707-722, 2019, doi: 10.1134/s0965545x18060044.

[8] X. Shen, J. L. Shamshina, P. Berton, G. Gurau, and R. D. Rogers, "Hydrogels based on cellulose and chitin: fabrication, properties, and applications," *Green Chemistry,* 10.1039/C5GC02396C vol. 18, no. 1, pp. 53-75, 2016, doi: 10.1039/C5GC02396C.

[9] J. R. Gross, "The Evolution of Absorbent Materials," in *Studies in Polymer Science*, vol. 8, L. Brannon-Peppas and R. S. Harland Eds.: Elsevier, 1990, pp. 3-22.

[10] A. Bashari, A. Rouhani Shirvan, and M. Shakeri, "Cellulose-based hydrogels for personal care products," *Polymers for Advanced Technologies,* vol. 29, no. 12, pp. 2853-2867, 2018, doi: 10.1002/pat.4290.

[11] H. M. Shewan and J. R. Stokes, "Review of techniques to manufacture micro-hydrogel particles for the food industry and their applications," *Journal of Food Engineering,* vol. 119, no. 4, pp. 781-792, 2013/12/01/ 2013, doi: https://doi.org/10.1016/j.jfoodeng.2013.06.046.

[12] R. Curvello, V. S. Raghuwanshi, and G. Garnier, "Engineering nanocellulose hydrogels for biomedical applications," *Advances in Colloid and Interface Science,* vol. 267, pp. 47-61, 2019/05/01/ 2019, doi: https://doi.org/10.1016/j.cis.2019.03.002.

[13] F. F. Montesano, A. Parente, P. Santamaria, A. Sannino, and F. Serio, "Biodegradable Superabsorbent Hydrogel IncreasesWater Retention Properties of Growing Media and Plant Growth," *Agriculture and Agricultural Science Procedia,* vol. 4, pp. 451-458, 2015, doi: 10.1016/j.aaspro.2015.03.052.

[14] E. S. Abrisham *et al.*, "Effects of a super absorbent polymer on soil properties and plant growth for use in land reclamation," *Arid land research and management,* vol. 32, no. 4, pp. 407-420, 2018, doi: https://doi.org/10.1080/15324982.2018.1506526.

[15] M. R. Guilherme *et al.*, "Superabsorbent hydrogels based on polysaccharides for application in agriculture as soil conditioner and nutrient carrier: A review," *European Polymer Journal,* vol. 72, pp. 365-385, 2015, doi: 10.1016/j.eurpolymj.2015.04.017.

[16] J. El-Asmar, H. Jaafar, I. Bashour, M. T. Farran, and I. P. Saoud, "Hydrogel Banding Improves Plant Growth, Survival, and Water Use Efficiency in Two Calcareous

Soils," *CLEAN – Soil, Air, Water,* vol. 45, no. 7, p. 1700251, 2017, doi: https://doi.org/10.1002/clen.201700251.

[17] Reddy Kathi S., "Effect of different doses of superabsorbent polymer (SAP) on water and nitrogen retention in soil, and on the growth and development of tomato and determination of optimal rate of SAP," Master of Science, Plant and soil science College of Graduate Studies Texas A&M University-Kingsville, Texas, 2019.

[18] Sivapalan Siva, "Improving crop production by the use of PAM: Potential benefits to Australian agriculture," presented at the Processdings 11th Australian agronomy conference, Geelong, Victoria, Australia, 2003.

[19] P. Chen, W. A. Zhang, W. Luo, and Y. e. Fang, "Synthesis of superabsorbent polymers by irradiation and their applications in agriculture," *Journal of Applied Polymer Science,* vol. 93, no. 4, pp. 1748-1755, 2004, doi: 10.1002/app.20612.

[20] M. R. Guilherme, A. V. Reis, A. T. Paulino, T. A. Moia, L. H. C. Mattoso, and E. B. Tambourgi, "Pectin-based polymer hydrogel as a carrier for release of agricultural nutrients and removal of heavy metals from wastewater," *Journal of Applied Polymer Science,* pp. n/a-n/a, 2010, doi: 10.1002/app.32123.

[21] M. A. Hubbe, A. Ayoub, J. S. Daystar, R. A. Venditti, and J. J. Pawlak, "Enhanced Absorbent Products Incorporating Cellulose and Its Derivatives: A Review," *2013,* Absorbency; Cellulosic materials; Fluff pulp; Superabsorbents; Hydrogels; Carboxymethylcellulose (CMC); Disposable; Rate of absorption; Life cycle analysis vol. 8, no. 4, p. 74, 2013-08-16 2013. [Online]. Available: https://ojs.cnr.ncsu.edu/index.php/BioRes/article/view/4379.

[22] N. Lavoine and L. Bergström, "Nanocellulose-based foams and aerogels: processing, properties, and applications," *Journal of Materials Chemistry A,* vol. 5, no. 31, pp. 16105-16117, 2017, doi: 10.1039/c7ta02807e.

[23] A. I. Raafat, M. Eid, and M. B. El-Arnaouty, "Radiation synthesis of superabsorbent CMC based hydrogels for agriculture applications," *Nuclear Instruments and Methods in Physics Research Section B: Beam Interactions with Materials and Atoms,* vol. 283, pp. 71-76, 2012, doi: 10.1016/j.nimb.2012.04.011.

[24] J. Pushpamalar, S. J. Langford, M. B. Ahmad, Y. Y. Lim, and K. Hashim, "Eco-friendly smart hydrogels for soil conditioning and sustain release fertilizer," *International Journal of Environmental Science and Technology,* vol. 15, no. 10, pp. 2059-2074, 2017, doi: 10.1007/s13762-017-1598-2.

[25] A. Sannino and L. Nicolais, "Concurrent effect of microporosity and chemical structure on the equilibrium sorption properties of cellulose-based hydrogels," *Polymer,* vol. 46, no. 13, pp. 4676-4685, 2005, doi: 10.1016/j.polymer.2005.03.072.

[26] S. Li and G. Chen, "Agricultural waste-derived superabsorbent hydrogels: Preparation, performance, and socioeconomic impacts," *Journal of Cleaner Production,* vol. 251, p. 119669, 2020/04/01/ 2020, doi: https://doi.org/10.1016/j.jclepro.2019.119669.

[27] L. Mendoza, L. Hossain, E. Downey, C. Scales, W. Batchelor, and G. Garnier, "Carboxylated nanocellulose foams as superabsorbents," *J Colloid Interface Sci,* vol. 538, pp. 433-439, Mar 7 2019, doi: 10.1016/j.jcis.2018.11.112.

[28] A. Isogai, T. Saito, and H. Fukuzumi, "TEMPO-oxidized cellulose nanofibers," *Nanoscale,* 10.1039/C0NR00583E vol. 3, no. 1, pp. 71-85, 2011, doi: 10.1039/C0NR00583E.

[29] R. M. Barajas-Ledesma, A. F. Patti, V. N. L. Wong, V. S. Raghuwanshi, and G. Garnier, "Engineering nanocellulose superabsorbent structure by controlling the drying rate," *Colloids and Surfaces A: Physicochemical and Engineering Aspects,* vol. 600, 2020, doi: 10.1016/j.colsurfa.2020.124943.

[30] C. R. Bauli, G. F. Lima, A. G. de Souza, R. R. Ferreira, and D. S. Rosa, "Eco-friendly carboxymethyl cellulose hydrogels filled with nanocellulose or nanoclays for agriculture applications as soil conditioning and nutrient carrier and their impact on cucumber growing," *Colloids and Surfaces A: Physicochemical and Engineering Aspects,* vol. 623, p. 126771, 2021/08/20/ 2021, doi: https://doi.org/10.1016/j.colsurfa.2021.126771.

[31] H. Zhang *et al.*, "Cellulose Anionic Hydrogels Based on Cellulose Nanofibers As Natural Stimulants for Seed Germination and Seedling Growth," *J Agric Food Chem,* vol. 65, no. 19, pp. 3785-3791, May 17 2017, doi: 10.1021/acs.jafc.6b05815.

[32] Y. Zhou, S. Fu, L. Zhang, and H. Zhan, "Superabsorbent nanocomposite hydrogels made of carboxylated cellulose nanofibrils and CMC-g-p(AA-co-AM)," *Carbohydrate Polymers,* vol. 97, no. 2, pp. 429-435, 2013/09/12/ 2013, doi: https://doi.org/10.1016/j.carbpol.2013.04.088.

[33] I. H. Mondal, *Cellulose-Based Superabsorbent Hydrogels* (Polymers and Polymeric Composites: A Reference Series). 2019.

[34] S. Ang, V. Haritos, and W. Batchelor, "Cellulose nanofibers from recycled and virgin wood pulp: A comparative study of fiber development," *Carbohydrate Polymers,* vol. 234, p. 115900, 2020/04/15/ 2020, doi: https://doi.org/10.1016/j.carbpol.2020.115900.

[35] R. F. Isbell, *The Australian soil classification*, Second edition. ed. Clayton South, VIC, Australia : CSIRO Publishing, 2016.

[36] S. C. U. Environmental Analysis Laboratory, . "Agricultural soil testing." https://www.scu.edu.au/environmental-analysis-laboratory---eal/analytical-services/agricultural-soil-testing/ (accessed 31/07/2020, 2020).

[37] R. M. Barajas-Ledesma, A. F. Patti, V. N. L. Wong, V. S. Raghuwanshi, and G. Garnier, "Engineering nanocellulose superabsorbent structure by controlling the drying rate," *Colloids and Surfaces A: Physicochemical and Engineering Aspects,* vol. 600, p. 124943, 2020/09/05/ 2020, doi: https://doi.org/10.1016/j.colsurfa.2020.124943.

[38] J. H. Dane and G. C. Topp, *Methods of soil analysis. Part 4, Physical methods*. Madison, Wisconsin : Soil Science Society of America, 2002.

[39] J. Burt, D. Phillips, and D. Gatter, "Growing chinese cabbage in Western Australia," Department of Agriculture and Food, Western Australia, 2006, vol. Bulletin 4673.

[40] L. van Zwieten *et al.*, "Influence of biochars on flux of N2O and CO2 from Ferrosol," (in English), *Australian Journal of Soil Research,* Article vol. 48, p. 555+, 2010 2010. [Online]. Available: https://link.gale.com/apps/doc/A241179274/AONE?u=monash&sid=AONE&xid=088435d9.

[41] P. Steduto, "Agricultural Water Use Efficiency (WUE) and Productivity (WP)," in *Water Encyclopedia*, pp. 558-560.

[42] A. Saha, B. Rattan, S. Sekharan, and U. Manna, "Quantifying the interactive effect of water absorbing polymer (WAP)-soil texture on plant available water content and irrigation frequency," *Geoderma,* vol. 368, p. 114310, 2020/06/01/ 2020, doi: https://doi.org/10.1016/j.geoderma.2020.114310.

[43] J. Akhter, K. Mahmood, K. A. Malik, A. Mardan, M. Ahmad, and M. Iqbal, "Effects of hydrogel amendment on water storage of sandy loam and loam soils and seedling growth of barley, wheat and chickpea," *Plant Soil and Environment,* vol. 50, pp. 463-469, 2018.

[44] M. Rahmati, A. Pohlmeier, S. M. A. Abasiyan, L. Weihermüller, and H. Vereecken, "Water Retention and Pore Size Distribution of a Biopolymeric-Amended Loam

Soil," *Vadose Zone Journal,* vol. 18, no. 1, p. 180205, 2019, doi: https://doi.org/10.2136/vzj2018.11.0205.

[45]   X. Bian, L. Zeng, Y. Deng, and X. Li, "The Role of Superabsorbent Polymer on Strength and Microstructure Development in Cemented Dredged Clay with High Water Content," (in eng), *Polymers (Basel),* vol. 10, no. 10, p. 1069, 2018, doi: 10.3390/polym10101069.

[46]   A. Satriani, M. Catalano, and E. Scalcione, "The role of superabsorbent hydrogel in bean crop cultivation under deficit irrigation conditions: A case-study in Southern Italy," *Agricultural Water Management,* vol. 195, pp. 114-119, 2018/01/01/ 2018, doi: https://doi.org/10.1016/j.agwat.2017.10.008.

[47]   A. Hüttermann, M. Zommorodi, and K. Reise, "Addition of hydrogels to soil for prolonging the survival of Pinus halepensis seedlings subjected to drought," *Soil and Tillage Research,* vol. 50, no. 3, pp. 295-304, 1999/05/01/ 1999, doi: https://doi.org/10.1016/S0167-1987(99)00023-9.

[48]   M. J. Zohuriaan-Mehr, H. Omidian, S. Doroudiani, and K. Kabiri, "Advances in non-hygienic applications of superabsorbent hydrogel materials," *Journal of Materials Science,* journal article vol. 45, no. 21, pp. 5711-5735, November 01 2010, doi: 10.1007/s10853-010-4780-1.

[49]   K. V. Sharman and M. Whitehouse, "Nitrogen drawdown index as a predictor of nitrogen requirements for Nephrolepis in sawdust media," *Scientia Horticulturae,* vol. 54, no. 1, pp. 23-33, 1993/04/01/ 1993, doi: https://doi.org/10.1016/0304-4238(93)90080-A.

[50]   K. A. Handreck, "Rapid assessment of the rate of nitrogen immobilisation in organic components of potting media: II. Nitrogen drawdown index and plant growth," *Communications in Soil Science and Plant Analysis,* vol. 23, no. 3-4, pp. 217-230, 1992/02/01 1992, doi: 10.1080/00103629209368584.

[51]   K. R. Kelley and F. J. Stevenson, "Forms and nature of organic N in soil," *Fertilizer Research,* Article vol. 42, no. 1-3, pp. 1-11, 1995, doi: 10.1007/BF00750495.

[52]   M. R. Hoosbeek, "Cycles of Soil: Carbon, Nitrogen, Phosphorus, Sulfur, Micronutrients, 2nd edition," *Soil science,* vol. 165, no. 2, pp. 185-187, 2000, doi: 10.1097/00010694-200002000-00010.

[53]   B. E. Jackson, R. D. Wright, and M. M. Alley, "Comparison of Fertilizer Nitrogen Availability, Nitrogen Immobilization, Substrate Carbon Dioxide Efflux, and Nutrient Leaching in Peat-lite, Pine Bark, and Pine Tree Substrates," (in English), *HortScience horts,* vol. 44, no. 3, p. 781, 01 Jun. 2009 2009, doi: 10.21273/hortsci.44.3.781.

THIS PAGE HAS BEEN INTENTIONALLY LEFT BLANK

CHAPTER 6:

BIODEGRADATION OF NANOCELLULOSE SUPERABSORBENT AND ITS EFFECT ON THE GROWTH OF SPINACH

THIS PAGE HAS BEEN INTENTIONALLY LEFT BLANK

PREFACE

Thus far, each chapter has contributed to evaluate the potential of nanocellulose SAPs for agricultural soils and how these can be engineered, enhancing their feasibility and performance. However, nanocellulose SAP performance is dependent on the type of soil. Soils vary greatly in texture, structure, chemical composition, cation exchange capacity, pH and many more properties. Each of these parameters can significantly affect the behaviour of the superabsorbent. Therefore, this chapter analyses the effect of two soils on the performance of nanocellulose SAP, and how this effect influences the growth of Spinach plants grown under water stress. This directly addresses the last research objective, which is to measure the effect of different soils on the water retention of nanocellulose and how this affects plant growth. A relationship between soil type and nanocellulose biodegradation was also determined.

In this study, two soils, a sandy soil and a clay loam soil, were amended with one application rate of nanocellulose SAP of 0.5 wt%. This application rate was chosen based on the results from Chapter 5 which showed no adverse effects on plant growth at 0.5% SAP. A pot trial whereby spinach plants were grown in these two soils with nanocellulose SAP was conducted. The effect of the superabsorbent on plant yield was measured. Soil was characterised in terms of soil porosity, bulk density and water retention. The effect of soil type on nanocellulose biodegradation was quantified through soil respiration and acid digestion methods.

THIS PAGE HAS BEEN INTENTIONALLY LEFT BLANK

Chapter 6: Biodegradation of nanocellulose superabsorbent and its effect on the growth of spinach

THIS PAGE HAS BEEN INTENTIONALLY LEFT BLANK

Biodegradation of nanocellulose superabsorbent and its effect on the growth of spinach

6.1 Abstract

In this study, spinach (*Spinacea oleracea*) plants were grown in two soils, a clay loam (CL) and a sandy (SD) soil, amended with nanocellulose superabsorbent at different levels of soil moisture. The effect of the superabsorbent on the soil properties, water management and plant biomass was measured and compared to soils treated with a commercial anionic polyacrylamide-based SAP. Plant biomass is the highest in SD soil amended with commercial superabsorbent. However, it decreases in the CL soil when superabsorbent is applied, independent of the SAP type. This effect is magnified when nanocellulose SAP is used and it is likely attributed to waterlogging stress and the fast biodegradation of this superabsorbent, where approximately 50% of the initial mass remains after 5 days of exposure. Future studies are needed to modify the structure of nanocellulose SAP to inhibit its biodegradation and increase its benefits for agricultural use.

6.2 Keywords

Nanocellulose superabsorbent, plant growth, spinach, water productivity, waterlogging, water retention, biodegradation.

6.3 Graphical Abstract
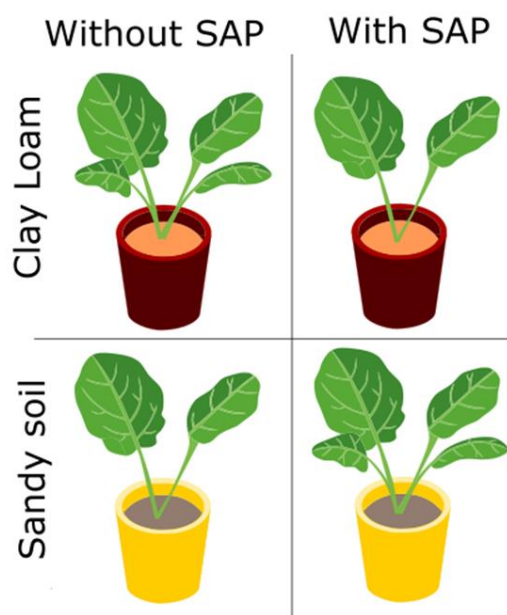
6.4 Introduction

Water stress is one of the most important limiting factors that affect plant growth and crop productivity, especially when this occurs at critical growth-stages of the cultivated crop [1]. The severity and longevity of water stress is influenced by many factors including rainfall amount, intensity and distribution [2]. One vital parameter that can help the agroecosystem to ameliorate the impact of extreme weather events (e.g. drought or intensive rain) is the soil water holding capacity (WHC) which measures the amount of water that a given soil can hold for crop use [3]. Hence, any improvements in WHC will have significant benefits in improving plant growth by reducing the effect of water stress.

Superabsorbent polymers (SAPs) can be used to increase soil WHC [4]. SAPs are hydrophilic polymers capable of absorbing large quantities of water and yet remain stable [5-8]. Their use in the horticultural and agricultural industries has improved soil water availability for plants [9]. As water reservoirs, SAPs have increased water retention in different types of soil, significantly reducing the irrigation water consumption [10, 11]. SAPs can also reduce

compaction tendency, increasing soil aeration and microbial activity [12]; thus, improving soil properties [4, 11, 13].

The effect of varying types and amounts of SAPs on plant growth has also been evaluated. El-Asmar et al. [14] found that superabsorbent addition to soils prolonged survival time of pine seedlings by 90%. Islam et al. [15] and Satriani et al. [16] have demonstrated that the SAP effects on plant yield are significantly magnified when plants are grown under deficit irrigation. Studies report that the use of superabsorbents can reduce crop evapotranspiration, increasing water use efficiency [16, 17].

One of the main drawbacks of superabsorbent polymers is that most are fossil fuel derived polyacrylamides (PAM) which exhibit poor environmental degradability. These SAPs release acrylate and acrylamide units when they break down in soil. Acrylamide is known to be carcinogenic, imposing a risk to the human health and the environment [18]. These increasing concerns have led to the development of environmentally-friendly superabsorbents from natural polymers including those made from lignocellulosic agricultural wastes [19], cellulose derivatives such as carboxymethyl cellulose (CMC) [20, 21] or hydroxyethyl cellulose (HEC) [22]. This is because of cellulose's desirable properties such as renewability, biodegradability and hydrophilicity [23, 24]. Most of these cellulosic based SAPS, however, are produced as composites in combination with acrylamide or acrylate which still exhibit poor biodegradability.

TEMPO-mediated oxidation is an alternative method to prepare cellulose-based superabsorbents [25]. This oxidation process selectively converts the primary alcohol groups in the cellulose fibres into carboxylate groups. The added electrostatic repulsion assists in the liberation of nano-scale fibres upon mechanical fibrillation at high shear forces [26]. The resulting material can be oven-dried, creating highly porous superabsorbent of high pore area,

exhibiting high swelling properties of up to 200 g of water/g of dry fibre [27]. Despite these characteristics, few studies have evaluated the application of these nanocellulose SAPs for agriculture [28]. Zhang et al. [29] reported that chemically cross-linked superabsorbents made from nanocellulose fibres (NCF) can be applied as soilless culture medium for plant growth. Bauli et al. [30] encapsulated NPK fertiliser in carboxymethylcellulose (CMC) superabsorbent filled with NCF. These authors found that the SAP was effective in slowing the release of fertiliser in water and soil. Few studies have measured the effect of nanocellulose-based SAPs on plant growth in a controlled soil environment nor their biodegradability. Limited information is available that relates the impact of these SAPs on different soils to plant yield and soil microbial activity. Singh et al recently reviewed a range of materials with their applications in soil and effects on plant growth including SAPs made of cellulosic materials [31]. A clear understanding of these responses is critical for application in agriculture.

Here, we present a greenhouse study in which we quantify the effect of nanocellulose SAP on spinach plants grown under different levels of soil moisture to simulate water-stress conditions. Experiments were conducted utilising two types of soils in which the total irrigation water required and water productivity were quantified. Results were compared to spinach grown in the same soils amended with a commercial PAM-based SAP. It was also our objective to measure the biodegradation of the novel nanocellulose-based SAP and to establish a relationship with the microbial activity.

6.5 Materials and methods

6.5.1 Materials and soil characteristics

Bleached Eucalyptus Kraft (BEK) pulp was provided by Australian Paper, Maryvale, Australia with a chemical composition of cellulose (78.8% ± 0.8), hemicellulose (17.7% ± 0.4), lignin (3.2% ± 0.1), extractives (0.3% ± 0.1) and ash (0.2% ± 0.1) [32]. Water\$ave BA was purchased

from Polymer Innovations. This is a commercial anionic polyacrylamide-based superabsorbent polymer (SAP). Sulphate of potash, super phosphate and urea were purchased from Richgro (Jandakot, Australia). Spinach (*Spinacea oleracea*) seeds were purchased from Mr. Fothergill's (South Windsor, Australia). Seed raising mix was purchased from Yates.

Two soil were used in this study. The first, a clay loam soil, was collected from a vegetable farm located in Werribee, Victoria (37°55'15"S; 144°42'6"E). The second, a sandy soil, was from a vegetable farm converted from pasture located in Cranbourne, Victoria (38°11'6"S; 145°18'50"E). The soils were classified as a Red Sodosol and a Podosol according to Isbell [33], respectively. These soils are referred to as clay loam (CL) and sandy (SD) hereafter. Both soils were collected at a depth of $0 - 20$ cm, air-dried and sieved to < 2 mm. Subsamples of 200 g were analysed for a range of key physicochemical properties (Table I) [34]. Additional properties are given in the supplementary material (Table SI).

Table I. Basic characteristics of the soils investigated. A comprehensive soil chemical analysis is provided in supplementary information (Table S1).

Parameter	Clay Loam (Red Sodosol)	Sandy (Podosol)
pH	8.1	5.7
Total Carbon (%)	1.3	1.2
Total Nitrogen (%)	0.12	0.05
C:N	10	25
Organic Matter (%)	2.2	2.0
Effective Cation Exchange Capacity ($cmol^+/Kg$)	18	2.6
Basic texture	Clay Loam	Sandy soil

Water holding capacity (g water/100 g soil)	40	23

6.5.2 Superabsorbent preparation

BEK pulp was used to prepare the nanocellulose SAP following the TEMPO-mediated oxidation protocol previously published to prepare oven-dried superabsorbents [35], a method adapted from Isogai et al. [26].

6.5.3 Soil water holding capacity

The soil water holding capacity (WHC) or field capacity of both soils was determined gravimetrically following the method provided by Dane and Topp [3] with values shown in Table 1 as g water / 100 g of soil.

6.5.4 Soil properties

The soil bulk density and porosity were calculated for both soils and with two types of superabsorbent: nanocellulose and commercial superabsorbent. The tests were conducted following a method adapted from Fan et al. [36]. Briefly, plastic funnels of 42.5 mm diameter with a filter paper placed at the bottom were weighed (W_0). For each soil type, 20 g of air-dried soil was mixed with 0.5 wt% of either nanocellulose or commercial SAP, added into the plastic funnel and then weighed (W_1). Treatments were then fully immersed in water for 24 h to allow the SAP to reach saturation. A control treatment for each soil type was also prepared and underwent the same immersion. After 24 h, treatments were raised and excess water was drained for 3 h. The height of the treatment (from the bottom of the funnel to the top of the soil – to calculate the total soil volume) and mass was recorded (W_2). Treatments were then dried in an oven at 65 °C until constant weight (W_3). Bulk density (g/cm^3) and total porosity (%) were calculated as follows:

$$Bulk\ density = \frac{(W_3 - W_0)}{V} x\ 100 \tag{1}$$

$$Total\ porosity = \frac{(W_2 - W_3)}{V} x 100 \tag{2}$$

6.5.5 Greenhouse spinach (*Spinacea oleracea*) pot experiments

A full factorial experimental design was set up in a greenhouse located at Monash University

Clayton campus to investigate effects of superabsorbent application and water stress on the

growth of spinach. The pot experiments involved: two types of superabsorbent, nanocellulose

and commercial; three moisture levels, 70%, 40% and 20% of soil's water holding capacity;

and two soil types, CL and SD soil. Each condition was prepared in replicates of five, giving

90 pots in total.

For each soil type, two treatments of soil amended with the dry superabsorbent were evaluated:

nanocellulose at 0.5 wt% (N0.5) and commercial SAP at 0.5 wt% (S0.5). Each treatment was

thoroughly mixed and placed in free-draining plastic pots of 14 cm diameter to reach a total of

1.2 kg and 1.3 kg of soil and superabsorbent for CL and SD soils, respectively. Deionised water

was then poured on top of the pots until water drops were observed dripping from the bottom.

The pots were then immersed in a tray with deionised water for 24 h to ensure complete

saturation of the superabsorbent in water uptake. After 24 h, the pots were raised and excess

water was drained for 3 h. The experiment also included a control treatment in which both soils

were not amended with superabsorbent (C0). Controls of both soils were irrigated to saturation

to be in line with the other treatments. A basal application of fertiliser was then added to all

pots based on soil analysis. The CL soils received N (from urea) at a rate of 100 kg ha^{-1}. For

the SD soils, the fertiliser rate was 100 kg ha^{-1} of N, 50 kg ha^{-1} of P (from super phosphate)

and 100 kg ha^{-1} of K (from sulphate of potash), respectively. Treatments were then allowed to

equilibrate for a further 24 h. Seedlings of spinach, previously grown in trays with seed raising

mix, were then transplanted at the two-leaf stage into the pots with soil treatments. For each treatment, three levels of soil moisture were studied: 70%, 40% or 20%.

Once the seedlings were transplanted, treatments were then allowed to reach the desired level of soil moisture. The soil moisture was measured and recorded daily by weighing of the pots and determining the water loss gravimetrically. Once they had reached the required soil moisture, each pot was then irrigated accordingly to maintain this at ±5%. A further fertiliser addition was conducted every two weeks at a rate of 20 kg ha^{-1} of N, 20 kg ha^{-1} of P and 20 kg ha^{-1} of K for both the CL and SD soils. All pots were arranged in a completely randomized block design. A schematic of the experimental setup is displayed in Figure 1.

Conditions in the greenhouse were as follows: for CL soils, temperature 27 °C ± 2 °C day and 19 °C ± 2 °C night. For plants grown in SD soils, temperature 26 °C ± 3 °C day and 16 °C ± 2 °C night. Light levels were maintained with supplemental lighting (12 h day length). Full spectrum high intensity discharge (HID) lights were used, with the illumination level ramped from 0-30 klux during the 24 h period.
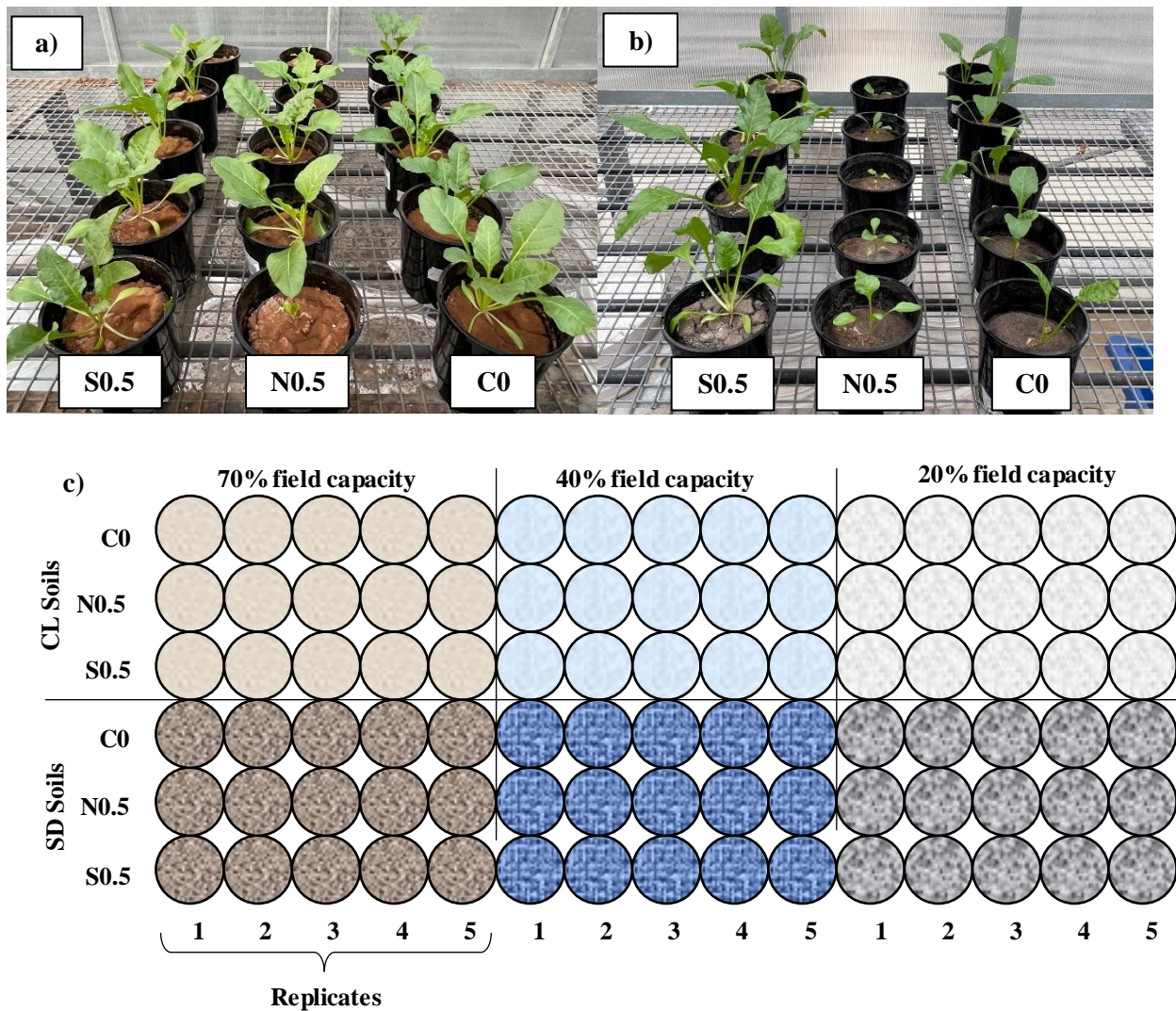
Figure 1. Pictures of the experimental setup at the time of harvesting, (a) spinach treatments in CL soils at 20% of soil moisture and (b) spinach treatments in SD soils at 20% of soil moisture. (c) Schematisation of the plant growth experiment. [1] The schematisation of the experiment aims to highlight the number of treatments only. All plants were arranged in a completely randomised design. [2] Here, treatments are referred to as control (C0), nanocellulose at 0.5 wt% (N0.5) and commercial superabsorbent at 0.5 wt% (S0.5).

6.5.6 Plant harvesting and soil analysis

Plants in the SD and CL soils were harvested 5- and 6-weeks post-transplanting, respectively. This was done by cutting the plant just below the cotyledons. Shoots were immediately weighed and the mass was recorded as shoot- fresh weight (SFW). These were then oven-dried for 3 days at 55 °C and the shoot- dry weight (SDW) was determined. Root biomass could not be reliably recovered because of the nature of the treatments. In CL soils, soil particles highly adhered to the spinach roots; and in SD soils, roots grew through the superabsorbent particles, making them difficult to recover.

Soil subsamples of 10 g were collected from each treatment to measure the amount of nanocellulose superabsorbent remaining at the end of the pot trial. This was done following the acid digestion method described in the biodegradation tests.

Soil water retention was calculated per treatment as follows:

$$Water\ retention\ (\%) = \frac{m_i}{m_o}\ x\ 100 \tag{3}$$

Where m_i refers to the mass of the treatment i, and m_o is the mass of the control. Both after 24h of being fully saturated with water.

At the end of the experiment, the total irrigation water required was determined. This value was used to calculate the water use efficiency or water productivity (WP) per treatment by dividing the shoot- dry weight (SDW) over the total irrigation water as follows:

$$Water\ productivity\ (WP) = \frac{SDW}{Total\ irrigation\ water} \tag{4}$$

6.5.7 Soil incubation studies

Soil incubation studies were performed for both soils and with two types of superabsorbent: nanocellulose and commercial SAP. For each type, 50 g of soil treatments were prepared with

0.5 wt% of application rate of superabsorbent. An additional control treatment was prepared without any superabsorbent for both soils. All treatments received a basal application of fertiliser based on soil analysis. The CL soils received N (from urea) at a rate of 100 kg ha^{-1}; and for the SD soils, the fertiliser rate was 100 kg ha^{-1} of N, 50 kg ha^{-1} of P (from super phosphate) and 100 kg ha^{-1} of K (from sulphate of potash), respectively. Each treatment, thoroughly mixed, was then placed in polypropylene containers of 120 mL and deionised water was added to reach 70% WHC. Treatments were incubated at 23 °C and 80% relative humidity. Soil moisture was maintained for the entire duration of the experiment by daily weighing of the containers and topping them up with deionised water when necessary. Each treatment was replicated five times.

Gas samples were collected at days 1, 3, 5, 7, 14, 21, 28 and 42 using the static chamber method adapted from van Zwieten et al. [37]. Briefly, the containers containing the incubated, treated soils were sealed and soil gas emissions were allowed to accumulate for exactly 10 minutes. The accumulated gases were then extracted using a gas tight syringe (SGE Analytical Scientific) and introduced into a pre-evacuated 12 mL Labco® exetainer vial through a septum. Collected gases were analysed for CO_2 on an Agilent Technologies 7890A Gas Chromatography – Thermal Conductivity Detector (GC-TCD) and GC-Flame Ionization Detector (FID), fitted with a Gerstel MultiPurpose Sampler (MPS) autosampler. The detector temperature was 250 °C. Helium was used as the carrier gas at 21 mL/min. The temperature of the column and oven was 60 °C.

6.5.8 Biodegradation tests

Nanocellulose superabsorbent biodegradation was evaluated in both the CL and SD soils. For each soil, superabsorbent was added to the soil at 0.5 wt% of application to prepare a total of 10 g of soil treatment. Similar to the soil incubation studies, an additional control treatment

was prepared without any superabsorbent for both soils. All treatments received the same basal application of fertiliser specified as the soil incubation studies. Each treatment was thoroughly mixed and placed in polypropylene containers of 25 mL. Deionised water was then added to reach 70% WHC. Treatments were incubated at 23 °C and 80% relative humidity. Soil moisture was maintained for the entire duration of the experiment by daily weighing of the treatments and topping them up with deionised water when necessary. Each treatment was conducted in five replicates. Treatments were destructively sampled at days 1, 3, 5, 7, 14, 21, 28, and 42, dried in an oven at 60 °C and stored frozen at -20 °C until required.

Biodegradation was measured using the acid digestion method adapted from Sluiter et al. [38] to hydrolyse the cellulose and oxidised cellulose in the soil to glucose and glucuronic acid which were then measured by High Performance Liquid Chromatography (HPLC). In brief, 3 mL of 72% sulphuric acid was added to 5 g of treated soil at room temperature. The mixture was incubated at room temperature for 60 min. During this time, the mixture was occasionally stirred every 5 to 10 minutes to ensure even acid – soil contact. Dilution to 4% sulphuric acid was then made by adding 83 mL of deionised water followed by autoclaving for 30 minutes at 121 °C. After cooling to room temperature, the soil was removed by filtration and the supernatant retained and neutralised to pH 5 using calcium carbonate. When neutralisation was complete, the solids were separated by centrifugation at 4400 rpm for 5 min. The supernatant was collected, filtered and analysed by HPLC using a BioRad Amminex HPX-87H column, 0.005 M sulphuric acid as the mobile phase, with a refractive index detector at a temperature of 40 °C, a column temperature of 60 °C and a flow rate of 0.4 mL/min. Because cellulose is a component already present in every soil, the nanocellulose SAP biodegradation was calculated as follows:

$$Biodegradation\ (\%) = \frac{(M_i - M_c)}{M_t}\ x\ 100 \tag{5}$$

Where M_i refers to the mass of cellulose in the treatment at time i, M_c is the mass of cellulose in the control and M_t means the total mass of cellulose added to the treatment.

6.5.9 Data analysis

All plant growth, water usage and biodegradation data were analysed by two-way ANOVA (analysis of variance) with the factors in the analysis being treatment and soil moisture. Soil respiration and biodegradation data were analysed by one-way ANOVA with factor in the analysis being treatment and soil type, respectively. Where significant differences were identified, pairwise comparisons were made with Tukey's honestly significant difference (HSD). Analyses were performed using GraphPad Prism 9.0.2.

6.6 Results

6.6.1 Effect on soil properties: water retention, total porosity and bulk density

The effect of superabsorbent application on soil properties was measured for clay loam (CL) and sandy (SD) soils, respectively (Figure 2). For both soils, water retention increases with the addition of SAP, independently of the superabsorbent type. The water retention in soils treated with commercial SAP was significantly higher compared to both the control and treatments with nanocellulose SAP. After the 24 h immersion in water, these soils retained approximately 180% and 220% more water than soils without superabsorbent (control) for the SD and CL soil, respectively. For both types of superabsorbent, the increase in water retention is higher when these are applied to SD soil than for CL soil.

For both soils, bulk density decreases with the application of superabsorbent, and soil porosity increases with SAP application. This effect is accentuated when commercial SAP is used. For SD soils, bulk density decreases from 1.3 to approximately 0.7 g/cm^3 with the application of commercial SAP with respect to the control. Similarly, the soil porosity in SD soil without SAP changes from 45% to 75% with the addition of commercial SAP. Similar effects where

observed in both soils treated with nanocellulose SAP but to a lesser extent. These results of bulk density and porosity agree with reported literature data about the application of SAP to soils [9, 39].
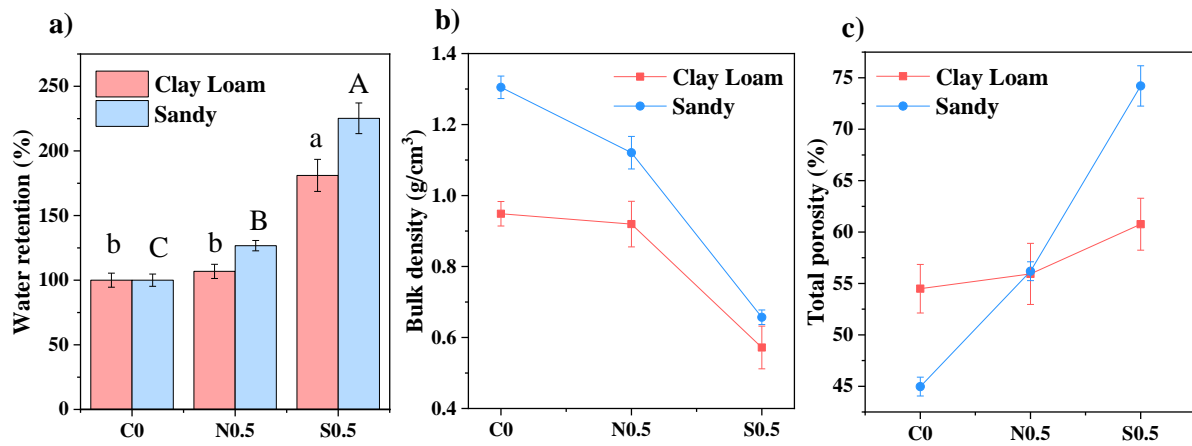
Figure 2. Effect of superabsorbent application on soil properties: (a) soil water retention (b) bulk density and (c) soil porosity. Results are reported as mean ± standard deviation (n=3). Bars with the same letters, lower case (for SD soil) and upper case (for CL soil), were not significantly different at the $p \leq 0.05$ level (Tukey's HSD). [1]: Here, treatments are referred to as control (C0), nanocellulose at 0.5 wt% (N0.5) and commercial superabsorbent at 0.5 wt% (S0.5).

6.6.2 Plant growth study summary analysis

In this study, the effect of treating two soil types with nanocellulose superabsorbent on plant growth under water stress was determined. The influence of two factors, treatment (T) and soil moisture (SM), was measured. Significant two-way interactions were found among the different response variables with results shown in Table 2. The following sections describe the effect of the superabsorbent on each of the response variables.

Table II. ANOVA summary of all response variables. Factors in the analysis were treatment (T) and soil moisture (SM). Both main effects and interactions are indicated. Here, ns = no significant difference, * is $p \leq 0.05$, ** represents $p \leq 0.01$, and **** is $p \leq 0.0001$.

	T	SM	T × SM
Clay loam (CL) soil			
Total irrigation water	*	****	**
Water productivity (WP)	****	****	****
Shoot dry weight (SDW)	****	****	****
Sandy (SD) soil			
Total irrigation water	**	****	ns
Water productivity (WP)	****	***	ns
Shoot dry weight (SDW)	****	***	ns

6.6.3 Effect of superabsorbent on water management

To measure the effect of superabsorbent application on the use of water, two variables were evaluated: total irrigation water required, which is the amount of water consumed by the plant or lost due to evaporation from the soil during the growing period; and water productivity, which is expressed as the ratio of dry biomass to the total water consumed. The total irrigation water was calculated for each soil type depending on treatment and soil moisture (Figure 3). Considering the soil treatments, the total water required to maintain each of the desired levels of soil moisture throughout the growing period is significantly lower in soil amended with nanocellulose SAP compared to the control, while no significant difference is observed in the water required between the control and commercial SAP. Both effects are independent of soil type or moisture (Figure 3a and 3c) and are related to the plant growth. When considered

separately from the soil treatments, the total water required in both the CL and SD soils significantly decreases with decreasing levels of soil moisture (Figure 3b and 3d).
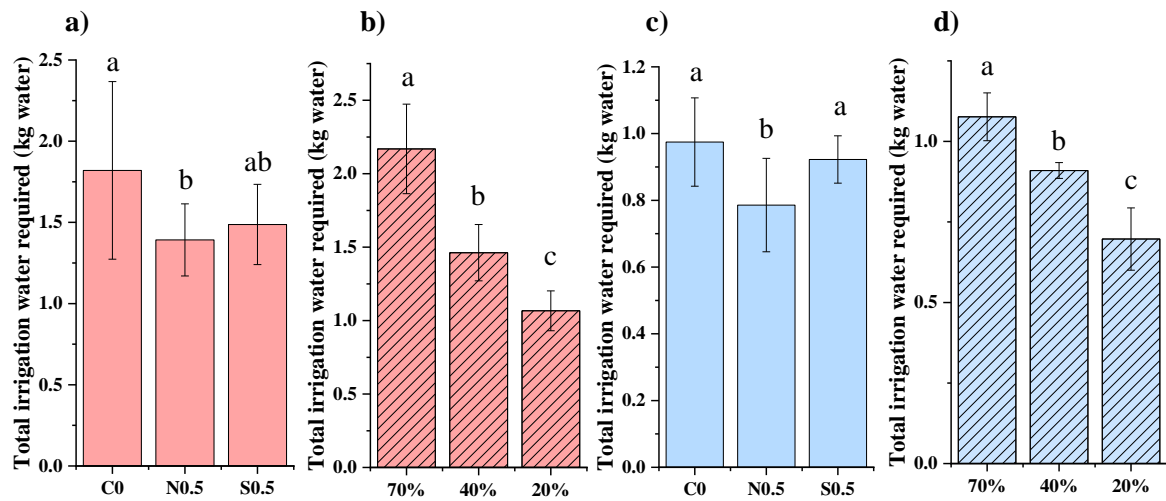
Figure 3. Total water required in the growth of spinach under the different treatments and levels of soil moisture. For CL soil (in red): (a) water loss in treatments irrespective of soil moisture and (b) soil moisture irrespective of treatment. For SD soil (in blue): (c) water loss in treatments irrespective of soil moisture and (d) soil moisture irrespective of treatment. Values are reported as mean ± standard deviation (n=5). Means followed by the same letter were not significantly different at the $p \leq 0.05$ level (Tukey's HSD), see Table II for details of ANOVA results.

Similarly, the water productivity (WP) was calculated for each treatment and different levels of soil moisture (Figure 4). For the CL soils, data analysis reveals significant two-way interactions between soil moisture and treatment (Table II). Interestingly, WP significantly decreases with the addition of superabsorbent, independent of soil type (Figure 4a). The opposite effect is observed in the SD soils, where WP is the highest in pots treated with commercial SAP, this is 2 times higher than the control, irrespective of the soil moisture (Figure 4c). For both soil types, WP at 20% of soil moisture is significantly lower than the other two moisture levels, irrespective of treatment (Figure 4b and 4d).
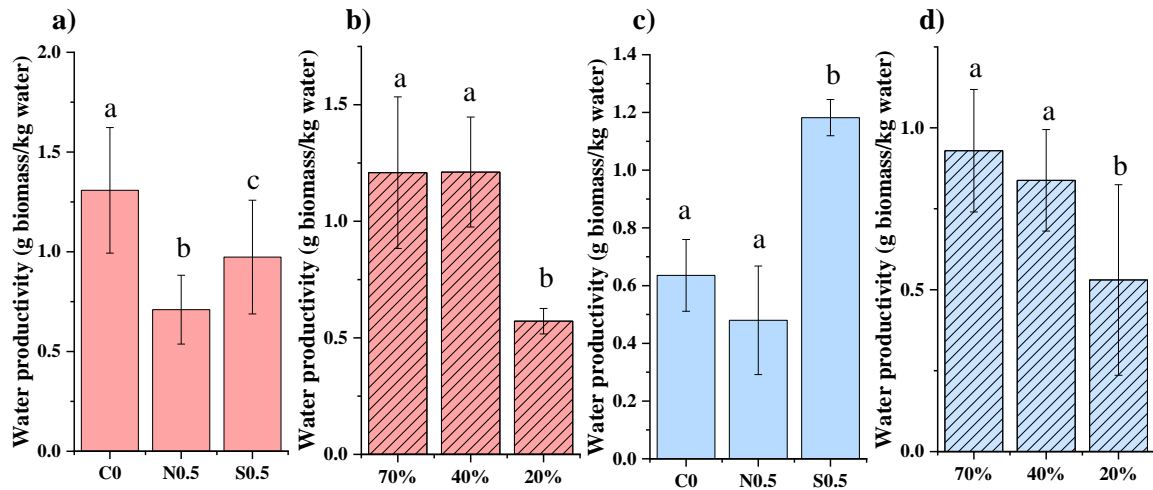
Figure 4. Water productivity (WP) of spinach grown in two soil types. For the CL soil (in red): (a) WP in treatments irrespective of soil moisture and (b) soil moisture irrespective of treatment. For the SD soil (in blue): (c) WP in treatments irrespective of soil moisture and (d) WP in soil moisture irrespective of treatment. Values are reported as mean ± standard deviation (n=5). Means followed by the same letter were not significantly different at the $p \leq 0.05$ level (Tukey's HSD), see Table II for details of ANOVA results.

6.6.4 Plant biomass

Clay loam soil. In most cases, the shoot dry weight (SDW) of all treatments decrease with decreasing level of soil moisture (Figure 5). There is a significant two-way interaction between soil treatment and the level of soil moisture (Table II). The SDW of spinach in treatments with superabsorbent is significantly lower than the control, at all levels of soil moisture. This effect is more accentuated in treatments with nanocellulose SAP. The SDW in these treatments is approximately 5 times lower than the control in the pots subjected to 70% of soil moisture. This difference is the greatest of all treatments (Figure 5a and 5b). When soil moisture is considered, the SDW decreases with decreasing levels of soil moisture, which highlights the response of plant growth under water stress.

Sandy soil. No significant interactions are observed between treatment and soil moisture (Table II). In general, the SDW decreases with decreasing levels of soil moisture, independently of treatment (Figure 5f). Considering the effect of treatment only, the SDW in pots with commercial SAP are significantly higher compared to the other treatments, irrespective of soil moisture. No significant difference in SDW is observed between the control and those with nanocellulose SAP (Figure 5e).
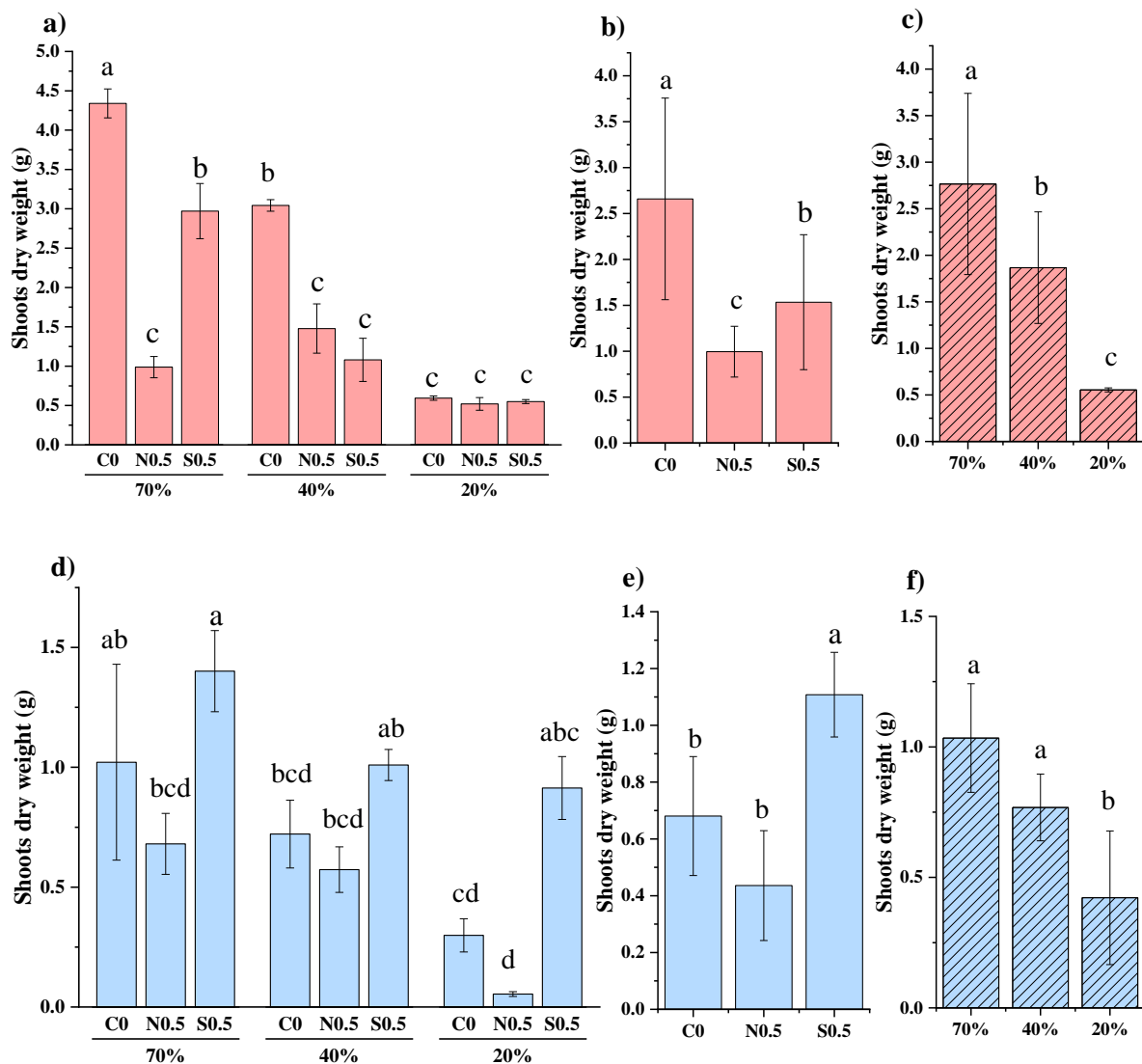
Figure 5. Shoot dry weight (SDW) of spinach grown in two soil types. For the CL soil (in red), (a) SDW under different levels of soil moisture and treatments, (b) SDW in treatments irrespective of soil moisture, and (c) SDW in soil moisture irrespective of

treatment. For the SD soil (in blue), (d) SDW under different levels of soil moisture and treatments, (e) SDW in treatments irrespective of soil moisture and (f) SDW in soil moisture irrespective of treatment. Values are reported as mean ± standard deviation (n=5). For each plot, means followed by the same letter were not significantly different at the $p \leq 0.05$ level (Tukey's HSD). Figures a and d highlight the difference at the two-way interaction (Treatment X Soil Moisture). See Table II for details of ANOVA results.

6.6.5 Microbial activity

In general, for both soil types, soil respiration rates (measured as CO_2 emissions) increase with time and application of nanocellulose SAP (Figure 6). After 40 days, the difference in soil respiration between the control and soils treated with nanocellulose SAP ranges between 14 g CO_2/m^2 to 28 g CO_2/m^2 for SD and CL soils, respectively. These results indicate the response of the soil microbial community to the presence of nanocellulose. Similarly, for both soil types, no significant difference is observed in soils amended with commercial superabsorbent and the controls.
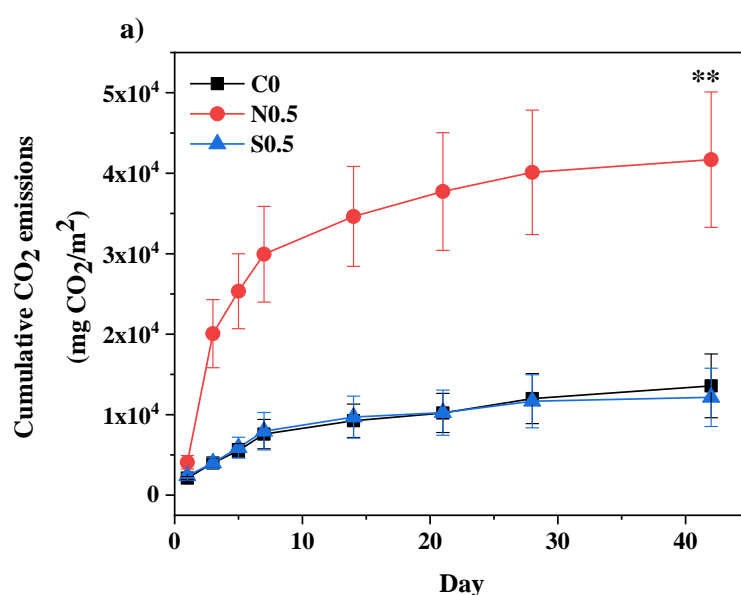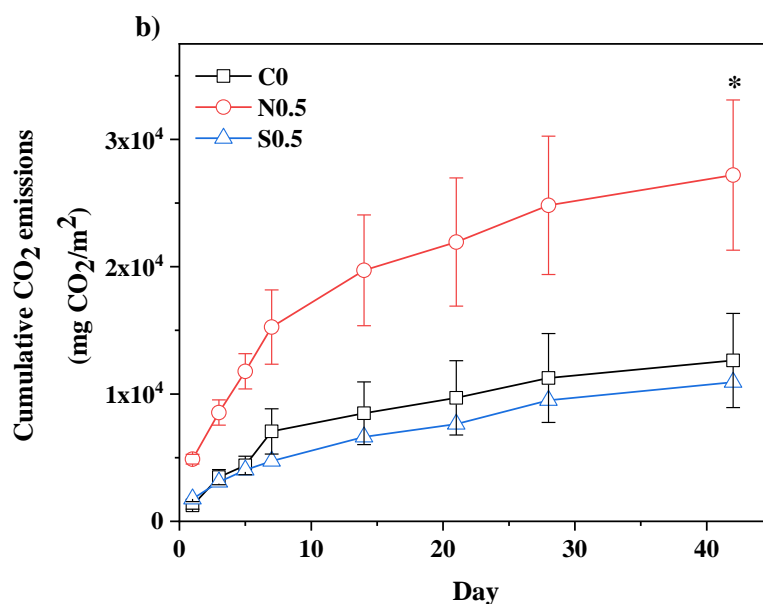
Figure 6. Cumulative CO_2 emissions of different soil treatments for: (a) CL soil and (b) SD soil. Results are reported as mean ± standard deviation (n=5). The asterisks above each data point show the level of significant difference compared to the control, C0. Here, * is $p \leq 0.01$, and ** shows $p \leq 0.001$.

6.6.6 Biodegradation

Biodegradation tests were conducted on the pots treated with nanocellulose SAP at the end of the plant experiment (Figure 7a). Both soils at all levels of soil moisture were tested. For both soil types, a minimum amount of superabsorbent remains after more than 35 days of exposure. For SD soils, no statistical difference is observed between treatments at any level of soil moisture. However, nanocellulose SAP in CL soil shows a significant difference when treated at 20% of soil moisture compared to those in 70 and 40%.

From the soil incubation studies, it is observed that the rate of nanocellulose biodegradation is dependent upon the soil type (Figure 7b). For both soils, the degradation of nanocellulose shows a similar trend. After an initial exponential increase during the first 7 days of exposure, SAP degradation rate decreases to reach a plateau. There is a significant difference in

nanocellulose biodegradation in both soils at day 7, where 50% and 30% of the initial mass remains in the SD and CL soils, respectively.
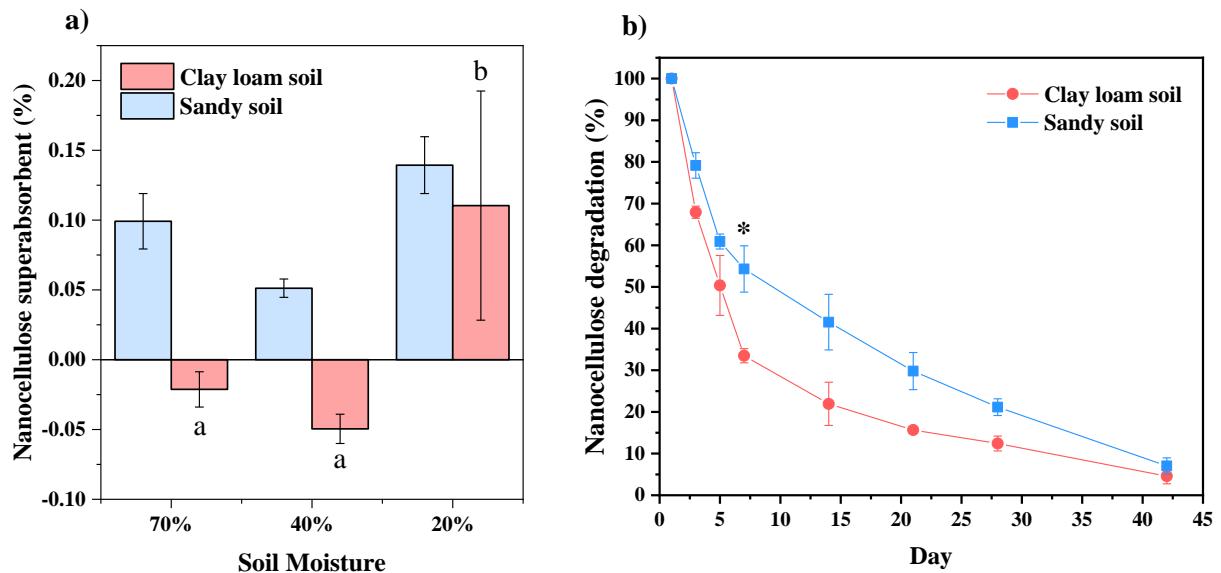
Figure 7. (a) Effect of soil type on the biodegradation of nanocellulose SAP over time. (b) Amount of nanocellulose superabsorbent remained at the end of the plant experiment for both soils. Results are reported as mean ± standard deviation (n=5). Bars followed by the same letter were not significantly different at the p ≤ 0.05 level (Tukey's HSD). The asterisk above day 7 in (b) shows the level of significant difference at the p ≤ 0.05.

6.7 Discussion

Several studies report that the amendment of SAP to soils can alleviate the impact of drought on plant growth, especially in arid regions [11]. This is because SAP addition can increase the soil water retention, improving plant growth when water supply is limited [40]. Similarly, studies suggest that the addition of SAP can improve the soil properties such as bulk density and soil porosity. These reflect the soil's ability to provide structural support, oxygen and water. Each of these indirectly affect plant growth.

In this study, for both soil types, soil porosity increased with the application of superabsorbent. An increase in soil porosity leads to an enhancement in the rate of seedling emergence and seed germination, root growth and density. Most important, it also increases soil aeration, increasing the oxygen availability in the root zone of plants and the soil microbial activity [9, 39, 41-43]. Similarly, for both soils, the addition of superabsorbent increases water retention, independently of the type of superabsorbent. This response agrees with previous literature. This is because the SAP granules occupy all the empty pores in the soil and fill them with additional water [44, 45], increasing the soil water holding capacity. However, for both types of superabsorbent, such increase in water retention is lower in the CL soils. This is due to the swelling mechanism of the SAP, which is driven by the difference in osmotic pressure across the polymer network (difference inside and outside) caused by the movement of the cations in the system [25]. These osmotic effects are diminished with increasing concentrations of salt, resulting in a decrease in swelling [46]. As noted here, the effective cation exchange capacity in the CL soil is higher than for the SD soil, being 18 and 2.6 $cmol^+/Kg$, respectively. In addition, the cation exchange capacity (CEC) of the CL soil is dominated by Ca^{2+} ions which are known to cause a greater impact in the swelling capacity of the superabsorbents [47].

Analysis of the total water required data revealed that the effect of soil moisture induced a higher response than the effect of treatment in both soils, where the water required significantly decreased with decreasing soil moisture. Differences in water requirement are correlated to the plant growth [48] which can be affected by water deficiency. Specially for spinach, studies have found a decrease in plant biomass when grown under water stress, leading to a decrease in water requirements [49].

Water productivity (WP) varied widely depending on the type of soil. Data analysis revealed that both, the treatment and soil type, had a significant effect. WP measures the ratio of total

biomass to irrigation water consumed. Interestingly, WP decreased in the CL soil with the addition of either SAP. These results contrast with most of the studies that rather suggest superabsorbents to increase water productivity [2, 15, 16, 50]; this observation is accentuated in treatments at 70% soil moisture. Because WP is related to plant biomass, its decrease is attributed to waterlogging stress which caused a decrease in the growth of spinach; this was noted in the reduction of SDW in treatments with SAP, at all levels of soil moisture (Figure 5a and 5b).

Waterlogging occurs when there is an excess of water in the plant's root zone, decreasing oxygen availability and leading to a reduction in plant growth, and in some cases, leading to plant death [51]. The waterlogging effect is important especially in clay loam soils. Because of the clay content, these soils have a greater water holding capacity than sandy soils. In the dispersive soils such as the clay loam, waterlogging can result in a collapse of the soil structure, blocking pores and leading to poor aeration. The increase in water retention caused by the addition of superabsorbent to CL soil is likely to have led to a waterlogging stress in spinach plants at the seedling stage. Previous studies have shown that waterlogging stress can appear when high concentrations of SAP to soils are employed [2, 52]. This is because superabsorbents can increase soil capillary porosity and decrease the air-filled porosity of soils, resulting in poor aeration [15]. This waterlogging stress led to an overall decrease in plant growth as it is observed in the reduction in SDW in treatments with superabsorbent, both commercial and nanocellulose. Another factor that may have contributed to the reduction in SDW in treatments with nanocellulose SAP at 70% soil moisture is the fast biodegradation of nanocellulose, occurring during the first week of the study. This effect released all the water taken up by the superabsorbent to the soil, likely inducing a higher waterlogging effect and causing a breakdown in soil structure which remained through the whole study. Thus, in line with previous studies, our findings suggest that the optimal concentration of SAP varies depending

on soil texture and dispersibility. SAPs should only be employed in areas with severe water stress [15, 50].

On the other hand, for SD soils, the SDW significantly increased with the application of commercial SAP. This is observed at all levels of soil moisture which, for this soil type, signifies the suitability of this SAP material as a water retention agent to promote plant growth under water stress. The SDW in soil amended with nanocellulose SAP was slightly lower than the control at all levels of soil moisture. Though this decrease was not low enough to represent a significant difference, the reduction in plant growth can be associated with a nitrogen deficiency caused by the immobilisation of nitrogen [53]. This occurs when large amounts of labile carbon (C) are added to soils, thereby increasing the activity of the soil microbial community. As a result, soil microbes use the available nitrogen in the soil for microbial growth and activity, limiting the nitrogen available for plant growth. The immobilisation of nitrogen is further impacted when lignocellulosic sources with high C content such as pine bark or sawdust are added to soils [53, 54]. The significant increase in soil respiration rates with application of nanocellulose SAP indicates an increase in the size of the microbial community which likely led to nitrogen drawdown. Immobilisation of nitrogen appears in treatments with carbon:nitrogen (C:N) ratios higher than 25:1 [55, 56]. For SD soil, the C:N molar ratio changed from 24 to 28 with the addition of nanocellulose SAP; which is a high C:N ratio at a level where immobilisation of nitrogen will occur [55, 56] (Table III).

Soil respiration rates are also related to the superabsorbent degradation in soil, where nanocellulose SAP degradation had a half-life of 5 and 7 days for CL and SD soils, respectively. The greater decomposition in the CL soils is due to its higher amount of organic matter, being able to support a larger microbial community with greater potential to decompose nanocellulose compared to that in SD soil [57]. This rate of decomposition supports previous

studies reporting the degradation of cellulose to mostly occur within 16 to 30 days [58, 59]. The rate of cellulose breakdown will vary between soils and with environmental conditions (moisture and temperature) [60], as observed in this study.

Table III. Total carbon (%), nitrogen (%) and C:N molar ratio of soil treatments measured by elemental analysis.

Treatment	Total carbon (%)	Total nitrogen (%)	C:N molar ratio
Clay Loam soil			
C0	1.3	0.13	12
N0.5	1.5	0.13	14
Sandy soil			
C0	1.2	0.056	24
N0.5	1.4	0.056	28

6.8 Conclusion

This study evaluated the effect of nanocellulose superabsorbent polymer (SAP) on the growth of spinach. Two soils, one a clay loam (CL) and the other a sandy soil (SD), were amended with nanocellulose SAP and spinach plants were grown at different levels of soil moisture to simulate water stress conditions. Soil water retention, porosity, water productivity (WP) and plant biomass were measured and the results were compared with those of soils treated with a commercial anionic polyacrylamide-based SAP. The biodegradation rate of the nanocellulose superabsorbent was determined and related to the soil microbial activity.

For both soils, porosity increased with the application of superabsorbent, independently of the SAP type. This effect was more accentuated in clay loam (CL) soils. Soil water retention significantly increased with the application of the commercial superabsorbent, being approximately 170% and 220% times more than the control for the clay loam (CL) and the

sandy (SD) soil, respectively. For both types of superabsorbent, the increase in water retention was lower in the CL soil. This is attributed to the effective cation exchange capacity which is about 8 times higher in the CL soil.

The effect of superabsorbent application on WP and plant biomass varied depending on the soil type. For the SD soil, WP and plant biomass were the highest in treatments with commercial superabsorbent, independent of soil moisture. For the CL soil, WP and plant biomass were significantly lower in treatments with superabsorbent compared to the control. This effect was magnified in treatments with nanocellulose superabsorbent and is likely attributed to waterlogging and the fast biodegradation of this SAP, where about 50% of the initial mass remained after 5 days of exposure in this soil. Immobilisation of nitrogen by the increasing microbial activity may have also contributed. This is supported by the significant increase in soil respiration rates when nanocellulose SAP is used in both soil types. This study identifies the commercial SAP to have a superior performance compared to nanocellulose superabsorbent. There is a need to overcome the waterlogging stress induced by SAP application. This can be achieved by adjusting the application rate of superabsorbent depending on the soil type. In addition, modification of the nanocellulose SAP physico-chemical structure is necessary to inhibit its biodegradation and fully increase its benefits for agricultural use.

6.10 References

[1] G. Bodner, A. Nakhforoosh, and H.-P. Kaul, "Management of crop water under drought: a review," *Agronomy for Sustainable Development,* vol. 35, no. 2, pp. 401-442, 2015/04/01 2015, doi: 10.1007/s13593-015-0283-4.

[2] A. M. AbdAllah, A. M. Mashaheet, and K. O. Burkey, "Super absorbent polymers mitigate drought stress in corn (Zea mays L.) grown under rainfed conditions," *Agricultural Water Management,* vol. 254, p. 106946, 2021/08/01/ 2021, doi: https://doi.org/10.1016/j.agwat.2021.106946.

[3] J. H. Dane and G. C. Topp, *Methods of soil analysis. Part 4, Physical methods.* Madison, Wisconsin : Soil Science Society of America, 2002.

[4] M. J. Zohuriaan-Mehr, Kabiri, Kourosh.,, "Superabsorbent Polymer Materials: A review," *Iranian Polymer Journal,* vol. 17, no. 6, pp. 451-477, 2008.

[5] E. M. Ahmed, "Hydrogel: Preparation, characterization, and applications: A review," *Journal of Advanced Research,* vol. 6, no. 2, pp. 105-121, 2015/03/01/ 2015, doi: https://doi.org/10.1016/j.jare.2013.07.006.

[6] S. Ghorbani *et al.*, "Hydrogels Based on Cellulose and its Derivatives: Applications, Synthesis, and Characteristics," *Polymer Science, Series A,* vol. 60, no. 6, pp. 707-722, 2019, doi: 10.1134/s0965545x18060044.

[7] X. Shen, J. L. Shamshina, P. Berton, G. Gurau, and R. D. Rogers, "Hydrogels based on cellulose and chitin: fabrication, properties, and applications," *Green Chemistry,* 10.1039/C5GC02396C vol. 18, no. 1, pp. 53-75, 2016, doi: 10.1039/C5GC02396C.

[8] J. R. Gross, "The Evolution of Absorbent Materials," in *Studies in Polymer Science*, vol. 8, L. Brannon-Peppas and R. S. Harland Eds.: Elsevier, 1990, pp. 3-22.

[9] F. F. Montesano, A. Parente, P. Santamaria, A. Sannino, and F. Serio, "Biodegradable Superabsorbent Hydrogel IncreasesWater Retention Properties of Growing Media and Plant Growth," *Agriculture and Agricultural Science Procedia,* vol. 4, pp. 451-458, 2015, doi: 10.1016/j.aaspro.2015.03.052.

[10] E. S. Abrisham *et al.*, "Effects of a super absorbent polymer on soil properties and plant growth for use in land reclamation," *Arid land research and management,* vol. 32, no. 4, pp. 407-420, 2018, doi: https://doi.org/10.1080/15324982.2018.1506526.

[11] M. R. Guilherme *et al.*, "Superabsorbent hydrogels based on polysaccharides for application in agriculture as soil conditioner and nutrient carrier: A review," *European Polymer Journal,* vol. 72, pp. 365-385, 2015, doi: 10.1016/j.eurpolymj.2015.04.017.

[12] M. J. Zohuriaan-Mehr, H. Omidian, S. Doroudiani, and K. Kabiri, "Advances in non-hygienic applications of superabsorbent hydrogel materials," *Journal of Materials Science,* journal article vol. 45, no. 21, pp. 5711-5735, November 01 2010, doi: 10.1007/s10853-010-4780-1.

[13] Reddy Kathi S., "Effect of different doses of superabsorbent polymer (SAP) on water and nitrogen retention in soil, and on the growth and development of tomato and determination of optimal rate of SAP," Master of Science, Plant and soil science College of Graduate Studies Texas A&M University-Kingsville, Texas, 2019.

[14] J. El-Asmar, H. Jaafar, I. Bashour, M. T. Farran, and I. P. Saoud, "Hydrogel Banding Improves Plant Growth, Survival, and Water Use Efficiency in Two Calcareous Soils," *CLEAN – Soil, Air, Water,* vol. 45, no. 7, p. 1700251, 2017, doi: https://doi.org/10.1002/clen.201700251.

[15] M. R. Islam, Y. Hu, S. Mao, J. Mao, A. E. Eneji, and X. Xue, "Effectiveness of a water-saving super-absorbent polymer in soil water conservation for corn (Zea mays L.) based on eco-physiological parameters," *Journal of the Science of Food and*

Agriculture, vol. 91, no. 11, pp. 1998-2005, 2011, doi: https://doi.org/10.1002/jsfa.4408.

[16] A. Satriani, M. Catalano, and E. Scalcione, "The role of superabsorbent hydrogel in bean crop cultivation under deficit irrigation conditions: A case-study in Southern Italy," *Agricultural Water Management,* vol. 195, pp. 114-119, 2018/01/01/ 2018, doi: https://doi.org/10.1016/j.agwat.2017.10.008.

[17] J. Akhter, K. Mahmood, K. A. Malik, A. Mardan, M. Ahmad, and M. Iqbal, "Effects of hydrogel amendment on water storage of sandy loam and loam soils and seedling growth of barley, wheat and chickpea," *Plant Soil and Environment,* vol. 50, pp. 463-469, 2018.

[18] J. Kumar, S. Das, and S. L. Teoh, "Dietary Acrylamide and the Risks of Developing Cancer: Facts to Ponder," (in eng), *Front Nutr,* vol. 5, pp. 14-14, 2018, doi: 10.3389/fnut.2018.00014.

[19] S. Li and G. Chen, "Agricultural waste-derived superabsorbent hydrogels: Preparation, performance, and socioeconomic impacts," *Journal of Cleaner Production,* vol. 251, p. 119669, 2020/04/01/ 2020, doi: https://doi.org/10.1016/j.jclepro.2019.119669.

[20] A. I. Raafat, M. Eid, and M. B. El-Arnaouty, "Radiation synthesis of superabsorbent CMC based hydrogels for agriculture applications," *Nuclear Instruments and Methods in Physics Research Section B: Beam Interactions with Materials and Atoms,* vol. 283, pp. 71-76, 2012, doi: 10.1016/j.nimb.2012.04.011.

[21] J. Pushpamalar, S. J. Langford, M. B. Ahmad, Y. Y. Lim, and K. Hashim, "Eco-friendly smart hydrogels for soil conditioning and sustain release fertilizer," *International Journal of Environmental Science and Technology,* vol. 15, no. 10, pp. 2059-2074, 2017, doi: 10.1007/s13762-017-1598-2.

[22] A. Sannino and L. Nicolais, "Concurrent effect of microporosity and chemical structure on the equilibrium sorption properties of cellulose-based hydrogels," *Polymer,* vol. 46, no. 13, pp. 4676-4685, 2005, doi: 10.1016/j.polymer.2005.03.072.

[23] M. A. Hubbe, A. Ayoub, J. S. Daystar, R. A. Venditti, and J. J. Pawlak, "Enhanced Absorbent Products Incorporating Cellulose and Its Derivatives: A Review," *2013,* Absorbency; Cellulosic materials; Fluff pulp; Superabsorbents; Hydrogels; Carboxymethylcellulose (CMC); Disposable; Rate of absorption; Life cycle analysis vol. 8, no. 4, p. 74, 2013-08-16 2013. [Online]. Available: https://ojs.cnr.ncsu.edu/index.php/BioRes/article/view/4379.

[24] N. Lavoine and L. Bergström, "Nanocellulose-based foams and aerogels: processing, properties, and applications," *Journal of Materials Chemistry A,* vol. 5, no. 31, pp. 16105-16117, 2017, doi: 10.1039/c7ta02807e.

[25] L. Mendoza, L. Hossain, E. Downey, C. Scales, W. Batchelor, and G. Garnier, "Carboxylated nanocellulose foams as superabsorbents," *J Colloid Interface Sci,* vol. 538, pp. 433-439, Mar 7 2019, doi: 10.1016/j.jcis.2018.11.112.

[26] A. Isogai, T. Saito, and H. Fukuzumi, "TEMPO-oxidized cellulose nanofibers," *Nanoscale,* 10.1039/C0NR00583E vol. 3, no. 1, pp. 71-85, 2011, doi: 10.1039/C0NR00583E.

[27] R. M. Barajas-Ledesma, A. F. Patti, V. N. L. Wong, V. S. Raghuwanshi, and G. Garnier, "Engineering nanocellulose superabsorbent structure by controlling the drying rate," *Colloids and Surfaces A: Physicochemical and Engineering Aspects,* vol. 600, 2020, doi: 10.1016/j.colsurfa.2020.124943.

[28] Y. Zhou, S. Fu, L. Zhang, and H. Zhan, "Superabsorbent nanocomposite hydrogels made of carboxylated cellulose nanofibrils and CMC-g-p(AA-co-AM),"

Carbohydrate Polymers, vol. 97, no. 2, pp. 429-435, 2013/09/12/ 2013, doi: https://doi.org/10.1016/j.carbpol.2013.04.088.

[29]   H. Zhang *et al.*, "Cellulose Anionic Hydrogels Based on Cellulose Nanofibers As Natural Stimulants for Seed Germination and Seedling Growth," *J Agric Food Chem,* vol. 65, no. 19, pp. 3785-3791, May 17 2017, doi: 10.1021/acs.jafc.6b05815.

[30]   C. R. Bauli, G. F. Lima, A. G. de Souza, R. R. Ferreira, and D. S. Rosa, "Eco-friendly carboxymethyl cellulose hydrogels filled with nanocellulose or nanoclays for agriculture applications as soil conditioning and nutrient carrier and their impact on cucumber growing," *Colloids and Surfaces A: Physicochemical and Engineering Aspects,* vol. 623, p. 126771, 2021/08/20/ 2021, doi: https://doi.org/10.1016/j.colsurfa.2021.126771.

[31]   N. Singh, S. Agarwal, A. Jain, and S. Khan, "3-Dimensional cross linked hydrophilic polymeric network "hydrogels": An agriculture boom," *Agricultural Water Management,* vol. 253, p. 106939, 2021/07/01/ 2021, doi: https://doi.org/10.1016/j.agwat.2021.106939.

[32]   S. Ang, V. Haritos, and W. Batchelor, "Cellulose nanofibers from recycled and virgin wood pulp: A comparative study of fiber development," *Carbohydrate Polymers,* vol. 234, p. 115900, 2020/04/15/ 2020, doi: https://doi.org/10.1016/j.carbpol.2020.115900.

[33]   R. F. Isbell, *The Australian soil classification*, Rev. ed. ed. Collingwood, VIC, Australia: Collingwood, VIC, Australia : CSIRO Pub., 2002.

[34]   S. C. U. Environmental Analysis Laboratory, . "Agricultural soil testing." https://www.scu.edu.au/environmental-analysis-laboratory---eal/analytical-services/agricultural-soil-testing/ (accessed 31/07/2020, 2020).

[35]   R. M. Barajas-Ledesma, A. F. Patti, V. N. L. Wong, V. S. Raghuwanshi, and G. Garnier, "Engineering nanocellulose superabsorbent structure by controlling the drying rate," *Colloids and Surfaces A: Physicochemical and Engineering Aspects,* vol. 600, p. 124943, 2020/09/05/ 2020, doi: https://doi.org/10.1016/j.colsurfa.2020.124943.

[36]   R. Fan, J. Luo, S. Yan, Y. Zhou, and Z. Zhang, "Effects of Biochar and Super Absorbent Polymer on Substrate Properties and Water Spinach Growth," *Pedosphere,* vol. 25, no. 5, pp. 737-748, 2015, doi: 10.1016/S1002-0160(15)30055-2.

[37]   L. van Zwieten *et al.*, "Influence of biochars on flux of N2O and CO2 from Ferrosol," (in English), *Australian Journal of Soil Research,* Article vol. 48, p. 555+, 2010 2010. [Online]. Available: https://link.gale.com/apps/doc/A241179274/AONE?u=monash&sid=AONE&xid=088435d9.

[38]   A. Sluiter *et al.*, "Determination of structural carbohydrates and lignin in biomass, in: Laboratory Analytical Procedure (LAP)," *National Renewable Energy Laboratory,* 01/01 2008.

[39]   N. Thombare, S. Mishra, M. Z. Siddiqui, U. Jha, D. Singh, and G. R. Mahajan, "Design and development of guar gum based novel, superabsorbent and moisture retaining hydrogels for agricultural applications," *Carbohydr Polym,* vol. 185, pp. 169-178, 2018, doi: 10.1016/j.carbpol.2018.01.018.

[40]   S. Sivapalan, "Improving crop production by the use of PAM: Potential benefits to Australian agriculture," presented at the Proceedings 11th Australian Agronomy Conference, Geelong, Victoria, Australia, 2003.

[41]   N. Thombare, S. Mishra, M. Z. Siddiqui, U. Jha, D. Singh, and G. R. Mahajan, "Design and development of guar gum based novel, superabsorbent and moisture

retaining hydrogels for agricultural applications," *Carbohydrate Polymers,* vol. 185, pp. 169-178, 2018/04/01/ 2018, doi: https://doi.org/10.1016/j.carbpol.2018.01.018.

[42] D. Sarmah and N. Karak, "Biodegradable superabsorbent hydrogel for water holding in soil and controlledвЂ‘release fertilizer," *Journal of applied polymer science,* vol. 137, no. 13, pp. 48495-n/a, 2020, doi: 10.1002/app.48495.

[43] H. A. A. El-Rehim, E.-S. A. Hegazy, and H. L. A. El-Mohdy, "Radiation synthesis of hydrogels to enhance sandy soils water retention and increase plant performance," *Journal of Applied Polymer Science,* vol. 93, no. 3, pp. 1360-1371, 2004, doi: https://doi.org/10.1002/app.20571.

[44] M. Rahmati, A. Pohlmeier, S. M. A. Abasiyan, L. Weihermüller, and H. Vereecken, "Water Retention and Pore Size Distribution of a Biopolymeric-Amended Loam Soil," *Vadose Zone Journal,* vol. 18, no. 1, p. 180205, 2019, doi: https://doi.org/10.2136/vzj2018.11.0205.

[45] X. Bian, L. Zeng, Y. Deng, and X. Li, "The Role of Superabsorbent Polymer on Strength and Microstructure Development in Cemented Dredged Clay with High Water Content," (in eng), *Polymers (Basel),* vol. 10, no. 10, p. 1069, 2018, doi: 10.3390/polym10101069.

[46] I. H. Mondal, *Cellulose-Based Superabsorbent Hydrogels* (Polymers and Polymeric Composites: A Reference Series). 2019.

[47] R. M. Barajas-Ledesma, L. Hossain, V. N. L. Wong, A. F. Patti, and G. Garnier, "Effect of the counter-ion on nanocellulose hydrogels and their superabsorbent structure and properties," *Journal of Colloid and Interface Science,* vol. 599, pp. 140-148, 2021/10/01/ 2021, doi: https://doi.org/10.1016/j.jcis.2021.04.065.

[48] M. Todorovic, "Crop Evapotranspiration," in *Water Encyclopedia*, pp. 571-579.

[49] A. Ünlükara, T. Yurtyeri, and B. Cemek, "Effects of Irrigation water salinity on evapotranspiration and spinach (Spinacia oleracea L. Matador) plant parameters in greenhouse indoor and outdoor conditions," *Agronomy Research,* vol. 15, pp. 2183-2194, 01/01 2017, doi: 10.15159/AR.17.041.

[50] H.-R. Fallahi, R. T. Kalantari, M. Aghhavani-Shajari, and M.-G. Soltanzadeh, "Effect of Super Absorbent Polymer and Irrigation Deficit on Water Use Efficiency, Growth and Yield of Cotton," (in English), *Notulae Scientia Biologicae,* vol. 7, no. 3, p. 338, 2015

[51] G. McDonald. "Waterlogging - the science." Department of primary industries and development. https://www.agric.wa.gov.au/waterlogging/waterlogging-%E2%80%93-science (accessed 31/05/2021, 2021).

[52] A. Chikara, M. C. Singh, R. Kumar, D. Parmar, and A. Kumar, "Performance of a new superabsorbent polymer on seedling and post planting growth and Water use pattern of chrysanthemum grown under controlled environment," *Acta horticulturae,* vol. 742, pp. 43-49, 04/01 2007, doi: 10.17660/ActaHortic.2007.742.5.

[53] K. V. Sharman and M. Whitehouse, "Nitrogen drawdown index as a predictor of nitrogen requirements for Nephrolepis in sawdust media," *Scientia Horticulturae,* vol. 54, no. 1, pp. 23-33, 1993/04/01/ 1993, doi: https://doi.org/10.1016/0304-4238(93)90080-A.

[54] K. A. Handreck, "Rapid assessment of the rate of nitrogen immobilisation in organic components of potting media: II. Nitrogen drawdown index and plant growth," *Communications in Soil Science and Plant Analysis,* vol. 23, no. 3-4, pp. 217-230, 1992/02/01 1992, doi: 10.1080/00103629209368584.

[55] K. R. Kelley and F. J. Stevenson, "Forms and nature of organic N in soil," *Fertilizer Research,* Article vol. 42, no. 1-3, pp. 1-11, 1995, doi: 10.1007/BF00750495.

[56] M. R. Hoosbeek, "Cycles of Soil: Carbon, Nitrogen, Phosphorus, Sulfur, Micronutrients, 2nd edition," *Soil science,* vol. 165, no. 2, pp. 185-187, 2000, doi: 10.1097/00010694-200002000-00010.

[57] B. P. Degens, "Microbial functional diversity can be influenced by the addition of simple organic substrates to soil," *Soil Biology and Biochemistry,* vol. 30, no. 14, pp. 1981-1988, 1998/12/01/ 1998, doi: https://doi.org/10.1016/S0038-0717(98)00070-4.

[58] A. Hadas, L. Kautsky, M. Goek, and E. Erman Kara, "Rates of decomposition of plant residues and available nitrogen in soil, related to residue composition through simulation of carbon and nitrogen turnover," *Soil Biology and Biochemistry,* vol. 36, no. 2, pp. 255-266, 2004/02/01/ 2004, doi: https://doi.org/10.1016/j.soilbio.2003.09.012.

[59] A. Hadas, S. Feigenbaum, M. Sofer, J. A. E. Molina, and C. E. Clapp, "Decomposition of Nitrogen-15-Labeled Wheat and Cellulose in Soil: Modeling Tracer Dynamics," *Soil Science Society of America Journal,* https://doi.org/10.2136/sssaj1993.03615995005700040019x vol. 57, no. 4, pp. 996-1001, 1993/07/01 1993, doi: https://doi.org/10.2136/sssaj1993.03615995005700040019x.

[60] H. P. Hartmann and T. Appel, "Calibration of near infrared spectra for measuring decomposing cellulose and green manure in soils," *Soil Biology and Biochemistry,* vol. 38, no. 5, pp. 887-897, 2006/05/01/ 2006, doi: https://doi.org/10.1016/j.soilbio.2005.08.005.

THIS PAGE HAS BEEN INTENTIONALLY LEFT BLANK

CHAPTER 7:
CONCLUSION AND PERSPECTIVES

THIS PAGE HAS BEEN INTENTIONALLY LEFT BLANK

Chapter 7: Conclusion and Perspectives

THIS PAGE HAS BEEN INTENTIONALLY LEFT BLANK

7.1 Conclusion

Superabsorbent polymers (SAP) are cross-linked networks of hydrophilic polymer chains with the ability to absorb water or fluids at hundreds time their own weight and remain stable. Their use in agriculture for soil water retention provides a strategy to improve the efficient use of water resources, because this industry uses about 70% of the water available for human consumption worldwide. However, most of the commercial SAPs are fossil-fuel derived polymers which are non-biodegradable and non-renewable. This necessitates the development of SAPs based on natural polymers such as cellulose, the world's most abundant biopolymer. Cellulose is 100% biodegradable, renewable and it has inherent hydrophilicity, which are all desirable characteristics to produce superabsorbents. Nanocellulose refers to the cellulose fibres with dimensions in the nanometre scale. Apart from the inherent properties of cellulose, nanocellulose can be easily functionalised and structured into a superabsorbent.

This thesis has identified nanocellulose superabsorbent as a promising substitute for the current fossil-fuel derived SAPs. First, the physical and chemical properties of nanocellulose SAPs were specifically designed to form a cost-effective material to use as a soil conditioner in agriculture. In the second part of this research, the potential of nanocellulose SAPs to increase water retention and improve soil properties and plant growth was measured.

7.1.1 Engineered nanocellulose superabsorbents for agricultural applications

7.1.1.1 Physical structure

Freeze-drying is the most common drying technique used to produce nanocellulose SAPs at laboratory scale. Although efficient and easy to control, this technique is expensive and difficult to perform on a large-scale, which can limit the application of these SAPs in agriculture. In this doctoral study, nanocellulose superabsorbents were therefore engineered by controlling the drying rate to produce novel and cost-effective superabsorbents with tunable

structures and pore properties. Five different drying methods, each providing a different rate of water removal, were tested. We raised the hypothesis that drying rate controls the structure of the resulting SAP cellulose network. The structure and pore properties of the SAPs were dictated by the drying technique used, which directly impacted the swelling capacity and kinetics. Freeze-drying SAPs exhibited a diffusion-controlled swelling mechanism whereas stress relaxation of the fibre network governed the absorption rate in oven-dried SAPs. Air-dried SAPs achieved the highest swelling capacity due to their high pore area and strong water bond interaction. Seed germination studies performed on two types of SAP confirmed the safe application of nanocellulose SAPs to plants.

7.1.1.2 Chemical structure

Another challenge in the production of nanocellulose superabsorbents is the presence of Na^+ ions in the nanofibre network which are introduced during the TEMPO-mediated oxidation of cellulose. Sodium is not desirable for agriculture related applications. Adding Na^+ to soils can have an adverse effect on water and oxygen availability and soil structure, imposing a stress on growing crops. Exchanging the cation with alternative cations can help in understanding the behaviour of the superabsorbent in soils where there is a natural mixture of exchangeable cations, including Mg^{2+}, Ca^{2+}, and K^+.

In the next engineering step, cellulose pulp was TEMPO-oxidised, ion-exchanged and fibrillated to produce nanocellulose hydrogels with varying extent of fibrillation and ionic cross-linking. Seven cations were tested. The hydrogels were further freeze-dried into superabsorbents (SAP). The type of ion and their interaction with the carboxylate groups dictated the fibrillation efficiency, which controlled the structure of the SAPs. The superabsorbent swelling at equilibrium was in the order of: $NH_4^+ > K^+ > Na^+ > Mg^{2+} > Zn^{2+} > Ca^{2+}$. Both NH_4^+-hydrogels and SAPs showed outstanding properties such as low pore diameter

and high pore area, achieving the highest swelling at equilibrium compared to the other cations. This was due to the ability of the NH_4^+ ions to rotate, which increased the number of available COO^- groups to bind with water, resulting in an increase in hydrogel stiffness, pore area and SAP swelling. The addition of NH_4^+ ions to the SAP network, also opens the possibility for the application of these SAPs as nutrient carriers. Nanocellulose SAP was demonstrated as a novel and sustainable alternative. By controlling its physical and chemical structure, this SAP can be tailored to suit a range of applications in agriculture.

7.1.2 Nanocellulose superabsorbent as soil conditioner

Superabsorbent polymers can be used to increase soil water retention, reduce irrigation water consumption to enable plants to survive longer in water limited conditions. Nanocellulose SAPs were evaluated as water retention agents for use in soils. A sandy soil was amended with three types of nanocellulose SAP at different application rates. The soil water retention increased with increasing application rate of superabsorbent. Adding freeze-dried SAP to soil resulted in the highest water retention, while soils treated with SAP oven-dried at 50 °C remained moist the longest. Such behaviour was attributed to the pore structure of both SAPs, as observed previously. For both, the increase in water content prolonged the period of water available for the plant by up to 20 days. The SAP performance decreased with subsequent hydration/dehydration cycles and as the SAP degraded. In the soil tested, SAP decomposition occurred within 30 days of exposure. Increasing the nutrient availability further increased the decomposition rate, independently of the type of SAP used. This research identified nanocellulose SAP produced through oven-drying at 50 °C as the best candidate for plant growth studies as this superabsorbent can retain soil moisture for longer and it is possible to produce on a large scale.

7.1.3 The role of nanocellulose superabsorbents in plant growth

Nanocellulose superabsorbents were first developed to optimize soil water retention; however, their role in plant growth needs to be determined. This was achieved by growing Tatsoi plants in a soil amended with varying rates of SAP. Two application rates of nanocellulose SAP were studied: 0.5 wt% and 1.0 wt%. Plant biomass significantly decreased in treatments with 1.0 wt% of nanocellulose SAP which was attributed to the immobilisation of nitrogen by microbial biomass. The increase in soil respiration rates with nanocellulose SAP further supports this finding. Plant biomass from treatments with 0.5 wt% of nanocellulose was similar to those without SAP. Thus, this application rate was selected for the subsequent studies.

7.1.4 The role of soil type in SAP performance

Soil properties, such as structure, water holding capacity, cation exchange capacity, pH and other features, vary widely. These features can greatly influence the SAP performance and its benefits for plants. To evaluate this, Spinach plants were grown in two soil types, a clay loam (CL) and a sandy soil (SD), both amended with 0.5 wt% of nanocellulose SAP. The results were compared with those of a commercial polyacrylamide-based SAP. For both soils, the addition of superabsorbent improved soil porosity and its water retention. Plant biomass varied widely depending on the type of soil. For the SD soils, plant biomass was the highest in treatments with commercial SAP. However, it significantly decreased in the CL soils treated with any type of superabsorbent, which was magnified using nanocellulose SAP. This finding is likely caused by waterlogging and the fast biodegradation of nanocellulose. Biodegradation tests indeed revealed that only about 50% of the initial mass of nanocellulose remained after 5 and 7 days of exposure in the CL and SD soils, respectively. This research identified the commercial superabsorbent to have a superior performance compared to nanocellulose.

7.2 Perspectives

This thesis engineered novel nanocellulose superabsorbents of controlled structure to increase soil water retention in agriculture. The production of cost-effective and efficient nanocellulose SAP was demonstrated by controlling the drying rate of the hydrogel precursor. The addition of multivalent ions confirmed the easy functionalisation of nanocellulose to suit a range of applications. For example, superabsorbents with minerals which contain K^+, Mg^{2+}, Zn^{2+} or NH_4^+ can also function as a controlled release for agrochemicals needed for plant growth.

The potential for nanocellulose SAPs to increase water retention in two soil types, one with low water holding capacity and another with high water holding capacity, was quantified. Although these soils were adopted as models, other soil types can be treated with nanocellulose superabsorbents and are likely to show similar outcomes. The superabsorbent application rate would need to be adapted in those cases. Future work could also explore the performance of these SAP as soil conditioners, conducting a full characterisation of the soils amended with nanocellulose. This implies analysing the changes in the soil properties including soil porosity, bulk density, soil compaction, and oxygen availability to understand how these may affect the plant growth. Indeed, this research demonstrated the potential of nanocellulose as a platform material for use in agriculture. Further modification of the nanocellulose SAP physical and chemical properties is necessary to decrease the rate of its biodegradation, and maximise its use for soil water retention. For example, nanocellulose can be cross-linked with other materials such as lignin to increase its stability in soil and provide a benign antimicrobial activity. The effect of introducing nanocellulose SAP on plant growth requires further exploration as well. Even though this thesis identified a potential nitrogen drawdown effect occurring with nanocellulose addition, there may be other factors limiting plant growth such as anaerobic conditions within the soil profile, or the effects of microbial growth which may also inhibit plant development. For this, a comprehensive nutrient analysis of the soil and plants

are needed which are beyond the scope of this study. Lastly, economic feasibility studies of the

production of nanocellulose superabsorbents, which considers their high biodegradability, and

the cost and ease of applying them in open field conditions, are required as well.

THIS PAGE HAS BEEN INTENTIONALLY LEFT BLANK

APPENDIX I:
SUPPLEMENTARY INFORMATION

THIS PAGE HAS BEEN INTENTIONALLY LEFT BLANK

Engineering nanocellulose superabsorbent structure by controlling the drying rate

Ruth M. Barajas-Ledesma[a], Antonio F. Patti[b], Vanessa N.L. Wong[c], Vikram Singh Raghuwanshi[a] and Gil Garnier[a*]

[a]Bioresource Processing Institute of Australia (BioPRIA) and Department of Chemical Engineering, Monash University, Clayton, VIC 3800, Australia
[b]School of Chemistry, Monash University, Clayton, VIC 3800, Australia
[c]School of Earth, Atmosphere & Environment, Monash University, Clayton, VIC 3800, Australia

*For correspondence: Gil.Garnier@Monash.edu

Figure S1. Schematic of the water retention value set up for the centrifuge.
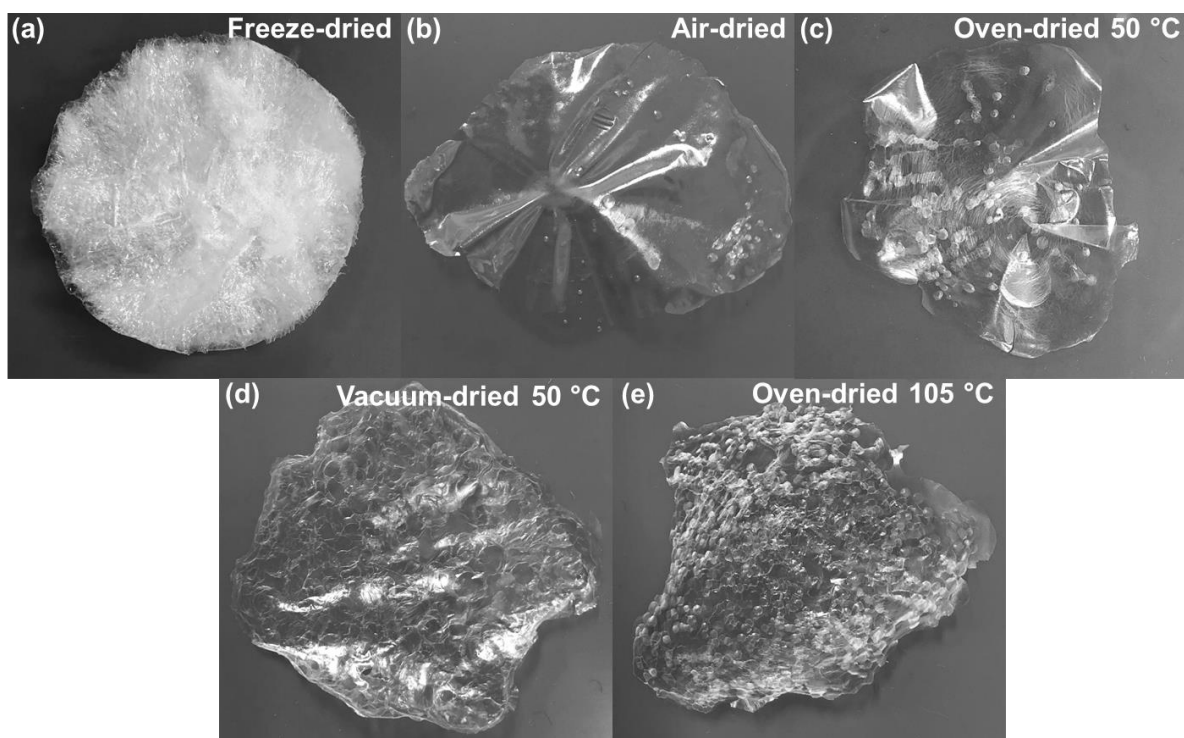
Figure S2. Photographs of nanocellulose superabsorbent produced with different drying methods: (a) Freeze-dried, (b) air-dried, (c) oven-dried 50 °C, (d) vacuum oven-dried 50 °C, (e) oven-dried 105 °C.
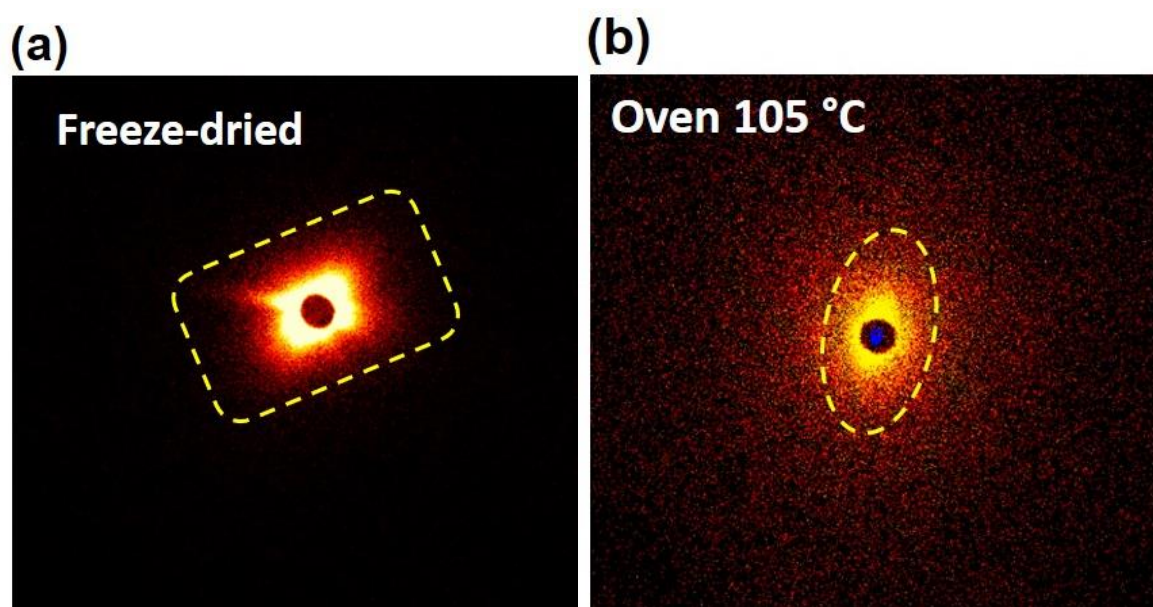
Figure S3. SAXS images of (a) freeze-dried and (b) oven-dried 105°C superabsorbents.

Radish on Oven-dried 50°C

Without superabsorbent

With superabsorbent

Figure S4. Radish seeds grown over oven-dried 50°C superabsorbents

Carboxylated nanocellulose superabsorbent: biodegradation and soil water retention properties

Ruth M. Barajas-Ledesma[a], Vanessa N.L. Wong[b], Karen Little[c], Antonio F. Patti[c] and Gil Garnier[a*]*

[a]Bioresource Processing Research Institute of Australia (BioPRIA) and Department of Chemical Engineering, Monash University, Clayton, VIC 3800, Australia
[b]School of Earth, Atmosphere & Environment, Monash University, Clayton, VIC 3800, Australia
[c]School of Chemistry, Monash University, Clayton, VIC 3800, Australia

*Email of corresponding authors: Gil.Garnier@Monash.edu and Antonio.Patti@Monash.edu

Tables

Table S1. Characteristics of the calcarosol soil selected for the experiments.

Parameter	Calcarosol
Electrical conductivity (dS/m)[a]	0.022
pH	6.80
Nitrate (mg/Kg)	2.2
Ammonium (mg/Kg)	1.5
Total Carbon (%)	0.12
Total Nitrogen (%)	0.03
Organic Matter (%)	0.20
Na^+ (mg/Kg)	14
Ca^{2+} (mg/Kg)	521
Mg^{2+} (mg/Kg)	139
K^+ (mg/Kg)	156
Phosphorus (mg/Kg)	22
Effective Cation Exchange Capacity ($cmol^+$/Kg)	4.21

[a]Electrical conductivity measured in a 1:5 soil:water extract.

Table S2. Characteristics of the calcarosol soil water extract used in the experiments.

Parameter	Water extract
pH	6.80
Electrical conductivity (µS/m)	536.02
Aluminium (mg/L)	31.90
Iron (mg/L)	16.40
Silicon (mg/L)	63.90
Calcium (mg/L)	9.27
Magnesium (mg/L)	4.44
Potassium (mg/L)	8.39
Sodium (mg/L)	72.60
Chloride (mg/L)	39.90
Sulphur (mg/L)	28.90
Phosphorus (mg/L)	9.90

Table S3. Comparison of the pore properties of nanocellulose SAP freeze-dried, oven-dried at 50 °C and at 105 °C [1]

Superabsorbent	Porosity (% ± S.D)	Pore area ($m^2g^{-1} \pm$ S.D.)	Pore volume (mL g^{-1})
Freeze-dried	94.5 ± 1.01	6.7 ± 0.44	20.2
Oven-dried at 50°C	48.7 ± 7.01	44.1 ± 0.30	0.3
Oven-dried at 105 °C	53.9 ± 2	0.2 ± 0.10	0.4

Figures
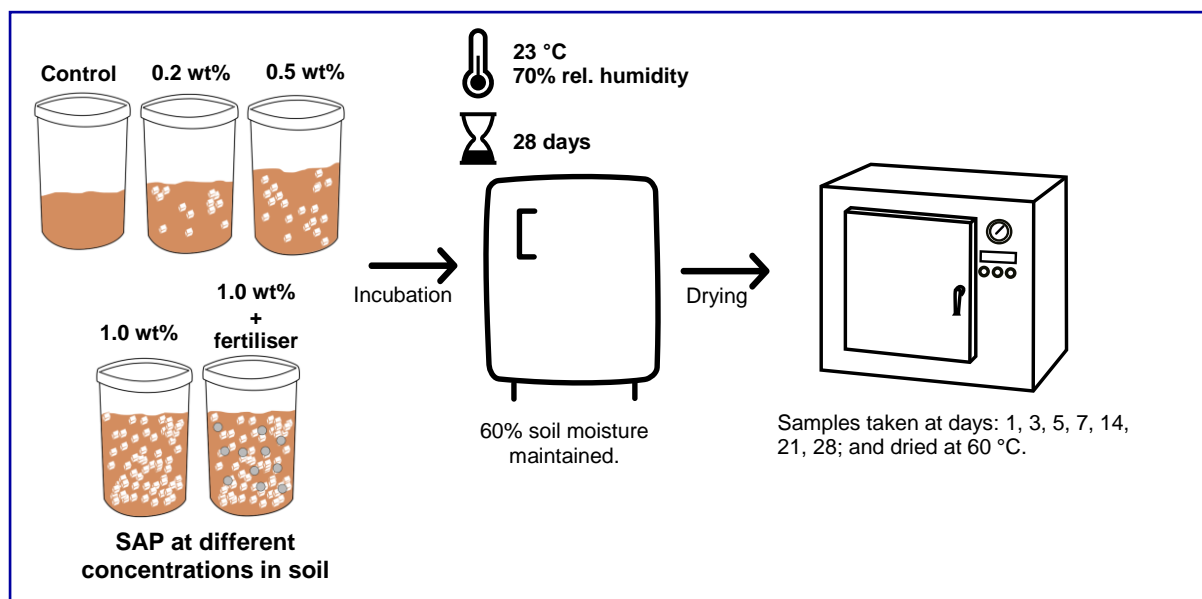
Figure S1. Scheme of the experimental set up for the biodegradation studies.
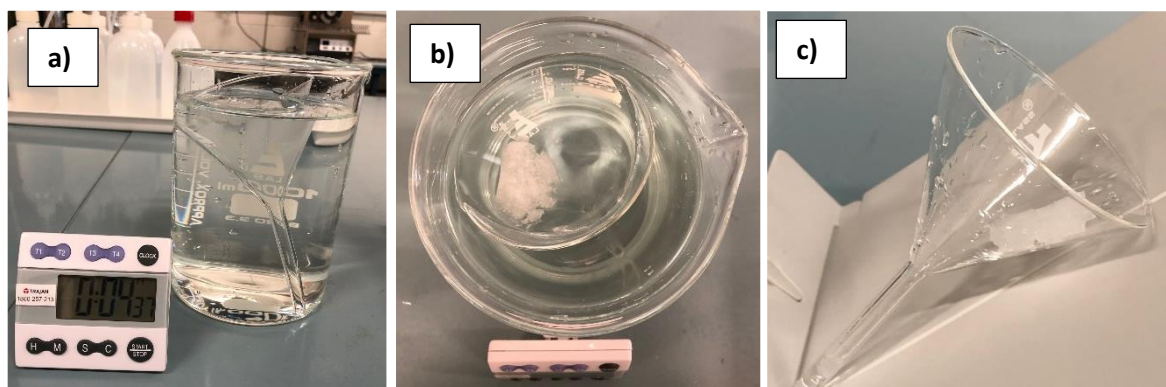
Figure S2. Photographs of the swelling experiments. (a) the superabsorbent sample is placed inside a funnel and immersed in deionised water. (b) the superabsorbent immersed in deionised water as viewed from the top. (c) After the selected period of time, the funnel is raised, and the excess water is allowed to drain and the sample is wiped.
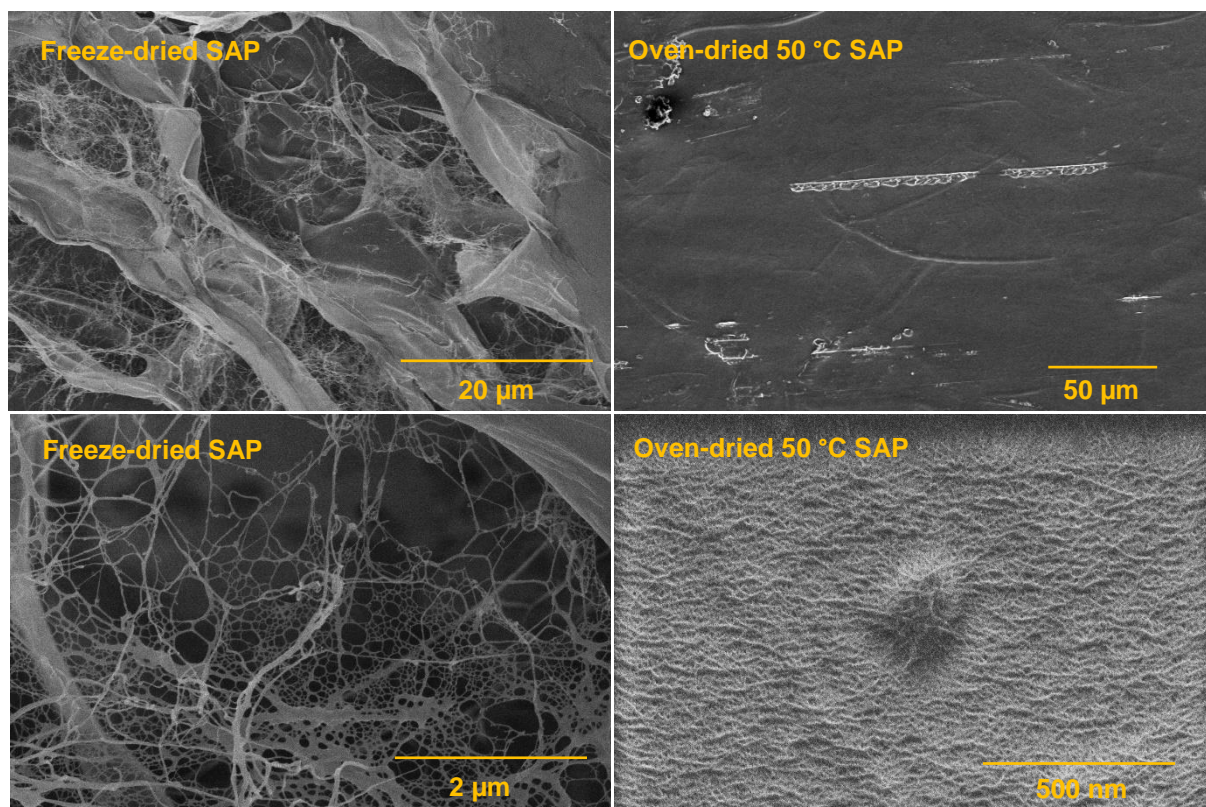
Figure S3. SEM images of the nanocellulose superabsorbents freeze-dried and oven-dried at 50 °C.

References

[1]   R. M. Barajas-Ledesma, A. F. Patti, V. N. L. Wong, V. S. Raghuwanshi, and G. Garnier, "Engineering nanocellulose superabsorbent structure by controlling the drying rate," *Colloids and Surfaces A: Physicochemical and Engineering Aspects,* vol. 600, p. 124943, 2020/09/05/ 2020, doi: https://doi.org/10.1016/j.colsurfa.2020.124943.

Effect of Nanocellulose-based superabsorbent on the early stage growth of tatsoi (*Brassica rapa narinosa*)

Ruth Barajas-Ledesma[a], Vanessa N.L. Wong[b], Karen Little[c], Gil Garnier[a]* and Antonio F. Patti[c]*

[a]Bioresource Processing Research Institute of Australia (BioPRIA) and Department of
[b]School of Chemistry, Monash University, Clayton, VIC 3800, Australia
[c]School of Earth, Atmosphere & Environment, Monash University, Clayton, VIC 3800, Australia
Chemical Engineering, Monash University, Clayton, VIC 3800, Australia

*For correspondence: Tony.patti@Monash.edu and Gil.garnier@Monash.edu

Table S1. Characteristics of the Podosol selected for the experiments. Soil was collected from a vegetable farm located in Cranbourne, Victoria, Australia.

Parameter	Podosol
Electrical conductivity (dS/m)*	0.028
pH	6.16
Total Carbon (%)	1.4
Nitrate (mg/Kg)	2.8
Ammonium (mg/Kg)	8.5
Na^+ (mg/Kg)	23
Ca^{2+} (mg/Kg)	316
Mg^{2+} (mg/Kg)	81
K^+ (mg/Kg)	<50
Phosphorus (mg/Kg)(Cowell)	14
Zinc (mg/Kg)	3.9
Manganese (mg/Kg)	2.0
Copper (mg/Kg)	0.77
Sulphur (mg/Kg)	3.5
Iron (mg/Kg)	125

Note: *Electrical conductivity measured in a 1:5 soil:water extract.
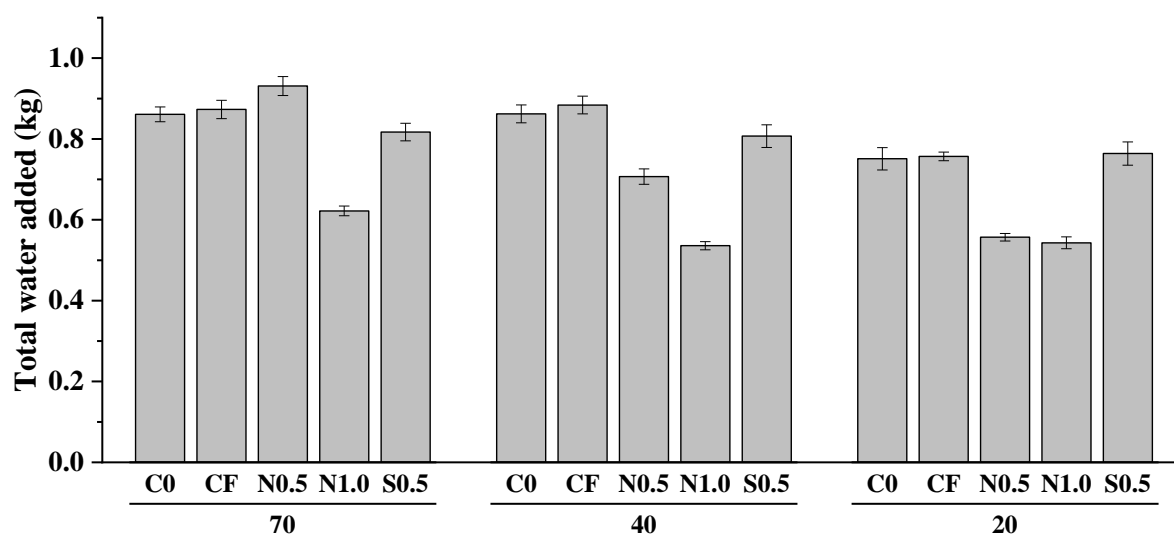
Figure S1. Total water added to tatsoi plants grown under different levels of soil moisture and treatments. Values are reported as mean ± standard deviation (n=5).
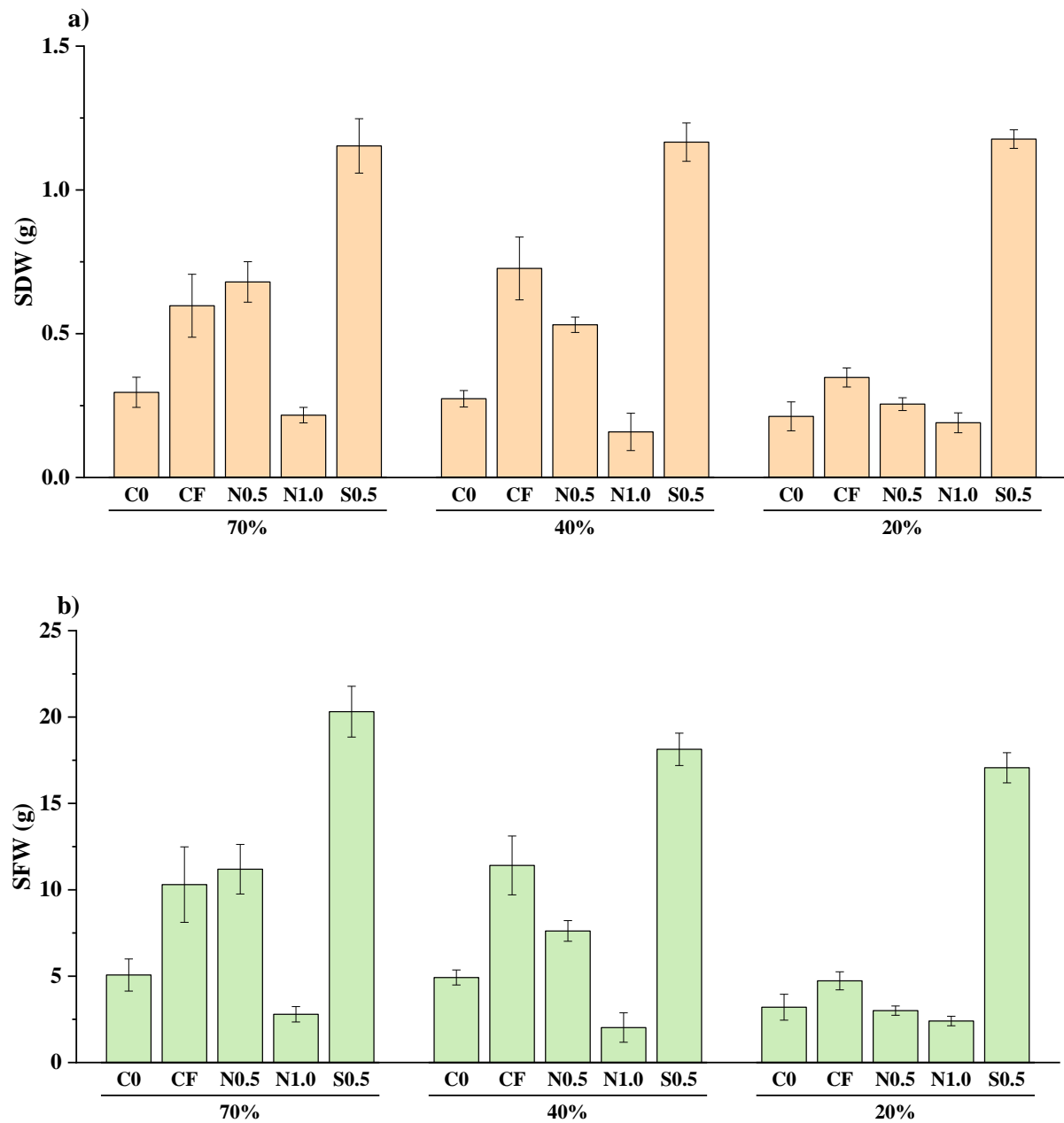
Figure S2. (a) Shoot dry weights (SDW) and (b) Shoot fresh weights (SFW) of Tatsoi plants grown under different levels of soil moisture and treatments. Values are reported as mean ± standard deviation (n=5).

Biodegradation of nanocellulose superabsorbent and its effect on the growth of spinach

Ruth M. Barajas-Ledesma[a], Craig W. Stocker[a], Vanessa N.L. Wong[b], Karen Little[c], Antonio F. Patti[c] and Gil Garnier[a*]*

[a]Bioresource Processing Research Institute of Australia (BioPRIA) and Department of Chemical Engineering, Monash University, Clayton, VIC 3800, Australia
[c]School of Earth, Atmosphere & Environment, Monash University, Clayton, VIC 3800, Australia
[b]School of Chemistry, Monash University, Clayton, VIC 3800, Australia

*For correspondence: Gil.Garnier@Monash.edu and Tony.Patti@Monash.edu

Table SI. Characteristics of the soils selected for the experiments. Red Sodosol was collected from a vegetable located in Werribee. Podosol soil was collected from a vegetable farm located in Cranbourne. Both locations in Victoria, Australia.

Parameter	Clay Loam (Red Sodosol)	Sandy (Podosol)
Electrical conductivity (dS/m)*	0.383	0.028
pH	8.1	5.7
Total Carbon (%)	1.3	1.2
Nitrate (mg/Kg)	18	4.9
Ammonium (mg/Kg)	3.5	0.36
Na^+ (mg/Kg)	254	31
Ca^{2+} (mg/Kg)	2,363	302
Mg^{2+} (mg/Kg)	417	49
K^+ (mg/Kg)	626	<50
Phosphorus (mg/Kg)(Cowell)	460	97
Zinc (mg/Kg)	2.6	2.4
Manganese (mg/Kg)	7.5	1.9
Copper (mg/Kg)	6.0	0.43
Sulphur (mg/Kg)	180	9.7
Iron (mg/Kg)	26	85

Note: *Electrical conductivity measured in a 1:5 soil:water extract.

APPENDIX II:

PUBLICATIONS INCLUDED IN THE THESIS IN THEIR PUBLISHED FORMAT

THIS PAGE HAS BEEN INTENTIONALLY LEFT BLANK

Contents lists available at ScienceDirect

Colloids and Surfaces A

Engineering nanocellulose superabsorbent structure by controlling the drying rate

Ruth M. Barajas-Ledesma[a], Antonio F. Patti[b], Vanessa N.L. Wong[c], Vikram Singh Raghuwanshi[a], Gil Garnier[a],*

[a] Bioresource Processing Research Institute of Australia (BioPRIA) and Department of Chemical Engineering, Monash University, Clayton, VIC 3800, Australia
[b] School of Chemistry, Monash University, Clayton, VIC 3800, Australia
[c] School of Earth, Atmosphere & Environment, Monash University, Clayton, VIC 3800, Australia

GRAPHICAL ABSTRACT

ARTICLE INFO

ABSTRACT

Hypothesis: The absorption performance and structure of superabsorbents prepared from carboxylated nanocellulose are strongly influenced by the rate of water removal. Their structure can be engineered by changing the drying profile.

Experiments: TEMPO-oxidised nanocellulose superabsorbents were prepared using five different drying techniques, each providing a distinct drying rate. The absorption capacity of deionised water was measured as a function of time and the swelling kinetics was determined, modelled and related to the superabsorbent structure. Superabsorbent phytotoxicity was assessed through seed emergence tests.

Findings: The absorption performance of nanocellulose superabsorbents is controlled by the drying rate. In most cases, drying the nanocellulose superabsorbents via evaporation increases the absorption capacity compared to freeze-dried superabsorbents. The best nanocellulose superabsorbent was the air-dried, absorbing around 230 g water/g dry fibre. The high absorption capacity of the evaporative dried superabsorbents is due to their high pore area which increases the interaction between water molecules and fibres. This leads to a stronger physical entrapment of water by capillary forces. Seed germination studies demonstrated that oven-dried 50 °C superabsorbent increased germination by 40 %. Carboxylated nanocellulose superabsorbents emerge as high-performance renewable materials which can be used extensively in many applications, including agriculture.

* Corresponding author.
 E-mail address: Gil.Garnier@Monash.edu (G. Garnier).

1. Introduction

Superabsorbent polymers (SAPs) are physically or chemically cross-linked three-dimensional (3D) networks made of linear or branched hydrophilic polymers [1]. Superabsorbents can absorb water or fluids at hundreds of times their own weight and remain stable in the swollen state [1–4]. The degree of swelling is governed by the mobility of ions from the external solution toward the centre of the superabsorbent, also known as counter-ion entropy, that induces an osmotic pressure difference across the material network [5,6]. Superabsorbents have been used in many applications including biomedicine [5], food and beverages [7], personal care and hygiene products [8], soil remediation and wastewater treatment [9] and agriculture [10]. In agriculture, SAPs can ameliorate water availability for plants [11]. These serve as soil conditioners, improving soil properties, reducing the irrigation water consumption, and increasing crop yield [12,13], and as nutrient carriers [13].

Most of the commercial superabsorbents are synthetic polymers, such as polyacrylamides or polyacrylates, which are non-biodegradable. Growing environmental and health concerns have driven the search for natural polymer-based superabsorbents, especially those made of polysaccharides, such as pectin or starch [14,15]. Cellulose, the most abundant polymer on earth, has also been investigated as a superabsorbent for its availability, low-cost, biodegradability, renewability and hydrophilicity [13,16]. Different synthesis methods have been examined to produce cellulose-based SAPs [17]. Among those, the TEMPO-mediation oxidation of cellulose is currently considered one of the most effective method for producing nanocellulose-based SAPs [6,18]. This process oxidises the easily accessible primary alcohol groups (C6) to the carboxylic acid, resulting in a cellulose structure containing some C6 carbons in carboxylic acid form. This surface modification provides the necessary electrostatic repulsion which assists the liberation of nanocellulose fibres upon mechanical fibrillation [19]. The resulting material, also referred to as hydrogel, consists of an entanglement of cellulose nanofibres (CNF) creating a porous material of high specific surface area [20]. Several reviews about nanocellulose-based material properties, production, structure and applications have been published [17,20–22].

A major challenge in the production of nanocellulose-based superabsorbents is to retain their porous structure during water removal. Different drying rates determined by the drying process have been examined to remove the water from hydrogels. Among these, freeze-drying has become the preferred method for laboratory preparation of highly-porous, ultralow-density solid SAPs of high water retention and swelling properties [20,23]. These are commonly known as foams or aerogels [20]. Freezing followed by sublimation of ice prevents the formation of capillary pressure, preserving the structure of the original dispersion. However, freeze-drying is not only expensive and difficult to perform on a large-scale [23], but it also produces low-density and fast swelling superabsorbent of limited application range. In agriculture, for example, a fast swelling rate can selectively sequester water, thus restricting the water availability to plants creating an undesirable water stress environment [12]. Thus, controlling the superabsorbent properties and structure which affect plant growth is crucial.

Evaporative-drying presents an alternative. Buchtová and Budtova [24] reported the evaporative vacuum drying at room temperature of microcrystalline cellulose dissolved in ionic liquids to produce superabsorbents with a volume shrinkage of 90 %, very low porosity and no measurable surface area because of the collapse of the porous polymer network. Beaumont et al. [25] compared the effects of oven-drying at 60 °C and freeze-drying on the redispersibility of TENCEL gel, composed of spherical cellulose II microparticles. Surprisingly, they showed that oven-dried superabsorbents had better colloidal stability and higher water retention than freeze-dried superabsorbents. This was attributed to the low process temperatures and superabsorbent additives, such as carboxylmethylcellulose, that minimises the

agglomeration and collapse of fibres during drying, referred to as hornification [26]. Hornification can also be minimised by preparing superabsorbents at high pH or by carboxylation of cellulose; a high-density of dissociated carboxylic groups prevents agglomeration by electrostatic stabilization [22,27].

While several studies have investigated the synthesis and formulation of cellulose-based superabsorbents, none have systematically compared the effect of drying rate and profile on the structure of nanocellulose superabsorbents nor related those to the absorption capacity and swelling kinetics. The effect of the drying rate on the morphology, porosity and pore properties of nanocellulose superabsorbent and how these properties influence plant growth remains poorly understood.

In this study, carboxylated nanocellulose hydrogels were prepared via TEMPO oxidation followed by high-pressure homogenization. This standard carboxylated nanocellulose hydrogel was dried to create a superabsorbent using five different drying techniques, each providing a different drying rate: freeze-drying, air-drying, vacuum drying, and oven-drying at high and low temperature. The superabsorbent absorption properties and the swelling kinetics were quantified. It is our objective to analyse the effect that drying rate has on the resulting superabsorbent structure and to establish the relationship with its absorption characteristics. Of special interest is the production of cellulose-based superabsorbents as hydro-retentor materials for applications in sustainable agriculture.

2. Materials and methods

2.1. Materials

Bleached Eucalyptus Kraft (BEK) pulp, containing around 90 % w/w of moisture was provided by Australian Paper, Maryvale, Australia. The chemical composition of the BEK pulp is displayed in Table 1 [28]. 2,2,6,6-Tetramethylpiperidine-1-oxyl (TEMPO) and sodium bromide (NaBr) were purchased from Sigma-Aldrich. Sodium hydroxide (NaOH) and hydrochloric acid (HCl) were diluted for solutions as required and purchased from Merck and ACL Laboratories, respectively. 12 % w/v sodium hypochlorite (NaClO) was purchased from Thermo Fisher Scientific and used as received. Radish (*Raphanus Sativus*) and cress (*Lepidium sativum L.*) seeds were purchased from Mr. Fothergill's (South Windsor, Australia).

2.2. Superabsorbent preparation

Nanocellulose superabsorbent was prepared following the TEMPO-mediated oxidation process developed by Isogai et al. [19]. Briefly, 25 g (dry weight) of BEK pulp was suspended in 2500 mL of water containing 0.4 g and 2.5 g of dissolved TEMPO and NaBr, respectively. The 12 % w/v NaClO was initially adjusted to pH 10 through addition of 36 % w/v HCl. The oxidation process started by adding 100 mL NaClO (6.6 mmol NaClO/g cellulose) drop-wise to the suspension under constant stirring. The pH of the reaction was kept at 10 via addition of 0.5 M NaOH. The reaction was maintained for 3 h or until no decrease in pH was observed. The oxidised fibres were washed with deionised water, recovered by filtration. The TEMPO-oxidised cellulose had a carboxylate content of 1.4 mmol/g as determined by conductivity

Table I

Chemical composition of BEK pulp in dry basis.

Chemical composition	Average content (% ± standard deviation)
Cellulose	78.7 ± 0.8
Hemicellulose	17.7 ± 0.4
Lignin	3.2 ± 0.1
Extractives	0.3 ± 0.1
Ash	0.2 ± 0.1

2

titration [29].

The TEMPO-oxidised cellulose was then dispersed in deionised water to achieve a concentration of 0.5 % w/v. Fibrillation was accomplished by using a high-pressure homogeniser (GEA Niro Soavi Homogeniser Panda) at 1000 bar and two passes.

After fibrillation, five drying techniques were employed to produce the superabsorbent: freeze-drying, air-drying, vacuum-drying at 50 °C and oven-drying at 50 °C and 105 °C. Freeze-dried nanocellulose superabsorbent was prepared by freezing the nanocellulose samples for at least 12 h at −80 °C. Once frozen, samples were freeze-dried (Christ Alpha 2-4 LD Plus) for 2 days. Air-dried samples were allowed to dry at ambient temperature (approx. 23 °C) until no difference in mass was observed. Vacuum oven-dried nanocellulose samples were prepared by drying in a vacuum oven (Thermoline Scientific Vacuum drying oven) at 50 °C until no difference in mass was observed. Oven-dried nanocellulose samples were prepared by drying in an oven at either 50 °C or 105 °C until no difference in mass was observed.

2.3. Characterisation

The structural morphology of all superabsorbents was analysed by SEM using a FEI Nova NanoSEM and a FEI Magellan 400. Samples were mounted on a metal stub coated with an Iridium layer less than 2 nm thick. Micrographs were obtained in high vacuum-mode.

The pore size distribution, porosity (total and at P = 1 atm) and pore surface of all samples were determined by mercury porosimetry (Micromeritics Autopore IV). Samples were degassed at 50 °C for at least 24 h prior testing. Two replicates per sample were conducted. In all measurements, the contact angle at the Hg-sample interface was assumed to be 130° and a testing pressure range from 0.1 to 60,000 psia was applied. The desired values were obtained through the Washburn Equation:

$$D = \frac{-4\gamma cos\theta}{P} \tag{1}$$

where D is the pore diameter, γ is the surface tension of mercury, θ refers to the contact angle between the mercury and the pore wall, and P is the applied pressure.

SAXS measurements were performed at the X-ray facility lab, Monash University with a Bruker N8 Horizon instrument using a CuKα (λ = 1.54 Å) micro-source. The sample to detector distance was 0.6 m which covers the q range between ~0.015 to 0.3 Å^{-1}. The scattered photons from the sample were collected on a 2D Vantec-500 detector (pixel size ~70 μm × 70 μm). Final scattering curves were obtained by radial averaging of scattering images with the Bruker EVA software.

2.4. Swelling and water retention studies

The swelling capacity of the superabsorbents prepared was evaluated in deionised water. Both swelling capacity and swelling rate were measured. The swelling capacity was determined by weighing the samples before and after immersion in deionised water for at least 24 h. The swelling capacity was calculated as follows:

$$Swelling \ capacity, \ Q = \frac{m_t - m_d}{m_d} \tag{2}$$

where m_t is the weight of the swollen superabsorbent at time t and m_d refers to the weight of the dried sample.

The swelling rate was evaluated by monitoring the weight gain of the samples after immersion in water over different periods of time and expressed as Q variations. Results are reported as the average and standard deviation of triplicates.

The water retention value (WRV) of all rehydrated superabsorbents was performed in triplicates following ISO 17190-6 [30]. The set up was adapted from Qingzheng Cheng [31]. Briefly, superabsorbent samples were immersed in deionised water for at least 48 h prior to

testing. Each wet sample was placed in a polypropylene mesh placed inside empty centrifugation tubes (supplementary information, S1). Centrifugation was carried out 3 min at a relative centrifugal force (RCF) of 250 G at room temperature. After centrifugation, the "wet weight" of the samples was measured. The samples were oven dried at 105 °C until they reached constant mass. The WRV was calculated as follows:

$$WRV = \frac{m_c - m_d}{m_d} \tag{3}$$

where m_c is the weight of the wet sample after centrifugation and m_d refers to the weight of the dry sample.

2.5. Seed germination tests

The impact of the superabsorbents, freeze-dried and oven-dried 50 °C, on the germination and growth of two plant species was assessed. The species selected were radish and cress.

Superabsorbent effects on seed germination were evaluated at concentrations of 2, 5, 10 g of superabsorbent/L. The application rate was within the recommended range for commercial superabsorbents [32]. For each treatment, different amounts of the nanocellulose before drying were spread on a filter paper according to the desired concentration. The filter paper was later freeze-dried or oven-dried at 50 °C, assuring even distribution of the superabsorbent on the filter paper. Once dried, the filter paper with the superabsorbent was placed in a 90 mm Petri dish and 5 mL of deionised water was poured. After the addition of water, 10 seeds of each species were placed on the wetted filter paper. Dishes were placed at room temperature in the dark. Four replicates of each treatment and the control (0 g/L – 5 mL of deionised water – dH₂O) were performed. Seed germination, defined as the seed having a radicle length > 5 mm [33], was evaluated every 12 h over a period of 7 days. The mean time to germination (MTG) of each plant species was calculated as follows:

$$MTG = \sum \frac{n \times d}{N} \tag{4}$$

where n is the number of seeds that germinated between each time period, d is the incubation period in minutes at that point and N is the total number of seeds that germinated in the treatment.

The germination index (GI) was determined for each species over a period of 48 h using the germination percentage and the radicle length:

$$Germination \ index \ (GI\%) = \frac{G_s}{G_c} \times \frac{L_s}{L_c} \times 100 \tag{5}$$

where Gs and Gc are the number of seeds that germinated in the sample and the control and Ls and Lc are the root lengths of the sample and the control, respectively. Germination index was measured as a percentage of control.

The germination studies data was analysed statistically using a One-way ANOVA (analysis of variance) to evaluate differences between the means of the different treatments. The Dunn's test was used to determine any significant differences (p < 0.05). ANOVA and Dunn's analyses were performed using SigmaPlot 13 (Sysstat, Chicago, IL).

3. Results

3.1. Swelling behaviour

The swelling capacity of the five nanocellulose superabsorbents was measured in deionised water as a function of time (Fig. 1). In general, all superabsorbents show a similar behaviour. After an initial absorption rate, swelling levels up to reach a plateau. The time required to reach maximum capacity ranged from a couple of hours, for freeze-dried superabsorbent, to 48 h for air-dried. Lyophilised superabsorbent is characterised by an initial rapid swelling with most of it occurring
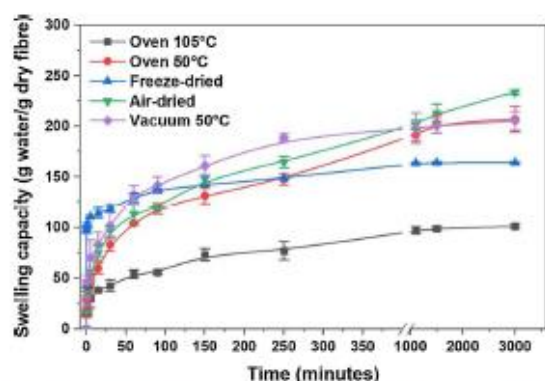
R.M. Barajas-Ledesma, et al.

Fig. 1. Swelling capacity of nanocellulose superabsorbents produced using five different drying techniques as a function of time. Results are reported as mean $\pm$ standard deviation (n = 3).

during the first minutes. These results are consistent with literature on freeze-dried nanocellulose superabsorbents [6]. For the samples dried via evaporation, the swelling rate is slower. Both freeze-dried and vacuum-dried samples reached their equilibrium capacity within 5 h whereas oven-dried samples at low and high temperature achieved equilibrium after 24 h.

The absorption capacity at equilibrium of all samples was measured over time until constant mass was observed (Fig. 1). The swelling at equilibrium is a function of the drying rate employed, dictated by the drying technique. Surprisingly, in all cases- except for oven drying at 105 °C-, drying the nanocellulose by evaporation increased its equilibrium capacity over freeze-dried superabsorbents. Air-dried superabsorbent has the highest water absorption capacity at 230 g water/g dry fibre.

The rate of water removal as a function of time was measured for all the superabsorbents (Fig. 2). A direct relationship between the absorption capacity and the drying rate is observed. Among evaporative-dried superabsorbents, air-dried superabsorbents show the slowest drying followed by oven-dried 50 °C and vacuum-dried 50 °C. Oven-dried 105 °C superabsorbents display the fastest drying rate and also the lowest swelling capacity.
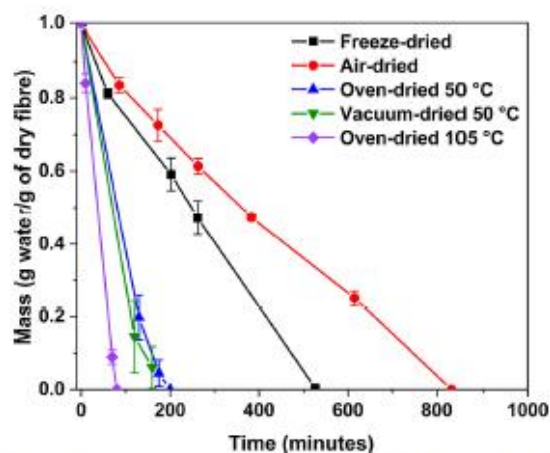
Fig. 2. Rate of water removal as a function of time of nanocellulose superabsorbents produced using five different drying techniques. Results are reported as mean $\pm$ standard deviation (n = 3).
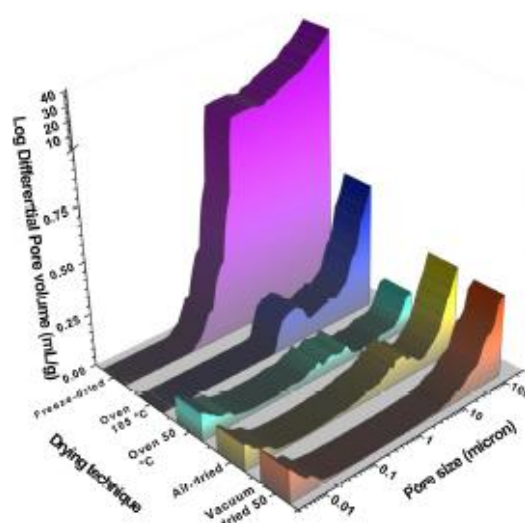
Fig. 3. Pore size distribution of nanocellulose superabsorbents using different drying techniques.

3.2. Pore size distribution

Mercury porosimetry was used to measure the pore size distribution of the nanocellulose superabsorbents prepared with the different drying techniques (Fig. 3). Pore size distribution notably changed depending on the drying mode categorized as freeze-drying or evaporative drying. Both freeze-dried superabsorbent and oven-dried 105 °C superabsorbent are characterised by a macroporous structure as defined by IUPAC [34] with no pores observed at a scale lower than 50 nm. Air-dried, oven-dried 50 °C and vacuum-dried 50°C superabsorbents all present a combination of macro, meso and micropores [34].

The relationship between bulk density, porosity, pore area (surface area) and volume of the superabsorbent is shown as a function of the drying technique in Fig. 4. Freeze-drying the nanocellulose superabsorbent produced an ultralight and highly porous material having a density lower than 170 kg/m³ and a porosity higher than 90 %. These characteristics are typical of freeze-dried superabsorbents also referred to as nanocellulose foams [20]. In all cases, evaporative drying produced porous nanocellulose superabsorbents of porosities ranging from 50 to 60 % and with densities in between 1000 and 1400 kg/m³. Vacuum-drying produced the superabsorbent of highest density (1400 kg/m³). Freeze-drying and oven-drying at 105 °C produced superabsorbents with the lowest pore area. These values were around 7 times lower than with the other drying techniques. Freeze-dried nanocellulose superabsorbents have the highest pore volume: around 20 mL/g. This value is 60 times higher than for superabsorbents prepared through evaporative-drying.

3.3. Structure

To analyse the structural morphology of the superabsorbents, scanning electron microscopy (SEM) imaging was performed (Fig. 5). The visual appearance of each superabsorbent is shown in the supplementary information, S2. The morphology of the superabsorbents strongly depends on the drying rate. At low magnification, freeze-dried superabsorbent is characterised by a sheet-like network of fibres with interconnected pores of several microns in diameter. This morphology is typical of freeze-dried materials [20,24]. In contrast, evaporative-dried superabsorbents present a transparent film-like structure with no

4
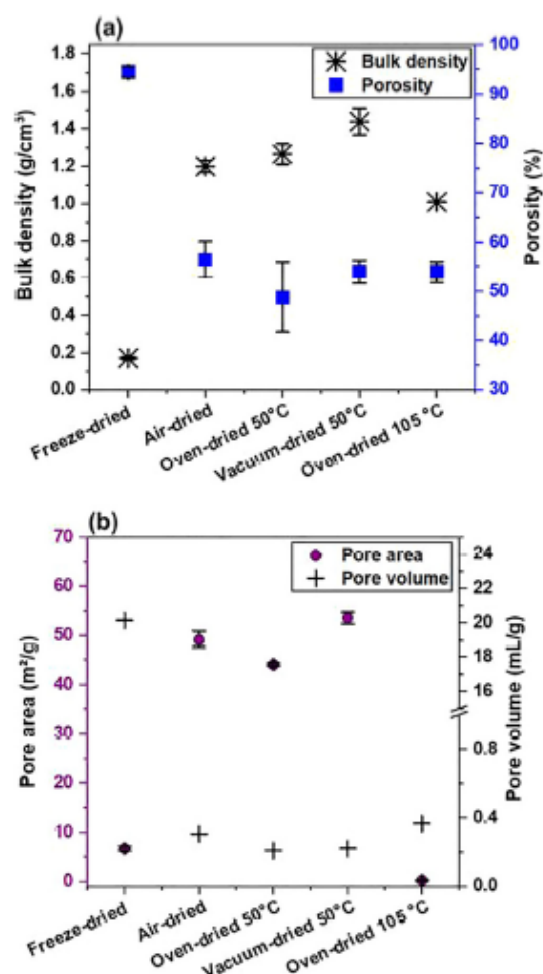
Fig. 4. (a) Porosity and bulk density of the different nanocellulose super-absorbents. (b) pore area and pore volume obtained through mercury por-osimetry. Total porosity was calculated as: Total porosity $= \left(\frac{pore\ volume}{skeletal\ volume\ +\ pore\ volume} \right) x\ 100\%.$

visible pores in the micrometre scale. For these, increasing the drying rate or temperature leads to an increase in surface roughness. Air-dried superabsorbent structure is homogeneous, soft and glassy whereas more micro-irregularities become evident as the temperature increases from 50 °C to 105 °C. These are due to fibre hornification which increases with temperature. At high magnification, freeze-dried superabsorbent forms a three-dimensional nanoporous network of fibres (Fig. 5a). The fibres are clearly visible and pore diameters range from 50 to 200 nm. The superabsorbents prepared by evaporation are characterised by two-dimensional structures of compact frames made of elemental entangled fibrils stacked on top of each other. Though the presence of small pores is observed in these cases, their diameter is difficult to measure by SEM due to the high density of fibres (Fig. 5b-d). The number of pores in oven-dried superabsorbent at 105 °C (Fig. 5e) is much lower than for the other evaporative-dried superabsorbents.

Small angle X-ray scattering (SAXS) was used to evaluate the pore structure and their distribution in the superabsorbents (Fig. 6). SAXS is a non-destructive method providing the morphology and distribution

of nanoscale structures over a complete volume [35–37]. The pore structure and distribution of the superabsorbents are dependent on the drying technique. In SAXS, superabsorbents air-dried, oven-dried 50 °C and vacuum-dried 50 °C display a uniform isotropic scattering. The pore size distribution from the SAXS curves were obtained by modelling the scattering using the sphere shape model [38] combined with the log-normal pore distribution. The pore size distribution evaluated from SAXS curve fitting is similar to the pore distributions from mercury porosimetry (Fig. 6d). However, the SAXS images of freeze-dried and oven-dried 105 °C superabsorbents show anisotropic scattering (sup-plementary information, S3) revealing the pores are not distributed in a particular direction. In both cases, the pore sizes are large and beyond the size range measurement of lab SAXS setup.

3.4. Phytotoxicity assays

To determine the effect of the superabsorbents in plants, a germi-nation experiment was conducted. Radish and cress seeds were treated with three different concentrations of 2 types of superabsorbents: freeze-dried and oven-dried 50 °C (to represent superabsorbents pro-duced via evaporation). The mean time to germination (MTG) of both species is shown in Fig. 7. There was no significant difference in the MTG between the dH_2O control (0 g/L) and the freeze-dried or oven-dried 50 °C treatments. The MTG remains constant in all cases.

The germination index (GI) was calculated by measuring the radicle length of seeds grown on the superabsorbents for 48 h (Fig. 8). Radish and cress seeds grown over freeze-dried superabsorbent show no sig-nificant difference between the dH_2O control and any of the freeze-dried concentrations. Radish seeds treated with oven-dried 50 °C su-perabsorbent exhibit an increase in GI between the concentrations of 2–5 g/L (compared with the control). In contrast, a slight decrease in GI is observed in cress seeds treated with oven-dried 50 °C superabsorbent at the highest concentration of 10 g/L.

4. Discussion

4.1. Effect of drying rate on the superabsorbent structure and swelling rate

Nanocellulose-based superabsorbents of varying structures were prepared by adjusting the drying rate controlled with the drying mode. We raise the hypothesis that the rate of water removal from the hy-drogel network controls its micro and nano structure. The effect of the structure on the swelling rate and superabsorption of nanocellulose was measured.

The structure of the superabsorbents was analysed by scanning electron microscopy (SEM), mercury porosimetry and small angle X-ray scattering (SAXS). While SEM provides three-dimensional and high-resolution images in a wide range of magnification, this technique is limited in quantifying material size and distribution [39]. Mercury porosimetry measures the pore size distribution which is used to cal-culate specific surface area and density. However, Hg porosiometry cannot quantify closed pores and measures the largest entrance of pores - not the actual inner size [40]. SAXS measurement generates the par-ticle size, distribution and shape variations [37]. The combination of these three techniques can define the superabsorbent structure both at the micro and nanoscale with certainty.

Freeze-dried superabsorbent achieved the fastest absorption rate (Fig. 1). This is due to their high porosity with the network of fibres forming pores ranging from 50 nm to 100 μm. Kuśtrowski, et al. [41] also reported similar pore properties for fast-swelling polysaccharides superabsorbents. High porosity polymeric networks allow fast water diffusion across the superabsorbent [13]. In general, superabsorbents dried by evaporation have a much slower swelling rate, with around 10 % of their capacity reached during the first minutes.

Two distinct regimes are observed in the swelling kinetics of na-nocellulose superabsorbents: (i) a steep initial uptake of water and (ii)
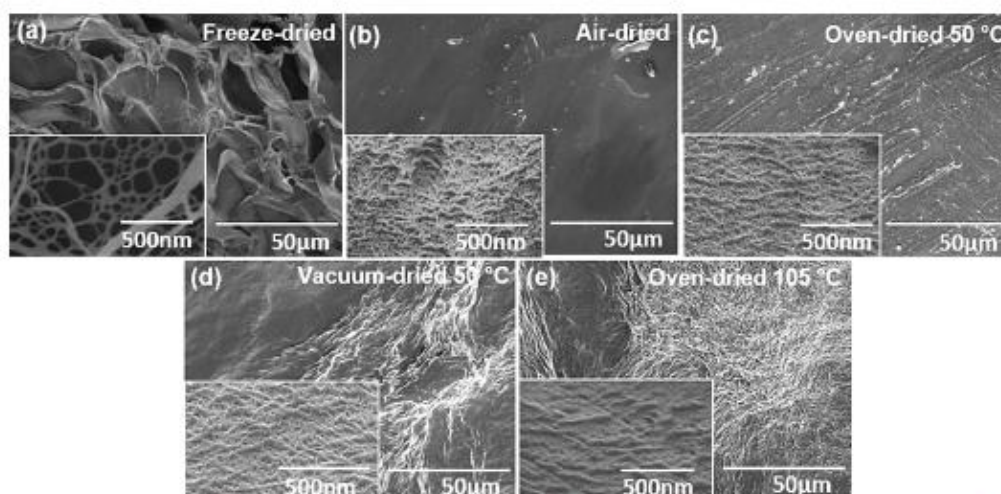
Fig. 5. SEM micrographs of the nanocellulose superabsorbent produced by changing the drying rate with the drying methods: (a) freeze-drying, (b) air-dried, (c) oven-dried at 50 °C, (d) vacuum oven-dried at 50 °C and (e) oven-dried 105 °C.
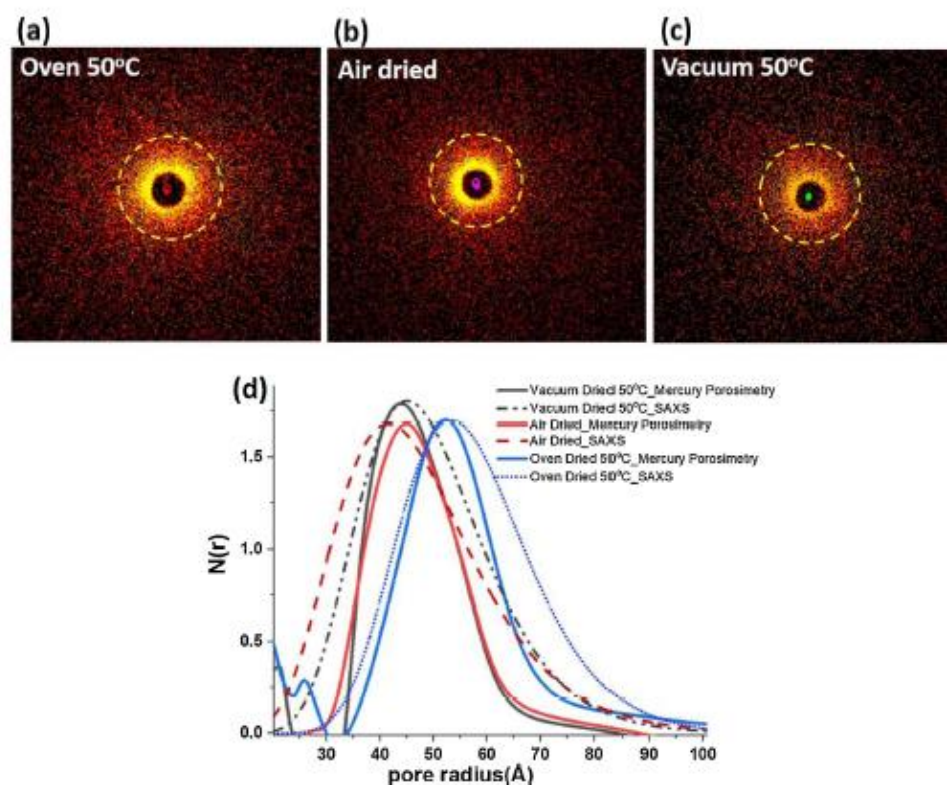
Fig. 6. Small angle X-ray scattering (SAXs) images of the nanocellulose superabsorbent produced at different drying rates: (a) air-dried, (b) oven-dried at 50 °C, (c) vacuum oven-dried at 50 °C. (d) Pore distribution of SAXs and mercury porosimetry tests. SAXS images of freeze-dried and oven-dried at 105 °C displayed in supporting information.
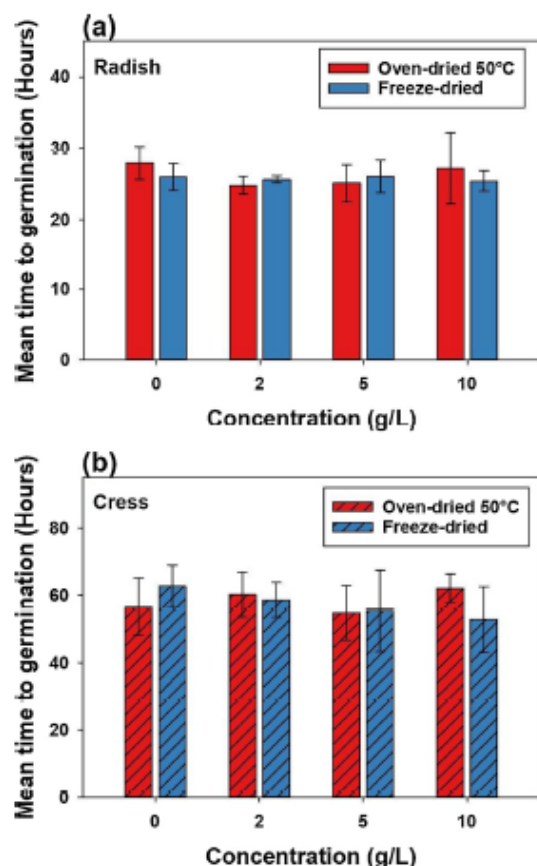
Fig. 7. Mean time to germination of (a) radish and (b) cress in the presence of increasing concentrations of two different types of superabsorbents: oven-dried 50 °C and freeze-dried. Results are reported as mean ± standard deviation (n = 4). Pictures of the phytotoxicity tests are shown in supplementary information, S4.

an asymptotical process towards the equilibrium swelling ratio. The effect of the drying technique on the swelling ratio was analysed using Schott's second-order kinetics model [42]

$$\frac{t}{Q_t} = \frac{1}{K_s Q_\infty^2} + \frac{1}{Q_\infty}t \tag{6}$$

where Q_∞ denotes the swelling capacity at equilibrium, K_s is the swelling rate constant, Q_t is the swelling capacity at time t. Because $K_{is} = K_s Q_\infty^2$, Eq. (6) can be expressed as:

$$\frac{t}{Q_t} = \frac{1}{K_{ts}} + \frac{1}{Q_\infty}t \tag{7}$$

where K_{is} refers to the initial swelling rate constant [43]. Plots of the average swelling rate (t/Q_t) versus time (t) are displayed in Fig. 9; the expected straight lines are achieved ($R^2 > 0.99$) in all cases. This confirms that the swelling process follows a second-order kinetic model. This model successfully described semicrystalline polymers such as cellulose or gelatin [6,42,43].

The swelling kinetic parameters K_s, K_{is} and Q_∞ obtained from the slopes and intercepts of the plots (Fig. 9) are listed in Table 2 . The theoretical absorption capacity at equilibrium (Q_{theo}) is similar to the experimental absorption capacity (Q_{actual}) in all cases. Both the initial

(K_{is}) and actual (K_s) swelling rate constants varied accordingly to the drying technique. K_{is} indicates the point where the buffer solution has permeated the entire film but before the polymer network stress relaxation retards swelling [42]. For freeze-dried superabsorbents, high porosity and pore size speed up the diffusion rate of water molecules into the superabsorbent, resulting in the highest K_{is}. In contrast, air-dried superabsorbents present a K_{is} around four times lower which indicates a slower diffusion rate of water molecules induced by the material porosity.

The swelling rate constant, K_s, is related to the solvent diffusion and relaxation process of the polymer chains [44]. Low values K_s suggest a rate controlled by stress relaxation in the swelling polymer network-not by diffusion-controlled swelling [42]. Air-dried superabsorbent presented the lowest K_s. The water molecules in this material diffused throughout the material during the first hour of immersion as shown by their soft and transparent appearance; however, equilibrium swelling was reached after 24 h. This indicates that the rate determining process is stress relaxation of the fibre network driven by the osmotic swelling pressure [42]. The same absorption mechanism applies to oven-dried at 50 °C and vacuum-dried at 50 °C. Freeze-dried superabsorbent reached saturation during the first minutes of experiment, suggesting a diffusion driven process. For the oven-dried superabsorbents at 105 °C, the swelling rate constant is higher than those from the other drying evaporation techniques. This indicates superabsorbent reaching saturation at a faster rate due to hornification, resulting in superabsorbents of smaller pores and inaccessible carboxylate groups, lowering swelling capacity.

4.2. Swelling capacity and water retention of nanocellulose superabsorbents

Two main variables are responsible for the superabsorption behaviour of nanocellulose. The first is porosity that enables diffusion of water molecules into the fibre network. This leads to the physical entrapment of water loosely held between nanofibres by capillary forces [6]. The second is the superabsorbent surface area. This facilitates the interaction between water and carboxylate groups (COO^-) and promotes hydrogen bonding. The fibre network expands and accommodates the influx of water through the relaxation of fibres driven by osmotic pressure [22,42]. The type of cations in the superabsorbent matrix also impacts water uptake [45]. However, only Na^+ was investigated in this study. Hence, the effects in the swelling capacity are directly related to the drying rate defining the structure of the superabsorbents.

Surprisingly, in all cases – except those dried at 105 °C – evaporative drying resulted in superabsorbents of higher swelling capacity than those produced by sublimation/freeze-drying. This contrasts from literature which reports that freeze-dried superabsorbent have higher absorption capacity than evaporative-dried superabsorbent [20,22,24,46]. This is because hornification in evaporative drying produces capillary pressure-induced stresses, shrinking pores and decreasing swelling capacity [24,25]. However, low-temperature drying and introducing anionic charges into the cellulose structure, such as carboxylate groups, minimise hornification of cellulose fibres [22,25,27]. These techniques were selected in our study.

Nevertheless, the high absorption capacity of our nanocellulose superabsorbents prepared by evaporative drying cannot be solely explained by the minimisation of hornification. Such performance is due to a combination of factors, all controlled by the drying rate. First, porosity and pore size enable physical entrapment of water into the superabsorbent network. This property is accentuated in freeze-dried superabsorbent having a porosity of > 90 %, which partly explains its absorption capacity [6]. The high absorption capacity of evaporative-dried superabsorbents is attributed largely to their high pore area higher than 45 m^2/g (Fig. 10). This increases the number of accessible COO^- groups participating in hydrogen bonding with water compared to freeze-dried superabsorbents, increasing the interaction of water

7
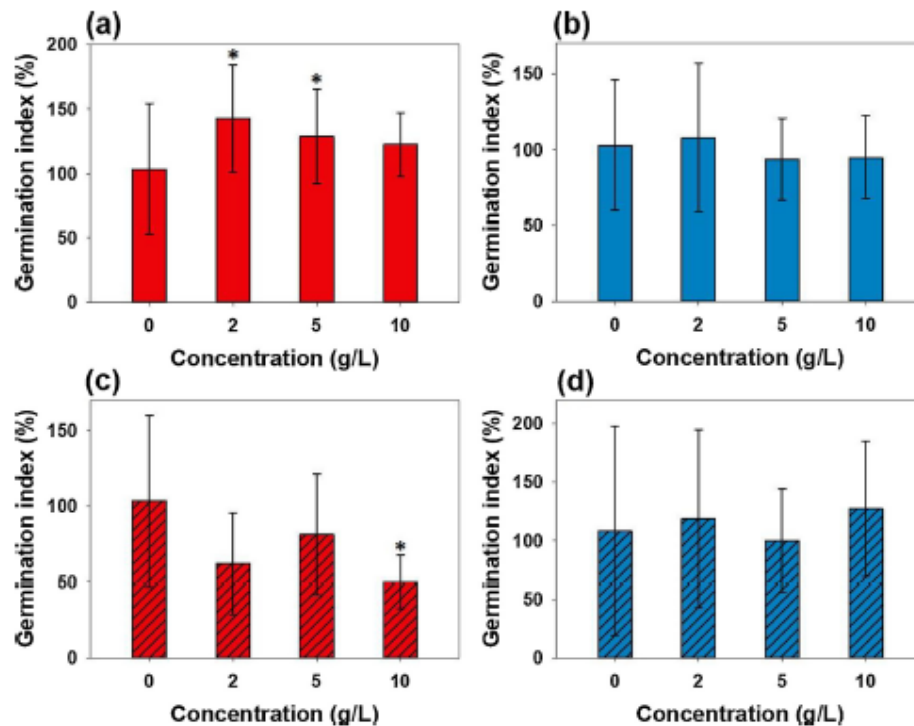
Fig. 8. Germination index of radish species treated with (a) oven-dried 50 °C and (b) freeze-dried superabsorbents, and cress species treated with (c) oven-dried 50 °C and (d) freeze-dried superabsorbents. Statistical difference according to ANOVA analysis followed by Dunn's test against 0 g/L concentration as control indicated as *P < 0.05, N = 4.
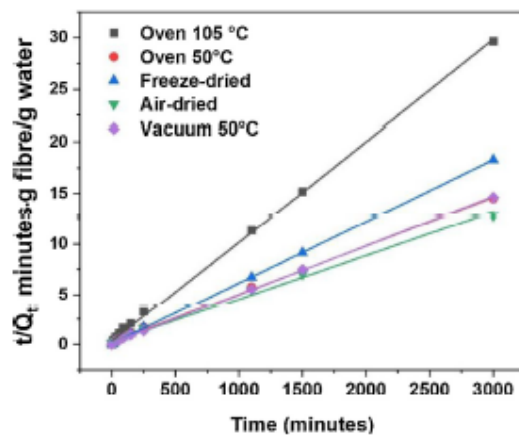
Fig. 9. Plots of t/Qt vs t according to Eq. 5 based on the experimental data displayed in Fig. 1.

Table II
Swelling kinetic parameters of the different superabsorbents.

Type	Qactual (g/g)	Qtheo (g/g)	Kis (g/g min)	Ks (10^{-5}, g/g min)
Oven-dried 105 °C	101.16	102.04	3.11	29.94
Oven-dried 50 °C	207.25	208.33	4.98	11.48
Freeze-dried	164.13	163.93	17.93	66.73
Air-dried	233.93	232.55	4.75	8.78
Vacuum 50 °C	205.43	204.08	9.95	23.91

adsorbed onto the polymer chains and swelling of the fibre network [47]. This, coupled with the pore size, lead to a stronger physical entrapment of water in between nanofibres by capillary forces.

These characteristics of evaporative-dried superabsorbents are given by rate of water removal. A relationship between this rate and the absorption capacity is observed. For these superabsorbents, Figs. 1 and 2 show that the slower the drying rate, the higher the absorption

capacity achieved. This is because slow rates lead to a more uniform arrangement of fibres, producing superabsorbents with macro, meso and micropores which results in high absorption capacity.

These hypotheses are also supported by the water retention values (WRV) shown in Fig. 10. A relationship between the pore area and the WRV is observed. Evaporative dried superabsorbents – except for those oven-dried at 105 °C – exhibit high pore area and high-water retention properties, while freeze-dried superabsorbent shows low pore area and low WRV. This is attributed to the large pore size which promotes the release of water molecules from the superabsorbent matrix.

4.3. Importance of nanocellulose superabsorbent structure in agriculture

Seed germination is one of the most important phases in the life cycle of a plant and is highly dependent on the existing environment [48]. Seed germination bioassays and early stage seedling growth studies are commonly used for determining toxicity effects in plants. In the development of novel materials as growing media, the absence of phytotoxicity is the first requirement [11]. In this study, seed
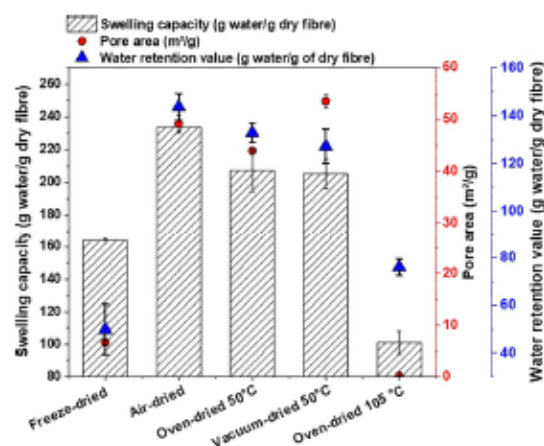
Fig. 10. Relationship between the drying technique, the swelling capacity, pore area and water retention value of nanocellulose superabsorbent.

germination and early stage seedling growth tests of radish and cress were conducted on two materials: freeze-dried and oven-dried 50 °C. The freeze-dried superabsorbent was chosen because of its difference in morphology compared to evaporative-dried superabsorbents, while oven-dried 50 °C was selected to represent superabsorbents dried via evaporation – the best condition for industrial scale production. Results show that any of the superabsorbents used in this study influenced the mean time to germination of either radish or cress seeds compared to the control (deionized water – dH_2O). This indicates that if seeds were to be grown in soil with nanocellulose superabsorbent, the time to emergence is unlikely to be affected, and hence its application in agriculture is safe for plants.

Moreover, radish seeds treated with oven-dried 50 °C exhibit an increase in the germination index by 30–40%. Such results are not observed in seeds treated with freeze-dried superabsorbent. This increase is attributed to the swelling kinetics of evaporative-dried superabsorbent being slower than freeze-dried superabsorbent, which increases the water availability at the early stage of seed germination. These positive effects confirm the results reported on superabsorbents improving seedling growth, regulating plants available water and reducing the detrimental effects produced by water stress [11,49].

5. Conclusion

A series of nanocellulose superabsorbents varying in pore properties was characterized in structure and swelling behaviour for application as hydro retentor in agriculture. Nanocellulose superabsorbent superabsorbents were prepared from TEMPO oxidized cellulose superabsorbents [6]. The structure of the nanocellulose superabsorbent was controlled with the drying rate of the superabsorbent. This was engineered with the drying process. Five methods, each providing a different rate of water removal, were studied. These include: freeze-dried, air-dried, vacuum-dried at 50 °C, and oven-dried at 50 °C and 105 °C. The effect of drying on the superabsorbent structure, swelling capacity, absorption rate, water retention and seed germination was analysed.

The structure of the nanocellulose superabsorbent, measured in terms of porosity, pore volume and area, is governed by the drying technique used. This structure directly impacts swelling capacity and kinetics. Freeze-dried superabsorbents are characterised by a three-dimensional macroporous network of fibres and pores ranging from 50 nm to 100 μm, whereas evaporative-dried superabsorbents form two-dimensional network of entangled fibrils stacked on top of each other. The high porosity and large pore size of freeze-dried

superabsorbents are responsible for their fastest absorption rate. These superabsorbents exhibit a diffusion-controlled swelling mechanism. The absorption mechanism of evaporative-dried superabsorbents is dictated by stress relaxation of the fibre network. Both mechanisms are described by a second-order kinetics model [42]. Air-dried superabsorbents have the highest swelling capacity. This is attributed to pore area and strong water bond interaction. Superabsorbents oven-dried at 105 °C have the lowest swelling capacity due to fibre hornification [25].

Seed germination of radish and cress seeds demonstrates that the nanocellulose-based superabsorbents tested in this study are suitable for agricultural use; the SAP performance was independent of the drying process. This study identified evaporative drying as the best drying technique to produce high capacity superabsorbents. This technique is far easier and cheaper than freeze-drying, decreasing production costs of nanocellulose superabsorbents.

CRediT authorship contribution statement

Ruth M. Barajas-Ledesma: Conceptualization, Validation, Methodology, Investigation, Software, Writing - original draft. **Antonio F. Patti:** Supervision, Writing - review & editing. **Vanessa N.L. Wong:** Supervision, Writing - review & editing. **Vikram Singh Raghuwanshi:** Validation, Software, Writing - review & editing. **Gil Garnier:** Visualization, Supervision, Writing - review & editing.

Declaration of Competing Interest

The authors declare that they have no known competing financial interests or personal relationships that could have appeared to influence the work reported in this paper.

Acknowledgements

Appendix A. Supplementary data

Supplementary material related to this article can be found, in the online version, at doi:https://doi.org/10.1016/j.colsurfa.2020.124943.

References

[1] J.R. Gross, The evolution of absorbent materials, in: L. Brannon-Peppas, R.S. Harland (Eds.), Studies in Polymer Science, vol. 8, Elsevier, 1990, pp. 3–22.
[2] E.M. Ahmed, Hydrogel: preparation, characterization, and applications: a review, J. Adv. Res. 6 (2) (2015) 105–121, https://doi.org/10.1016/j.jare.2013.07.006.
[3] S. Ghorbani, et al., Hydrogels based on cellulose and its derivatives: applications, synthesis, and characteristics, Polym. Sci. Ser. A 60 (6) (2019) 707–722, https://doi.org/10.1134/s0965545x18060044.
[4] X. Shen, J.L. Shamshina, P. Berton, G. Gurau, R.D. Rogers, Hydrogels based on cellulose and chitin: fabrication, properties, and applications, Green Chem. 18 (1) (2016) 53–75, https://doi.org/10.1039/C5GC02396C.
[5] R. Curvello, V.S. Raghuwanshi, G. Garnier, Engineering nanocellulose hydrogels for biomedical applications, Adv. Colloid Interface Sci. 267 (2019) 47–61, https://doi.org/10.1016/j.cis.2019.03.002.
[6] L. Mendoza, L. Hossain, E. Downey, C. Scales, W. Batchelor, G. Garnier, Carboxylated nanocellulose foams as superabsorbents, J. Colloid Interface Sci. 538 (March) (2019) 433–439, https://doi.org/10.1016/j.jcis.2018.11.112.
[7] H.M. Shewan, J.R. Stokes, Review of techniques to manufacture micro-hydrogel particles for the food industry and their applications, J. Food Eng. 119 (4) (2013) 781–792, https://doi.org/10.1016/j.jfoodeng.2013.06.046.
[8] A. Bashari, A. Rouhani Shirvan, M. Shakeri, Cellulose-based hydrogels for personal care products, Polym. Adv. Technol. 29 (12) (2018) 2853–2867, https://doi.org/10.1002/pat.4290.
[9] S. Basak, N. Nandi, S. Paul, I.W. Hamley, A. Banerjee, A tripeptide-based self-shrinking hydrogel for waste-water treatment: removal of toxic organic dyes and

lead (Pb2+) ions, Chem. Commun. 53 (43) (2017) 5910–5913, https://doi.org/10.1039/C7CC01774J.

[10] T.M. Neethu, P.K. Dubey, A.R. Kaswala, Prospects and applications of hydrogel technology in agriculture, Int. J. Curr. Microbiol. Appl. Sci. 7 (05) (2018) 3155–3162, https://doi.org/10.20546/ijcmas.2018.705.369.

[11] F.F. Montesano, A. Parente, P. Santamaria, A. Sannino, F. Serio, Biodegradable Superabsorbent Hydrogel Increases Water Retention Properties of Growing Media and Plant Growth, Agric. Agric. Sci. Procedia 4 (2015) 451–458, https://doi.org/10.1016/j.aaspro.2015.03.052.

[12] M.J. Zohuriaan-Mehr, Kourosh Kabiri, Superabsorbent polymer materials: a review, Iran. Polym. J. 17 (6) (2008) 451–477.

[13] M.R. Guilherme, et al., Superabsorbent hydrogels based on polysaccharides for application in agriculture as soil conditioner and nutrient carrier: a review, Eur. Polym. J. 72 (2015) 365–385, https://doi.org/10.1016/j.eurpolymj.2015.04.017.

[14] M.R. Guilherme, A.V. Reis, A.T. Paulino, T.A. Moia, L.H.C. Mattoso, E.B. Tambourgi, Pectin-based polymer hydrogel as a carrier for release of agricultural nutrients and removal of heavy metals from wastewater, J. Appl. Polym. Sci. (2010), https://doi.org/10.1002/app.32123 pp. n/a-n/a.

[15] J. Zhang, L. Wang, A. Wang, Preparation and swelling behavior of fast-swelling superabsorbent hydrogels based on starch-g-poly(acrylic acid-co-sodium acrylate), Macromol. Mater. Eng. 291 (6) (2006) 612–620, https://doi.org/10.1002/mame.200500387.

[16] S. Varanasi, R. He, W. Batchelor, Estimation of cellulose nanofibre aspect ratio from measurements of fibre suspension gel point, Cellulose 20 (4) (2013) 1885–1896, https://doi.org/10.1007/s10570-013-9972-9.

[17] S.M.F. Kabir, P.P. Sikdar, B. Haque, M.A.R. Bhuiyan, A. Ali, M.N. Islam, Cellulose-based hydrogel materials: chemistry, properties and their prospective applications, Prog. Biomater. 7 (September (3)) (2018) 153–174, https://doi.org/10.1007/s40204-018-0095-0.

[18] Q. Li, S. McGinnis, C. Sydnor, A. Wong, S. Renneckar, Nanocellulose Life Cycle Assessment, ACS Sustain. Chem. Eng. 1 (8) (2013) 919–928, https://doi.org/10.1021/sc4000225.

[19] A. Isogai, T. Saito, H. Fukuzumi, TEMPO-oxidized cellulose nanofibers, Nanoscale 3 (1) (2011) 71–85, https://doi.org/10.1039/C0NR00583E.

[20] N. Lavoine, L. Bergström, Nanocellulose-based foams and aerogels: processing, properties, and applications, J. Mater. Chem. A 5 (31) (2017) 16105–16117, https://doi.org/10.1039/c7ta02807e.

[21] K.J. De France, T. Hoare, E.D. Cranston, Review of Hydrogels and Aerogels Containing Nanocellulose, Chem. Mater. 29 (11) (2017) 4609–4631, https://doi.org/10.1021/acs.chemmater.7b00531.

[22] I.H. Mondal, Cellulose-Based Superabsorbent Hydrogels (Polymers and Polymeric Composites: A Reference Series), (2019).

[23] Z. Pakowski, Modern methods of drying nanomaterials, Transp. Porous Media 66 (1–2) (2006) 19–27, https://doi.org/10.1007/s11242-006-9019-x.

[24] N. Buchtová, T. Budtova, Cellulose aero-, cryo- and xerogels: towards understanding of morphology control, Cellulose 23 (August (4)) (2016) 2585–2595, https://doi.org/10.1007/s10570-016-0960-8.

[25] M. Beaumont, J. König, M. Opietnik, A. Potthast, T. Rosenau, Drying of a cellulose II gel: effect of physical modification and redispersibility in water, Cellulose 24 (3) (2017) 1199–1209, https://doi.org/10.1007/s10570-016-1166-9.

[26] N. Butchosa, Q. Zhou, Water redispersible cellulose nanofibrils adsorbed with carboxymethyl cellulose, Cellulose 21 (December (6)) (2014) 4349–4358, https://doi.org/10.1007/s10570-014-0452-7.

[27] T. Lindstrom, G. Carlsson, The effect of carboxyl groups and their ionic form during drying on the hornification of cellulose fibers, svensk papperstidning (1982) R146.

[28] S. Ang, V. Haritos, W. Batchelor, Cellulose nanofibers from recycled and virgin wood pulp: a comparative study of fiber development, Carbohydr. Polym. 234 (2020) 115900, https://doi.org/10.1016/j.carbpol.2020.115900.

[29] T. Saito, A. Isogai, TEMPO-Mediated Oxidation of Native Cellulose. The Effect of Oxidation Conditions on Chemical and Crystal Structures of the Water-Insoluble

Fractions, Biomacromolecules 5 (5) (2004) 1983–1989, https://doi.org/10.1021/bm0497769.

[30] Urine-absorbing aids for incontinence - Test methods for characterizing polymer-based absorbent materials ISO 17190-17196, Geneva, 2001.

[31] J.W. Qingzheng Cheng, Joseph F. McNeel, Peter M. Jacobson, Water retention value measurements of cellulosic materials using a centrifuge technique, BioResources 5 (3) (2010) 1945–1954.

[32] S. Karnani, Viji, Hydrogel Agriculture Technology (Accessed 06 February 2020), http://vikaspedia.in/agriculture/best-practices/sustainable-agriculture/crop-management/hydrogel-agriculture-technology.

[33] K.P. Mosse, A.F. Patti, E.W. Christen, T.R. Cavagnaro, Winery wastewater inhibits seed germination and vegetative growth of common crop species, J. Hazard. Mater. 180 (August (1–3)) (2010) 63–70, https://doi.org/10.1016/j.jhazmat.2010.02.069.

[34] IUPAC, Compendium of Chemical Terminology, 2nd ed. (the "Gold Book"), Blackwell Scientific Publications, Oxford, 1997.

[35] V.S. Raghuwanshi, et al., Cationic polyacrylamide induced nanoparticles assembly in a cellulose nanofiber network, J. Colloid Interface Sci. 529 (2018) 180–186, https://doi.org/10.1016/j.jcis.2018.06.009.

[36] V.S. Raghuwanshi, U.M. Garusinghe, J. Ilavsky, W.J. Batchelor, G. Garnier, Effect of nanoparticles size and polyelectrolyte on nanoparticles aggregation in a cellulose fibrous matrix, J. Colloid Interface Sci. 510 (2018) 190–198, https://doi.org/10.1016/j.jcis.2017.09.064.

[37] O. Glatter, O. Kratky, Small Angle X-Ray Scattering, Academic Press, London, New York, 1982.

[38] V.S. Raghuwanshi, M. Ochmann, F. Polzer, A. Hoell, K. Rademann, Self-assembly of gold nanoparticles on deep eutectic solvent (DES) surfaces, Chem. Commun. 50 (63) (2014) 8693–8696, https://doi.org/10.1039/C4CC02588A.

[39] L.C. Gomes, J.M.R. Moreira, J.M. Simões, L.F. Melo, F.J. Mergulhão, Biofilm localization in the vertical wall of shaking 96-well plates (in eng), Scientifica (Cairo) 2014 (2014) 231083, https://doi.org/10.1155/2014/231083.

[40] H. Giesche, Mercury porosimetry: a general (practical) overview, Part. Part. Syst. Charact. 23 (1) (2006) 9–19, https://doi.org/10.1002/ppsc.200601009.

[41] P. Kuśtrowski, P. Natkański, A. Rokicińska, and E. Witek, Polymer Hydrogel-Clay (Nano) Composites in Polymer Gels, (Gels Horizons: From Science to Smart Materials, 2018, Chapter 1, pp. 1–62.

[42] H. Schott, Swelling kinetics of polymers, J. Macromol. Sci. Part B- Phys. 31 (1) (2006) 1–9, https://doi.org/10.1080/00222349208215453.

[43] X. Shi, W. Wang, A. Wang, pH-responsive sodium alginate-based superporous hydrogel generated by an anionic surfactant micelle templating, Carbohydr. Polym. 94 (1) (2013) 449–455, https://doi.org/10.1016/j.carbpol.2013.01.019.

[44] F. Rosa, J. Bordado, M. Casquilho, Kinetics of water absorbency in AA/AMPS co-polymers: applications of a diffusion–relaxation model, Polymer 43 (1) (2002) 63–70, https://doi.org/10.1016/S0032-3861(01)00596-1.

[45] I. Homma, H. Fukuzumi, T. Saito, A. Isogai, Effects of carboxyl-group counter-ions on biodegradation behaviors of TEMPO-oxidized cellulose fibers and nanofibril films, Cellulose 20 (5) (2013) 2505–2515, https://doi.org/10.1007/s10570-013-0020-6.

[46] J. Nemoto, T. Soyama, T. Saito, A. Isogai, Nanoporous networks prepared by simple air drying of aqueous TEMPO-oxidized cellulose nanofibril dispersions, Biomacromolecules 13 (March (3)) (2012) 943–946, https://doi.org/10.1021/bm300041k.

[47] Z. Xia, M. Patchan, J. Maranchi, J. Elisseeff, M. Trexler, Determination of cross-linking density of hydrogels prepared from microcrystalline cellulose, J. Appl. Polym. Sci. 127 (6) (2013) 4537–4541, https://doi.org/10.1002/app.38052.

[48] A.G. Rombola, et al., Relationships between chemical characteristics and phyto-toxicity of biochar from poultry litter pyrolysis, J. Agric. Food Chem. 63 (August (30)) (2015) 6660–6667, https://doi.org/10.1021/acs.jafc.5b01540.

[49] M.K. Akhter, K.A. Malik, A. Mardan, M. Ahmad, M.M. Iqbal, Effects of hydrogel amendment on water storage of sandy loam and loam soils and seedling growth of barley, wheat and chickpea, Plant Soil Environ. 50 (10) (2004) 463–469.

10

Regular Article

Effect of the counter-ion on nanocellulose hydrogels and their superabsorbent structure and properties

Ruth M. Barajas-Ledesma [a], Laila Hossain [a], Vanessa N.L. Wong [c], Antonio F. Patti [b], Gil Garnier [a,*]

[a] Bioresource Processing Research Institute of Australia (BioPRIA) and Department of Chemical Engineering, Monash University, Clayton, VIC 3800, Australia
[b] School of Chemistry, Monash University, Clayton, VIC 3800, Australia
[c] School of Earth, Atmosphere & Environment, Monash University, Clayton, VIC 3800, Australia

GRAPHICAL ABSTRACT

ARTICLE INFO

ABSTRACT

Hypothesis: Carboxylated nanocellulose gels and superabsorbents (SAPs) can be engineered by ion exchange of TEMPO treated cellulose fibers with different cations prior to shearing, thus creating a nanofibrous network ionically cross-linked. The structure and properties of these materials are highly influenced by the type counter-ion used as it controls both the degree of fibrillation and crosslinking.

Experiments: Functionalised nanocellulose SAPs were made using TEMPO-mediated oxidation followed by ion-exchange before fibrillation into a hydrogel and freeze-drying. Seven different cations were tested: 4 of valency 1 (H, Na, K, NH_4), and 3 of valency 2 (Ca, Mg, and Zn). The effect of the counter-ion on the gelation mechanism and the superabsorbent performance was evaluated. The SAP absorption capacity in deionised water was related to the superabsorbent structure and morphology.

Findings: The gel stability of nanocellulose superabsorbents is governed by the counter-ion type and valency. The viscoelastic properties of all nanocellulose hydrogels are controlled by its elastic regime, that is storage modulus (G') > loss modulus (G''). The type of cation dictates the rheology of these gels by altering the fibrillation efficiency due to the extent of ionic cross-links occurring before and after fibrillation. The driving force for gelation in monovalent gels is due to the coupling of nanofibrils by physical interactions, creating an electrostatic stabilisation of the ionised COO^- groups at high shear forces. Cation – carboxylate interactions dominate the gelation in divalent gels by supressing the repulsive charges

generated by the COO^- and also creating interfibril connections via ionic-crosslinks, as confirmed by the zeta potentials. The superabsorption performance is dominated by the counter-ion and is in the order of: $NH_4^+ > K^+ > Na^+ > Mg^{2+} > Zn^{2+} > Ca^{2+}$. NH_4^+-SAPs present the slowest kinetics and the highest absorption capacity. Its high pore area, which extends the number of accessible carboxyl groups that participates in hydrogen bonding with water, is responsible for this behaviour. Nanocellulose SAPs are attractive renewable materials, suited for many applications, including as nutrient cation carriers in agriculture.

1. Introduction

Hydrogels are characterised by cross-linked networks of hydrophilic polymers that hold large amounts of water and remain stable [1–4]. The gelation mechanism is controlled by the density and type of cross-linking, physical or chemical. For physically cross-linked hydrogels, gelation is due to physical interacting forces such as van der Waals, hydrogen bonding, electrostatic and chain entanglements, among others [5]. Chemically cross-linked hydrogels undergo chemical reactions that covalently cross-linked the polymer network. These hydrogels are typically strong and permanent [5]. The formation of ionically-crosslinked hydrogels has been reported when metal salts are added to the polymer network, inducing gelation by screening repulsive charges [6,7].

Hydrogels can be used as superabsorbent polymers (SAPs) by removing the water of the network which, for nanocellulose, is often achieved by freeze-drying [8,9]. The resulting material from freeze-drying appears as a foamy-like structure, also referred to as nanocellulose foam or aerogel [8,10]. Their swelling is dictated by the movement of the counter-ions from outside to inside the superabsorbent, causing an osmotic pressure difference across the network [11]. These materials are found in numerous applications such as hygiene and personal care products [12], agriculture [13] and biomedicine [14]. In agriculture, SAPs can act as soil conditioners, increasing plant water availability and soil water retention [15,16], and as slow release fertilisers or nutrient carriers [16].

The majority of the available superabsorbents are fossil fuel derived polymers which degrade slowly and raise health and environmental concerns due to the formation of microplastic particles that can be harmful to soil biota [17–19]. These environmental issues have driven the development of superabsorbents from natural polymers, especially those made of starch [20], pectin [21], alginate [22], or cellulose [23,24]. From these, cellulose, the most abundant carbohydrate and biopolymer on earth, is often preferred as source material due its biodegradability, availability and hydrophilicity [16,25]. Cellulose-based SAPs can be produced through the 2,2,6,6-tetramethylpiperidine-1-oxyl (TEMPO)-mediated oxidation of cellulose followed by (freeze)drying. This process converts the primary alcohol groups of cellulose into sodium carboxylate groups [26], and adds the required electrostatic repulsion which forms nanocellulose hydrogels upon mechanical fibrillation. Nanocellulose-based SAPs are regarded as highly-porous materials with high swelling and water retention properties [8,27].

The sodium ions present in the polymer matrix is not desirable for agricultural related applications of nanocellulose superabsorbents. Adding sodium to soils will have an adverse effect on soil structure, oxygen and water availability and can impose a stress on growing crops, resulting in a decrease of yields or crop failure [28]. The exchange of the counter-ion with others can tailor this material not only as a superabsorbent, but also as a nutrient carrier for plants. Literature suggests that the cation can significantly influence the properties of cellulose-based materials. Homma, Fukuzumi, Saito and Isogai [29] found that the biodegradation rate of TEMPO-oxidised nanofibril films is greatly influenced by the

counter-ion; Na^+ are reported to have the fastest rate and Cu^{2+} the lowest. Dong, Snyder, Williams and Andzelm [6] revealed that the storage modulus (G') of cellulose nanofibril hydrogels increase with increasing valency of the metal cation and are strongly associated to the binding energy of the COO^- groups with the nanofibers. Yang, Xu and Han [7] showed that cellulose nanofibers (CNF) covalently cross-linked with polyacrylamide (PAAm) can be reinforced with multivalent cations to create hydrogels of high stiffness and toughness. The addition of these ionic-links between the metal cation and CNF improves hardness and elasticity by 600% compared to pristine gels.

Ionically cross-linked nanocellulose hydrogels can be prepared by subjecting the TEMPO-oxidised nanocellulose to an aqueous salt solution before or after fibrillation, with most of the studies using the latter. This technique consists on adding the salt solution dropwise to a dispersion of TEMPO-oxidised cellulose nanofibers, without stirring, which are left standing overnight [6,7,30,31]. This process selectively substitutes the sodium ions present in the dispersion with another ion of stronger affinity. However, this technique is not only slow – which can sometimes take up to 5 days [30]- but also challenging to scale up, thus limiting the application range.

While several studies investigated the effect that different metal cations have on the gelation of nanocellulose-based hydrogels, none have studied the effect of the different cations on the viscoelastic properties of nanocellulose hydrogels nor associated those to the superabsorption performance. Similarly, while some studies suggested that the addition of salt solution after fibrillation results in the formation of heterogenous clumps and the loss of the gel structure [32], the effect of the cation on the fibrillation efficiency upon homogenisation is unknown.

Here, TEMPO mediated oxidation was used to prepare carboxylated nanocellulose hydrogels. The oxidised fibres were subjected to an acid wash with HCl to remove all Na^+ cations present, followed by fibre re-suspension in different salt solutions, homogenisation and freeze-drying. The fibrillation efficiency, hydrogel rheology and SAP structure and swelling properties were measured. This study innovates by the technique used to prepare ionically cross-linked SAPs. The addition of these cations can not only assist in the transition of the superabsorbent as a hydro-retentor material to a nutrient carrier material for applications in sustainable agriculture, but also help in understanding the behaviour of superabsorbent in soils where there is a natural mixture of exchangeable cations, including Ca^{2+}, Mg^{2+} and K^+.

2. Materials and methods

2.1. Materials

Bleached Eucalyptus Kraft (BEK) pulp was provided by Australian Paper, Maryvale, Australia with a chemical composition of cellulose (78.8% ± 0.8), hemicellulose (17.7% ± 0.4), lignin (3.2% ± 0.1), extractives (0.3% ± 0.1) and ash (0.2% ± 0.1) [33]. Sodium hypochlorite (NaClO) at 12% w/v was purchased from Thermo Fisher Scientific and used as received. 2,2,6,6-Tetramethylpiperi

dine-1-oxyl (TEMPO) and Sodium bromide (NaBr) were purchased from Sigma-Aldrich. Sodium hydroxide (NaOH) and hydrochloric acid (HCl) were purchased from ACL Laboratories and Merck, respectively, and diluted for solutions as needed. Zinc sulfate monohydrate (ZnSO$_4$·H$_2$O), sodium sulfate anhydrous (Na$_2$SO$_4$), ammonium sulfate ((NH$_4$)$_2$SO$_4$) and potassium sulfate (K$_2$SO$_4$) were purchased from Sigma-Aldrich. Calcium sulfate hemihydrate (CaSO$_4$·½H$_2$O) and Copper (II) sulfate pentahydrate (CuSO$_4$·5H$_2$O) were purchased from Westlab. Magnesium sulfate anhydrous (MgSO$_4$) was purchased from Merck. 70% Nitric acid (HNO$_3$) was purchased from Ajax Finechem.

2.2. Synthesis of carboxylated cellulose

The oxidation process was based on a previously developed method [26]. In brief, 25 g of BEK pulp (dry basis) was dispersed in 2500 mL of water with 2.5 g and 0.4 g of dissolved sodium bromide and TEMPO, respectively. Prior to the oxidation process, the sodium hypochlorite at 12% w/v was adjusted to pH 10 through the addition of hydrochloric acid at 36% w/v. To achieve a carboxylate content of 1.4 mmol/g of dry fibre, 100 mL of sodium hypochlorite was added drop-wise to the suspension whilst stirring. The pH of the reaction was maintained at 10 by adding 0.5 M NaOH. The reaction was complete when the change in pH was negligible. The oxidised cellulose was washed with deionised water, filtrated and stored refrigerated at 4 °C until required. The sodium carboxylate content of the TEMPO oxidised cellulose was 1.4 mmol/g dry fibre and was measured by conductivity titration [34].

2.3. Ion exchange treatment of carboxylated cellulose

The ion exchange treatment employed was based on a previously reported method [29]. 1 g of the TEMPO-oxidised fibres, containing sodium carboxylate groups, was suspended in 1 L of 0.01 M HCl and stirred for 1 h. The oxidised cellulose pulp was later washed with Milli-Q water and filtrated. The oxidised pulp with protonated carboxyl groups was then re-suspended in 1 L of salt solution and stirred for 3 h at room temperature. The number of moles of salt dissolved in the suspension was fixed to be 10 times as much as the calculated carboxylate groups present in the oxidised cellulose. After 3 h, the salt treated cellulose fibres were washed with Milli-Q water, filtrated and stored refrigerated at 4 °C until required. The following solutions were used for the ion-exchange treatment: hydrochloric acid (HCl), sodium sulfate (Na$_2$SO$_4$), zinc sulfate (ZnSO$_4$), potassium sulfate (K$_2$SO$_4$), ammonium sulfate ((NH$_4$)$_2$SO$_4$), copper (II) sulfate pentahydrate (CuSO$_4$), calcium sulfate (CaSO$_4$), magnesium sulfate (MgSO$_4$). Sulfate anion salts were selected to negate the effect of the anion and for its suitability for agriculture.

2.4. Preparation of nanocellulose hydrogel and superabsorbent

To prepare the nanocellulose hydrogel, the TEMPO-oxidised fibres treated with the various counter-ions were suspended in Milli-Q water to achieve a concentration of solids of 0.5% w/v and fibrillated through high pressure homogenisation (GEA Niro Soavi Homogeniser Panda) at 800 bar and two passes. To produce the nanocellulose superabsorbent, the resulting hydrogel from homogenisation was stored for at least 12 h at −80 °C and freeze-dried for 48 h using a Christ Alpha 2–4 LD Plus.

2.5. Characterisation

Freeze-dried nanocellulose SAP was characterised using a Fourier Transform Infrared (FTIR) spectrometer (Agilent Technologies Cary 630 FTIR).

The counter-ion content in nanocellulose hydrogels was analysed by either elemental analysis (HCNS) using a Perkin Elmer 2400 Series II analyser, for NH$_4^+$ and H$^+$ gels, or by inductively coupled plasma – optical emission spectrometry (ICP-OES), for all other ions. For ICP-OES analysis, 3 g of nanocellulose hydrogel was placed in crucibles and ashed using a muffle furnace, based on a previously reported method [35]. Temperature ramped to 600 °C over 3 h and kept for a further 3 h. The metal residues left in the crucible were dissolved using 1 mL of 70% HNO$_3$ and diluted with Milli-Q water to achieve a total volume of 15 mL. The dissolved metals were then analysed by ICP-OES using a Perkin-Elmer Avio 200. Each sample was analysed in triplicate.

The zeta potential of the nanocellulose hydrogels was measured following the method described by Mendoza, Hossain, Browne, Raghuwanshi, Simon and Garnier [36]. Briefly, 1 mL of each salt treated gel was diluted to a concentration 0.01% and sonicated using an ultrasonic homogeniser at 70% amplitude (ON/OFF, 5 s) and 19.5 kHz for 2 min. Large cellulose fibres were removed by centrifugation for 5 min at 4400 rpm. The zeta potential was measured using a Brookhaven Nanobrook Omni. Each sample was analysed 5 times.

The viscoelastic properties of nanocellulose hydrogels were evaluated using a rheometer (Anton Paar MCR302) at 25 °C. A cone (0.997°) and plate (49.975 mm) geometry was selected for Na$^+$, K$^+$ and NH$_4^+$ and a cup and bob for H$^+$, Mg^{2+}, Ca^{2+} and Zn^{2+} ions. During the measurements, a solvent trap was employed to maintain a constant temperature. The amplitude sweep was varied from 0.01 to 100% at a constant frequency of 1 Hz.

The morphology of the SAPs was observed using scanning electron microscopy (SEM) (FEI Magellan 400). Nanocellulose foams were placed on a metal stub and coated with an Iridium layer of less than 2 nm thick.

The porosity, pore size distribution and pore properties of all SAPs were measured by mercury porosimetry (Micromeritics Autopore IV). Samples were degassed at 50 °C for at least 24 h prior testing and analysed in triplicates. The testing pressure ranged from 0.1 to 60,000 psia was applied.

The swelling or absorption capacity of nanocellulose SAPs was quantified in Milli-Q water. The swelling rate and absorption were measured by weighing the samples before and after immersion in water over different periods of time (1, 5, 15, 30, 60, 90, and 150 min) at room temperature. The following equation was used to determine the swelling capacity:

$$Swelling\ capacity, Q = \frac{m_t - m_d}{m_d} \qquad (1)$$

where m_t refers to the weight of the swollen gel at time t and m_d is the weight of the dried sample.

3. Results

TEMPO oxidised BEK pulp, which had a carboxylate content of 1.4 mmol/g dry fibre and was washed with acid, was first dispersed into different salt solutions of varying valency and cation type and then homogenised under high shear forces, thus forming hydrogels. These hydrogels were characterised in chemical structure and ion content. Rheology was used to evaluate the cross-linking density and fibrillation efficiency. Hydrogels were then lyophilised and the aerogels produced were analysed for morphology, pore size distribution and swelling in water.

3.1. Ion exchange of carboxyl-group counter-ions

The FT-IR spectra and the zeta potential of the hydrogels prepared with the various counter-ions is displayed in Fig. 1a and b, respectively. The presence of a band at 1720 cm^{-1} for the H$^+$-hydrogel indicates the conversion of the Na$^+$ carboxylate groups from the TEMPO-mediated oxidation to carboxylic acid groups using the acid treatment (Fig. 1a). All samples with monovalent ions (Na$^+$, K$^+$ and NH$_4^+$) and divalent ions (Mg^{2+}, Ca^{2+} and Zn^{2+}) show a sharp peak at 1600 cm^{-1}, distinctive of the C=O stretching groups, which confirms the presence of the carboxylate functional group which will be associated with the respective counter-ions. Interestingly, the zeta potential of the nanocellulose hydrogels decreased with increasing ion valency. Monovalent hydrogels have a zeta potential ranging from −80 mV to −74 mV; for divalent, it ranges from −50 to −35 mV. Ca^{2+}-hydrogels have the lowest surface charge of all samples (Fig. 1b). The difference between and among the valencies is significant, as previously reported [37].

The degree of counter-ion exchange from the protonated carboxyl group to other cations was evaluated through ICP-OES analysis (Fig. 2). NH$_4^+$ ions were determined by HCNS analysis, also shown in Fig. 2. Except for Zn^{2+}-gels, the measured counter-ion content of all ions is similar to that calculated by stoichiometry – 1.4 and 0.7 mmol/g dry fibre for mono and divalent cation gels, respectively. This confirms the complete conversion of the protonated carboxyl groups to their respective carboxylate salt. Samples with divalent ions formed cationic carboxylate groups with 1:2 (cation-COO) molar ratio, corresponding to (COO)$_2$-cation structures ionically cross-linked. The increase in the measured counter-ion content of Zn^{2+}-gels higher than the calculated value can be attributed to an excess of salt solution that was not completely removed upon washing.

3.2. Viscoelastic properties

The effect of the counter-ions on the gelation properties of the nanocellulose hydrogels was measured by rheology. The viscosity curves of all gels are presented in Fig. 3a. In general, increasing shear rate decreases viscosity. This is known as a shear-thinning behaviour and is common in nanocellulose gels [38,39]. Gels with divalent ions have lower shear viscosity than those with monovalent ions.
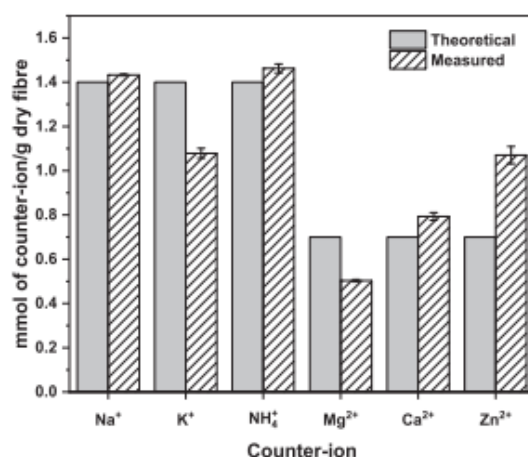
Fig. 2. Counter-ion content of the TEMPO-oxidised nanocellulose sheared after the ion exchange treatment. Measurements are determined from ICP-OES and HCNS analysis. Results are reported as mean ± standard deviation (n = 3).

The storage modulus or solid-like behaviour (G') and the loss modulus or liquid-like behaviour (G") were evaluated as a function of shear strain in oscillatory flow mode (Fig. 3d-e). The viscoelastic properties of the nanocellulose gels is governed by the elastic regime in all cases, noted by a higher G' than G" over the strain range. The storage modulus of the gels decreases with increasing ion valency. Monovalent gels, except those with H$^+$ ion, exhibit an elastic modulus an order of magnitude higher than all divalent ions providing an indication of fibre crosslinking in between the gel matrix [7]. Gel stiffness, described by the G' values (Fig. 3b), is in the order of NH$_4^+$ ≫ Na$^+$ > K$^+$ > Mg^{2+} > Zn^{2+} > Ca^{2+} > H$^+$. Similarly, gel relaxation, described by G" values (Fig. 3c), is in the decreasing order of NH$_4^+$ ≫ Na$^+$ > K$^+$ > Mg^{2+} > Ca^{2+} − Zn^{2+} > H$^+$. The linear viscoelastic region (LVR) changes for both curves, G' and G", depending on the valency and type of counter-ion. Both hydrogels display a similar LVR regime that drops at a shear strain of 10%. Finally, the difference between the G' and the G" values for monovalent gels is an order of magnitude higher than for divalent
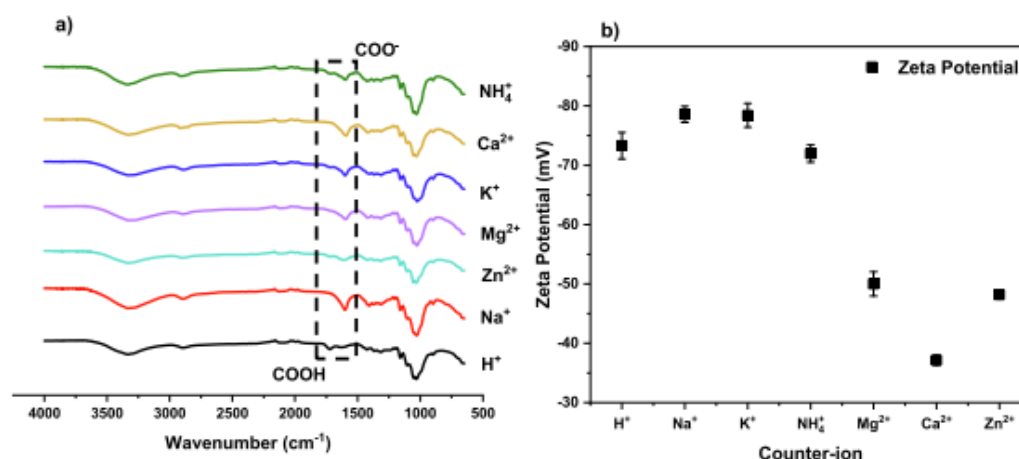

Fig. 1. (a) FT-IR spectra and (b) zeta potential of TEMPO-oxidised nanocellulose pretreated with different counter-ions. The dashed line highlights the absorption bands for COO− and COOH groups. Results are reported as mean ± standard deviation (n = 3).
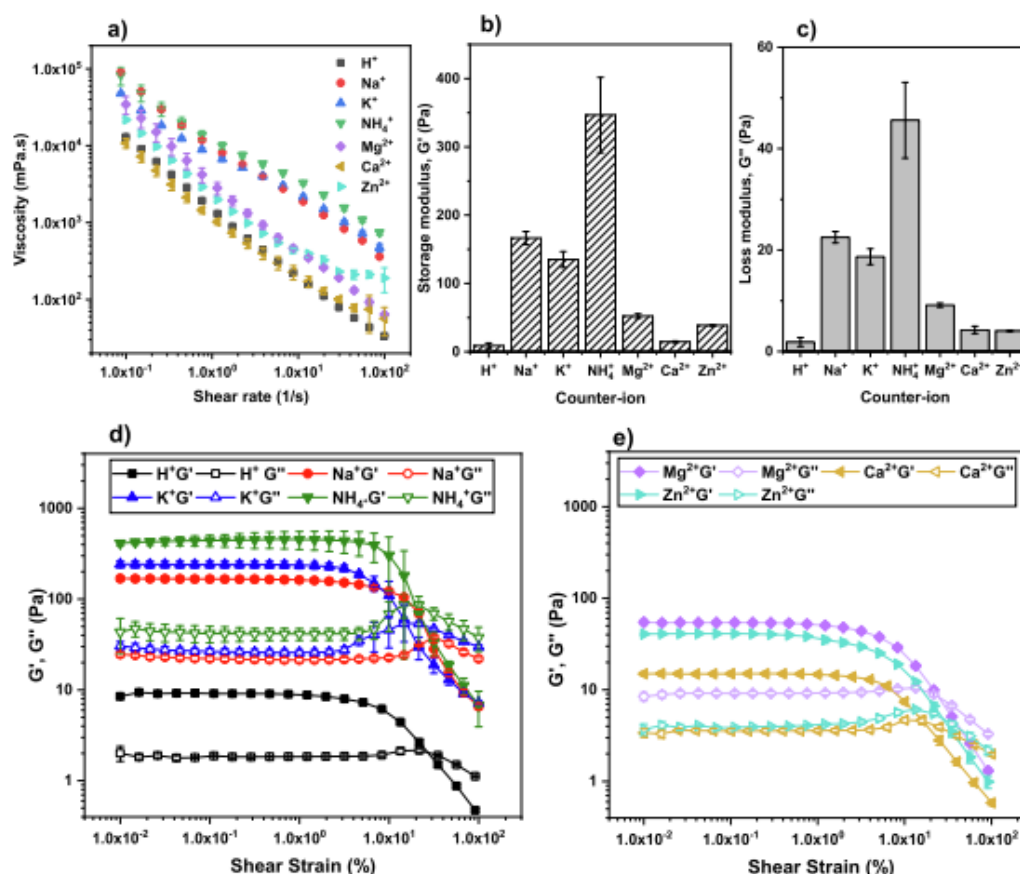
Fig. 3. Rheological properties of TEMPO-oxidised nanocellulose sheared with different counter-ions: (a) viscosity curves, (b) nanocellulose gel stiffness and (c) relaxation represented by the storage modulus (G') and the loss modulus (G"), storage (G') and loss (G") modulus of (d) monovalent and (e) divalent ions. Results are reported as mean ± standard deviation (n = 3).

gels. This suggests that monovalent gels are mostly dominated by the elastic character, whereas divalent and H⁺ gels are dictated by both the elastic and the viscous behaviour in the same proportion.

3.3. Morphology

Nanocellulose-based aerogels were prepared by freeze-drying. SEM imaging was employed to analyse the morphology (Fig. 4). The internal structure strongly depends on the counter-ion present in the superabsorbent. Though all treatments produced SAPs with very porous structures, the pore shape, size and fibre arrangement differ. Monovalent ions form SAPs characterised by an entanglement of fibres which results in open and porous three-dimensional assemblies (Fig. 4a-d). Fibres are clearly visible, forming foam structures with pore diameters ranging from 10 to 300 nm. In contrast, superabsorbents with divalent ions are characterised by a more homogeneous and organised structure. Pores are detected, but the cellulose fibres are still connected to each other, not entangled (Fig. 4e-g). Pore diameters range between 30 and 200 nm.

3.4. Pore size

The pore size distribution of the nanocellulose superabsorbents was evaluated using mercury porosimetry (Fig. 5a). Pore size dis-

tribution is controlled by the counter-ion present in the SAP. Apart from NH_4^+, all monovalent and divalent ions form SAP with a micro-porous structure. No visible pores are noted at a scale lower than 2 μm. Superabsorbents made with NH_4^+ counter-ion display a combination of micro, meso and macropores of size ranging from 5 nm to up to 100 μm, classified by IUPAC [40].

The pore properties of the superabsorbents is expressed as a function of the counter-ion (Fig. 5a-c). NH_4^+-based superabsorbents exhibit the highest pore area, more than 15 times higher than any of the other SAPs. It also has the smallest pore diameter, in the range of 2–5 nm, which is about 6 times smaller than for the other materials. Apart from this, there are no other major difference observed in the SAPs prepared with the other monovalent and divalent ions. The pore volume is slightly smaller for superabsorbents with monovalent ions than for divalent ions, ranging from 25–30 mL/g and 32–37 mL/g, respectively. The porosity of all the SAPs is in between 90 and 94%, which is typical of freeze-dried superabsorbents [8].

3.5. Swelling

The degree of swelling of the nanocellulose SAPs was quantified in Milli-Q water and evaluated as over time (Fig. 6). All superabsorbents perform similarly, with swelling uptake reaching a plateau after an initial absorption rate. Apart from NH_4^+,

144

Fig. 4. SEM images of the nanocellulose superabsorbent made from freeze-drying nanocellulose hydrogels of TEMPO-treated cellulose sheared with different counter-ions: (a) H$^+$, (b) Na$^+$, (c) K$^+$, (d) NH$_4^+$, (e) Mg^{2+}, (f) Ca^{2+} and (g) Zn^{2+}.
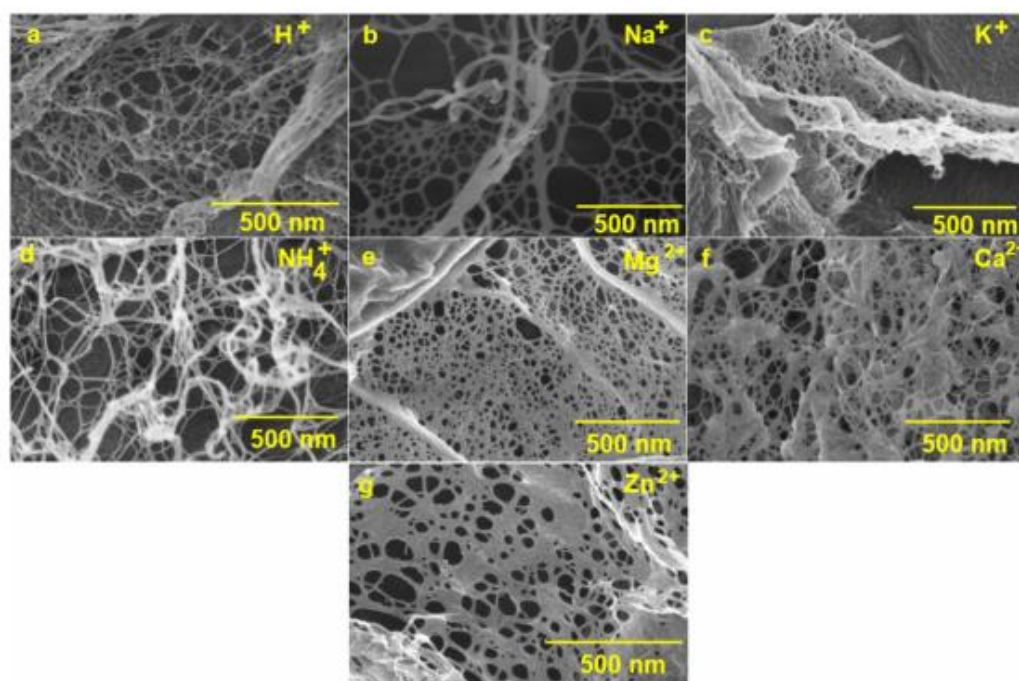
superabsorbents show an initial rapid swelling, achieving equilibrium as soon as they are immersed in water. SAP with NH$_4^+$ counter-ion is characterised a slow swelling rate.

The type of counter-ion dictates the SAP swelling at equilibrium (Fig. 7). Ammonium-based SAP achieves the highest swelling capacity of approximately 130 g water/g dry fibre. This is followed by the other monovalent ions, K$^+$ and Na$^+$, in order, respectively. SAPs with valency two ions report a lower swelling capacity, with Ca^{2+} being the lowest of all.

4. Discussion

TEMPO-mediated oxidation is the most commonly used method to produce nanocellulose hydrogels. This introduces sodium carboxylates at the C6 glycosidic position which contributes to the liberation of cellulose fibres upon homogenisation. However, the presence of sodium counter-ions may limit the application range of this material. This study evaluated the effects that different counter-ions have on the properties of both nanocellulose hydrogels and superabsorbents via ion exchange treatment prior fibrillation.

The FT-IR spectra analysis confirms the evidence of the carboxylate groups balanced by different cations or protonated carboxyl groups. This is noted by the presence of their characteristic peak of metal carboxylate group at −1600 cm^{-1}. However, the intensity of this peak is lower for hydrogels with Zn^{2+} and NH$_4^+$ ions. In these cases, the FT-IR spectra also show a small peak at −1720 cm^{-1} which corresponds to protonated carboxyl groups. This suggests that not all the carboxyl groups were converted to the corresponding metal carboxylate group [29,41]. This is because of the pH of

ZnSO$_4$ and NH$_4$SO$_4$ solutions being 4.8 and 5.5 respectively, which promotes the partial formation of free carboxylic acid.

Except for Zn^{2+}-gels, the addition of multivalent ions forms cation carboxylate groups with molar ratios of 1:1 and 1:2 for monovalent cations (NH$_4^+$, H$^+$, Na$^+$, K$^+$) and divalent cations (Zn^{2+}, Ca^{2+}, Mg^{2+}), respectively. Divalent cations have a higher solvation volume and binding energy than monovalent cations which allows interfibril interactions, leading to ionic cross-linking between multiple fibres [6]. These ionic links generate strong interactions with numerous carboxylate groups, bridging cellulose nanofibers by attractive forces that screen the electrostatic repulsion between neighbouring nanofibres [7]. This screening effect governs the gel stability and increases with increasing concentration and counter-ion valency [42]. This is confirmed with the surface charge of the hydrogels, being almost half that of monovalent gels, indicating the formation of significant cohesive interactions between nanofibrils due to the strength of these interfibril connections [6]. The surface charge, measured by zeta potential, is related to the physical stability of these gels by electrostatic repulsion of individual fibres. Values higher than +/−30 mV can develop enough repulsive force to reach good colloidal stability. On the other hand, smaller values can lead to flocculation and particle aggregation [43]. In this case, the low zeta potential values of divalent gels, with Ca^{2+}-gels being close to the threshold of agglomeration, led to a decrease in the degree of nanofibrillation, exhibited by the substantial fibril aggregation observed in the nanocellulose dispersion after fibrillation and in the morphology of the aerogels upon drying (Fig. 4) [36]. Fibril aggregation was also observed in gels with H$^+$ ions. In this case, gel stability is governed by the protonated carboxyl groups which decrease the electrostatic repulsion and surface charge, allowing the fibres to come closer as the van
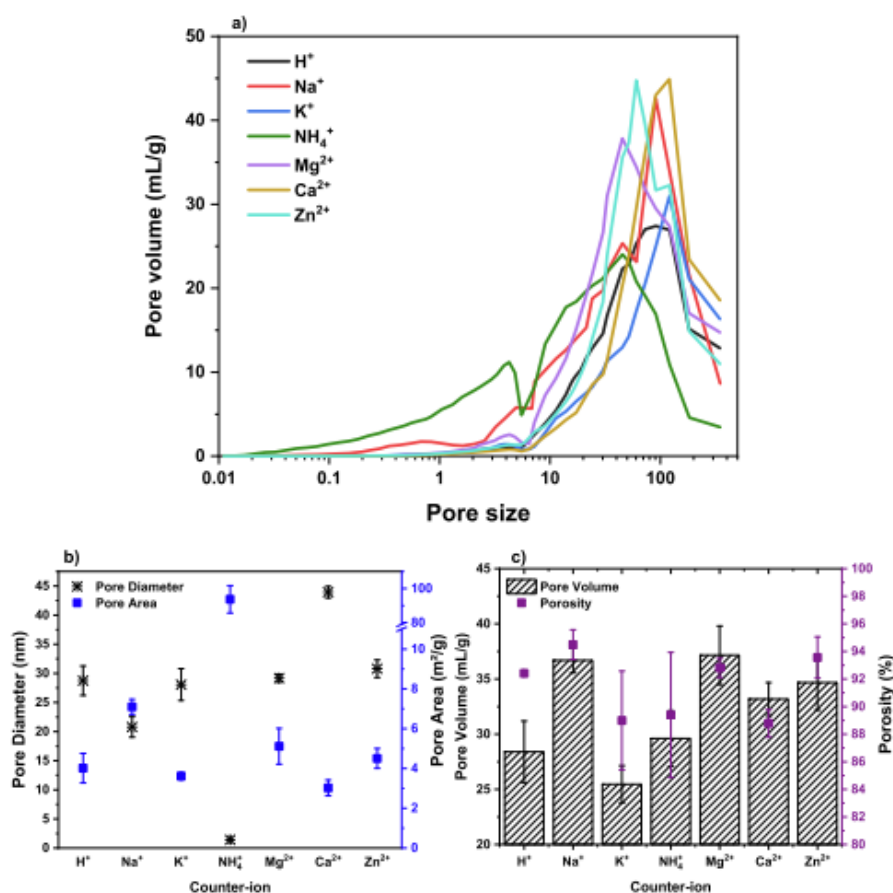
Fig. 5. Pore properties of the nanocellulose superabsorbents with different counter-ions: (a) pore size distribution (b) pore diameter and pore area, and (c) porosity and pore volume. Results are reported as mean +/− standard deviation (n = 3).
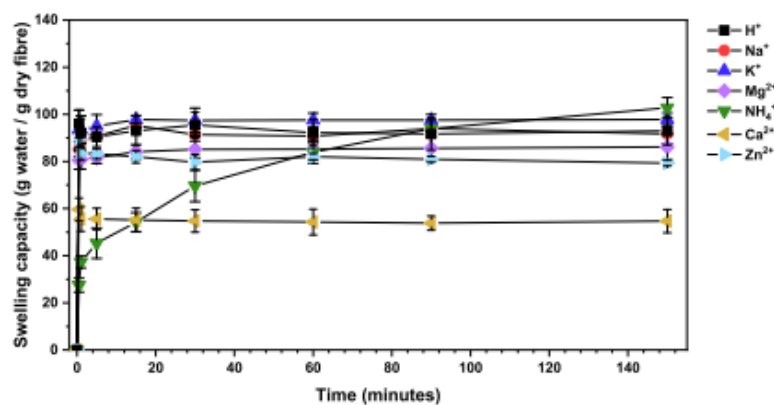
Fig. 6. Effect of the counter-ion on the degree of swelling of nanocellulose superabsorbents over time. Results are reported as mean ± standard deviation (n = 3).

der Waals forces become dominant, resulting in a decrease in the degree of fibrillation [32,44]. In contrast, monovalent ionic gels lack the interfibril cross-linking interactions as observed with the viscoelastic properties. Thus, the driving force for gelation is due to the coupling of nanofibrils by physical interactions that creates an electrostatic stabilisation of the ionised COO⁻ groups when high
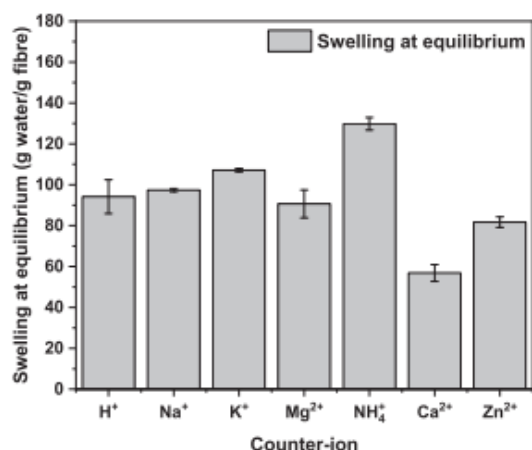
Fig. 7. Effect of the counter-ion on the swelling capacity of nanocellulose superabsorbents at equilibrium. Results are reported as mean +/- standard deviation (n = 3).

shear forces are applied to the oxidised fibres [6,32], forming stronger and more stable materials.

The type of counter-ion governs the superabsorption performance. The interaction of the counter-ion with the cellulose nanofibers can be explained by two main variables. For monovalent ions, the swelling at equilibrium follows the Hofmeister effect. This effect relates the behaviour of hydrophilic colloids in the presence of salts and is attributed to the size and hydration of ions [45]. According to the Hofmeister effect, stability of hydrophilic particles follows the indirect series as: $NH_4^+ > K^+ > Na^+$. Where ions on the left will adsorb more strongly to a hydrophilic substrate [45]. This cation specificity coincides with the measured values of swelling capacity and is attributed to negative volume exclusion entropy generated by the cation hydration. This results in an increase of the strength of the electrostatic repulsive forces which increases the entanglement of nanocellulose fibres [46,47]. Thus, increasing the absorption capacity due to the increase in hydrogen bonding between the COO^- available to interact with water [48] and also contributing to the swelling of the fibre network [10].

These repulsive forces are screened in the presence of divalent cations, as van der Waals forces become dominant and strong cation-carboxylate bonds are created [6]. Cellulose nanofibers come closer, decreasing the fibre ability to entangle upon fibrillation and thus, decreasing the swelling capacity. In this case, swelling is mainly attributed to the available pore volume, where swelling increases with increasing pore volume and decreases in the order of $Mg^{2+} > Zn^{2+} > Ca^{2+}$. This difference in pore volume depending on the counter-ion can be associated to the cation radii, where the increment in ionic radii of valency two cations results in a decrease in swelling (Mg^{2+} (72 pm) < Ca^{2+} (100 pm)) [49].

Lastly, of all the cations studied, NH_4^+ produced gels and superabsorbents with remarkable properties: high gel stiffness and stability, high SAP pore area and swelling, and slow swelling kinetics. Such performance is attributed to the unique ability of the ammonium cation to rotate [50]. This ability creates additional hydrogen bonds between the water molecules and the nanofiber network, resulting in a higher fibrillation efficiency upon homogenisation. This increase in fibre entanglement is observed in the small pore size and wide pore distribution of this SAP (Fig. 4d, 5a and 5b), increasing the pore area by an order of magnitude. This expands the number of available carboxyl groups able to participate with hydrogen bonding, resulting in a high gel stiffness. This also

increases the swelling of the nanofibre network and the amount of water adsorbed to the polymer chains, responsible for the high swelling of this superabsorbent [51].

5. Conclusion

A number of nanocellulose hydrogels varying in the extent of cellulose fiberization and ion cross-linking was prepared and freeze-dried into superabsorbents (SAP). Gel and SAP were characterized in terms of rheology, aerogel structure, gelation mechanism and swelling behaviour. Carboxylated nanocellulose was prepared from TEMPO oxidized cellulose followed by ion exchange in a series of salt solutions prior to high shear homogenization into a gel [10]. Seven cations were ion exchanged to the COO^- groups. These are: H^+, Na^+, K^+, NH_4^+, Ca^{2+}, Mg^{2+} and Zn^{2+}; the anion was sulfate. The effect of the cation on the gelation properties and mechanism, superabsorbent structure, swelling capacity and absorption rate was analysed.

FT-IR and ICP-OES analyses confirm the formation of metal carboxylate groups with 1:1 (metal-COO) molar ratio for monovalent cations and 1:2 M ratio for divalent cations, which corresponds to $(COO)_2$-metal structures ionically cross-linked. The gel stability of the nanocellulose is governed by the valency and the type of cation. Gelation in monovalent gels is due to the coupling of nanofibrils by physical interactions which creates an electrostatic stabilisation of the ionised carboxyl groups during the high shear forces of homogenizing [6,32]. In contrast, for divalent gels, the driving force for gelation is due to strong interfibril connections via ionic-crosslinks which screen the repulsive forces between carboxylate groups, enabling fibres to associate together. The type of ion and their interaction with the COO^- groups determine the efficiency of fibrillation during homogenization, which affects the structure of the hydrogels and aerogels made of those. This aerogel structure directly impacts swelling capacity and kinetics. Swelling at equilibrium is in order of: $NH_4^+ > K^+ > Na^+ > Mg^{2+} > Zn^{2+} > Ca^{2+}$. The swelling capacity of monovalent SAPs follows the Hofmeister effect and is related to the size and hydration of ions. For divalent SAPs, absorption is caused by their difference in pore volume given by the ionic radii. The remarkable properties of NH_4^+ gel and SAP, compared to the other cations, are attributed to the ability of the ammonium cation to rotate, which increases the number of available carboxyl groups that engage in hydrogen bonding, resulting in an increase in pore area, gel stiffness and SAP swelling [51].

This study not only demonstrates the potential of nanocellulose-based SAPs with different cations to suit a range of applications but also innovates on the preparation method, that is by performing ion exchange before fibrillation -and not after- resulting in a cheaper and faster process than the conventional treatment. The addition of these cations can assist in the transition of the superabsorbent as a hydro-retentor to a nutrient carrier material, increasing the benefits of this material for agricultural and food use.

CRediT authorship contribution statement

Ruth M. Barajas-Ledesma: Conceptualization, Visualization, Methodology, Investigation, Software, Writing - original draft. **Laila Hossain:** Methodology, Software, Formal analysis, Writing - review & editing. **Vanessa N.L. Wong:** Supervision, Writing - review & editing. **Antonio F. Patti:** Supervision, Writing - review & editing. **Gil Garnier:** Visualization, Supervision, Writing - review & editing.

Declaration of Competing Interest

The authors declare that they have no known competing financial interests or personal relationships that could have appeared to influence the work reported in this paper.

Acknowledgement

References

[1] E.M. Ahmed, Hydrogel: preparation, characterization, and applications: a review, J. Adv. Res. 6 (2) (2015) 105–121.

[2] S. Ghorbani, H. Eyni, S.R. Bazaz, H. Nazari, L.S. Asl, H. Zaferani, V. Kiani, A.A. Mehrizi, M. Soleimani, Hydrogels based on cellulose and its derivatives: applications, synthesis, and characteristics, Polym. Sci., Ser. A 60 (6) (2019) 707–722.

[3] X. Shen, J.L. Shamshina, P. Berton, G. Gurau, R.D. Rogers, Hydrogels based on cellulose and chitin: fabrication, properties, and applications, Green Chem. 18 (1) (2016) 53–75.

[4] J.R. Gross, The Evolution of Absorbent Materials, in: L. Brannon-Peppas, R.S. Harland (Eds.), Studies in Polymer Science, Elsevier, 1990, pp. 3–22.

[5] R. Curvello, V.S. Raghuwanshi, G. Garnier, Engineering nanocellulose hydrogels for biomedical applications, Adv. Colloid Interface Sci. 267 (2019) 47–61.

[6] H. Dong, J.F. Snyder, K.S. Williams, J.W. Andzelm, Cation-induced hydrogels of cellulose nanofibrils with tunable moduli, Biomacromolecules 14 (9) (2013) 3338–3345.

[7] J. Yang, F. Xu, C.-R. Han, Metal ion mediated cellulose nanofibrils transient network in covalently cross-linked hydrogels: mechanistic insight into morphology and dynamics, Biomacromolecules 18 (3) (2017) 1019–1028.

[8] N. Lavoine, L. Bergström, Nanocellulose-based foams and aerogels: processing, properties, and applications, J. Mater. Chem. A 5 (31) (2017) 16105–16117.

[9] K.J. De France, T. Hoare, E.D. Cranston, Review of hydrogels and aerogels containing nanocellulose, Chem. Mater. 29 (11) (2017) 4609–4631.

[10] L. Mendoza, L. Hossain, E. Downey, C. Scales, W. Batchelor, G. Garnier, Carboxylated nanocellulose foams as superabsorbents, J. Colloid Interface Sci. 538 (2019) 433–439.

[11] J. Grignon, A.M. Scallan, Effect of pH and neutral salts upon the swelling of cellulose gels, J. Appl. Polym. Sci. 25 (12) (1980) 2829–2843.

[12] A. Bashari, A. Rouhani Shirvan, M. Shakeri, Cellulose-based hydrogels for personal care products, Polym. Adv. Technol. 29 (12) (2018) 2853–2867.

[13] T.M. Neethu, P.K. Dubey, A.R. Kaswala, Prospects and applications of hydrogel technology in agriculture, Int. J. Curr. Microbiol. Appl. Sci. 7 (05) (2018) 3155–3162.

[14] R. Curvello, G. Garnier, Cationic cross-linked nanocellulose-based matrices for the growth and recovery of intestinal organoids, Biomacromolecules 22 (2) (2021) 701–709.

[15] M.J. Zohuriaan-Mehr, K. Kabiri, Superabsorbent polymer materials: a review, Iran. Polym. J. 17 (6) (2008) 451–477.

[16] M.R. Guilherme, F.A. Aouada, A.R. Fajardo, A.F. Martins, A.T. Paulino, M.F.T. Davi, A.F. Rubira, E.C. Muniz, Superabsorbent hydrogels based on polysaccharides for application in agriculture as soil conditioner and nutrient carrier: a review, Eur. Polym. J. 72 (2015) 365–385.

[17] Z. Steinmetz, C. Wollmann, M. Schaefer, C. Buchmann, J. David, J. Tröger, K. Muñoz, O. Frör, G.E. Schaumann, Plastic mulching in agriculture. Trading short-term agronomic benefits for long-term soil degradation?, Sci Total Environ. 550 (2016) 690–705.

[18] A.A. Horton, A. Walton, D.J. Spurgeon, E. Lahive, C. Svendsen, Microplastics in freshwater and terrestrial environments: evaluating the current understanding to identify the knowledge gaps and future research priorities, Sci. Total Environ. 586 (2017) 127–141.

[19] L. Ramos, G. Berenstein, E.A. Hughes, A. Zalts, J.M. Montserrat, Polyethylene film incorporation into the horticultural soil of small periurban production units in Argentina, Sci. Total Environ. 523 (2015) 74–81.

[20] P. Chen, W.A. Zhang, W. Luo, Y.e. Fang, Synthesis of superabsorbent polymers by irradiation and their applications in agriculture, J. Appl. Polym. Sci. 93(4) (2004) 1748-1755.

[21] M.R. Guilherme, A.V. Reis, A.T. Paulino, T.A. Moia, L.H.C. Mattoso, E.B. Tambourgi, Pectin-based polymer hydrogel as a carrier for release of agricultural nutrients and removal of heavy metals from wastewater, J. Appl. Polym. Sci. (2010) n/a-n/a.

[22] X. Shi, W. Wang, A. Wang, pH-responsive sodium alginate-based superporous hydrogel generated by an anionic surfactant micelle templating, Carbohydr. Polym. 94 (1) (2013) 449–455.

[23] A. Sannino, C. Demitri, M. Madaghiele, Biodegradable cellulose-based hydrogels: design and applications, Materials 2 (2) (2009) 353–373.

[24] J. De Guzman, K. Dela Peña, J. Ytac Dorothy, T. Tumolva, Synthesis and characterization of ionically-crosslinked κ-carrageenan/sodium alginate/carboxymethyl cellulose hydrogel blends for soil water retention and fertilizer release, Solid State Phenom. 304 (2020) 59–65.

[25] S. Varanasi, R. He, W. Batchelor, Estimation of cellulose nanofibre aspect ratio from measurements of fibre suspension gel point, Cellulose 20 (4) (2013) 1885–1896.

[26] A. Isogai, T. Saito, H. Fukuzumi, TEMPO-oxidized cellulose nanofibers, Nanoscale 3 (1) (2011) 71–85.

[27] Z. Pakowski, Modern methods of drying nanomaterials, Transp. Porous Media 66 (1–2) (2006) 19–27.

[28] E. Bresler, Saline and Sodic Soils Principles-Dynamics-Modeling, 1st ed, Berlin, Heidelberg : Springer Berlin Heidelberg : Imprint: Springer, 1982.

[29] I. Homma, H. Fukuzumi, T. Saito, A. Isogai, Effects of carboxyl-group counter-ions on biodegradation behaviors of TEMPO-oxidized cellulose fibers and nanofibril films, Cellulose 20 (5) (2013) 2505–2515.

[30] H. Dong, J.F. Snyder, D.T. Tran, J.L. Leadore, Hydrogel, aerogel and film of cellulose nanofibrils functionalized with silver nanoparticles, Carbohydr. Polym. 95 (2) (2013) 760–767.

[31] M. Chau, S.E. Sriskandha, D. Pichugin, H. Thérien-Aubin, D. Nykypanchuk, G. Chauve, M. Méthot, J. Bouchard, O. Gang, E. Kumacheva, Ion-mediated gelation of aqueous suspensions of cellulose nanocrystals, Biomacromolecules 16 (8) (2015) 2455–2462.

[32] L. Mendoza, W. Batchelor, R.F. Tabor, G. Garnier, Gelation mechanism of cellulose nanofibre gels: a colloids and interfacial perspective, J. Colloid Interface Sci. 509 (2018) 39–46.

[33] S. Ang, V. Haritos, W. Batchelor, Cellulose nanofibers from recycled and virgin wood pulp: a comparative study of fiber development, Carbohydr. Polym. 234 (2020) 115900.

[34] T. Saito, A. Isogai, TEMPO-mediated oxidation of native cellulose. The effect of oxidation conditions on chemical and crystal structures of the water-insoluble fractions, Biomacromolecules 5 (5) (2004) 1983–1989.

[35] M. Maliha, M. Herdman, R. Brammananth, M. McDonald, R. Coppel, M. Werrett, P. Andrews, W. Batchelor, Bismuth phosphinate incorporated nanocellulose sheets with antimicrobial and barrier properties for packaging applications, J. Cleaner Prod. 246 (2020) 119016.

[36] D.J. Mendoza, L. Hossain, C. Browne, V.S. Raghuwanshi, G.P. Simon, G. Garnier, Controlling the transparency and rheology of nanocellulose gels with the extent of carboxylation, Carbohydr. Polym. 245 (2020) 116566.

[37] R. Prathapan, R. Thapa, G. Garnier, R.F. Tabor, Modulating the zeta potential of cellulose nanocrystals using salts and surfactants, Colloids Surf., A 509 (2016) 11–18.

[38] I. Besbes, S. Alila, S. Boufi, Nanofibrillated cellulose from TEMPO-oxidized eucalyptus fibres: effect of the carboxyl content, Carbohydr. Polym. 84 (3) (2011) 975–983.

[39] O. Nechyporchuk, M.N. Belgacem, F. Pignon, Current progress in rheology of cellulose nanofibril suspensions, Biomacromolecules 17 (7) (2016) 2311–2320.

[40] IUPAC, Compendium of Chemical Terminology, second ed. (the "Gold Book"), Blackwell Scientific Publications, Oxford, 1997.

[41] T. Saito, T. Uematsu, S. Kimura, T. Enomae, A. Isogai, Self-aligned integration of native cellulose nanofibrils towards producing diverse bulk materials, Soft Matter 7 (19) (2011) 8804–8809.

[42] J.N. Israelachvili, Intermolecular and surface forces, third ed., Academic Press, Burlington, Massachusetts, 2011.

[43] E. Joseph, G. Singhvi, Chapter 4 - multifunctional nanocrystals for cancer therapy: a potential nanocarrier, in: A.M. Grumezescu (Ed.), Nanomaterials for Drug Delivery and Therapy, William Andrew Publishing, 2019, pp. 91–116.

[44] A.B. Fall, S.B. Lindström, O. Sundman, L. Ödberg, L. Wågberg, Colloidal stability of aqueous nanofibrillated cellulose dispersions, Langmuir 27 (18) (2011) 11332–11338.

[45] T. Oncsik, G. Trefalt, M. Borkovec, I. Szilagyi, Specific ion effects on particle aggregation induced by monovalent salts within the hofmeister series, Langmuir 31 (13) (2015) 3799–3807.

[46] H. Huang, E. Ruckenstein, Effect of hydration of ions on double-layer repulsion and the hofmeister series, J. Phys. Chem. Lett. 4 (21) (2013) 3725–3727.

[47] E. Ruckenstein, H. Huang, Specific ion effects on double layer forces through ion hydration, Colloids Surf., A 459 (2014) 151–156.

[48] R.M. Barajas-Ledesma, A.F. Patti, V.N.L. Wong, V.S. Raghuwanshi, G. Garnier, Engineering nanocellulose superabsorbent structure by controlling the drying rate, Colloids Surf., A 600 (2020) 124943.

[49] R.D. Shannon, Revised effective ionic radii and systematic studies of interatomic distances in halides and chalcogenides, Acta Crystallogr. Sect. A 32 (5) (1976) 751–767.

[50] J. Guo, L. Zhou, A. Zen, A. Michaelides, X. Wu, E. Wang, L. Xu, J. Chen, Hydration of NH4+ in water: bifurcated hydrogen bonding structures and fast rotational dynamics, Phys. Rev. Lett. 125 (10) (2020) 106001.

[51] Z. Xia, M. Patchan, J. Maranchi, J. Elisseeff, M. Trexler, Determination of crosslinking density of hydrogels prepared from microcrystalline cellulose, J. Appl. Polym. Sci. 127 (6) (2013) 4537–4541.

APPENDIX III:
CO-AUTHORED PUBLICATIONS NOT INCLUDED IN THE THESIS

THIS PAGE HAS BEEN INTENTIONALLY LEFT BLANK

Engineering laminated paper for SARS-CoV-2 medical gowns

Laila Hossain [a,b,1], Maisha Maliha [a,b,1], Ruth Barajas-Ledesma [a,b,1], Jinhee Kim [b], Kevin Putera [b], Dinesh Subedi [c], Joanne Tanner [a,b], Jeremy J. Barr [c], Mark M. Banaszak Holl [b], Gil Garnier [a,b,*]

[a] Bioresource Processing Research Institute of Australia (BioPRIA), Australia
[b] Department of Chemical Engineering, Monash University, VIC, 3800, Australia
[c] School of Biological Sciences, Monash University, VIC, 3800, Australia

ARTICLE INFO

ABSTRACT

The COVID-19 pandemic has highlighted the need for diversity in the market and alternative materials for personal protective equipment (PPE). Paper has high coatability for tunable barrier performance, and an agile production process, making it a potential substitute for polyolefin-derived PPE materials. Bleached and newsprint papers were laminated with polyethylene (PE) coatings of different thicknesses, and characterised for their potential use as medical gowns for healthcare workers and COVID-19 patients. Thicker PE lamination improved coating homogeneity and water vapour resistance. 49 GSM bleached paper with 16 GSM PE coating showed high tensile and seam strength, and low water vapour transmission rate (WVTR). Phi-X174 bacteriophage testing revealed that paper laminated with 15 GSM coating hinders virus penetration. This research demonstrates that PE laminated paper is a promising material for low cost viral protective gowns.

1. Introduction

In March 2020, the World Health Organisation declared the outbreak of COVID-19 to be a global pandemic. The highly infectious nature of the virus SARS-CoV-2, which causes COVID-19, has made the prevention of person-to-person transmission a critical mechanism to halt the spread of the disease. The use of personal protective equipment (PPE) is therefore vitally important [1]. Without appropriate protection from exposure to the SARS-CoV-2 virus, front-line health care workers are at great personal risk, and represent a critical transmission link to other patients and their families [2]. The rapid spread of COVID-19 and the consequential increase in demand for PPE has resulted in significant worldwide PPE shortages, including medical gowns.

Medical gowns are designed to prevent the transmission of pathogens to the wearer from an infected patient's body fluids [3,4]. These have been shown to be superior to apron-style coverings in the reduction of contamination from splashes [5,6]. According to the American Food, Drug and Cosmetic act [7], PPE used in healthcare facilities is considered to be a medical device. PPE is categorised as either a Class I (low to moderate risk) or Class II (moderate to high risk) device by the USFDA [8]. Medical gowns are classified as Class II medical devices, for which regulatory standards must be met for commercialisation [9]. According to the AAMI PB70 standard, the four tests required for the barrier performance of medical gowns are water, hydrostatic pressure, blood penetration and virus penetration resistance [10]. Based on their performance in these tests, medical gowns are categorised from level 1 (low protection) to level 4 (high protection) [11].

In the absence of genuine and appropriate PPE, many workers have been forced to adopt makeshift solutions, such as wearing plastic garbage bags as gowns, which do not meet any of the above standards [12]. Public Health England sought to mitigate the shortage of appropriate PPE by allowing the use of reusable laboratory coats and patient gowns made of washable, woven fabrics as alternatives to disposable, non-woven gowns [13]. Many PPE manufacturers have increased or introduced the production of reusable gowns to meet the increasing demand [14–16]. However, some products only meet level 2 [17] or level 3 [18] regulatory requirements. Granzow [19] demonstrated that reusable woven fabric gowns have a lower resistance to microorganism and liquid penetration than disposable non-woven polypropylene gowns, which achieve the best liquid penetration resistance.

The global pandemic, spike in demand, and shortage of traditional PPE materials suitable for viral transmission protection has driven biopolymer researchers, virologists, and biomedical experts to collaborate and explore low cost alternative materials for medical gowns and

other PPE [20]. Laminated paper is a non-woven material with significant potential for use as medical gowns. The inherent properties, ubiquitous availability, low cost, and agile paper production and lamination processes make this material widely available, suitable to address the health-care criteria, and able to adapt to rapid changes in demand during a pandemic event or other emergency that results in critical PPE shortage situations. Laminated paper materials are attracting attention for their physical properties, as well as their renewability and biodegradability in many industries including packaging [21–23], superabsorbents [24–27], membranes [28,29] and biomedical [30–32]. However, the use of paper-based protective apparel has not yet been reported.

This study presents engineered and optimised laminated paper composite materials for medical gowns. Paper as the base material provides the mechanical strength, and a thin laminated coating of polyethylene acts as a barrier to increase the level of viral protection of the gowns. The effects of basis weight, laminate thickness, and combinations thereof on the composite performance were determined. The mechanical and barrier properties, viral protection, and liquid resistance of the composites were quantified. The ease of gown manufacture and performance with respect to the regulatory requirements for Level 4 medical gowns were critically evaluated. Finally, bespoke prototypes were designed and manufactured from the optimised laminated paper material, and feedback from health-care workers was sought to demonstrate the application.

2. Methodology

2.1. Materials

Polyethylene was provided by Qenos Pty Ltd. Machine glazed bleached eucalyptus paper and newsprint paper were provided by Opal, Maryvale, VIC, Australia (formerly known as Australian Paper) and Norske Skog Boyer, Australia, respectively. Anhydrous calcium chloride was purchased from Sigma Aldrich. The surfactant polysorbate 80 was purchased from Sigma-Aldrich, Australia. Whatman filter paper 602H was obtained from Bio-Strategy Pty limited Australia.

2.2. Preparation of laminated paper

The base sheets were coated on one or two sides with a blend of low density polyethylene (LDPE) and linear low-density polyethylene (LLDPE), referred to simply as polyethylene (PE) in this paper. Paper samples were coated at Opal Specialty Paper, VIC, Australia (formerly known as Orora) by extrusion coating. In this process, polyethylene is melted at high temperature (300 °C to 320 °C) and pressure, extruded through a slit die and laminated onto a paper substrate at high temperature through a nip roll assembly. The nip roll assembly consists of a rubber-covered pressure roll and water-cooled chill roll. The paper is fed from the rubber-covered pressure roll into the nip where lamination is achieved by pressing the polyethylene and paper layer together. The formed laminate is rapidly cooled down by water-cooled chill roll (15 °C to 30 °C) and collected by a wind-up mechanism. The sample description and composition is given in Table 1.

2.3. Sample thickness

The thickness of the material was measured using the L&W Micrometer (model no. 222). The sample thickness was calculated as the average of 5 random points for 5 replicates.

2.4. Coating defect analysis

2.4.1. Fluorescence and optical imaging
Fluorescence staining was employed to detect defects in the PE coating, followed by optical microscopy in transmission and reflectance

Table 1
Description and composition of laminated paper materials examined in this study.

Sample code	Sample Details	
	Base sheet	Laminate
N42/10	Newsprint 42 GSM	Polyethylene 10 GSM
N51/10	Newsprint 51 GSM	Polyethylene 10 GSM
B44/0	Bleached 44 GSM	–
B44/6	Bleached 44 GSM	Polyethylene 6 GSM
B44/10	Bleached 44 GSM	Polyethylene 10 GSM
B44/15	Bleached 44 GSM	Polyethylene 15 GSM
B49/0	Bleached 49 GSM	–
B49/16	Bleached 49 GSM	Polyethylene 16 GSM
15/B49/16	Bleached 49 GSM	Double side coated with Polyethylene 15 GSM and 16 GSM

mode to visualise the overall coating morphology. In theory, the fluorescence dye should stain defects on PE coating if the nature of the defect is a hole in the coating that exposes the underlying paper. Diluted propidium iodide (PI) solution was prepared by mixing 20 μL of stock solution (10 mM) with 80 μL of deionised water, then passing through a 0.2 μm syringe filter before spraying the solution onto the coated side(s) of the sample. PI droplets on the coated surface were dried by wicking with a delicate task wipe (Kimwipe), and the surface was rinsed with deionised water to remove any residue on the coated surface before a final drying with Kimwipe. Fluorescence images of the pinhole structures were taken with the PE coated side up using a Nikon upright microscope (model DS-Ri2) employing a TRITC filter (Ex 540/24, DM 565, BA 605/55) with 10x objective lens. The entire surface was scanned before capturing images of the location(s) with the largest observed pinholes. Pinhole defects appeared as red spots on the sample during fluorescence imaging. Pinholes were not always visible in the optical images. Transmission (brightfield) and reflectance images were captured sequentially at the same location using the same microscope. Reflectance images were captured with a coloured filter to enhance contrast. A fine tipped marker was used to circle the pinhole location on the PE coating to direct the subsequent acquisition of topography and chemical composition information with AFM-IR.

2.4.2. Atomic force microscopy – infrared spectroscopy (AFM-IR)
The AFM-IR data were collected with a Bruker NanoIR3 system. AFM images of pinholes identified during fluorescence and optical imaging were captured areas of 3 × 3 μm to 30 × 30 μm at 0.7 Hz line scan rate with 100–200 pixel density on each edge using contact mode probes (Model: PR-EX-nIR2-10). Two to four height images were stitched together depending on the defect size in order to visualise the defect topography. Four IR spectra within the range 790–1850 cm^{-1} were taken at locations of interest with 18.74% laser power, 2.9% duty cycle, and 2429 pt IR focus spot. The resonant frequency of the tip was tuned to around 265 kHz. IR imaging was performed with IR peaks unique to PE and cellulose – 1464 cm^{-1} and 1062 cm^{-1}, attributed to CH$_2$ wag and C–O stretch, respectively – to acquire IR maps of the PE-to-cellulose ratio on the coated surface.

2.5. Mechanical properties

2.5.1. Tensile strength
Bare and laminated paper samples were tested for tensile strength in accordance with the TAPPI T402 standard using an Instron tensile tester

(model 5965). The samples were cut into 50 mm wide strips by laser cutter and tested at a constant strain rate of 10 mm/min. Five replicates were measured in each direction (machine direction: MD and cross direction: CD). Geometric mean tensile (GMT) was calculated by the square root of the product of the MD tensile load and CD tensile load at break.

$$GMT = \sqrt{(\text{Tensile load at MD} \times \text{Tensile load at CD})}$$

2.5.2. Tear strength

Tear strength was measured following ASTM D5587-15. Rectangular samples of dimension 150 mm by 75 mm were cut by laser cutter (Epilog Laser). Following the standard, an isosceles trapezoid template of 25 mm by 102 mm was drawn for each sample. A preliminary cut 15 mm long was made at the centre of the 25 mm edge. Samples were tested using an Instron tensile tester (model 5965) at a constant strain rate of 300 mm/min. Five replicates were measured for each direction (machine direction: MD and cross direction: CD) and the arithmetic mean value is reported.

2.5.3. Seam strength

Seam strength was measured following ASTM D751-19. Rectangular samples with a dimension of 50 mm by 203 mm were cut by laser cutter (Epilog Laser). The sample was folded in half with the fold parallel to the short direction of the sample. The fold was sewn in a seam (stitch type: 301) approximately 100 mm from one end using a Janome N190 sewing machine with polyester thread (Gutermann 274 yds/vgs) and a denim needle (denim needle 16; 15 × 1DE). The fold was cut after seaming, and the samples unfolded at the seam or strength testing using an Instron tensile tester (model 5965) at a constant strain rate of 300 mm/min. Five replicates were measured for each direction (machine direction: MD and cross direction: CD) and the arithmetic mean value is reported. For thermofused samples, the samples were folded similarly as described for sewn samples. Then the samples were cut through the fold and thermofused by a heat sealer (Sunbeam VAC 780).

2.5.4. Statistical analysis

The tensile and the seam strengths were analysed to determine the variance in the results from each type of sample, and to determine whether there were statistically significant differences between them. This was done using GraphPad Prism 8.0.2 by one-way analysis of variance (ANOVA) for the whole set of data, followed by Tukey's post hoc test to compare individual samples.

2.6. Barrier properties

2.6.1. Water penetration

Impact penetration tests were evaluated in triplicate following the standard AATCC TM42-2017e [33]. Samples and blotting papers were conditioned at 21 °C and 50% relative humidity for at least 4 h before testing. Once conditioned, each sample was clamped under a spring clamp located at the top of a stand with an inclination of 45°. Another spring clamp with a weigh of 0.5 kg was clamped at the free end of the sample. A previously weighed blotting paper was placed beneath the sample.

A funnel with a spray nozzle at the bottom was placed 0.6 m above the top of the inclined stand (measured from the middle). The nozzle had 25 holes of 1 mm diameter. 500 mL of deionised water was poured into the funnel and allowed to spray under gravity onto the sample. The weight of the blotter paper was measured immediately after the water spraying finished.

2.6.2. Hydrostatic pressure

Hydrostatic pressure tests were performed in triplicate using a set up adapted from the standard AATCC TM127-2018 [34]. Samples were conditioned at 21 °C and 50% relative humidity for at least 4 h before

testing. A pre-fabricated polypropylene tube of 15 cm diameter and 100 cm height with two clear plaques at the bottom was used to conduct the tests. Each sample was inserted in between these plaques and tighten with screws. Deionised water was poured inside the tube with the sample at the bottom until leaks were observed. The height of the water in the tube was recorded.

2.6.3. Water vapour transmission rate

The water vapour transmission rate (WVTR) of the samples was measured using the desiccant method according to the standard ASTM E96. The samples were dried in an oven at 105 °C for at least 4 h prior to the test. Permeability cups containing pre-dried calcium chloride were sealed with the laminated side (outside surface) of the samples facing the desiccant, and the paper side (inside surface) facing the environment. The WVTR testing was conducted at 23 °C and 50% relative humidity. The change in mass of the cups with time was recorded and plotted. The slope of the rate of change of mass was used to calculate the water vapour transmission rate.

2.7. Virus protection

2.7.1. Preparation of phage suspension

Bacteriophage Phi-X174 was used in this assay as a model virus as it is non-pathogenic to humans. Phi-X174 was propagated using host Escherichia coli C ATCC 13706. The lysate was purified following the Phage-on-Tap protocol [35]. Chloroform extraction was not performed during phage purification of the lysate due to incompatibility with the test materials. The phage titre was determined by the soft agar overlay method, in which phage lysate was diluted 10 fold in bacteriophage nutrient broth [Bacto-tryptone (8.0 ± 0.1) g + Potassium chloride (5.0 ± 0.06) g + Calcium chloride (0.2 ± 0.003) g + Purified water (pH 5.3) (1 000 ± 12.5) ml] with surfactant [poly-sorbate 80 (0.1 ± 0.001 25) ml] to simulate the surface tension range for blood and body fluids.

2.7.2. Penetration test

The resistance of the material to Bacteriophage Phi-X174 was studied using the standard method ISO 16604:2004 (E). Herein, Phi-X174 in liquid was used in contact with the outside surface (laminated side) of the material. 90 mm diameter sample were tested in a penetration cell of diameter 70 mm. The penetration test cell and the samples were steam sterilised at 121 °C and 214 kPa for 15 min before each test. The sample was placed within the penetration cell, and the cell was closed by torqueing the bolts to 2.8 Nm each. The cell was covered with the transparent cover and mounted vertically in the apparatus for the penetration test. The cell was filled with 75 ± 2 mL of approximately 10^7 plaque forming units (pfu)/mL of Phi-X174 (challenge suspension) using a syringe and needle. The liquid was subjected to 0 kPa for 5 min followed by 20 kPa for 5 min. The cell was visually inspected for any sign of visible liquid penetration to the inside surface from the outside surface. At the end of the test, the challenge suspension was collected by opening the drain valve. The inside surface of the material (paper side) was washed with 5 mL of sterile nutrient broth, referred to as assay fluid. The entire surface area was brought into contact with the assay fluid by swirling the cell manually. If penetration was observed visually at any point earlier than the completion of the test, the cell was drained immediately and the assay fluid was collected and examined by viral titration using the soft agar overlay method with the media specified in the ISO 16604:2004 (E) protocol. The total number of plaques was counted. The sample passed the test if the count was less than 1 pfu/mL and vice versa. Positive and negative controls were performed using Whatman filter paper 602H and a heavy gauge polypropylene autoclavable bag material, respectively. All experiments were performed in triplicate.

Settle plates were performed to ensure there was no airborne contamination during any stage of the experiment. The agar plates containing E. coli C were exposed for 15–20 min at the locations of phage

3

titration and the penetration testing area. Material compatibility testing was performed to ensure there was no phage inactivation by the sample or the material of the penetration cell. This was done by pouring 10 mL of the phage suspension of 2200 pfu/ml onto the surface of the test material while it was in the cell. The lysate was then collected after 10 min of exposure to the sample and the cell. Phage titration was performed on this lysate as described above.

2.8. Ash content

The ash in the paper laminate composites were tested using the standard method TAPPI T211. Samples of known mass were combusted in an electrical muffle furnace (Model no. BT7670 Tetlow kilns & furnaces) at 525 °C for 3 h and the mass of the resulting ash was recorded. The moisture content was measured by keeping the samples of known mass in 105 °C for 4 h and recording the dried mass. The ash content was calculated as follows:

$$\text{Ash content } (\%) = \frac{\text{Weight of ash } (g)}{\text{Weight of paper sample (moisture free)}(g)} \times 100$$

3. Results

This study aimed to characterise laminated paper composite materials for their potential use as medical gown. The paper laminate composites were analysed by combining optical microscope and AFM-IR to detect surface composition and topographical heterogeneity of the base sheet-laminate interface, thus relating permeability to composite structure. The mechanical properties of the laminate materials, including tensile strength, seam strength and tear strength, were also analysed to quantify the effect of each layer. The materials were further tested against AAMI PB 70 for level 4 medical gowns, for which the required properties are >30 N for tensile and seam strength and >10 N

for tear strength. The barrier properties of the composites were tested against both water and a bacteriophage virus to determine the role and importance of each layer.

3.1. Coating morphology

Laminate integrity is key in achieving the required level of viral protection. However, the PE coating must also be as thin as possible for economic purposes, and to optimise wearer comfort. Further, analysis of the level of adhesion and the morphology of the interface can reveal a new understanding of the diffusion and barrier properties of laminated papers. Here, we combine advanced optical microscopy with AFM-IR analysis to probe and quantify the surface and interface between the layers of laminated paper.

3.1.1. PE coating morphology visualised with optical microscopy and AFM-IR

The surface and interface between the layers of the laminated papers were measured through advanced optical microscopy combined with AFM-IR analysis (Fig. 1). The optical microscopy transmission (brightfield) image shows the underlying cellulose fibres while the reflectance image reveals coating morphology. Pinholes were not readily detectable in the brightfield images, but a faint hue of the dye was occasionally observed. The reflectance images show heterogeneous coating morphology across the samples. The images of the two thinnest laminate layers and base sheet thicknesses (B44/6 and B44/10) show light and dark domains, revealing higher amorphous arrangement of PE chains (dark) than the semi-crystalline domains (light), which is consistent with the AFM-IR observations (Fig. 2) [36]. Samples B44/15, B49/16 and 15/B49/16 show no distinct light and dark domains; however, an overall dense bubble morphology indicates air trapped in the melt.
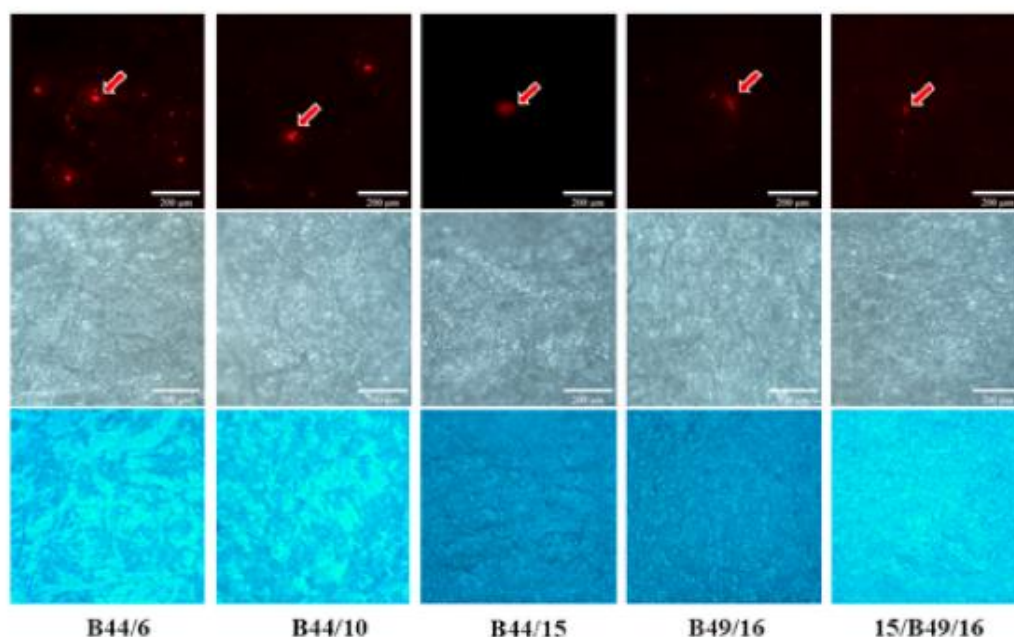
Fig. 1. Optical microscopy of laminate paper composites (scalebar: 200 μm) with PI staining. Fluorescence (top row), transmission (brightfield) (middle row) and reflectance with coloured filter (bottom row) images of propidium-iodide (PI) stained samples with various base sheet and laminate layer thicknesses. Fluorescence images reveal pinholes (in red), brightfield shows cellulose fibres and reflectance images highlight coating morphology. (For interpretation of the references to colour in this figure legend, the reader is referred to the Web version of this article.)

4
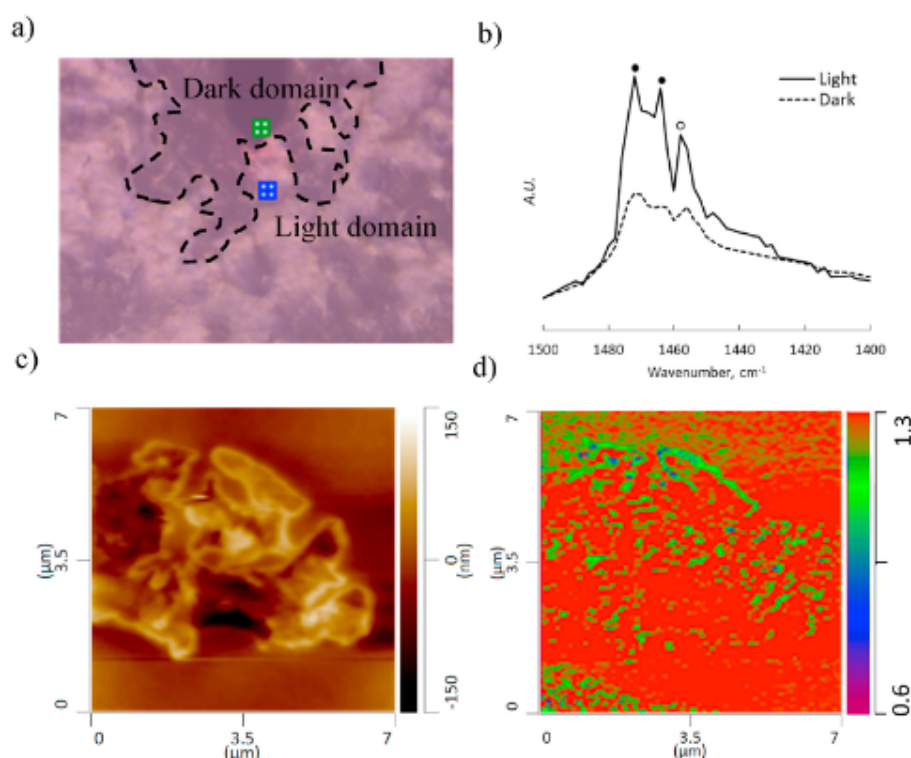
Fig. 2. Characterisation of the heterogeneous coating morphology of sample B44/10: a) NanoIR3 Optical microscopy view (375 × 282 μm) of the coating surface showing light and dark domains. b) AFM-IR spectrum showing the prominent CH$_2$ bending peaks of semicrystalline PE (solid circles, 1472 cm^{-1}, 1464 cm^{-1}) and amorphous PE (open circle, 1458 cm^{-1}). Dark domains have higher intensity due to semi-crystalline bands compared to the light regions, which show diminished semi-crystalline band signal intensity and similar intensity from the amorphous band. c) AFM topography map of a dark domain showing uneven surface morphology. D) PE (1464 cm^{-1}) -to-Cellulose (1062 cm^{-1}) IR ratio map of region (c) showing distinct PE rich (red) and PE poor (green) areas at the edges of the uneven surface topography. (For interpretation of the references to colour in this figure legend, the reader is referred to the Web version of this article.)

3.1.2. Pinholes visualised with fluorescence microscopy and AFM-IR

The fluorescence and optical images of selected samples after propidium iodide staining are displayed in Fig. 1. Fluorescence images show that the thinner laminate layer has the most pinholes while the thickest base sheet shows the least. The AFM topography images reveal two types of defect morphologies for pinholes. The first morphology is a protrusion of cellulose fibres through the coating from the base sheet due to insufficient amount of coating material (Fig. 3A); the other is a crater-like defect due to uneven coating (Fig. 3b). The AFM-IR shows an increase in the cellulose signal (1064 cm^{-1}) peak closer to the bottom of the crater-like defect than at shallower regions, indicating a thinner layer of the polyethylene coating at the base of the crater. The protruding fibre features give an even stronger cellulose signal at 1064 cm^{-1} in addition to a deformation of the polyethylene peak (1464 cm^{-1}) with lowered intensity and widened base. For protrusion defects, the IR composition map of polyethylene-to-cellulose ratio revealed poor polyethylene coating (Fig. 3c). A simultaneous measurement of the relative stiffness of the material was collected by tracking the resonant frequency of the AFM tip. The protruded defect generated higher frequencies than the surrounding area, indicating that a PE poor region can introduce mechanical heterogeneity, such as domains with high relative stiffness contrast compared to that of surrounding areas due to exposed cellulose material from base sheet (Fig. 3d).

3.2. Mechanical properties

Achieving the required mechanical properties with paper laminate materials, particularly high tensile strength, is expected to be challenging. Here, the effect of the type and thickness of paper base-sheet and the thickness of the PE coating are analysed. The material strength must also be preserved upon gown assembly, therefore two seam options, sewn and fused, are presented and analysed here.

3.2.1. Tensile strength

The mechanical properties of the laminated paper samples were expressed as the geometric mean tensile (GMT) at break point. Results are presented in Fig. 4. The dotted line represents the strength required (30N) for level 4 medical gown materials according to AAMI PB 70. All samples except the two newsprint composites meet the requirement. The newsprint composites (N42/10 and N51/10) have a lower GMT compared to those of bleached paper. These results indicate that pulp type plays an important role in governing the composite strength.

Increasing the thickness of the laminate for the same bleached base-sheet (B44/6, B44/10, B44/16) does not change the GMT significantly, nor does increasing the base sheet grammage from 44 to 49 GSM (B49/0 and B49/16). The effect of laminate thickness is also negligible when paper is coated on a single side. However, coating on both sides (15/B49/16) improves GMT significantly compared to single side coating.
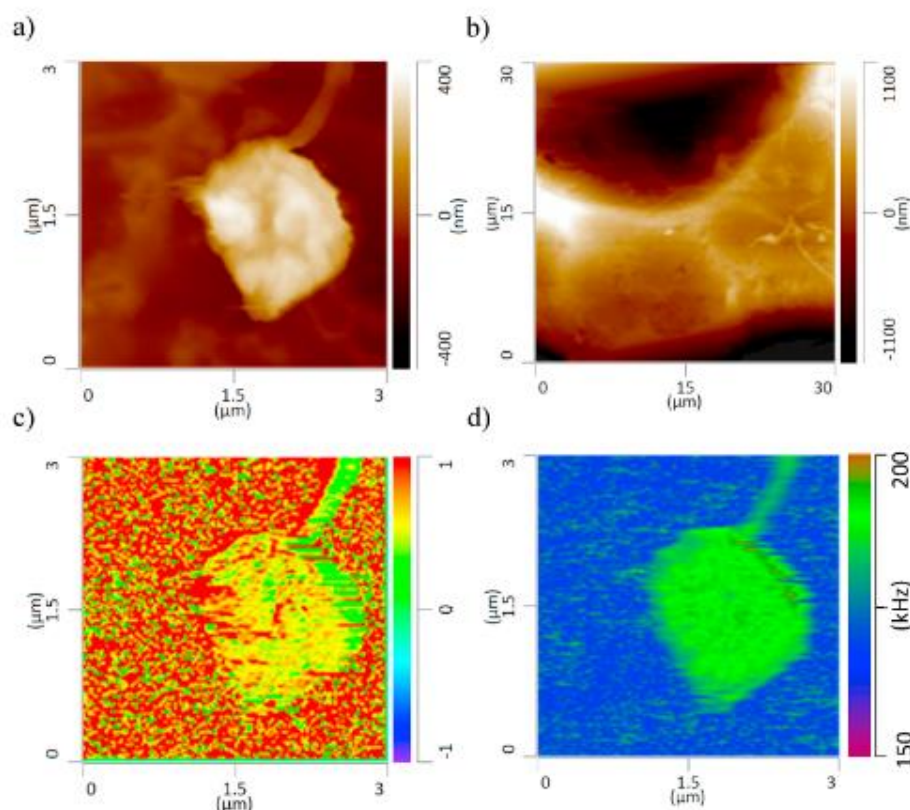
5

Fig. 3. Evidence of pinhole defect morphologies detected by AFM-IR characterization. a) An AFM topography map of a protruding defect (type 1) and b) An AFM topography map of a concave crater-like defect (type 2). c) PE (1464 cm^{-1}) -to-Cellulose(1062 cm^{-1}) IR ratio map of a protruding defect in A showing reduced IR absorption of 1464 cm^{-1} indicating poor PE coating on cellulose base sheet. d) PLL frequency map showing that protruding defects introduce domains with high relative stiffness contrast.
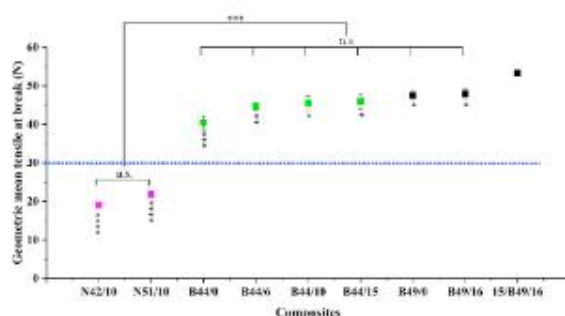

Fig. 4. Geometric mean tensile strength at break point for the different laminate composites. The dotted line shows the AAMI PB 70 requirement. The asterisks brackets show statistically significant differences between the indicated data points and groups. The asterisks below each data point show the level of significance when compared with 15/B49/16. Here, n.s. represents "not statistically significant", * represents $p < 0.05$, ** is for $p < 0.01$, *** for $p < 0.001$ and **** corresponds to $p < 0.0001$.

3.2.2. Seam strength

Seam strength was measured for both sewn and thermofused sample assemblies (Fig. 5). Slippage occurred for sewn seams at a low force for the unlaminated bleached paper with a 44 GSM base sheet (B44/0).

Increasing the laminate thickness on this base sheet (B44/6, B44/10, B44/16) or increasing the base sheet grammage (B49/0) does not affect seam strength significantly. However, when higher GSM base sheets were laminated on one side (B49/16), the seam strength improved considerably. Coating the sample on both sides (15/B49/16) improves the seam strength compared to its single-sided laminated counterpart (B49/16). This material (15/B49/16) has significantly higher seam strength than the unlaminated base sheets (B44/0 and B49/0) and the laminated base sheet with a lower GSM (B44/6,10,15). Therefore, it appears that both base sheet and laminate layers contribute to seam strength.

Thermofused composites did not show any difference in seam strength, irrespective of base sheet grammage, laminate thickness, or double-sided coating. Moreover, none of the thermofused composites samples meet the seam strength required (30 N) for by AAMI PB 70 for level 4 medical gowns (Fig. 5b). However, the thermofuser used here was a kitchen heat seal and thus might not have provided sufficient heat.

3.3. Barrier properties

Paper laminate barrier properties are important to ensure protection from the surrounding environment. Here, the effect of the thickness of paper base sheet and the thickness of the coating are evaluated.

3.3.1. Water resistant

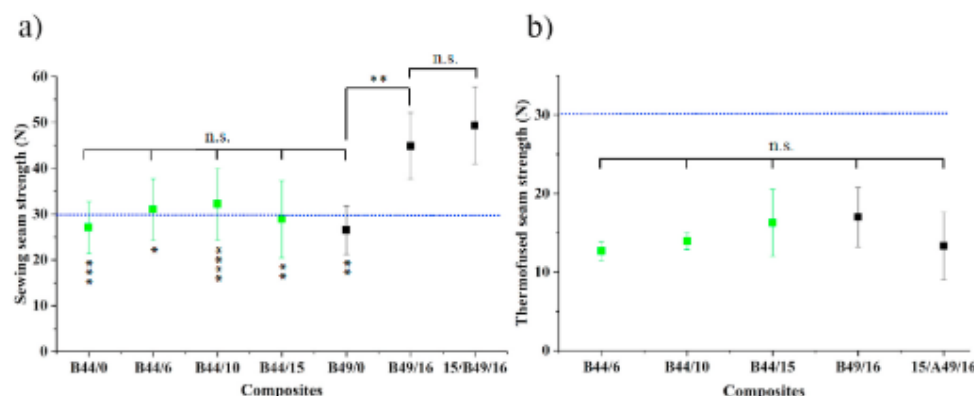The water resistance of the composites was measured through

Fig. 5. Seam strength after (a) sewing and (b) thermofusing for the different laminate composites. The dotted line shows the AAMI PB 70 requirement. The asterisks brackets show statistically significant differences between data points and groups. The asterisks below each data point show the level of significance compared to 15/B49/16. Here, n.s. represents not statistically significant, * is $p \leq 0.05$, ** shows $p \leq 0.01$, *** for $p \leq 0.001$ and **** corresponds to $p \leq 0.0001$.

hydrostatic pressure and impact penetration tests with results displayed in Table SI and Fig. 6. The hydrostatic pressure increased with increasing base sheet thickness. However, a more substantial increase was observed when the effect of the laminate was considered simultaneously. For A44/0 and A49/0, hydrostatic pressure was 24 and 37 cm, respectively. These values increased above 98 cm when a coating layer was added.

Water penetration values decreased with increasing base sheet thickness. Similar to the hydrostatic pressure tests, the greatest impact was noted when a laminate layer was included. For A44/0 and A49/0, water penetration was 0.11 and 0.06 g, respectively, decreasing to below 0.3 g when a coating layer was added.

3.3.2. Water vapour transmission rate

Materials without a PE layer showed the highest water vapour transmission rate (WVTR) (Fig. 7). WVTR values were similar for different base sheet thickness (A44/0 and A49/0). However, introducing a PE layer to the base sheet decreased the WVTR by 94% for A44/6 (31.3 g/m^2.day) compared to the base sheet A44/0 (530.4 g/m^2.day). Increasing the laminate layer thickness further reduced the WVTR. The lowest WTVR (2.4 g/m^2.day) occurred when a laminate layer was applied to both sides of a base sheet (15/B49/16).
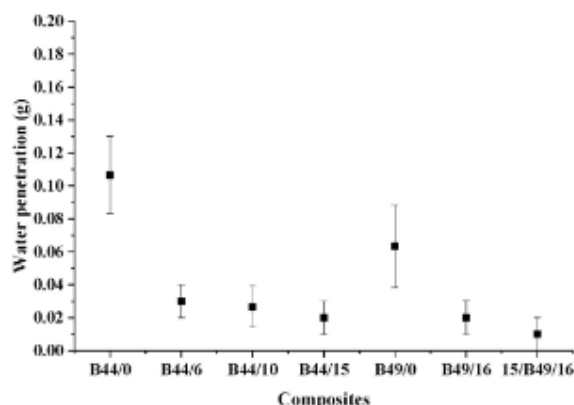

Fig. 6. Water penetration of the different samples.
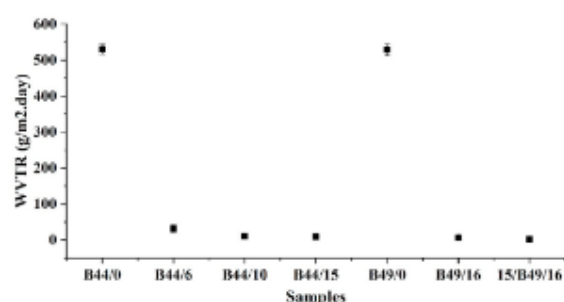
Fig. 7. Water vapour transmission rate for the different laminate composites.

3.4. Virus protection

The ability of the laminate materials to resist the penetration of viruses was tested using a surrogate virion Phi-X174 bacteriophage. The penetration of a virus suspension containing 10^7 pfu/mL from one side of the material to the other side was tested. Table S2 shows the resistance of the bleached paper samples coated with laminates of different thickness to virus penetration. The samples with a higher PE lamination passed the penetration tests irrespective of the paper type and base sheet grammage. The samples with low PE lamination (A44/6 and A44/10) failed the penetration test, whereas those with higher lamination (A44/15 and A49/16) could withstand a pressure of 20 kPa without allowing the virus particles to penetrate, thereby passing the test. The double coated sample (15/A49/16) also passed the test. The experimental method was validated with positive and negative controls. The positive control, which was a filter paper having a pore size of 2 μm, provided no barrier to the virus particles. The impermeable polyethylene material, with very low wettability and a small pore size, showed in no penetration of the virus suspension even under pressure.

Virus sizes usually range between 24 and 200 nm. The Phi-X174 bacteriophage tested here was reported to have an icosahedral shape with external spikes on each vertex, with a diameter of 25 nm excluding the spikes [37]. This virus particle is reported to be 34 ± 2 nm in size, including the spikes [38]. The viral species causing the COVID-19 outbreak is SARS-CoV-2. SARS-CoV-2 virions are spherical in shape, also containing glycoprotein spikes, and their diameter ranges from 60

nm to 140 nm [39,40]. SARS-CoV-2 viruses are larger than the microbe tested. It is therefore concluded that materials that provides barrier to the Phi-X174 bacteriophage would also resist penetration by the SARS-CoV-2 virus.

3.5. Ash content

The ash content signifies the presence of inorganic residues from wood pulp, the paper making process, and paper fillers. The ash content of the newsprint (N42/10) and bleached paper (B44/10) having the same laminate coating were $1.35 \pm 0.36\%$ and $0.50 \pm 0.07\%$. The ash content of the newsprint sample was significantly higher than the bleached sample. The ash content of the uncoated bleached paper (B44/0) is $0.21 \pm 0.12\%$, which shows that the 10 GSM coating also has some contribution to the ash.

4. Discussion

Paper based materials have never been reported for use as medical gowns. Thus, their prospect in this area remains poorly understood. At first, this material may seem to be an injudicious choice because of its perceived weakness, high porosity and high wicking ability. However, two events have challenged this perception. The first is the COVID crisis that has drastically limited access to typical polyolefin non-woven gown materials, which are predominantly manufactured in Asia [41,42]. In contrast, paper is manufactured on all the inhabited continents, and indeed, in most countries. The second is the advance of paper as an engineered material. Substantial progress in strength and barrier performance has been achieved in the last decade. However, commodity paper has yet to be reported as an accessible medical gown material, without the use of advanced technologies such as nanocellulose and assembling systems. This section has two objectives. The first is to investigate the property-structure relationship of laminated papers in the context of COVID-19 medical gown materials; the second is to determine if and how the current gown standard (AAMI PB 70) can be met with paper technology.

The AAMI PB 70 standard states the mechanical and barrier property requirements for medical gowns. Hence, these were studied to understand the suitability of the base sheet-laminate combination for Level 4 medical gowns, the highest level of protection. Special attention was dedicated to coating homogeneity, which was identified as a critical factor to ensure both reliability and safety of the material in COVID-19 medical gowns.

4.1. Material morphology

Defects in the laminate layer may compromise the barrier and mechanical function of laminated paper during use as COVID-19 surgical and isolation gowns. Due to the sub-micron size of the SARS-CoV-2 virus, a high resolution technique, namely AFM-IR, was utilised to acquire nanoscale structural and composition information regarding material defects by revealing these features with fluorescence staining. The concept is to stain the paper underneath the laminated surface with a fluorescent dye, which gives highly sensitive detection of any defects present.

Fluorescence stained regions, or pinholes, are defects which are more prevalent in composites with lower grammage base sheets, which introduces more pores in the sheet, or thinner laminate layers providing inadequate coverage over the rough paper surface. AFM-IR characterization reveals protruding (type 1) or crater like (type 2) defect morphologies with circular to ellipsoidal shapes that are 1–30 μm on the longest axis. Samples of the lowest base sheet grammage and thinner laminate layers (B44/6) have the largest type 1 and type 2 defects. The number of defects reduces with increasing laminate layer thickness (B44/15); in addition, an increase in base sheet grammage also aids in reducing the number and size of defects. The IR absorption of type 1

defects displays stronger absorptions around 1060 cm^{-1} and a reduced absorption around 1466 cm^{-1}. Type 2 defects exhibit an increase in absorption around 1060 cm^{-1} nearer the bottom of the crater. In addition, the relative stiffness of a type 1 defect is significantly higher than that of the surrounding material. This suggests protruding defects result from the base sheet having little to no coating while crater defects consists of regions with a thinner laminate layer with nano-holes at the bottom of the crater. Both types of defects must be mitigated as defects initiate tears and reduces barrier function, especially type 1 defects. However, mechanical and barrier test results must also be considered when determining the base sheet and laminate layer thicknesses (which determine the minimum number of defects) required for a functional yet economical medical gown.

AFM-IR analysis of light and dark domains visualised with optical microscopy reveals a heterogeneous coating morphology with distinct domains of semi-crystalline (light) and amorphous (dark) arrangement of polyethylene in materials with the lowest base sheet grammage (B44/6 and B44/10). While the nature of these domains does not indicate defects of the laminate layer, it does indicate reduced uniformity and molecular orientation, which may imply poor material function and impact laminate adhesion. Sollogoub et al. used optical microscopy to demonstrate that a substrate surface of higher roughness and lower polymer thickness had poor adhesion because the polymer had not reached the bottom of all the substrate surface irregularities due to the polymer flow being halted by crystallization or solidification [43]. Optical microscopy is thus a simple way to gauge the potential quality of laminate adhesion and to identify macroscopic coating defects.

4.2. Material performance

4.1.1. Effect of base sheet type

Two different types of base sheets were evaluated: Newsprint paper and Bleached Kraft paper. Newsprint paper is made from softwood pulp (yellow pine) by thermomechanical pulping, which involves refining (grinding) under saturated vapour to separate the fibres from wood [44] at temperatures above the glass temperature (T_g) of lignin. Newsprint paper retains most of its lignin and some of the hemicelluloses. In contrast, bleached Kraft paper is produced from hardwood (Eucalyptus) by chemical (Kraft) pulping, followed by bleaching. In Kraft pulping, wood chips are pre-steamed and mixed with a hot mixture of sodium hydroxide, sodium sulphide and water, which reacts with lignin to separate the cellulose fibres [45]. Around 90% of the lignin and most of the hemicelluloses are removed in this process. The chemical composition and wood polymer distribution of the two types of paper are thus significantly different. The most critically different properties are the length and therefore bonding abilities of the fibres with Pine fibres (L = 2 mm and D = 20 μm) being significantly coarser than Eucalyptus fibres (L = 0.8 mm, D = 8 μm).

The base sheet type directly affects strength, measured here as the maximum tensile force at rupture [46]. Composites made from Kraft-based paper are twice as strong (GMT) as bleached newsprint (N42/10 and N51/10). This is attributed to the high lignin content in the newsprint paper, which decreases fibre-fibre bonding by the limiting hydrogen bonding ability and reducing fibre conformability, resulting in a lower GMT. Wet end chemistry is not expected to play any significant role as only retention aids and sizing agents (internal and surface for Bleached Kraft paper) are used; there are no wet/dry strengths agents. Further, the Kraft paper contains no filler while the Newsprint likely contains some $CaCO_3$ from the recycling process. This supposition is supported by the ash content analysis, which shows that the newsprint composites (N42/10) has a higher ash content compared to the bleached Kraft paper (B44/10).

4.1.2. Effect of base sheet and laminate thickness

Virus penetration of these composites is entirely dependent on the laminate thickness; base sheet type and thickness has no effect. Samples

with thin laminate show penetration of the virus suspension from the outside (laminated) surface to the inside. A lower grammage base sheet (44 GSM) can provide full protection to virus particles only when the PE layer is above 15 GSM. Granzow et al. showed that gowns made of polypropylene resist fluid strikethrough and microorganism penetration better than those made of polyester or cotton [19]. Thus, it is the polymer coating on the laminated gowns that dictate the level of virus protection. Image analysis confirms that thinner laminates have a heterogeneous coating morphology, and defects may allow virus penetration. Coating thicknesses above 15 GSM show lower coating heterogeneity and less pinhole defects. Therefore, a thicker laminate coating should provide improved virus protection.

Increasing the laminate layer or base sheet thickness does not result in a statistically significant difference in the tensile strength. This is confirmed by the similar GMT results observed for the 44 GSM base sheet composite tested at three laminate layer thickness. The laminate layer mainly contributes to the flexibility or 'drapability' of the composite, and provides a hydrophobic barrier and viral barrier.

For seam strength, sewing outperforms thermofusing. Sewn seam slippage (displacement of thread) occurs at a low force for the unlaminated bleached paper and for laminated bleached papers with lower base sheet grammage. For the 44 GSM base sheets, increasing the laminate thickness does not affect the seam strength significantly. However, the seam strength improves significantly with laminated (one side) 49 GSM base sheets. Coating the sample on both sides further increases seam strength compared to unlaminated base sheets with the same grammage (B49/0). This indicates that both the base sheet and laminate layer contribute to seam strength. For the thermofused composites, increasing the base sheet thickness or the laminate thickness does not affect the seam strength, which is universally poor.

The presence of the laminate has a conspicuous effect on the barrier properties of the composites. The hydrostatic pressure of the paper composites significantly increases when a laminate layer is added, independent of the laminate thickness. Similar results are observed for water resistance and the water vapour transmission rate of laminated samples, which confirms that the polymer coating is responsible for the permeability and hydrophobicity of these composites [47].

4.1.3. Meeting standard requirements

16 GSM polyethylene lamination on a 49 GSM Kraft pulp base sheet is a suitable material for the production of Level 4 isolation gowns, as per the requirements of AAMI PB 70, providing the highest level of protection [10]. According to ASTM F3352-19, the laminated composite developed in this study meets the standard requirements for tensile and seam strength (matching or exceeding 30 N) [48]. The analysis indicates that the best combination is a 49 GSM base sheet with 16 GSM PE layer. Although the tear strength of all the laminated composites is lower than the standard requirement, this can potentially be improved by including a thin polypropylene (PP) layer between the composite base sheet and laminate layer, or with a tape or mesh at the ends, preventing crack propagation.

5. Conclusion

This study investigates polyethylene (PE) laminated paper as a novel material for the manufacture of disposable medical gowns meeting the stringent requirements for SARS-CoV-2 protection. Medical gowns have standards to meet in tensile strength, tear strength, seam strength, water penetration, hydrostatic pressure and viral protection.

Bleached and newsprint papers of varying basis weights were laminated with a polyethylene coating (on one or both sides). The laminated composites were characterised for coating morphology (optical microscopy and IR-AFM), mechanical properties, water resistance, water-vapour permeability and viral penetration. The performance achieved were compared to the medical gown material standards.

The water resistance of the laminated papers meets the standard requirements regardless of the laminate thickness or the base sheet grammage. The mechanical strength of the composite results from the type of paper base sheet, with bleached paper being the strongest. The virus protection is dependent on the laminate thickness; a minimum PE coating of 15 GSM is required for viral resistance, regardless of the paper base sheet. Image analysis of the laminated paper surface reveals coating heterogeneity in thinly coated laminates. A thicker coating is required for achieving a coating morphology free of defects, which is imperative for providing good viral protection. The laminated materials met all tensile and seam strength requirements; however, they failed the tear strength standard. A simple solution might be the addition of a tape or mesh at the ends, thus preventing crack propagation in paper. This research presented and validated PE laminated paper as a new material for medical gown and COVID-19 PPE equipment production.

Declaration of competing interest

The authors declare that they have no known competing financial interests or personal relationships that could have appeared to influence the work reported in this paper.

Appendix A. Supplementary data

Supplementary data to this article can be found online at https://doi.org/10.1016/j.polymer.2021.123643.

References

[1] N.J. Rowan, J.G. Laffey, Challenges and solutions for addressing critical shortage of supply chain for personal and protective equipment (PPE) arising from Coronavirus disease (COVID19) pandemic - case study from the Republic of Ireland, Sci. Total Environ. 725 (2020) 138532.
[2] L. Vogel, Canada's PPE crisis isn't over yet, say doctors, Can. Med. Assoc. J. 192 (20) (2020) E563. E563.
[3] N. Shimasaki, M. Hara, R. Kikuno, K. Shinohara, A highly sensitive assay using synthetic blood containing test microbes for evaluation of the penetration resistance of protective clothing material under applied pressure, Biocontrol Sci. 21 (3) (2016) 141–152.
[4] F.S. Kilinc, A review of isolation gowns in healthcare: fabric and gown properties, J.Eng. fibres.Fabr 10 (3) (2015), 155892501501000313.
[5] Y. Guo, Y. Li, P.L. Wong, Environment and body contamination: a comparison of two different removal methods in three types of personal protective clothing, Am. J. Infect. Contr. 42 (4) (2014) e39–e45.
[6] Verbeek, J.H., B. Rajamaki, S. Ijaz, R. Sauni, E. Toomey, B. Blackwood, C. Tikka, J. H. Ruotsalainen, and F.S.K. Balci, Personal protective equipment for preventing highly infectious diseases due to exposure to contaminated body fluids in healthcare staff. Cochrane Database Syst. Rev., (4).2020.
[7] U.S. Food and Drug Administration, Enforcement policy for gowns, other apparel, and gloves during the coronavirus disease (COVID-19) public health emergency, in: U.S.D.o.H.a.H. Services, United States of America, 2020.
[8] Administration, U.S.F.D. Medical gowns [cited 2020 27 May]; Available from: https://www.fda.gov/medical-devices/personal-protective-equipment-infection-control/medical-gowns, 2020.

[9] F.S.K. Balci, Isolation gowns in health care settings: laboratory studies, regulations and standards, and potential barriers of gown selection and use, Am. J. Infect. Contr. 44 (1) (2016) 104–111.

[10] A.A.M.I. PB70, Liquid barrier performance and classification of protective apparel and drapes intended for use in health care facilities, Association for the Advancement of Medical Instrumentation, Arlington (VA), 2012.

[11] Association for the Advancement of Medical Instrumentation, Selection and use of protective apparel and surgical drapes in health care facilities, Technical Information Report: TIR11: 2005 (2005).

[12] E. Bowden, C. Campanile, B. Golding, Worker at NYC Hospital where Nurses Wear Trash Bags as Protection Dies from Coronavirus. New York Post, 2020.

[13] Coronavirus BBC, UK Failed to Stockpile Crucial PPE, in BBC, 2020 (United Kingdom).

[14] Ford Ramps up PPE Production amidst Collaboration with Thermo Fisher on COVID-19 Test Kits, in Legal Monitor Worldwide, 2020. NA.

[15] HanesBrands, HanesBrands begins production of medical gowns in addition to cloth face coverings to supplement personal protection supply during COVID-19 pandemic, in: Medical Letter on the CDC & FDA, 2020, p. 1342. Atlanta.

[16] From Sanitizer to Gloves to Gowns, Wisconsin Company Vonco Steps up to Combat COVID-19 in America, in Plus Company Updates, 2020. NA.

[17] Dow, Partners to develop and donate level 2 medical isolation gowns, in: M2 Pharma, NA, 2020.

[18] PPE company starts production of reusable gowns, coveralls in response to COVID-19, in: Legal Monitor Worldwide, NA, 2020.

[19] J.W. Granzow, J.W. Smith, R.L. Nichols, R.S. Waterman, A.C. Muzik, Evaluation of the protective value of hospital gowns against blood strike-through and methicillin-resistant Staphylococcus aureus penetration, Am. J. Infect. Contr. 26 (2) (1998) 85–93.

[20] T. Dargaville, K. Spann, M. Celina, Opinion to address a potential personal protective equipment shortage in the global community during the COVID-19 outbreak, Polym. Degrad. Stabil. (2020) 109162.

[21] M.A. El-Samahy, S.A.A. Mohamed, M.H. Abdel Rehim, M.E. Mohram, Synthesis of hybrid paper sheets with enhanced air barrier and antimicrobial properties for food packaging, Carbohydr. Polym. 168 (Supplement C) (2017) 212–219.

[22] M. Maliha, M. Herdman, R. Brammananth, M. McDonald, R. Coppel, M. Werrett, P. Andrews, W. Batchelor, Bismuth phosphinate incorporated nanocellulose sheets with antimicrobial and barrier properties for packaging applications, J. Clean. Prod. 246 (2019).

[23] G. Rodionova, M. Lenes, Ø. Eriksen, Ø. Gregersen, Surface chemical modification of microfibrillated cellulose: improvement of barrier properties for packaging applications, Cellulose 18 (1) (2011) 127–134.

[24] L. Mendoza, L. Hossain, E. Downey, C. Scales, W. Batchelor, G. Garnier, Carboxylated nanocellulose foams as superabsorbents, J. Colloid Interface Sci. 538 (2019) 433–439.

[25] M.N. Alam, L.P. Christopher, Natural cellulose-chitosan cross-linked superabsorbent hydrogels with superior swelling properties, ACS Sustain. Chem. Eng. 6 (7) (2018) 8736–8742.

[26] A.M.A. Hasan, M.E.-S. Abdel-Raouf, Cellulose-based superabsorbent hydrogels, in: M.I.H. Mondal (Ed.), Cellulose-Based Superabsorbent Hydrogels, Springer International Publishing, Cham, 2019, pp. 245–267.

[27] R.M. Barajas-Ledesma, A.F. Patti, V.N.L. Wong, V.S. Raghuwanshi, G. Garnier, Engineering nanocellulose superabsorbent structure by controlling the drying rate, Colloid. Surface. Physicochem. Eng. Aspect. 600 (2020) 124943.

[28] G. Metreveli, L. Wågberg, E. Emmoth, S. Belák, M. Strømme, A. Mihranyan, A size-exclusion nanocellulose filter paper for virus removal, Advanced Healthcare Materials 3 (10) (2014) 1546–1550.

[29] A. Onur, A. Ng, G. Garnier, W. Batchelor, Engineering cellulose fibre inorganic composites for depth filtration and adsorption, Separ. Purif. Technol. 203 (2018) 209–216.

[30] A. Basu, G. Celma, M. Strømme, N. Ferraz, In vitro and in vivo evaluation of the wound healing properties of nanofibrillated cellulose hydrogels, ACS Applied Bio Materials 1 (6) (2018) 1853–1863.

[31] E. Caló, V.V. Khutoryanskiy, Biomedical applications of hydrogels: a review of patents and commercial products, Eur. Polym. J. 65 (2015) 252–267.

[32] M. Jorfi, E.J. Foster, Recent Advances in Nanocellulose for Biomedical Applications, 2015 n/a-n/a.

[33] AATCC TM42-2017e, Test Method for Water Resistance: Impact Penetration test, AATCC, North Carolina, USA, 2017.

[34] AATCC TM127-2018, Test Method For Water Resistance: Hydrostatic Pressure, North Carolina, 2018.

[35] N. Bonilla, M.I. Rojas, G. Netto Flores Cruz, S.H. Hung, F. Rohwer, J.J. Barr, Phage on tap-a quick and efficient protocol for the preparation of bacteriophage laboratory stocks, PeerJ 4 (2016), e2261.

[36] H. Hagemann, R. Snyder, A. Peacock, L. Mandelkern, Quantitative infrared methods for the measurement of crystallinity and its temperature dependence: polyethylene, Macromolecules 22 (9) (1989) 3600–3606.

[37] K. Yazaki, Electron microscopic studies of bacteriophage phi X174 intact and 'eclipsing' particles, and the genome by the staining, and shadowing method, J. Virol Methods 2 (3) (1981) 159–167.

[38] M.E. Bayer, R.W. DeBlois, Diffusion constant and dimension of bacteriophage phi X174 as determined by self-beat laser light spectroscopy and electron microscopy, J. Virol. 14 (4) (1974) 975–980.

[39] N. Zhu, D. Zhang, W. Wang, X. Li, B. Yang, J. Song, X. Zhao, B. Huang, W. Shi, R. Lu, P. Niu, F. Zhan, X. Ma, D. Wang, W. Xu, G. Wu, G.F. Gao, W. Tan, A novel coronavirus from patients with pneumonia in China, 2019, N. Engl. J. Med. 382 (8) (2020) 727–733.

[40] Y.M. Bar-On, A. Flamholz, R. Phillips, R. Milo, SARS-CoV-2 (COVID-19) by the numbers, eLife 9 (2020), e57309.

[41] J.M.R. Andrew, B. Mike, At war with no Ammo: doctors say shortage of protective gear is drive, in: The New York Times, The New York Times, New York, 2020.

[42] The Food and Drug Administration, FAQs on shortages o surgical masks and gowns during the COVID-19 Pandemic [cited 2020 5/11/2020]; Available from: htt ps://www.fda.gov/medical-devices/personal-protective-equipment-infection-control/faqs-shortages-surgical-masks-and-gowns-during-covid-19-pandemic, 2020.

[43] C. Sollogoub, P. Montmitonnet, Y. Demay, J.-F. Agassant, P. Deparis, Origin of the bubble defect in the extrusion coating process, Polym. Eng. Sci. 51 (2) (2011) 347–362.

[44] Skog Norske, Newsprint [cited 2020 1/10/2020]; Available from: https://www.norskeskog.com/Products/Newsprint, 2020.

[45] J. Fernández-Rodríguez, X. Erdocia, F. Hernández-Ramos, M.G. Alriols, J. Labidi, Lignin separation and fractionation by ultrafiltration, in: Separation of Functional Molecules in Food by Membrane Technology, Elsevier, 2019, pp. 229–265.

[46] A. TUTU, U. YILMAZ, M. ÇĞÇEKLER, Effects of physical Properties of some Papers on offset printing quality, in IV, in: International Multidisciplinary Eurasian Congress, 2017. Rome-Italy.

[47] P.W. Klein, in: Morgan, P. Claypool (Eds.), Fundamentals of Plastics Thermoforming, San Rafael, Calif.: San Rafael, Calif, Morgan & Claypool Publishers, 2009.

[48] F3352-19, A., Standard Specification for Isolation Gowns Intended for Use in Healthcare Facilities, ASTM International, West Conshohocken, PA, 2019.

APPENDIX IV:
STUDIES NOT INCLUDED IN THE THESIS

THIS PAGE HAS BEEN INTENTIONALLY LEFT BLANK

Characterisation and phytotoxic effects of torrefied wood derived from the Furacell process

Ruth M. Barajas-Ledesma[a], Antonio F. Patti[b], Vanessa N.L. Wong[c], Des Richardson[d] and Gil Garnier[a*]

[a]Bioresource Processing Institute of Australia (BioPRIA) and Department of Chemical Engineering, Monash University, Clayton, VIC 3800, Australia
[b]School of Chemistry, Monash University, Clayton, VIC 3800, Australia
[c]School of Earth, Atmosphere & Environment, Monash University, Clayton, VIC 3800, Australia
[d]Norske Skog, Tasmania, Australia.

*For correspondence: Gil.Garnier@Monash.edu

Abstract

Hypothesis: The Furacell process involves the slow pyrolysis of plant biomass and yields a significant portion of torrefied wood with traces of sulfolane (TWS). Torrefied wood is a carbon-rich solid material that has the potential to be used as a soil amendment due to its carbon stability and its chemical properties. Sulfolane, on the other hand, can be a potential phytotoxic compound. This study investigated the feasibility of TWS as a soil additive and the phytotoxic effect of sulfolane and other water-soluble compounds on plant growth was evaluated.

Experiments: TWS from the Furacell process was characterized physically and chemically. The effects of hot water extraction of sulfolane and pyrolysis for reducing TWS toxicity were assessed. The phytotoxicity of these materials was estimated by means of standard germination and seedling growth tests for assessing the toxicity of soil amendments [1, 2]. Toxicity tests were evaluated on radish (*Raphanus Sativus*) and cress (*Lepidium sativum L.*) seeds conducted in water suspensions (at 2, 20, 40, 100 and 200 g/L).

Findings: TWS caused a significant delay in germination and inhibited plant growth of radish and cress seeds. No germination was observed at concentrations higher than 100 g/L for both

species. The inhibition to germination due to TWS was substantially suppressed after hot water extraction of sulfolane and other water-soluble elements; however, germination index remained low (20% average compared to the control – water only) at concentrations higher than 20 g/L. The pyrolysis of TWS to convert the material to char at a temperature of 500 °C did not have an impact on reducing the toxicity of the material which suggested that an element of toxicity coming from the tars in TWS persevered. Through these findings it was concluded that the high phytotoxicity of TWS is partially attributed to the hydrophilic substances derived from the process that are removable by water washing such as sulfolane, and to the presence phenolic and furanic compounds. Further studies are needed to quantify and evaluate the effect of tars in the phytotoxicity of TWS.

1.0 Introduction

Torrefied wood is the brown to black uniform carbonaceous product derived from the incomplete combustion of plant biomass through slow pyrolysis. Torrefied wood can be used for energy production [3], carbonized nanomaterials [4, 5], waste management [6], gasification [3] and soil amendment [7]. Among these, its use as soil additive has attracted vast interest due to its capabilities to mitigate agro-environmental stresses through the permanent storage of CO_2, soil nutrient retention, pH correction, and crop yield improvement [6, 8].

The physical and chemical properties of torrefied wood are influenced by the properties of the feedstock and by pyrolysis conditions such as temperature and residence time [9]. Feedstocks differ depending on its elemental composition, moisture content, and lignin, cellulose and hemicellulose content. During pyrolysis, plant biomass undergoes a variety of physical, chemical and molecular transformations. Pyrolysis involves alterations in the O/C and H/C ratios, porosity, surface area [10], and an increase of aromatic ring structures and a decrease in O-H and CH_3 [9]. The molar H/C ratio is used to correlate the degree of the thermochemical alteration of the material. A H/C limit higher than 0.7 is used to distinguish torrefied wood from char, a more aromatic plant biomass-derived carbonaceous material.

In addition, the effects of torrefied wood are highly variable depending on its application rate, soil characteristics and plant species that have an impact in the outcomes reported in the literature that range from an increase in plant productivity to evident plant growth inhibition [9, 11].

The Furacell process involves the slow pyrolysis of plant biomass and sulfolane, and yields a significant portion of torrefied wood contaminated with traces of sulfolane that is used in the process [12, 13]. Sulfolane has been recently reported to affect human fertility and the

development of unborn children [14-16]. For this reason, its presence in agricultural soils has raised concerns related to its possible toxicity impact in plants.

Few studies have been published that assess the effects of sulfolane in plants. Most of them focussed on how sulfolane is taken up by plants and how these plants can be used for soil bioremediation. For example, Doucette, et al. [17] showed that sulfolane is significantly absorbed by cattails and accumulated in the leaf tips. In their experiment, sulfolane concentrations in the leaf tips were as high as 33,000 mg/kg dry weight for exposure of 200 mg/L of sulfolane in water. The uptake and translocation of sulfolane were found to be a function of exposure concentration and water transpired. Similar outcomes were outlined by Headley, et al. [18] and Guerrero [19]. These studies were conducted for non-edible plants only and did not investigate potential phytotoxicity effects of sulfolane.

Seed germination is one of the most important phases in the life cycle of a plant, and it is highly dependent on the existing environment [11]. Thus, seed germination bioassays and early stage seedling growth studies have been commonly used as a basis for determining toxicity effects in plants. These studies measure soil toxicity directly, and also consider the indirect impact of water-soluble compounds present in the sample [20]. Numerous scientific studies have used germination tests for evaluating the toxicity of carbonaceous materials derived from biomass pyrolysis [11, 21, 22].

There are several methods available in the literature for reducing the toxicity of torrefied wood as well as for the extraction of sulfolane from solid matter. Rombola, et al. [11] demonstrated that inhibition to germination can be suppressed if the biomass-derived material is washed with water prior germination studies. Rogovska, et al. [23] observed that the negative effects of different biomass-derived materials on seedling growth can be eliminated if they are leached with water before the germination tests. Anderson and Richardson [13] demonstrated that

sulfolane can be extracted from torrefied wood using pressurised hot water and that the extraction rate of sulfolane is doubled when using pressurised hot water compared with using ethyl acetate.

The aim of this study was to evaluate the phytotoxicity of the torrefied wood with sulfolane (TWS) formed in the Furacell process by using standard seed germination and seedling growth tests, and to identify possible relationships with its chemical characteristics. To this purpose, germination tests with radish and cress seeds were executed with the TWS at different concentrations. The effects of hot water extraction and pyrolysis on seed germination were evaluated on the TWS. Lastly, a comparison of the pyrolysed TWS was made with pyrolysed pine sawdust (PS) thermally treated at the same conditions.

2.0 Materials and Methods

2.1 Feedstock and torrefied wood preparation.
Pine sawdust and TWS with approximately 3 wt% of sulfolane residue were kindly provided from a pulp and paper company in Tasmania. The TWS was manually ground using a mortar and pestle to reduce its particle size from 4 mm in average to less than 500 µm for the germination tests.

2.2 Torrefied wood post-treatments.
The hot water extraction of sulfolane in TWS was performed in 6 cycles. Each cycle involved application of the following conditions: about 20 g of TWS was suspended in 1000 mL of deionized water in a 1500 mL beaker at 90 °C and mechanically stirred for 8 h. After extraction, the material was sonicated at a power output of 750 Watts and a frequency of 20 kHz for one hour using a sonics vibra-cell high-intensity ultrasonic processor. The aqueous phase was separated by filtration. After this cycle, fresh deionized water was added to the solid TWS product and the process was repeated six more times. The final solid TWS product left (re-

named as cleaned torrefied wood – CTW) after the seventh hot water extraction was dried overnight at 104 °C in an oven and utilized for germination tests.

Batch pyrolysis experiments were conducted on the PS, TWS, and CTW to produce char. About 10 g of the desired feedstock was placed uniformly inside a Tetlow muffle furnace initially purged with nitrogen and then kept under a constant nitrogen atmosphere. Pyrolysis was performed at 500 °C for 30 min at a heating rate of 8 °C/min. According to the feedstock labelling, the samples were named as following: CPS, CTWS, CCTW.

2.3 Feedstock and TWS characterisation.

Fourier-transform infrared spectroscopy (FT-IR) was performed with 4 cm^{-1} resolution measuring the absorbance from 4000 to 600 cm^{-1} on an Agilent Cary 360 FT-IR/ATR spectrophotometer equipped with a single-bounce diamond.

Elemental composition (HCNS) of pine sawdust and TWS were determined by combustion using a Perkin Elmer 2400 Series II analyser. The ash composition was calculated by way of thermal analysis using a Mettler Toledo GC 200 thermal analyser. About 5 mg of each sample was placed in an Al_2O_3 pan and heated at room temperature to 900 °C under a nitrogen atmosphere; thereafter, samples were exposed to an air current. The residual mass left was used to determine the ash content. The oxygen content was calculated from the mass balance as follows:

$$O\% = 100 - (C + H + N + ash)\%$$

The pH was determined following International Biochar Initiative (IBI) guidelines [24]. Briefly, a 1:20 (w:v) solution of material:deionized water was prepared and stirred for 90 minutes prior pH measurement using a 914 Metrohm pH/Conductometer analyser.

The high heating value (HHV) was calculated according to the following equation based on the elemental composition of the material [25]:

$$HHV\ (KJkg^{-1}) = 3.55C^2 - 232C - 2230H + 51.2CH + 131N + 20600 \quad (1)$$

The composition of sulfolane and other water-soluble compounds in the TWS, the CTW and the eluates obtained from the extraction post-treatment were analysed using a SHIMADZU GC-2010 Plus gas chromatograph analyser. Table I shows the solvents used as standard for each material.

Table I. Standard solvents used for gas chromatography analysis.

Sample	Standard solvent
TWS	Water
CTW	Water
Extraction eluates	Water

Thermogravimetric analysis (TGA) and derivative (DTG) curves were obtained using the Mettler Toledo GC 200 thermal analyser mentioned above. The method used was as follows: moisture was evaporated by heating each sample up to 110 °C using a heating rate of 25 °Cmin^{-1} and held for 10 min. Volatile compounds were removed using a heating rate of 25 °C min^{-1} up to 900 °C. These steps were performed at a N_2 gas rate of 20 mL min^{-1}. The final step consisted in introducing an air current at 900 °C for 30 min to oxidize fixed carbon and determine ash content.

Mass and Energy yield, and mass energy density were calculated according to Poudel, et al. [26] and Gogoi, et al. [27]:

$$\text{Mass yield } (Y_{mass}) = \frac{\text{mass after pyrolysis}}{\text{mass of raw sample}} \times 100\% \quad (2)$$

$$\text{Energy yield } (Y_{energy}) = Y_{mass} \times \frac{\text{HHV (pyrolysed sample)}}{\text{HHV (raw sample)}} \times 100\% \quad (3)$$

$$Mass\ energy\ density = \frac{Energy\ yield}{Mass\ yield} \quad (4)$$

2.4 Seed germination studies

The impact of both the TWS and CTW and their respective chars on the germination of two plant species was assessed. The species considered were radish (*Raphanus Sativus* supplied by Mr. Fothergill's) and cress (*Lepidium sativum L.* supplied by Mr. Fothergill's). Both species are considered sensitive to toxic organic compounds such as polyphenols [28].

The germination effects were evaluated at concentrations of 2, 20, 40, 100, 200 g/L by measuring the required amount of solid material and mixing it with 5 mL of deionized water depending on the desired concentration. The application rate was within the range of published recommendations and experiments [10]. For each treatment, 10 seeds of each species were placed on a filter paper wetted with 5 mL of the required concentration in a 90 mm Petri dish. Dishes were placed at room temperature in the dark. Four replicates of each treatment and the control (0 g/L – 5 ml of deionized water) were performed. Seed germination, defined as the seed having a radicle length > 5mm [1], was evaluated 12-hourly over a period of 7 days. The mean time to germination (MTG) of each plant species was calculated as follows:

$$MTG = \sum \frac{n \times d}{N}$$

Where n is the number of seeds that germinated between each time period, d is the incubation period in minutes at that point and N is the total number of seeds that germinated in the treatment.

In addition, the germination index was determined for each species over a period of 168 h using the germination percentage and the radicle length:

$$Germination\ index = \frac{G_s}{G_c} \times \frac{L_s}{L_c} \times 100$$

Where Gs and Gc are the number of seeds that germinated in the sample and the control and Ls and Lc are the root lengths of the sample and the control, respectively. Germination index is measured as a percentage of control.

2.5 Data analysis

The retrieved data from the germination studies were analysed statistically using One-way and Two-way ANOVA (analysis of variance) to determine differences between the means of the different treatments. Student-Newman-Keuls (SNK) tests were used where significant differences were found ($p < 0.05$). ANOVA and SNK analyses were performed using SigmaPlot 13 (Sysstat, Chicago, IL).

3.0 Results

3.1 Material characterisation.

The characteristics of pine sawdust (PS), torrefied wood with sulfolane (TWS) and clean torrefied wood (CTW) are shown and compared with their respective chars in Table II. The chemical characteristics of the PS were consistent with typical composition values found in the literature [3, 29, 30].

Table II. Proximate and elemental analysis of pine sawdust (PS), torrefied wood with sulfolane (TWS), clean torrefied wood (CTW) and their respective chars (indicated with the prefix C) produced at 500 °C (indicated in suffix) for 30 min. All on dry basis.

Sample	pH	Moisture (%)	C (wt%)	H (wt%)	N (wt%)	Ash (wt%)	O (wt%)	S (wt%)	Atomic ratio H:C	Atomic ratio O:C
PS	4.83	31	46.62	6.54	0.06	0.29	46.49	<0.3	1.684	0.749
TWS	2.12	2.1	56.84	4.95	0.17	4.15	33.88	<0.3	1.045	0.4448
CTW	3.07	2	59.02	4.84	0.09	3.58	32.46	<0.3	0.986	0.413
CPS500	7.52	ND	85.45	2.45	0.25	6.66	5.21	<0.3	0.341	0.046
CTWS500	2.23	ND	75.48	2.10	0.23	7.87	14.32	<0.3	0.333	0.142
CCTW500	2.69	ND	79.11	1.91	0.19	7.87	10.91	<0.3	0.290	0.105

Table III shows the calorific values (HHV), yields and mass energy densities of the torrefied

woods and the chars produced from the pyrolysis of pine sawdust, TWS and CTW. The yield

of the chars from TWS and CTW was reported based on pine sawdust as raw material. The

mass yield of the chars produced was in line with data reported in the literature: around 20-

30% for pine sawdust [6, 31] and between 30-40% for torrefied wood [27, 32]. The energy

yield (or energy efficiency) indicates the ratio of energy available of the material to initial

energy content of the raw biomass. In general, the mass and the energy yield decreased with

the increase in the thermochemical conversion of pine. The decrease in mass was due to its loss

of moisture and its thermal decomposition to form gaseous products such as CO, CO_2, H_2O,

acetic acid and other compounds [26].

Table III. Calorific value (HHV), mass yield, energy yield and mass energy density of torrefied

wood with sulfolane (TWS), clean torrefied wood (CTW) and their respective chars (prefix C).

Sample	Calorific value (MJ/kg)	Mass yield (%)	Energy yield (%)	Mass energy density
PS	18.53	-	-	-
TWS	22.78	65	79.9	1.23
CTW	23.12	65	81.1	1.25
CPS500	31.93	21	36.2	1.72
CTWS500	26.77	38.4	55.4	1.44
CCTW500	28.01	35.1	53.1	1.51

Figure 1 shows the thermogravimetric (TG) and the derivative thermogravimetry (DTG) curves

of PS, TWS, CTW and their respective chars. Differences in the thermo-degradability between

the feedstock and their respective chars were evident. All samples exhibited an initial weight loss at 100 °C, attributed to moisture loss. The highest changes in the lost fraction of weight were observed at a temperature range between 250 – 450 °C. PS displayed 65% of weight loss at a temperature between 350 – 400 °C, associated to the decomposition of cellulose occurring in the temperature range of 315 – 400 °C [33]. TWS and CTW also exhibited a similar trend at this temperature range but to a lower degree. This is because the cellulose in the torrefied materials had already been partially modified by the Furacell heating process.
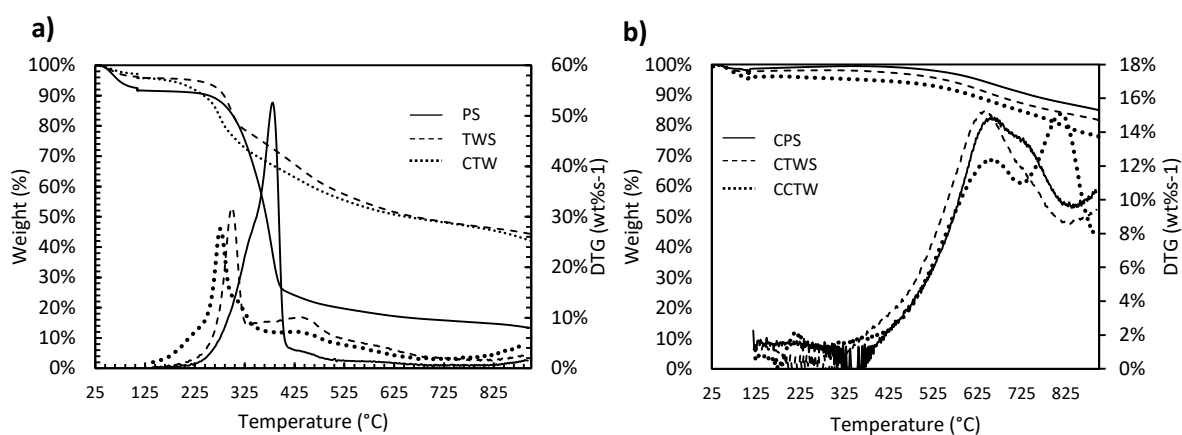

Figure 1. TGA and DTG curves of a) pine sawdust (PS), torrefied wood (TWS) and CTW samples. b) TG curves for pine feedstock, TWS and CTW samples.The DTG curves of TWS and CTW of in Figure 1a also displayed a distinct weight loss in the temperature range of 280 – 320 °C and a difference between these curves of approximately 4 %wt was observed. This difference was attributed to the removal of sulfolane since TWS showed a peak in the DTG signal at 275 °C, a temperature lower than the boiling point of sulfolane of 285 °C [15], and CTW had this peak at 300 °C.

Overall, the TG and DTG curves of the chars in Figure 1b produced at 500 °C suggested that the pyrolysis underwent complete carbonisation of the initial feedstock since no thermo-degradable fraction below this temperature was observed. This was also supported by the low

values of the H:C ratios [34]. Likewise, the steady weight loss above 530 °C in the chars was attributed to the degradation temperature of lignin that occurs slowly between 140 to 900 °C [6, 33].

Figure 2 shows the evolution of the FT-IR spectra of PS, TWS and CTWS as a function of the temperature at which they were processed or charring temperature. In principle, pine sawdust was characterised for its cellulosic and lignin content exhibited as O–H, C–O and its aliphatic (C–H) bonds.

The evolution of FT-IR spectra of lignocellulosic biomass displayed in Figure 2 shows the dehydration of cellulosic and ligneous components ($3500 - 3200$ cm^{-1}) that increased with the charring temperature. The TWS300 spectrum exhibited stronger C=O and C=C stretching vibrations ($1700 - 1600$ cm^{-1}) indicating the formation of lignin/cellulose-derived transformation products (multiple peaks at $1600 - 700$ cm^{-1}), aromatic components ($885 - 750$ cm^{-1}), and a decreased intensity of the 1080 cm^{-1} band for C–O skeletal vibrations, common in the functional groups of cellulose, hemicellulose and lignin [35]. All of these were linked to the processing temperature of torrefied wood in the Furacell^{TM} process. This supported the hypothesis that this material was torrefied wood or char in transition, where small volatile dissociation products are created as a result of dehydration of plant materials and depolymerisation of plant biopolymers as described by Keiluweit, et al. [36]. Finally, the CTWS500 spectrum was used to verify the effective conversion of the material to char. Heating the material to 500 °C resulted in more substantial chemical transformations. Bands due to hydrogen bonded O-H stretching ($3200 - 3500$ cm^{-1}) of water molecules and C-O (1080 cm^{-1}) decreased intensity or were completely absent. Absorption of aliphatic C-H stretching (2935 and 2885 cm^{-1}) declined compared to TWS300 spectrum. An increase of intensity at $885 - 752$ cm^{-1} relative to $1650 - 1500$ cm^{-1} indicated a larger degree of condensation which suggested that smaller aromatic units condensed into larger sheets [37].
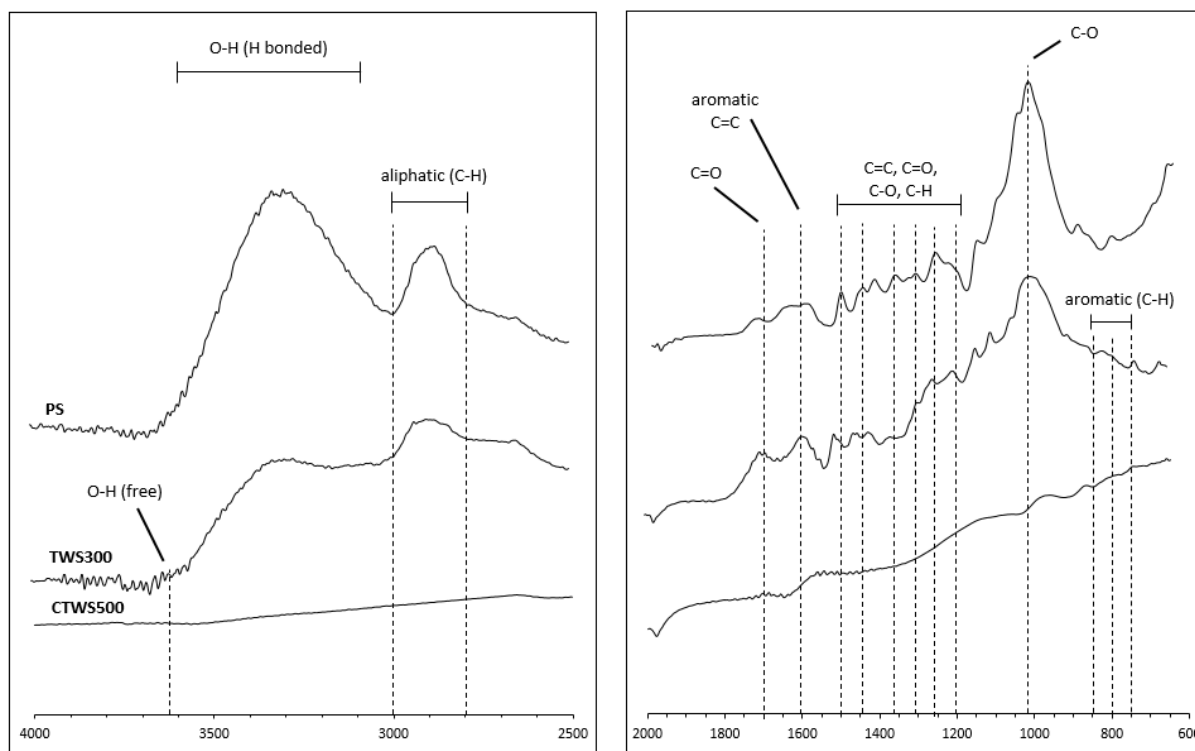
Figure 2. Stacked FT-IR of pine sawdust (PS), torrefied wood (TWS) and char from torrefied wood (CTWS500) samples.

3.2 Assessment of phytotoxicity of TWS and mitigation methods

3.2.1. Effect of TWS as received

In the first germination experiment, radish and cress seeds were treated under five different concentrations of torrefied wood as received: 2, 20, 40, 100, and 200 g/L. It was observed that the mean time to germination (MTG) and the germination index (GI) in both species increased with increasing TWS concentration. No germination was observed at concentrations higher than 40 g/L for all species which outlines the heavy toxicity effect TWS had on plant species (see Figure 3).
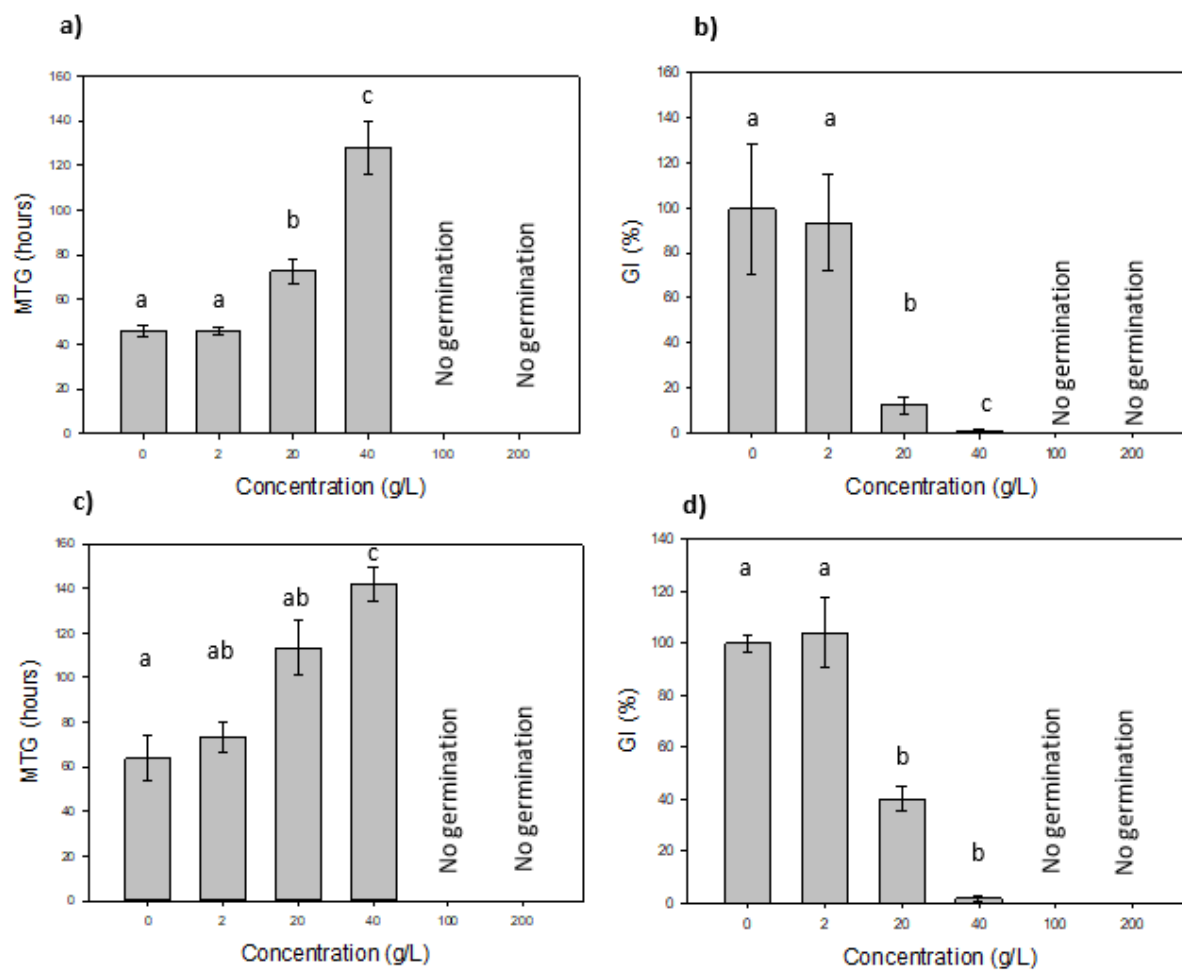
Figure 3. Mean time to germination and germination index of radish (a and b) and cress (c and d) in the presence of **TWS** concentrations. Means (+- S.E.) followed by the same letter are not significantly different at the P < 0.05 level, as determined by SNK's test.

Radish seeds showed no substantial difference in MTG or GI between the control and 2g/L. However, they showed a significant increase in MTG between 2 and 20 g/L, or greater. A similar trend was observed for cress species where MTG increased with increasing concentration up to 40 g/L, and no germination was noted at higher concentrations.

The GI decreased with increasing TWS concentration for all species. For the species considered in this experiment, the GI was significantly lower where seeds were treated at high

concentrations of TWS in comparison with dH$_2$O control. The GI changed from 100% at dH$_2$O control to 1.6% and 1.3% at a concentration of 40 g/L for radish and cress, respectively.

3.4.2. Extractable compounds

Hot water was used to extract the chemicals present in the TWS such as sulfolane, acetic acid, furfural and levoglucosenone (LGO). Figure 4 presents the concentrations of sulfolane before and after the hot water extraction process.
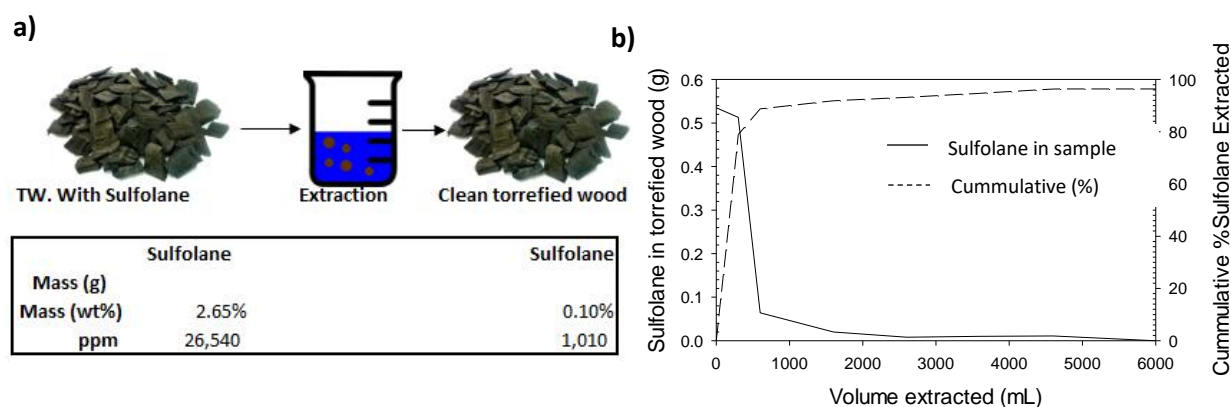

Figure 4. a) Concentrations of Sulfolane before and after extraction. b) Elution profile of Sulfolane extracted from the torrefied wood.

Figure 4b shows that approximately 80% of the sulfolane present in the initial torrefied wood was removed in the first extraction cycle which confirms the effectiveness of the method. Nevertheless, it was also observed that the remaining material after the extraction had still some traces of sulfolane left (see Figure 4a). Overall, the extraction process removed 96% of the initial sulfolane in the TWS. Similar yields were reported by Anderson and Richardson [13], who used pressurised hot water to extract sulfolane from torrefied wood.

 The concentration of other specific potentially toxic compounds extracted from the TWS is shown in Table IV. Acetic acid, furfural and levoglucosenone (LGO) are products from the pyrolysis of biomass in the Furacell process and were expected to be found in the TWS. In general, it was observed that the concentration of each compound decreased on each extraction

cycle. Apart from sulfolane, the concentration of all of the other compounds was negligible in the CTW.

Table IV. Concentration of extractable compounds in 25 g of torrefied wood.

Sample/ Extraction cycle	Concentration (wt%)				Extracted mass (g)			
	Acetic acid	Furfural	LGO	Sulfolane	Acetic acid	Furfural	LGO	Sulfolane
TWS	0.07	0.067	0.258	2.654	0.017	0.016	0.063	0.65
1	0.021	0.012	0.025	0.171	0.063	0.036	0.075	0.513
2	0.002	0.004	0.005	0.021	0.006	0.012	0.015	0.064
3	0	0	0	0.002	0	0	0	0.02
4	0.001	0.001	0.001	0.001	0.008	0.01	0.08	0.008
5	0	0.001	0.001	0.001	0	0.01	0.01	0.01
6	0	0	0.01	0.001	0	0	0.01	0.01
7	0	0	0.01	0	0	0	0.01	0
CTW	0	0	0	0.101	0	0	0	0.024

3.4.3. Germination tests after TWS post-treatment

Germination assays were performed with the product left after the hot water extraction (labelled clean torrefied wood – CTW). Germination tests were also performed with the chars produced from the TWS and CTW, and they were compared with char produced from pine sawdust (PS) – a clean source. All of the germination tests were conducted at 5 different concentrations of solid material mixed with deionized water: 2, 20, 40, 100 and 200 g/L for radish and cress seeds. Deionized water was used as a control. Figure 5 shows the results of the germination tests performed with CTW.

The inhibitory effects of TWS significantly decreased after the hot water extraction process. Figure 6 presents pictures of the germinations assays of radish seeds treated with 40 g/L of TWS and CTW after 7 days of experiment. More pictures of the treatments are shown in the supplementary information.

The ANOVA tests indicated that MTG for radish seeds was constant over the dH_2O control and the treatments up to 40 g/L. In this experiment, the lowest MTG observed was 40 hours on average, whereas the highest MTG reported was 78 hours at a concentration of 200 g/L. Similarly, MTG of cress species was 71 hours in average and the ANOVA tests showed that no substantial difference was observed between the dH_2O and all the treatments. It should be noted that both plant species germinated at concentrations of 100 and 200 g/L, in contrast to the results observed for TWS.
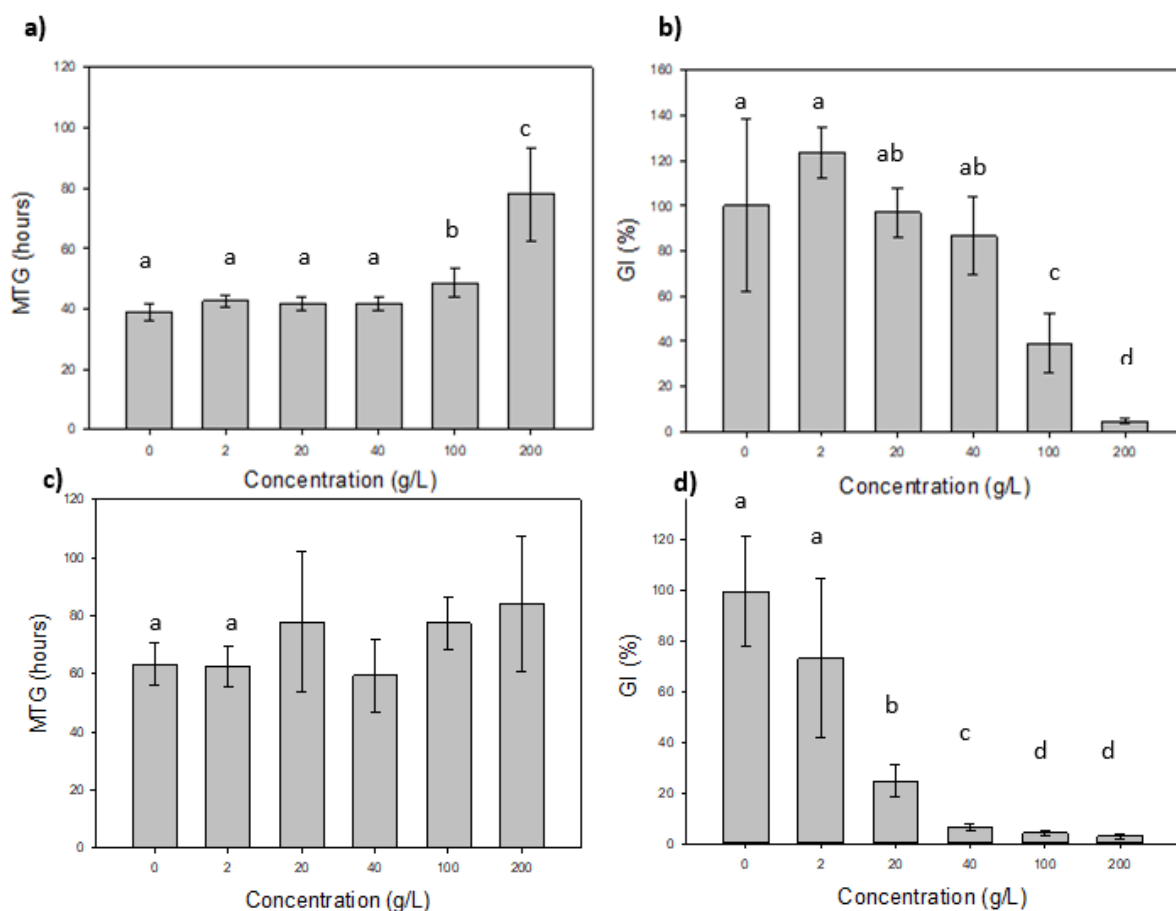
Figure 5. Mean time to germination and germination index of radish (a and b) and cress (c and d) in the presence of clean torrefied wood (CTW) concentrations. Means (+- S.E.) followed by the same letter are not significantly different at the P < 0.05 level, as determined by SNK's test
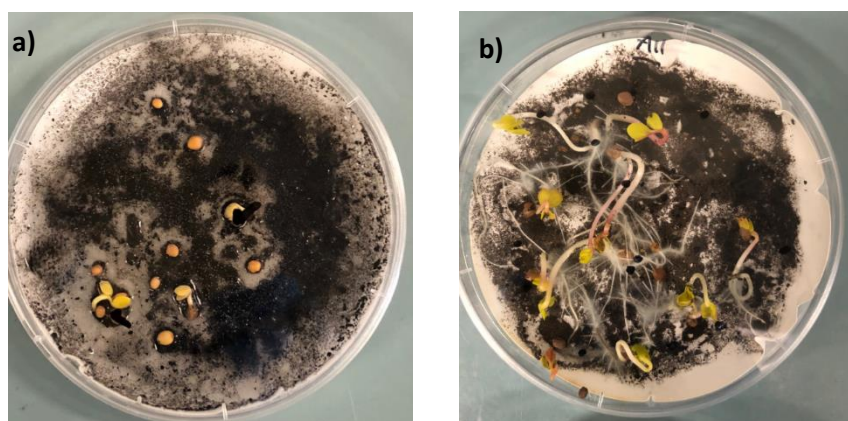

Figure 6. Germination assays of radish seeds treated at concentrations of 40 g/L of TWS a) and CTW b). Photos taken after 7 days of experiment.

A partial improvement in the GI was also observed for all species treated with cleaned torrefied wood (CTW). Though the GI of radish seeds remained constant between the dH_2O control and the treatments up to 40 g/L, the roots barely grew at 200 g/L. A similar trend was observed for cress species. Here, a significant difference was noted between the control and the concentrations after 2 g/L which suggested that the clean torrefied wood still had some elements of toxicity. These observations are supported by Rogovska, et al. [23], who evaluated the effects of chars on seedling growth of corn seeds and found that growth inhibition was significantly reduced when the chars were washed with water prior to germination tests. The effect of the chars on seed germination of radish and cress is presented in Figure 7. Additional graphs of individual materials can be found in the supplementary information at the end of this APPENDIX.
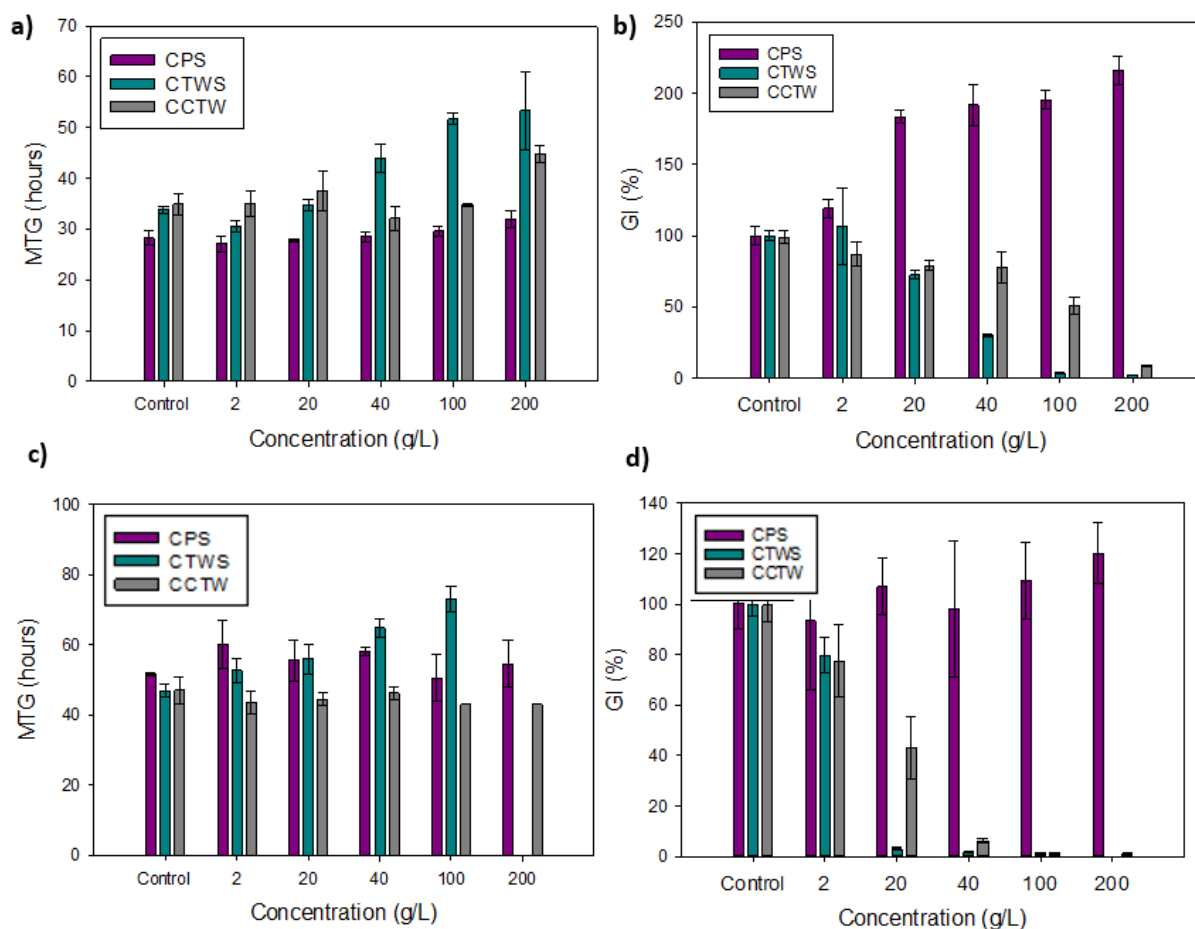
Figure 7. Mean time to germination and germination index of radish (a and b) and cress (c and d) in the presence of char from pine sawdust (CPS), char from torrefied wood with sulfolane (CTWS) and char from clean torrefied wood (CCTW). All at different concentrations.

Figure 7a and 7c show that there was no significant difference in the MTG between the dH_2O control and the chars produced from PS and CTW. However, both species showed an increase in MTG when treated with char produced from TWS where cress seeds did not germinate at the highest concentration of 200 g/L.

On the other hand, Figure 7b and 7d clearly indicates that GI in both species was severely affected by the chars produced from the torrefied wood, both TWS and CTW. This impact was more acute in cress seeds where germination indexes harshly decreased after a concentration

of 2 g/L which indicated that the conversion of the torrefied wood to char did not have any effect in reducing the toxicity of torrefied wood. Comparing the GI of chars from TWS and CTW with char from pine sawdust, it is clearly observed that an element of toxicity still persists in the torrefied wood even after converting it to char, especially when char is produced from the torrefied wood as received (TWS) (see figure 8).

Interestingly, char from pine sawdust exhibited positive effects in the germination of radish seeds (figure 7b). This was used to confirm the hypothesis of how an adequate char should perform to improve plant growth. Similar results were presented by Gell, et al. [38], who found that poultry char produced at 550 °C increased radish root elongation in 134%.
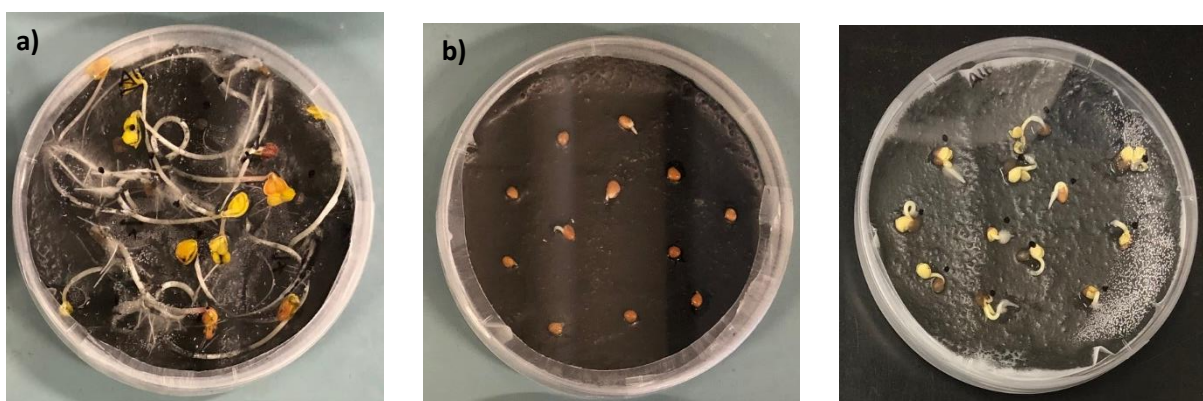

Figure 8. Germination assays of radish seeds treated at concentrations of 200 g/L of char from pine sawdust (CPS), (b) char from torrefied wood with sulfolane (CTWS) and (c) char from clean torrefied wood (CCTW). Photos taken after 7 days of experiment.

4.0 Discussion

4.1 Material characterisation

The H:C atomic ratio shown in Table II displays values of 1.045 and 0.986 of TWS and CTW respectively. This validated the hypothesis that the material did not undergo full thermochemical conversion to char and therefore it was torrefied wood and not char. According

to the International Char Initiative (IBI) [24], only materials with an H:C atomic ratio less than 0.7 are recognized as thermochemically converted materials or chars. Looking at the H:C ratios of the chars produced, it was observed that for all cases the H:C atomic ratio was less than 0.7 which confirmed the successful thermochemical conversion of the biomass into char. These findings were strengthened by the O:C values of 0.44 and 0.14 of TWS and CTWS respectively. a According to Spokas [39], a boundary of O:C atomic ratio of less than 0.2 is used to divide thermo-chemical conversion products from combustion residues. Lastly, the percent of sulphur of <0.3% in the CTW was used to verified the effective removal of sulfolane from the torrefied wood.

Comparing the calorific values (HHV) in Table III of the chars produced and the torrefied wood with the HHV value of pine, it was observed that the HHV increased as the thermochemical conversion of pine took place. This was because of the increase in the concentration of C-C and C-H bonds in the material after the removal of the C-O bonds verified in the decrease of the O:C atomic ratios [27]. However, it should be noted that the higher the HHV, the lower the mass and energy yield of the material produced. This indicates a trade-off between the energy content in the material and its total available mass which is explained by the mass energy density. Hence, it is concluded that the closest the value is to 1 the more energy efficient the material is.

4.2 Assessment of phytotoxicity of TWS and mitigation methods

4.2.1. Effect of TWS as received

The significant delay in seed germination and the severe decrease in plant growth for both radish and cress seeds suggest that TWS had inhibitory effects in the time to germination and germination index of both species. Though the mechanisms of the phytotoxicity are difficult to predict, previous studies have shown that both species are sensitive to the presence of aliphatic and aromatic hydrocarbons [38] present in the material, and to phenolic compounds derived

from the decomposition of lignin [30]. These observations are strongly supported by the results of Trifonova, et al. [40], who showed that the phenols and furans present in the torrefied wood inhibited germination of tomato seeds. Such compounds were found to be generated during biomass pyrolysis at low temperatures. They found that the phytotoxicity of torrefied wood decreases when biological treatment is used.

Similarly, the presence of sulfolane in TWS is likely to have a phytotoxic impact. Doucette, et al. [17] investigated the uptake of sulfolane in plants by growing cattails hydroponically in aqueous solutions with sulfolane. They found that sulfolane is taken up passively by cattails, it ends in the leaves where it gets accumulated. Though no phytotoxicity effect was reported by the authors, the concentrations of sulfolane used in the experiments were much lower than the concentrations presented in this study (20 to 200 ppm compared to 50 to 5,300 ppm respectively) to eliminate the possibility of sulfolane causing growth inhibition in plants. Likewise, in the study by Doucette, et al. [17], the plants were allowed to grow for several weeks prior to their exposure to sulfolane meaning that germination tests could not be assessed.

4.2.2. Germination tests after TWS post-treatments

Germination assays of CTW indicated that even though MTG results for cress species were similar across all CTW concentrations and control, GI results revealed that a high phytotoxic effect still persists in cress seeds since the GI decreased as CTW concentration increased (i.e. seeds germinated but the plant did not grow). Such observations were reported by Gell, et al. [38], who found that thermally treated biomass at low-temperature pyrolysis exhibit more phytotoxic effects. These are attributed to the tars present in the torrefied wood. Tars are produced during the pyrolysis process and they are mainly composed of a mixture of hydrocarbons. They are not water-soluble and therefore cannot be removed with hot water.

It is not yet known which element(s) of the torrefied wood are likely to be responsible for the chronic phytotoxicity observed. Figure 9 compares the germination index depending on the

torrefied wood post-treatment for radish and cress. Results showed that CTW and its respective char had less inhibitory effects as compared to the others. In fact, char from CTW had little a reduction in phytotoxicity compared with CTW alone. This strongly supports the hypothesis that the water-soluble compounds such as furfural, phenols and sulfolane present in the torrefied wood are partly responsible for inhibiting seed germination as suggested by Buss and Masek [21] and Trifonova, et al. [40].
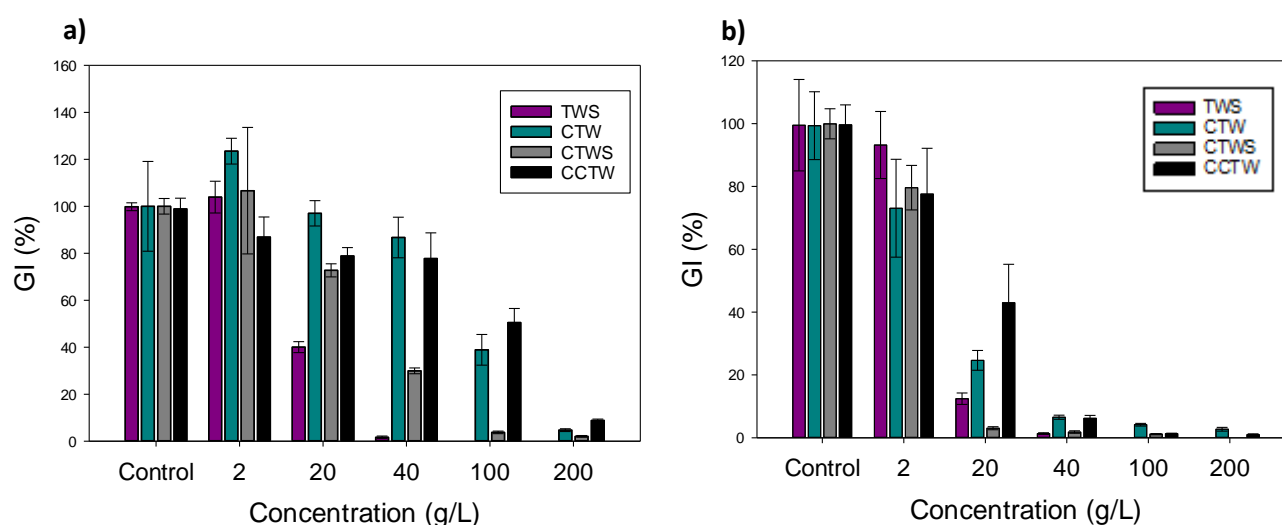

Figure 9. Germination index of radish (a) and cress (b) seeds in the presence of different treatments. Means (+- S.E.).

Soil acidity is known to be a major growth-limiting factor for plants [41]. High acidity levels in soils are known to result in inhibited plant growth as they are associated with plant diseases. Robson and Abbott [42] suggest that the main effect of unfavourable pH is to prolong the stage of growth during which the plant is more susceptible to infection. During the toxicity studies, some fungal growth was observed in both species treated with high concentrations of TWS and CTW (100 and 200 g/L). It was believed that this fungal growth was due to the acid conditions of the experiment (pH < 3); however, the pH of both species treated at lowest concentration of both TWS and CTW was between 3 and 3.5, and no fungal growth was detected which suggested that the pH was not solely responsible for the observed phytotoxicity.

Lastly, it was suggested that some chemical compounds in the residuals tars of the chars may have direct toxicity effects in plant growth [43]. Buss and Masek [21] showed that softwood char contaminated with high volatile organic compounds totally inhibits cress seed germination at concentrations higher than 1 g. They also found that water-soluble constituents of the char induced heavy toxicity to germination which was also confirmed in this study. Gell, et al. [8] showed that chars from low-temperature pyrolysis exhibit more phytotoxic effects than chars produced at high temperatures. This is because pyrolysis at low temperature produces higher levels of tars which is likely to occur in this case. The results in Figure 7b and 7d indicates that char from pine sawdust did not exhibit any inhibitory effects on plant growth, unlike to what was observed for chars of TWS and CTW. Thus, strongly supporting the hypothesis that TWS and CTW chars contain more tars than PS char because of their previous thermal treatment that happened in the Furacell process. Moreover, Yang, et al. [44] showed that "tar-free" char can be achieved if the pyrolysis temperature is higher than 500 °C. Nevertheless, further processing of the material with organic extraction or solid-phase adsorption is needed to quantify the amount and impact of tars in plant toxicity.

5.0 Conclusion

Germination assays of radish and cress seeds were found to be a suitable method for determining phytotoxicity. This study demonstrated that the torrefied wood of the Furacell process delays the germination and inhibits vegetative growth of radish and cress.

This study showed that washing the torrefied wood with hot water was a suitable method to extract water-soluble compounds such as acetic acid, furfural and sulfolane present in the material. The mass of sulfolane in the material before and after the extraction process was 0.65 g and 0.024 g respectively. Hence, the extraction process successfully removed 96% of the sulfolane content in the torrefied wood.

Whilst removing the sulfolane and other water-soluble compounds from the torrefied wood showed an improvement in the time to germination and early growth of radish and cress species, the material remains toxic to plant growth as it impacted the germination index of cress seeds.

The production of char from pine sawdust exhibited positive effects in the germination of radish seeds and served as a positive indicator for comparing the toxicity effects of the chars produced from the torrefied wood.

Similarly, no difference was observed between the clean torrefied wood (CTW) and its respective char (CCTW) which suggests that converting the torrefied wood to char does not reduce its phytotoxicity.

The data presented in this report indicate that the torrefied wood from the Furacell process is negatively affecting the early growth and development of the species tested. This effect is attributed to the composition of tars present in the material. However, further studies such as organic extraction with ethyl acetate or solid-phase adsorption of tars are needed to quantify and evaluate the effect of tars in the material.

6.0 Bibliography

[1]   K. P. Mosse, A. F. Patti, E. W. Christen, and T. R. Cavagnaro, "Winery wastewater inhibits seed germination and vegetative growth of common crop species," *J Hazard Mater,* vol. 180, no. 1-3, pp. 63-70, Aug 15 2010, doi: 10.1016/j.jhazmat.2010.02.069.

[2]   *Seed Germination/root elongation toxicity test*, USEPA, Washington, DC, 1992.

[3]   A. Eseyin, P. Steele, and C. U. Pittman, Jr., "Current trends in the production and applications of torrefied wood/biomass - A review," *Bioresources,* vol. 10, no. 4, pp. 8812-8858, 2015.

[4]   J. McDonald-Wharry, M. Manley-Harris, and K. Pickering, "Carbonisation of biomass-derived chars and the thermal reduction of a graphene oxide sample studied using Raman spectroscopy," *Carbon,* vol. 59, pp. 383-405, 2013, doi: 10.1016/j.carbon.2013.03.033.

[5]   T. Somanathan, K. Prasad, K. K. Ostrikov, A. Saravanan, and V. M. Krishna, "Graphene Oxide Synthesis from Agro Waste," *Nanomaterials (Basel),* vol. 5, no. 2, pp. 826-834, May 20 2015, doi: 10.3390/nano5020826.
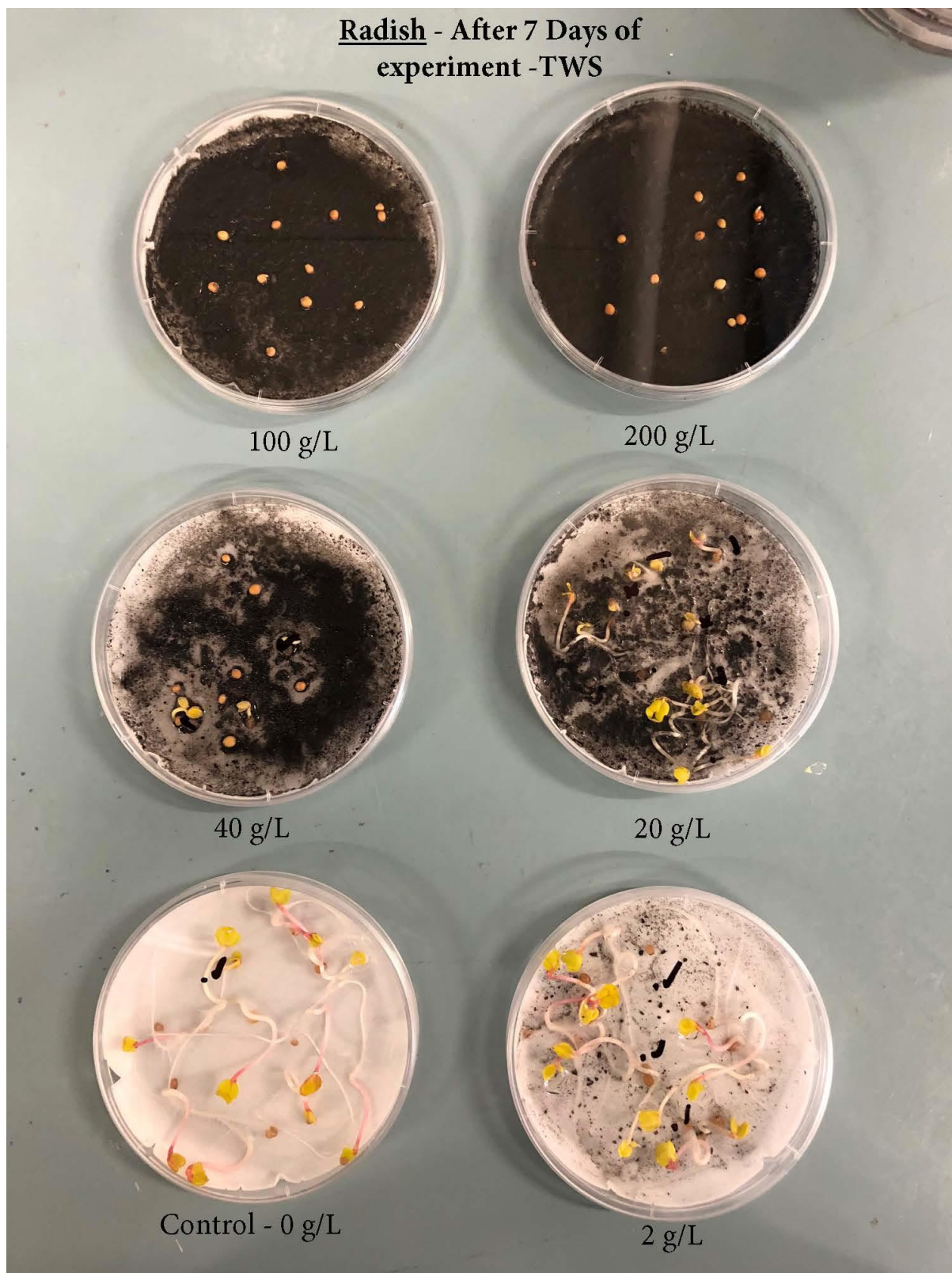
[6]   N. Gómez, J. G. Rosas, J. Cara, O. Martínez, J. A. Alburquerque, and M. E. Sánchez, "Slow pyrolysis of relevant biomasses in the Mediterranean basin. Part 1. Effect of temperature on process performance on a pilot scale," *Journal of Cleaner Production,* vol. 120, pp. 181-190, 2016/05/01/ 2016, doi: https://doi.org/10.1016/j.jclepro.2014.10.082.

[7]   S. Kuppusamy, P. Thavamani, M. Megharaj, K. Venkateswarlu, and R. Naidu, "Agronomic and remedial benefits and risks of applying biochar to soil: Current knowledge and future research directions," *Environ Int,* vol. 87, pp. 1-12, Feb 2016, doi: 10.1016/j.envint.2015.10.018.

[8]   K. Gell, J. van Groenigen, and M. L. Cayuela, "Residues of bioenergy production chains as soil amendments: Immediate and temporal phytotoxicity," *Journal of Hazardous Materials,* vol. 186, no. 2, pp. 2017-2025, 2011/02/28/ 2011, doi: https://doi.org/10.1016/j.jhazmat.2010.12.105.

[9]   S. Kloss *et al.*, "Characterization of Slow Pyrolysis Biochars: Effects of Feedstocks and Pyrolysis Temperature on Biochar Properties," (in English), *Journal of Environmental Quality,* vol. 41, no. 4, pp. 990-1000, Jul 2012

2017-11-19 2012. [Online].

[10]   J. Lehmann and S. Joseph, *Biochar for Environmental Management : Science and Technology*. London, UNITED STATES: Routledge, 2009.

[11]   A. G. Rombola *et al.*, "Relationships between Chemical Characteristics and Phytotoxicity of Biochar from Poultry Litter Pyrolysis," *J Agric Food Chem,* vol. 63, no. 30, pp. 6660-7, Aug 5 2015, doi: 10.1021/acs.jafc.5b01540.

[12]   D. E. Richardson and W. D. Raverty, "Predicted environmental effects from liquid emissions in the manufacture of levoglucosenone and Cyrene™," *APPITA,* vol. 69, no. 4, pp. 344-351, 2016.

[13]   S. A. Anderson and D. E. Richardson, "Analysis of Sulfolane in Biochar," 2017.

[14]   C. M. Thompson, D. W. Gaylor, J. A. Tachovsky, C. Perry, M. C. Carakostas, and L. C. Haws, "Development of a chronic noncancer oral reference dose and drinking water screening level for sulfolane using benchmark dose modeling," *J Appl Toxicol,* vol. 33, no. 12, pp. 1395-406, Dec 2013, doi: 10.1002/jat.2799.

[15]   Chevron Phillips, "Sulfolane Safety Data Sheet," 2018.

[16]   D. Prat *et al.*, "CHEM21 selection guide of classical- and less classical-solvents," *Green Chemistry,* vol. 18, no. 1, pp. 288-296, 2016, doi: 10.1039/c5gc01008j.

[17]   W. J. Doucette, J. K. Chard, B. J. Moore, W. J. Staudt, and J. V. Headley, "Uptake of sulfolane and diisopropanolamine (DIPA) by cattails (Typha latifolia)," *Microchemical Journal,* vol. 81, no. 1, pp. 41-49, 2005, doi: 10.1016/j.microc.2005.01.015.

[18]   J. V. Headley, L. C. Dickson, and K. M. Peru, "Comparison of Levels of Sulfolane and Diisopropanolamine in Natural Wetland Vegetation Exposed to Gas-Condensate Contaminated Ground Water," *Communications in Soil Science and Plant Analysis,* vol. 33, no. 15-18, pp. 3531-3544, 2007, doi: 10.1081/css-120014546.

[19]   H. Guerrero, "Fate of sulfolane in a hydroponic cattail system," Master of Science, Civil and Environmental Engineering Utah State University, Utah, 2004.

[20]   *Seed germination/root elongation toxicity test*, US EPA, Washington DC., 1992.

[21]   W. Buss and O. Masek, "Mobile organic compounds in biochar - a potential source of contamination - phytotoxic effects on cress seed (Lepidium sativum) germination," *J Environ Manage,* vol. 137, pp. 111-9, May 1 2014, doi: 10.1016/j.jenvman.2014.01.045.
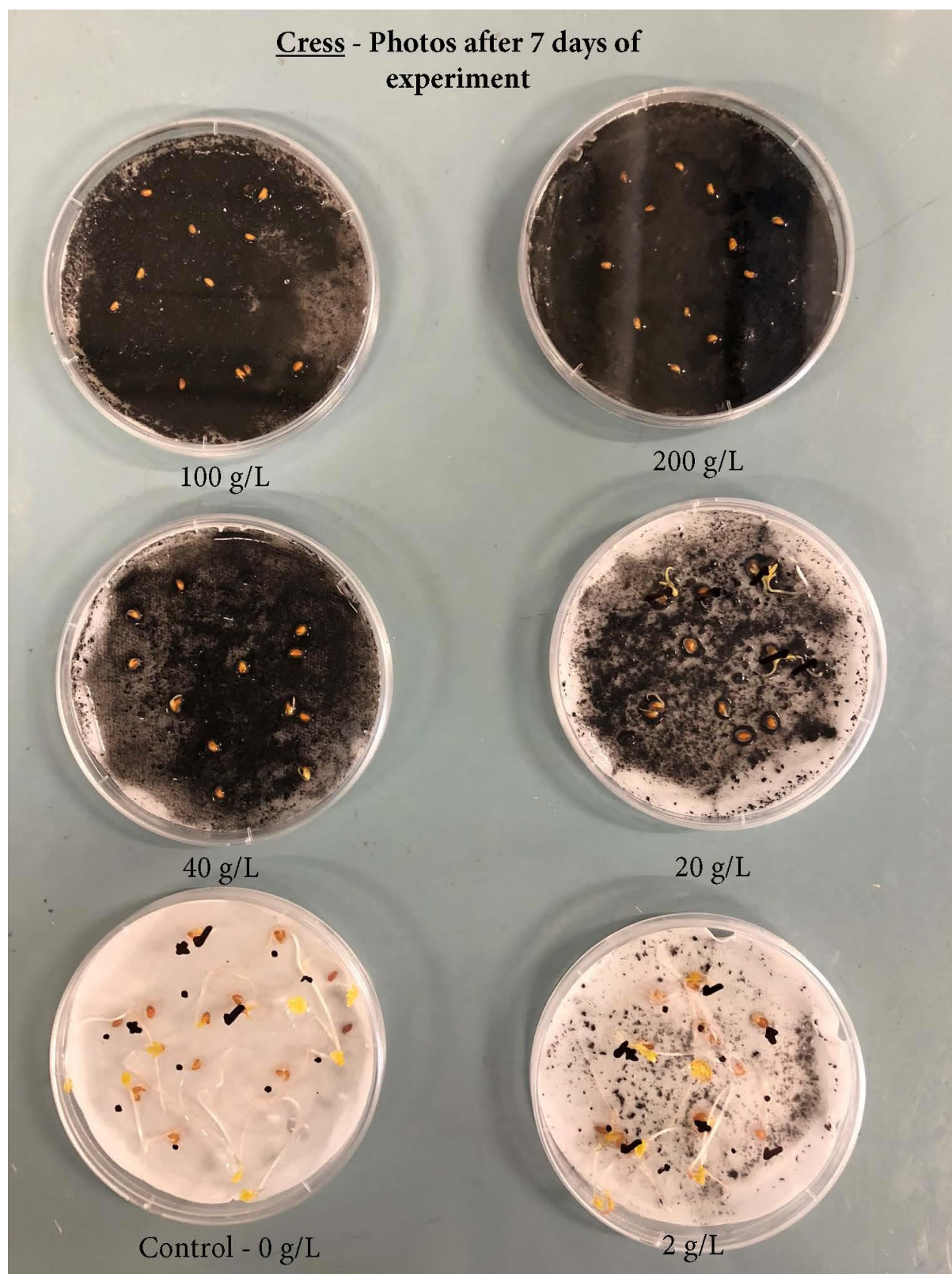
[22] Y. Li *et al.*, "Mitigating biochar phytotoxicity via lanthanum (La) participation in pyrolysis," *Environ Sci Pollut Res Int,* vol. 24, no. 11, pp. 10267-10278, Apr 2017, doi: 10.1007/s11356-017-8653-x.

[23] N. Rogovska, D. Laird, R. M. Cruse, S. Trabue, and E. Heaton, "Germination Tests for Assessing Biochar Quality," (in English), *Journal of Environmental Quality,* vol. 41, no. 4, pp. 1014-22, Jul 2012

2017-11-19 2012. [Online].

[24] *Standardized Product Definition and Product Testing Guidelines for Biochar that Is Used in Soil*, Product Definition and Specification Standards IBI-STD-2.1, International Biochar Initiave, 2015.

[25] A. Friedl, E. Padouvas, H. Rotter, and K. Varmuza, "Prediction of heating values of biomass fuel from elemental composition," *Analytica Chimica Acta,* vol. 544, no. 1, pp. 191-198, 2005/07/15/ 2005, doi: https://doi.org/10.1016/j.aca.2005.01.041.

[26] J. Poudel, T.-I. Ohm, and S. C. Oh, "A study on torrefaction of food waste," *Fuel,* vol. 140, pp. 275-281, 2015/01/15/ 2015, doi: https://doi.org/10.1016/j.fuel.2014.09.120.

[27] D. Gogoi *et al.*, "Effect of torrefaction on yield and quality of pyrolytic products of arecanut husk: An agro-processing wastes," *Bioresource Technology,* vol. 242, pp. 36-44, 2017/10/01/ 2017, doi: https://doi.org/10.1016/j.biortech.2017.03.169.

[28] F. Fornes and R. M. Belda, "Acidification with nitric acid improves chemical characteristics and reduces phytotoxicity of alkaline chars," *J Environ Manage,* vol. 191, pp. 237-243, Apr 15 2017, doi: 10.1016/j.jenvman.2017.01.026.

[29] S. Arnsfeld, D. Senk, and H. W. Gudenau, "The qualification of torrefied wooden biomass and agricultural wastes products for gasification processes," *Journal of Analytical and Applied Pyrolysis,* vol. 107, pp. 133-141, 2014, doi: 10.1016/j.jaap.2014.02.013.

[30] J. S. Tumuluru, S. Sokhansanj, J. R. Hess, C. T. Wright, and R. D. Boardman, "A review on biomass torrefaction process and product properties for energy applications," (in English), *Industrial Biotechnology,* Report vol. 7, p. 384+, 2011/10//

// 2011. [Online]. Available: http://link.galegroup.com.ezproxy.lib.monash.edu.au/apps/doc/A272510994/AONE?u=monash&sid=AONE&xid=6341b79f.

[31] S. Meyer, B. Glaser, and P. Quicker, "Technical, Economical, and Climate-Related Aspects of Biochar Production Technologies: A Literature Review," *Environmental Science & Technology,* vol. 45, no. 22, pp. 9473-9483, 2011/11/15 2011, doi: 10.1021/es201792c.

[32] A. Zheng *et al.*, "Effect of torrefaction on structure and fast pyrolysis behavior of corncobs," *Bioresource Technology,* vol. 128, pp. 370-377, 2013/01/01/ 2013, doi: https://doi.org/10.1016/j.biortech.2012.10.067.

[33] V. Dhyani and T. Bhaskar, "A comprehensive review on the pyrolysis of lignocellulosic biomass," *Renewable Energy,* vol. 129, pp. 695-716, 2018/12/01/ 2018, doi: https://doi.org/10.1016/j.renene.2017.04.035.

[34] K. Hammes, R. J. Smernik, J. O. Skjemstad, and M. W. I. Schmidt, "Characterisation and evaluation of reference materials for black carbon analysis using elemental composition, colour, BET surface area and 13C NMR spectroscopy," *Applied Geochemistry,* vol. 23, no. 8, pp. 2113-2122, 2008/08/01/ 2008, doi: https://doi.org/10.1016/j.apgeochem.2008.04.023.

[35] I. Pastorova, R. Botto, P. Arisz, and J. Boon, "Cellulose char structure: a combined analytical Py-GC-MS, FTIR, and NMR study " *Carbohydrate Research* vol. 262, pp. 27-47, 1994.

[36] M. Keiluweit, P. Nico, M. Johnson, and M. Kleber, "Dynamic Molecular Structure of Plant Biomass-Derived Black Carbon (Biochar)," *Environ Sci Technol,* vol. 44, pp. 1247-1253, 2010.

[37] Y. Guo and R. M. Bustin, "FTIR spectroscopy and reflectance of modern charcoals and fungal decayed woods: implications for studies of inertinite in coals," *International Journal of Coal Geology,* vol. 37, no. 1, pp. 29-53, 1998/09/01/ 1998, doi: https://doi.org/10.1016/S0166-5162(98)00019-6.

[38] K. Gell, J. van Groenigen, and M. L. Cayuela, "Residues of bioenergy production chains as soil amendments: immediate and temporal phytotoxicity," *J Hazard Mater,* vol. 186, no. 2-3, pp. 2017-25, Feb 28 2011, doi: 10.1016/j.jhazmat.2010.12.105.

[39] K. A. Spokas, "Review of the stability of biochar in soils: predictability of O:C molar ratios," *Carbon Management,* vol. 1, no. 2, pp. 289-303, 2014, doi: 10.4155/cmt.10.32.

[40] R. Trifonova, J. Postma, M. T. Schilder, and J. D. van Elsas, "Microbial Enrichment of a Novel Growing Substrate and its Effect on Plant Growth," (in English), *Microbial Ecology,* vol. 58, no. 3, pp. 632-41, Oct 2009

2014-08-02 2009, doi: http://dx.doi.org/10.1007/s00248-009-9518-8.

[41] P. S. Kidd and J. Proctor, "Why plants grow poorly on very acid soils: are ecologists missing the obvious?," *Journal of Experimental Botany,* vol. 52, no. 357, pp. 791-799, 2001, doi: 10.1093/jexbot/52.357.791.

[42] A. D. Robson and L. K. Abbott, "4 - The Effect of Soil Acidity on Microbial Activity in Soils," in *Soil Acidity and Plant Growth*, A. D. Robson Ed.: Academic Press, 1989, pp. 139-165.

[43] C. R. Smith, E. M. Buzan, and J. W. Lee, "Potential Impact of Biochar Water-Extractable Substances on Environmental Sustainability," *ACS Sustainable Chemistry & Engineering,* vol. 1, no. 1, pp. 118-126, 2013/01/07 2013, doi: 10.1021/sc300063f.

[44] H. Yang, S. Kudo, S. Hazeyama, K. Noringa, O. Mašek, and J.-i. Hayashi, "Detailed Analysis of Residual Volatiles in Chars from the Pyrolysis of Biomass and Lignite," *Energy & Fuels,* vol. 27, no. 6, pp. 3209-3223, 2013/06/20 2013, doi: 10.1021/ef4001192.
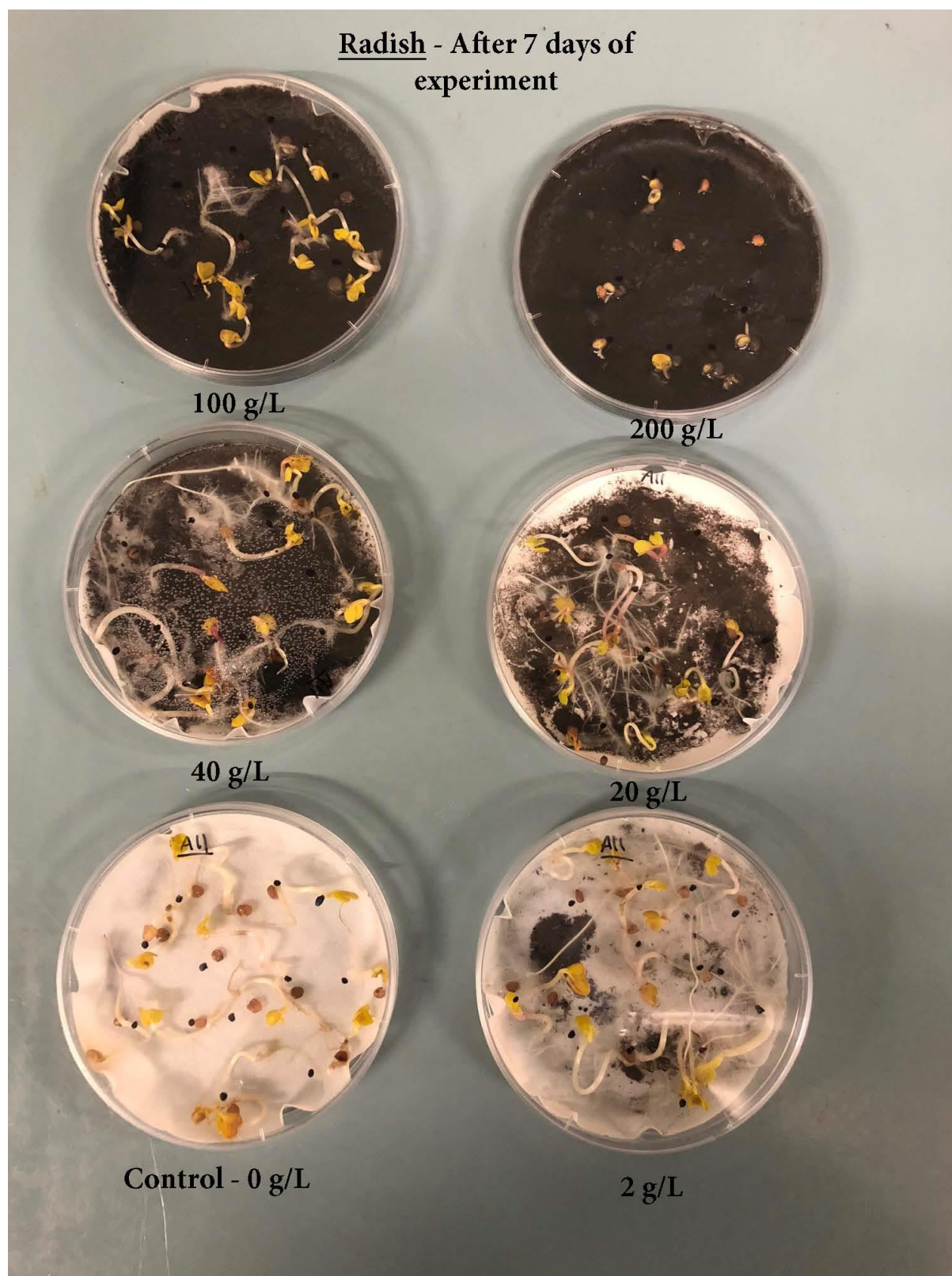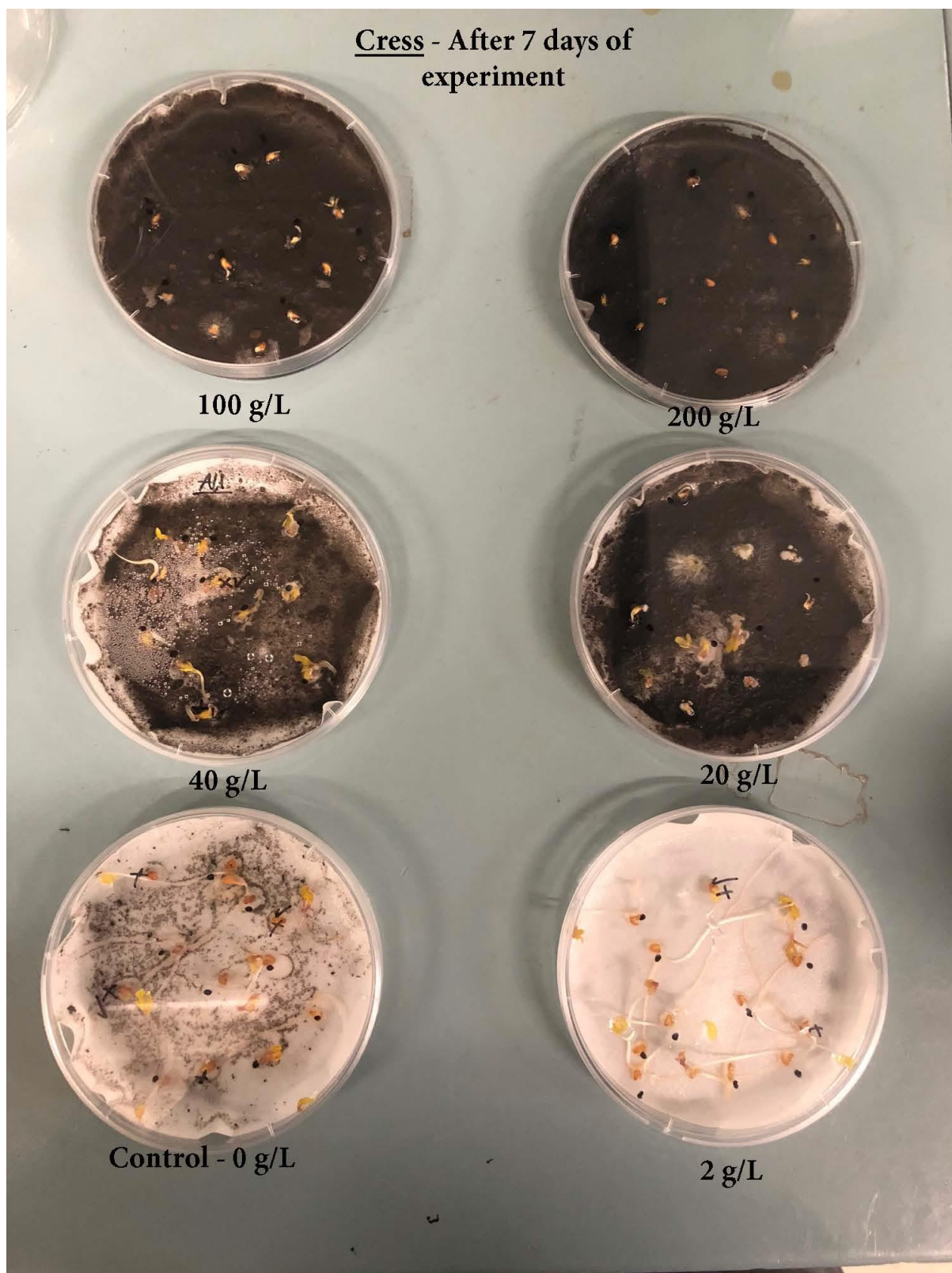
Supplementary information

A. Germination assays performed with torrefied wood with sulfolane (TWS)

Radish - After 7 Days of experiment -TWS

100 g/L   200 g/L

40 g/L   20 g/L

Control - 0 g/L   2 g/L

Cress - Photos after 7 days of experiment

100 g/L

200 g/L

40 g/L

20 g/L

Control - 0 g/L

2 g/L

B. Germination assays performed with clean torrefied wood with sulfolane (CTW)

Radish - After 7 days of experiment

Cress - After 7 days of experiment

100 g/L

200 g/L

40 g/L

20 g/L

Control - 0 g/L

2 g/L

C. Mean time to germination (MTG) and Germination index (GI) of radish and cress seeds treated with different biochars at different concentrations.
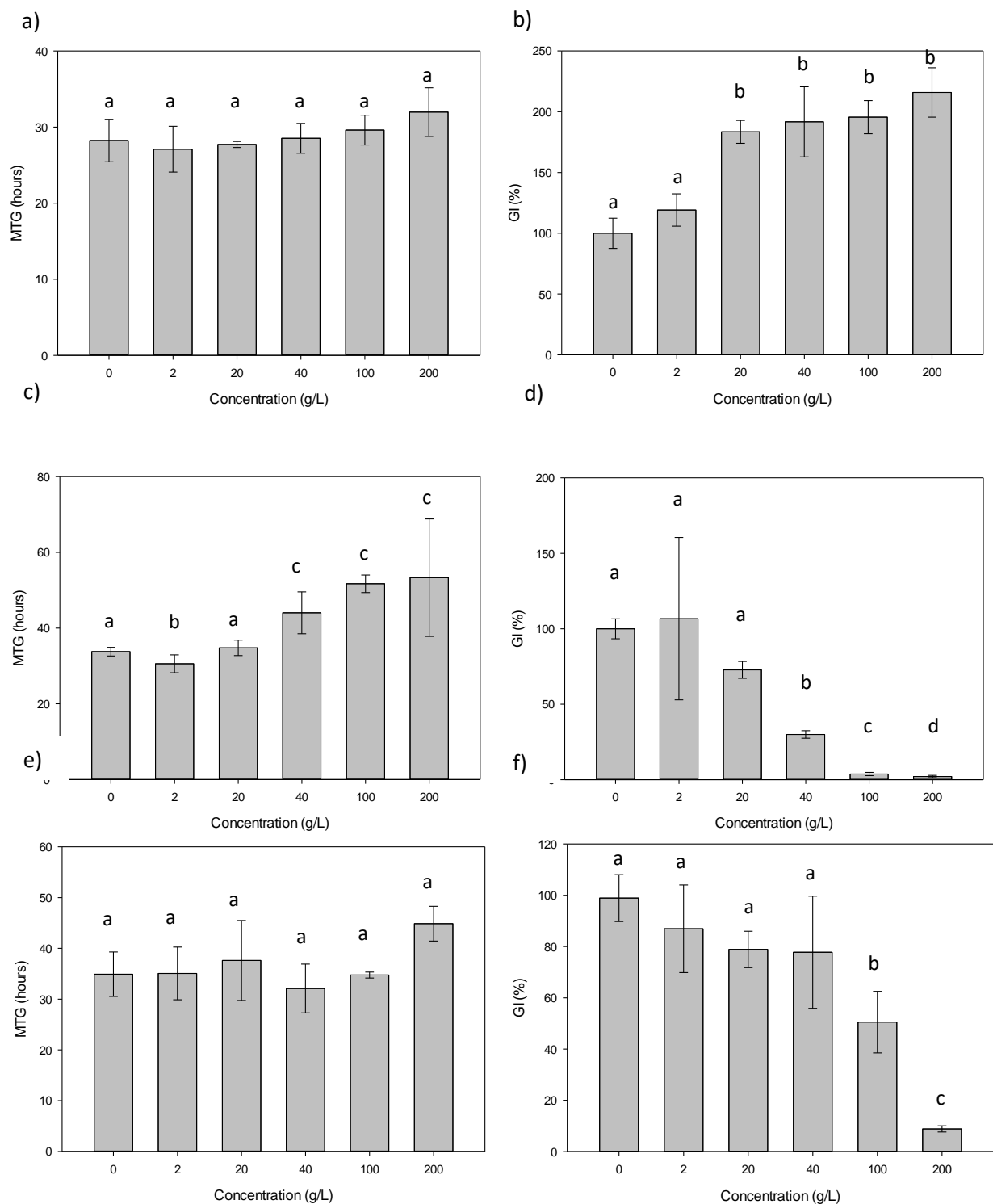

Figure 9. Mean time to germination and germination index of radish in the presence of char produced from pine sawdust (CPS) (a and b), char produced from TWS (CTWS) (c and d), and

char produced from CTW (CCTW) (e and f). Means (+- S.E.) followed by the same letter are not significantly different at the P < 0.05 level, as determined by SNK's test.
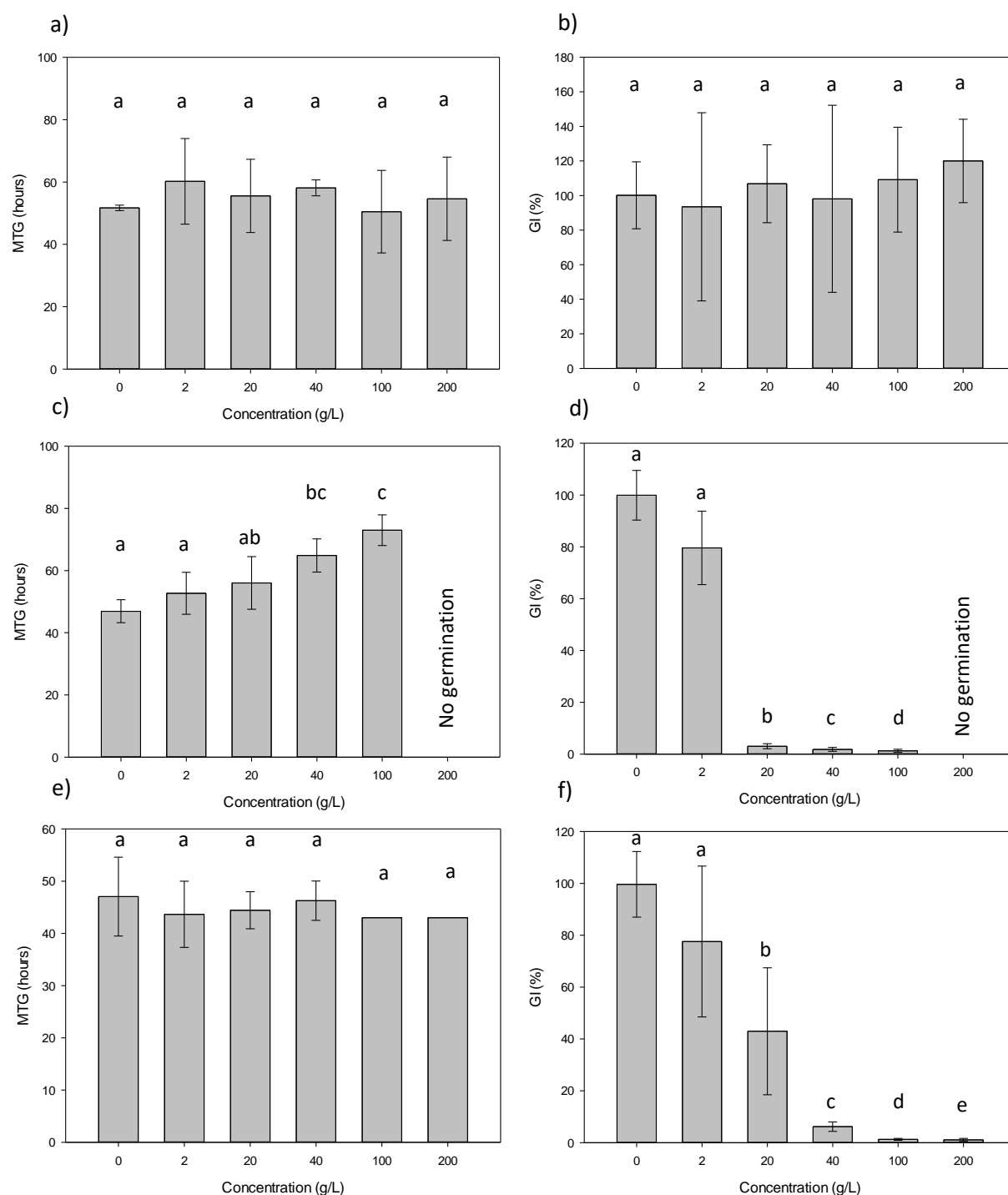

Figure 10. Mean time to germination and germination index of cress in the presence of char produced from pine sawdust (CPS) (a and b), char produced from TWS (CTWS) (c and d), and

char produced from CTW (CCTW) (e and f). Means (+- S.E.) followed by the same letter are

not significantly different at the $P < 0.05$ level, as determined by SNK's test.